THE UNIVERSITY OF CHICAGO

SEX DIFFERENCES IN THE CIRCADIAN AND ULTRADIAN RHYTHMS OF MICE

A DISSERTATION SUBMITTED TO

THE FACULTY OF THE DIVISION OF THE SOCIAL SCIENCES

IN CANDIDACY FOR THE DEGREE OF

DOCTOR OF PHILOSOPHY

DEPARTMENT OF PSYCHOLOGY

BY

JONATHAN PARKS RIGGLE

CHICAGO, ILLINOIS

AUGUST 2022

Dedication

To my mother.

To my supporting father

To the sisters who kept me sharp.

To the roommates who gave me a home.

To the friends who held me somewhat sane.

To the undergrads who enabled all the research.

To the lab mates who helped me along the way, innumerably.

To all the rodents whose lives were used to advance the research.

To the many professors who offered me their time and ear as guidance.

To the cats who slapped me awake for food and, as a byproduct, experiments.

To the mentor who instructed me and guided me, sometimes curious, and sometimes furious,

To Science.

Dedications are poor compensation.

“You’re going have to get much smarter very quickly.”

-Jeff Vandermeer

Table of Contents

List of Figures

List of Tables

Acknowledgements

Despite what is commonly said, a dissertation is done in isolation, usually in the squinty hours of that liminal space between night and morning with an accumulation of coffee mugs, gum wrappers, tea mugs (for when you've decided you've had enough of the strong stuff), vaguely appetizing food remnants, and empty diet coke cans (for when you've decided you are a fool and assuredly have not had enough of the strong stuff)... Nevertheless, a large modicum of thanks is due to those whose support allows you to get to and descend into such a state (and hopefully come out again).

First, I must thank my mother, Dr. Martha Anne Pendleton Riggle, for instilling in me both a strong moral compass to guide me through unfamiliar waters and an abiding independence for when my road grew lonesome and treacherous. As for my father, Dr. Karl Parks Riggle, I have the utmost gratitude for his being a moral paragon in my life and always trying to find new ways to understand and love me, even when normal communication failed us. To my sisters, Dr. Brittany and (the soon to be Dr.) Kirsten Riggle, thank you for loving me, supporting me, and occasionally kicking my tuches when I got too full of myself.

To my loving friends, your contributions defy page limits (or will at least strain my committee's patience) so in brief I will express my eternal appreciation and hope that I may be as good a friend to all of you as you have been to me. For my lab mates, Dana Beach, Jharnae Love, and Dr. Kenneth Onishi, you all are awesome and I am deeply indebted to you for the ears you lent to all my rants and hare-brained ideas. Finally, to Dr. Leslie Kay, Dr. Xiaoxi Zhuang, Dr. Irving Zucker, Dr. Greg Norman, and most of all Dr. Brian J. Prendergast, words cannot express my gratitude for all the mentorship on my scientific journey.

Abstract

Biological rhythms in behavior and physiology are pervasive and provide temporal structure to an organism's basic biological functions. Circadian rhythms are generated by a cellular transcriptional-translational feedback loop consisting of 'clock genes' and their protein products, interacting in a 24 h loop. But biological timekeeping happens over many timescales. Circadian rhythms occur on a daily timescale (~24 h e.g., sleep, activity, metabolism), whereas ultradian rhythms persist at sub-daily timescales (~1-6 h e.g., sleep stages, activity bouts, meal patterns). Understanding how circadian and ultradian rhythms work in isolation, and perhaps more importantly, how they interact, holds the potential for deeper insights into behavior and physiology. Females are historically underrepresented in behavioral neuroscience, and this bias extends to the study of biological rhythms (chronobiology). Although sex differences have been reported in rhythmic aspects of humans and non-human behavior, clock-driven behaviors, and clock-dependent pathology, the assumption that females and males rely on the same molecular mechanisms, to the same degree, to generate circadian rhythms has not been rigorously examined. Ultradian rhythms, while ubiquitous, have garnered far less empirical study as compared to circadian rhythms, and females are similarly neglected in this domain. I conducted several experiments to interrogate sex differences in circadian and ultradian rhythms, and their regulation by environmental and epigenetic processes.

In the first experiment (Chapter 3), I investigated whether male and female mice are equally dependent a core clock gene (Period 2; *per2*) for the generation and maintenance of circadian rhythms in behavior. I showed that both males and females lacking two functional copies of the *per2* gene exhibited a loss of circadian rhythms, but this circadian arrhythmia manifested differently between the sexes: compared to males, females became arrhythmic

faster, and far more females became arrhythmic. Male gonadal hormones were responsible for this sex difference in circadian dependence on *per2*.

In Experiment 2 (Chapter 4), I developed and validated a novel analytical technique, based on wavelet time series analyses, for quantifying ultradian rhythms, which have been difficult to accurately and precisely quantify, in part because of the properties that define them: multimodal periods, non-stationarity, circadian harmonics, and diurnal modulation. Using extensive simulations and empirical validations, I confirmed the technique's accuracy and precision; I then used the wavelet-technique to identify robust and repeatable sex differences in ultradian rhythms of mice and to quantify how gonadal hormones and seasonal changes in photoperiod affect these sex differences.

Returning to the circadian system, in Experiment 3 (Chapter 5), I tested the hypothesis that the individual differences in the effects of the *per2* knockout, identified in Experiment 1, were a consequence of the state of the circadian clock network. I found that lighting manipulations known to perturb the circadian clock failed to alter the effects of the *per2* gene on most aspects of circadian behavior, indicating that an animal's recent photic experience is likely irrelevant, and that circadian disruption in the $Per2^{m/m}$ mutant mouse model may reflect stochastic rather than established circadian processes.

Finally, in Experiment 4 (Chapter 6), I extended my investigation of sex differences in behavior to examine whether epigenetic processes can contribute to variability in circadian and ultradian rhythms. These studies evaluated the role of the RNA methylation reader gene *ythdf1*. Using male and female mutant mice deficient in *ythdf1*, I documented numerous changes in circadian behavior that manifested only in one sex.

Taken together, these findings indicate that the core molecular machinery of the circadian clock is sexually-differentiated. This sex difference does not appear to be modifiable by manipulations that strongly disrupt circadian network coherence, but it is clearly maintained by concurrent gonadal hormone secretion. The novel analytical techniques described here will permit more accurate and precise quantification of sex differences in circadian and ultradian patterns of behavior, in both sexes, furthering our understanding of how sex differences in biological timekeeping are influenced by interoceptive (circadian network coherence, hormones, epigenetics) and exteroceptive (photoperiod) cues.

Chapter 1: Background and General Information

Life and time are inextricably linked. As the earth orbits the sun, day turns into night and the seasons progress, life responds accordingly. Organisms, no matter if they are single celled bacteria, sessile plants, or animals, do not function the same at night as during the day, nor in winter as in summer. Their physiology and behavior change in accordance to their external time. But they do not do so purely based on stimuli such as the presence and absence of light or changes in temperature— a warm day in midwinter does not cause apple trees to flower (Zhang et al., 2019). Life has evolved temporal order: the capacity to internalize and keep time at many different levels concurrently, organizing its behavior and physiology rhythmically in concert with its environment.

Chronobiology, the study of biological timing, seeks to grapple with questions of how interactions of behavior, physiology, and different periods of time occur. For example: why migratory humpback whales do not breed out of season and yet still can adapt to changing ocean temperatures (Ramp et al., 2015); how the loss of the ability to generate daily time affects the survival of chipmunks in the wild (DeCoursey et al., 2000); and for what reasons meadow vole behavior is organized in 2-3 hour intervals (Gerkema et al., 1993; Gerkema et al., 1990; Gerkema & van der Leest, 1991). The complex mechanisms needed to provide this chronological structure in the face of seasonally, daily, and intra-daily environmental challenges are not fully understood, nor are the ways that events occurring across these different levels of time interact (Daan et al., 2011). Biological timing has been shown to vary across sex and species, yet many of its properties and principles endure across these dimensions (Vansteensel et al., 2008; Yan & Silver, 2016). Moreover, its malfunction is frequently deleterious to both physical and mental

health (Evans et al., 2013; Walker et al., 2020). Understanding how life "gets timing right" and why it occasionally gets it wrong has widespread implications both in basic biology and clinical outcomes: from animal migration to cancer (Savvidis & Koutsilieris, 2012; Stevenson et al., 2015). Concerted efforts have been made toward this understanding— the 2017 Nobel Prize in Physiology or Medicine was awarded to Hall, Rosbash and Young's for their discoveries of the molecular mechanisms controlling the circadian rhythms, but major gaps in understanding still exist.

Two big questions remaining in chronobiology center on: (1) what the properties of intradaily rhythms (ultradian rhythms; URs) are, and (2) how the sexes differ in biological timekeeping. In the case of ultradian rhythms despite widespread observation of these rhythmicities across a host of behaviors and physiological processes, the mechanistic underpinning and many of the basic properties of URs remain poorly understood. As for the role of sex, while the existence of sex differences in biological rhythms has been well established (Butler et al., 2017; Yan & Silver, 2016), much of the basic work into the mechanisms of timekeeping has been conducted without consideration of sex, despite sex differences proven importance to health (Bailey & Silver, 2014; Zucker & Prendergast, 2020).

The research described in this dissertation further explores the role of different levels of biological time in laboratory mice at both behavioral and molecular levels. A general background is reviewed below, followed by novel experiments which address new questions in chronobiology. Special attention is paid both to how biological clock mechanisms differ between the sexes and to the development of tools to better quantify the role of intradaily ultradian organization.

Conserved Ubiquity of Biological Timekeeping

Biological timing is ubiquitous. Animals migrate at specific times of year, breed seasonally, or hibernate during the winter. Creatures furred and feathered exploit different temporal niches: foraging at night, grazing during the day, or hunting insects at dawn or dusk. Seasonal (~1 year), daily (~24 hour), and intra-daily (0.5-6 hour) cycles in plants (McClung, 2006), likewise occur in fungi (Dunlap & Loros, 2006) and animals ranging from octopuses to grizzly bears (Bloch et al., 2013; Cobb et al., 1995; Jansen et al., 2016; Meisel et al., 2002; Vansteensel et al., 2008; Yates & Yates, 2008). Even the more nebulous daily rhythms of sleep are accepted to have temporal structure, being arranged into short basic rest activity cycles (Kleitman, 1982), an organization that seems to be recapitulated in body temperature fluctuation and feeding behavior (Blessing & Ootsuka, 2016). Mounting evidence indicates that ~24 hour rhythms known as 'circadian' (from the latin *circa* meaning around and *dies* meaning day) can be found in every cell in the human body, even anucleated red blood cells (O'Neill & Reddy, 2011). And anywhere from 10% to 50% of the genome is circadian in its gene expression (Turek, 2016; Zhang et al., 2014). Timekeeping is so pervasive that it has been demonstrated in all three domains of life (Whitehead et al., 2009).

The adaptive significance of rhythms is likely three-fold: rhythms permit entrainment of an organism with periodicities in its external environment, facilitate synchrony among the innumerable clocks/rhythms within the organism itself, and flexibly keep time during intervals in which the external environment is no longer a helpful cue. Below I briefly address these.

Entrainment: No matter the organism, seasonal and daily circadian rhythms have evolved to provide synchrony with predictable environmental geoperiodicities such as light, day length (photoperiod), and in some cases temperature, with great degree of evolutionary conservation

and convergence in function and mechanisms (Glaser & Stanewsky, 2005; Lahiri et al., 2005). This phenomenon is a process known as entrainment. Importantly, in virtually every instance where daily and seasonal rhythms have been documented, they have been shown to be driven by endogenous timers. That is, while they may be modified by environmental input they do not require any external stimuli to maintain their rhythmicity, even if in the case of interval timers that need stimulus to reinitiate their rhythmic interval (Paul et al., 2008; Stevenson et al., 2017). The environmental cues that drive entrainment are called *Zeitgebers*, from the German for 'time giver'. In terrestrial organisms, light has emerged as the most salient for entrainment. Indeed both unicellular and multicellular organisms have been shown to use light to encode seasonal and daily information (Ouyang et al., 1998; Pittendrigh & Minis, 1972).

Internal Synchrony: This coordination of the external world with internal clocks is only effective if synchrony is achieved in the multiple oscillatory component internal environment. In single celled organisms, e.g. cyanobacteria, this may manifest as orchestration of multiphasic, rhythmic gene expression (Liu et al., 1995). In multicellular organisms where every cell and tissue has its own clock, each timepiece must work in concert in order to achieve normal function. When desynchrony occurs, it results in pathological systems/network events such as jet lag, metabolic syndromes and immune dysfunction, both in humans and animal models (Evans & Davidson, 2013; Haspel et al., 2020), demonstrating the functional importance of clock alignment.

Bout Structure: Beyond entrainment and internal coordination, organisms have a need to keep time on timescales not directly synchronized to any known external geoperiodicities (Goh et al., 2019). These intra-daily URs with periods in the 0.5-6 h range provide internal temporal order, and allow organisms to consolidate behavior and physiology into bout structures which

may be both more efficacious and energetically efficient (Guillot & Meyer, 1997; Scannapieco et al., 2009; Veldhuis, 2008; Yates & Yates, 2008). Ultradian hormone pulsatility has been shown to be necessary for many hormones to operate at maximum efficiency (Veldhuis, 2008). And the utility of URs becomes readily apparent when zeitgeibers linked to geoperiodicites are no longer available naturally. When constant light or darkness emerge near the Arctic or Antarctic solstices, reindeer and ptarmigan exhibit feeding, body temperature, and locomotor activity rhythms that are purely ultradian in structure, during these intervals (Bloch et al., 2013). Similar observations have been reported during avian, mammalian, and eusocial insect reproductive events, as well as during avian migration (Bloch et al., 2013; Prendergast, Beery, et al., 2012; Yerushalmi & Green, 2009).

In keeping with this adaptive significance, all three of these temporal domains: seasonal, circadian, and ultradian, have mechanisms of timekeeping with show a great deal of evolutionary conservation, but also convergence as biological rhythms are thought to have evolved multiple times.

Shared Mechanisms: Melatonin is important for seasonal rhythms in both animals (Stevenson et al., 2017) and plants (Zhang et al., 2019). Drosophila and murine daily clocks are very similar in mechanism, using many of the same molecular components(Tataroglu & Emery, 2015). Even fungal or bacterial daily rhythms function on similar operational principles— the use of negative feedback loops (Dunlap & Loros, 2006; Ouyang et al., 1998); and temperature compensation (Kidd et al., 2015) to maintain period homeostasis. Such similarities may also be present in ultradian rhythms, but their mechanisms are not well enough understood to permit such inferences (Prendergast & Zucker, 2016). Regardless, while it is easy to prematurely assign evolutionary and ecological importance to a pattern of chronobiological laboratory observations

(Daan et al., 2011; Riede et al., 2017), evidence suggests that biological timekeeping evolved many times independently (Young & Kay, 2001), and recent work has shown that mutant mice with an impaired ability to generate circadian rhythms are at a considerable adaptive disadvantage compared to their intact wildtype counterparts (Spoelstra et al., 2016). Moreover, even when selective pressures wanes for the ability to entrain daily periodicities, circadian rhythms persist. A wonderful illustration of this occurs in blind Mexican cavefish who have lived deep underground, separated long enough from their river cousins to regressively evolve nonfunctional eyes and lose pigmentation, yet still exhibit the capacity to entrain to light and to generate circadian rhythms in the laboratory, albeit dampened (Beale et al., 2013). A similar finding had been discovered in entirely subterranean naked mole rats (Yerushalmi & Green, 2009). In summation, the available data supports the idea that the function and mechanisms of biological timekeeping both are conserved and convergent.

Importance of Biological Time

Homeostasis: Why biological timekeeping is of important enough to evolve independently multiple times and then be conserved and ubiquitous can be understood at multiple levels. One framework focuses on energy conservation and survival (i.e. homeostasis). The work of Bernard and Cannon first developed the idea of homeostasis. Under Cannon's conceptualization, organisms have equilibria (set points) of temperature, concentration, etc. which hold the internal milieu (or internal environment) at values that optimize adaption and survival. Negative feedback loops are used to re-establish the set points when environmental influences push physiological variables outside the normal range, destabilizing the system (Cannon, 1929). Biological rhythms may seem initially at odds with this conceptualization, as daily changes seem

to superficially defy homeostatic control, the defense of a set point would presumably counteract any rhythmicity. Potential environmental threats are not constant in their likelihood to perturb homeostasis though, depending on the time of day and year: predation, dehydration, hypo/hyperthermia, availability of food all change and these shifts are predictable— hypothermia is less of a threat in the summer, as is a nocturnal predator during the day. Biological rhythms allow organisms to anticipate a dynamic environment and modify their set points rhythmically, expending more energy on homeostatic defense only when threat perturbation is more likely to be high (McEwen & Wingfield, 2010). Indeed foundational work demonstrated that many homeostatic set points oscillate throughout the day and year (Buijs et al., 2019). Taken together the importance of biological clocks may be described as an augmentation of homeostasis. A variation on the theme.

Energy Conservation: Biological clocks confer upon individuals the ability to not only anticipate changing threats of perturbation, but also schedule changes in physiology in anticipation, thus optimizing energy balance. For example, over the course of a year, many ultimate factors directly relevant to survival, such as temperature, mate availability, and food abundance fluctuate from year to year, but proximate factors such as day length are highly stable across years— for example, a spring thaw occurs on a different date every year, but every year a specific day length will predict spring (Stevenson et al., 2017). This is ultimately linked to energy availability. In mammals it is adaptive to give birth during seasons when energy is readily available, because lactation greatly increases energy demands and offspring are particularly vulnerable to environmental change, (Hill, 1992; Paul et al., 2008; Stevenson et al., 2015). Likewise it is beneficial for hibernating animals like ground squirrels to prioritize acquiring extra energy during seasons when it is readily available to prepare themselves for winter and emerge

from hibernation only when enough food available to survive (Paul et al., 2008). Use of day length as a predicative cue confers upon them stability in organizing these behaviors across evolutionary time. Rhythmicity is under strong selective pressure. On a shorter time scale, an animals' daily temporal niche is also subject to such ultimate-proximate linkages. By manipulating predictable connections between environmental cues (food availability, predation, temperature, and availability of water) and the light/dark cycle it is possible to make a nocturnal animal become diurnal and vice versa. Animals then optimize their daily distribution of behavior based on the constraints of their circadian environment (Riede et al., 2017). Ultradian rhythm may also optimize the expenditure of resources, the bout structure they exhibit is very energy efficient (Guillot & Meyer, 1997). Biological clocks across many time scales, then, appear to permit the energetic optimization of physiology by predicting environmental events.

Coordination of Behavior across Multiple Temporal Domains: Beyond anticipating perturbation, and energy conservation, biological timing allows organisms to interface with many different timescales concurrently exhibiting behaviors and physiology that are concordant not only with season, but time of day, and state of rest. A rhetorical device to assist: consider that the early bird gets the worm. To do so, she must marshal a whole host of physical systems that change over changing time scales and she must do so in proper order. First, she must wake before her prey wriggles free of the ground, initiating glucocorticoid pulses many hours in advance to prepare metabolically for the challenge (Pilorz et al., 2018), but not so early as to be vulnerable to nocturnal predators. Awake, the dozens of hormones that converge to induce hunger must pulse in concert as she hunts (Ahima & Antwi, 2008; Kaiya et al., 2013). She must also allocate enough energy to remain alert and elude predators, outcompeting other would-be worm snatchers (Pilorz et al., 2018). Even when the she seizes her prey, the task is not complete

as her metabolism must be ready to digest the worm while her immune, digestive, and excretory systems are ready to process potential hazards the worm brings with it (Pacha & Sumova, 2013; Zheng et al., 2020). Depending on her size, though, one worm may not be enough. If she needs to eat again in the same day, she will need time to digest and continuing to forage extends the time she is vulnerable to potential predators (DeCoursey et al., 2000; Elderbrock et al., 2020; Gerkema & Verhulst, 1990; Yerushalmi & Green, 2009), instead she will wait a short interval of time before all the timing events of the first foraging interval are repeated. Depending on the season, however, this whole time course may be reshaped. If she is migrating her feeding activity may shift entirely (Bloch et al., 2013). At every step of the early bird getting the worm then, timing is required and coordinated across many temporal domains. That is why, beyond concepts like homeostasis, energy conservation, biological timekeeping is important, because it allows organisms to structure their behavior and physiology across many different levels of time concurrently and optimize for survival.

Models of the Circadian Timing System in Mammals:

Organization and Coordination of Clocks: Mammals have endogenous circadian oscillators in every cell of the body, driven by transcriptional-translational feedback loops (TTFLs; expanded on in more detail later) but they need structural organization in order to properly internally synchronize and entrain to their environment. It is possible that identical intrinsic period lengths could lead to spontaneous synchronization (Evans & Gorman, 2016), however in mammals the evidence would suggest that intrinsic period differs by tissue (Abe et al., 2002; Balsalobre, 2002; Evans & Gorman, 2016; Granados-Fuentes et al., 2004). Synchrony of every circadian oscillator could be mediated by simultaneous entrainment of independent oscillators (Fig. 1.1A), but desynchrony does not occur in constant conditions, arguing against such a

possibility (Evans & Gorman, 2016). Thus the mammalian circadian system must have two basic features: (1) mechanisms of coupling each cellular oscillator and (2) a pacemaker or coupled pacemakers which encodes time information from the external environmental and impose their period (the interval between successive occurrences of the rhythm) and phase (the timing of the rhythm with respect to externals cues) on other oscillatory cells, tissues, and organs, (Fig. 1.1B-C; (Evans & Gorman, 2016)

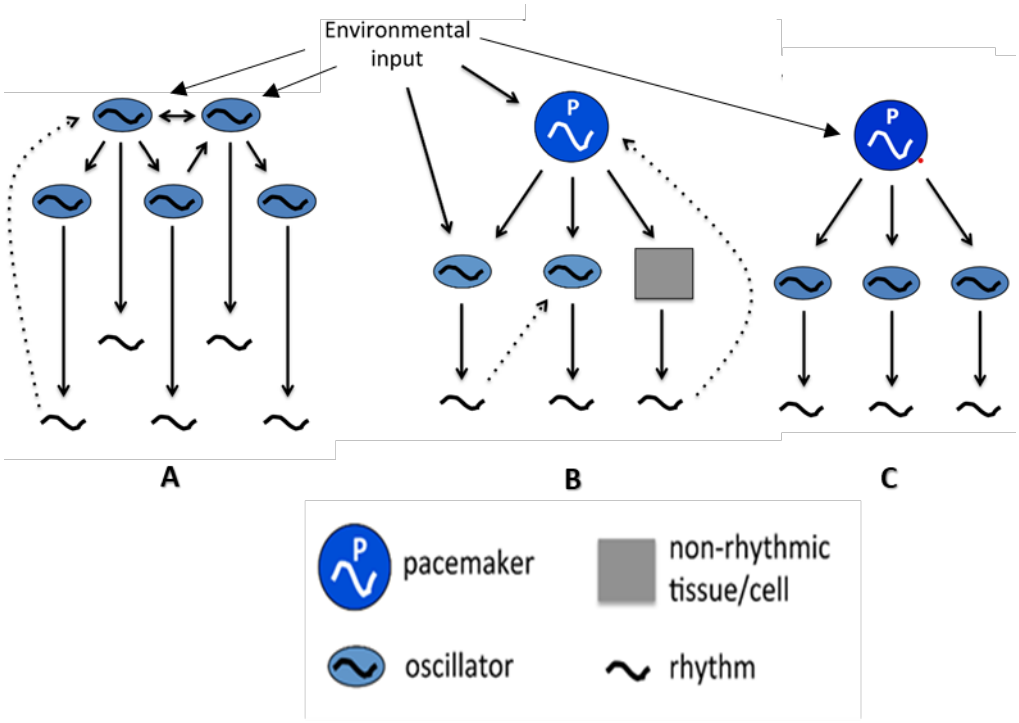

Figure 1: Models of pacemaker organization

(A) No pacemaker model: oscillators are synched with the outside world simultaneously and no pacemaker drive intra-organismal synchrony. (B) Reciprocal pacemaker model: a pacemaker has access to the external environment and imposes period and phase on all subordinate oscillators and non-oscillatory structures. Feedback exists back on the pacemaker. (C) Rigid hierarchical pacemaker model: a pacemaker has access to the external environment and imposes period and phase on all subordinate oscillators and non-oscillatory structures. Peripheral feedback does not exists back on the central pacemaker.

Dynamic Entrainment: Although entrainment is often studied in acute preparations (jet lag, single light pulses (Reebs & Mrosovsky, 1989; Stephan, 1983), in naturalistic contexts,

entrainment is not performed on a constant *zeitgeiber*—the availability of light, food, and temperature all vary with the seasons. Thus as photoperiod/day length increase and decrease throughout the year, entrainment, must adjusted accordingly— expanding and compressing activity duration (τ) and changing its phase relationship with the onset and offset of light and dark (Daan & Pittendrigh, 1976). Beyond just seasonal fluctuations in *zeitgeibers*, though, non-periodic masking events occur all the time: circadian disruption due to sickness, social influences, pregnancy, etc., and animals must adjust to stay in phase with outside world. However, they must do so transiently, without entraining to the new cue. Indeed, when light is provided in too short or long intervals (T Cycles) rats have been shown to be unable to maintain entrainment (Stephan, 1983), because entrainment is only possible within a narrow band of T Cycles such that transient cues cannot permanently disrupt biological clocks. As a final note, entrainment is most often studied via models that examine entrainment of the organism to the environment, but it is assumed that similar dynamic, continuous entrainment is occurring among distinct cellular- and tissue-level circadian oscillators distributed throughout the body on a daily basis. This is seldom studies directly, however, with few exceptions (Evans et al., 2013).

SCN as a Pacemaker: Of course, in order for rhythms to entrain, they must first be generated, and over the past 5 decades, a substantial body of evidence supports a role for specific brain nuclei as a pacemaker for the generation of mammalian circadian rhythms. In mammals, the suprachiasmatic nucleus (SCN) of the hypothalamus has been demonstrated function as the circadian pacemaker. It has been shown to be necessary for organism-wide circadian rhythms—in electrolytically lesioned rats, hamsters and mice: circadian rhythms in adrenal corticosterone, body temperature, water drinking, and locomotor activity are abolished when animals are removed from presence of *zeitgebers* and placed in constant conditions (Stephan and Zucker

1972; Moore and Eichner 1972). This work has been replicated and extended to other mammals (rodents and non-human primates) in hundreds of studies (Fuller et al., 1981; Ralph et al., 1990; Reppert et al., 1981; Yoo et al., 2005). The SCN is also sufficient to set the phase and period of organism wide circadian rhythms. Inouye and Kawamura (1979) electrically isolated the SCN containing hypothalamus with a Halasz knife in rats blinded by bilateral ocular enucleation, demonstrated using electrical recording that while the rest of the brain became circadian arrhythmic, circadian electrical rhythms persisted within the hypothalamic island. Furthermore, they found an inverse phase relationship between circadian electrical rhythms in the rest of the hypothalamic island and the SCN suggesting it was the source of this rhythmicity (Inouye & Kawamura, 1979). Transplant work in hamsters by Ralph and colleagues has further supported this conclusion. When SCN lesioned hamsters were given fetal SCN transplants from mutant hamsters with genomically altered intrinsic circadian period, the transplant not only restored circadian function put instilled the mutant period in a wild type background (Ralph et al., 1990) indicating that the SCN is sufficient for organism wide period synchrony. These data together with work by Silver (1996) suggest that in order to have synchronized and endogenous rhythmicity across the mammalian body the SCN pacemaker is required.

SCN and Zeitgebers: In order to entrain a mammal to its environment, the circadian pacemaker in the SCN, must have access to *zeitgeibers* from the external environment. In mammals the photic *zeitgeber,* light*,* remain the most salient for circadian entrainment. Light must be perceived at the retina, and via redundant retinal cellular inputs: photoreceptive rods, cones, or ganglion cells (Panda et al., 2005) and accesses the SCN directly via the retinal hypothalamic tract (RHT) of the optic nerve or indirectly via the thalamic intergeniculate leaflet. In the SCN, RHT terminals release glutamate which activates intracellular mechanisms that shift

the TTFL (Golombek & Rosenstein, 2010). Acute circadian responses to light can be characterized by a psychophysical function known as a phase response curve (PRC) which indicates the magnitude of circadian shift in time as a function of when in the circadian cycle light is encountered (Golombek & Rosenstein, 2010; Johnson, 1999; Wams et al., 2017). The PRC to light typically has an amplitude of several hours in each direction (advance and delay shifts), underscoring the potency of light as a circadian zeitgeiber (Johnson, 1999).

Nonphotic zeitgebers, such as social cues can entrain circadian rhythms too (Wams et al., 2017). Bats caged in a dark cave can be entrained by their uninhibited conspecifics (Marimuthu et al., 1981). It is possible to phase shift circadian rhythms with social cues and this has been demonstrated repeatedly in many different animal species (Wams et al., 2017). Even human and non-human primates can effectively use social cues for entrainment when conditions like total blindness preclude the use of photic *zeitgeibers* (Erkert & Schardt, 1991; Klerman et al., 1998; Wams et al., 2017). Nonphotic *zeitgebers* are unlikely to directly access the SCN. Though their neural pathways are less understood, in hamsters lesions of the intergeniculate leaflet(IGL) prevented the response to certain nonphotic cues, and the serotonergic raphe nucleus (which projects both on to the SCN and IGL) has emerged as potentially important substrate for non-photic *zeitgeiber* entrainment (Fig 1.2; (Wams et al., 2017). The SCN then is not only the circadian pacemaker but also a site of *zeitgeiber* integration. Despite a number of idiosyncratic examples of potent, ecologically-meaningful circadian responses to nonphotic zeitgeibers, in common mammalian circadian research models, PRCs to most NPZs are substantially lower in amplitude than PRCs to light, underscoring their secondary role in mediating entrainment (Mrosovsky, 1996).

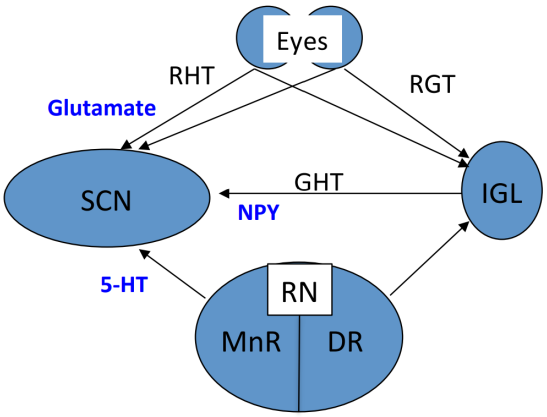

RHT = retinohypothalamic tract; IGL = intergeniculate leaflet of the thalamus;
GHT = geniculohypothalamic tract; RN = Raphe nucleus; MnR = median Raphe nucleus;
DR = dorsal Raphe nucleus

Figure 2: Direct and indirect pathways of entrainment into the SCN

Glutaminergic input from the retinohypothalmic tract, NPY input from the geniculohypothalamic tract, and serotonergic input from the median Raphe nucleus have emerged as three major pathways that mediate entrainment.

Dual Oscillator Model: A theoretical model has emerged to account for limits of entrainment and entrainment to changing photoperiods, and is founded in the work of Pittendrigh and Daan. Although formulated and based in nocturnal organisms, it is likely relevant to all mammals that live in a photic environment. It demarcates two oscillators, an evening (E) oscillator responsible for the onset of activity and a morning (M) oscillator responsible for the offset the next morning. All other things being equal, the E oscillator is thought to have a τ less than 24 h and the M a τ greater than 24 h, suggesting that they should run away from each other i.e. splitting. However, because these oscillators can phase advance or delay based on when they encounter light in their respective cycles (expanded on later) under stable entrainment conditions the phase delay of the E oscillator and the phase advance of M oscillator counter their natural drift away from each

other and keep them coupled. When photoperiod is changed this destabilizes the system causing the oscillators to drift toward or apart from each other until a new stable equilibrium is achieved (Evans & Gorman, 2016). Moreover, when T cycles are too short or long the E and M oscillators will not be appropriately phase shifted and thus will not be stably entrained. This model then can account for both limits of entrainment and entrainment to shifting photoperiods.

Evidence of SCN Photoperiod Response: The SCN is sensitive to photoperiod. In line with the dual oscillator model, physiological and behavioral evidence supports the SCN being sensitive to photoperiod. For example, with long enough photoperiods it is even possible to shift the GABAergic neurons of the SCN from inhibitory to excitatory (Myung et al., 2015), and reorganize the SCN network (Evans et al., 2013). Sumova and colleagues showed that light induced C-fos expression in the rat SCN changes with changing day length and recent work by Azzi and fellows have demonstrated that DNA methylation shifts dynamically with photoperiod in the SCN and helps reorganize the network to respond (Azzi et al., 2014; Azzi et al., 2017; Sumova et al., 1995).

Evidence for a Dual Oscillator Model: Behavioral and genomic observation support the idea that multiple distinct oscillatory components within the SCN coordinate with one another to form a functional dynamic pacemaker (Daan & Pittendrigh, 1976; Evans & Gorman, 2016; Pittendrigh, 1960). In constant light (LL), many nocturnal rodents exhibit circadian arrhythmia or a behavior known as 'splitting', in which activity bifurcates into two activity rest bout that drift apart from each other before stabilizing in an antiphase relation. Notably, this splitting can be reversed with exposure to constant darkness (DD). Moreover, the onset and offset of rhythmicity appear to be differentially regulated and changing the photoperiod, the duration of light compared to dark within a 24 hour can change the dynamics of these interactions (Schwartz

et al., 1987). It is possible to split the output of the SCN both at a behavioral and physiological level, between each lobe of the SCN and within (Evans & Gorman, 2016). Electrical activity recapitulates the behavioral oscillations but bifurcations in activity have not been consistently mapped within the SCN or between bitlateral lobes (Evans & Gorman, 2016). Emerging evidence though has documented that splitting behavior is absent in mice with genomic ablation of genes critical to circadian function and moreover the E&M oscillators can also disappear following the knockout of these genes, suggesting a genomic basis to the dual oscillator model(Schwartz et al., 2011).

Complex Hierarchical Clock Models: Linking the SCN to the external world is not sufficient for the robust circadian oscillations seen in physiology and behavior. After the phase and period of the circadian pacemaker are entrained to environmental cues they still must be systematically distributed to peripheral oscillators. Earlier models conceptualized the circadian system as one of a superordinate oscillator/pacemaker over multiple subordinate oscillators (Figure 1.1C; (Evans & Gorman, 2016), but emerging evidence suggests that this is an oversimplification. SCN-lesioned mice, genomically modified to have a luciferase reporter on one of the oscillatory genes in the TTFL underlying their cell autonomous circadian rhythms, exhibit a loss of coherent organism-level circadian rhythms, but robust circadian rhythms persist in desynchronized peripheral tissues (Yoo et al., 2005). Moreover, it is possible to restore circadian rhythms in SCN-lesioned mice with methamphetamine and timed food access. This rescue is not simply a bypass of the SCN. These rescued oscillators do not use the same mechanisms of molecular timekeeping as SCN-organized circadian rhythms and thus are separable (Mohawk et al., 2009; Pendergast & Yamazaki, 2018; Tataroglu et al., 2006). Finally, inconsistent with a unidirectional system in which a superordinate pacemaker imposes its period and phase on subordinate

oscillator, circadian activity output (Edgar et al. 1991) and peripheral oscillators such as the gut bacterial network (Niimi & Takahashi, 2019; Weger et al., 2019) have been shown to feedback back on to the clock. Newer models of circadian organization, thus interpret the SCN as more of a conductor of independent oscillators in the periphery which receive extra-SCN zeitgeber information and modify the SCN's timekeeping in turn (Patton & Hastings, 2018). Nevertheless, this elevation of the independence of peripheral timekeeping does not preclude the continued importance or uniqueness of the SCN. Nor does it suggest that the mammalian circadian time system is better understood as a distributed system of clocks like that of the avian system (Cassone, 2014). Unlike peripheral tissues whose circadian rhythmicity rapidly dampens in vitro culture, circadian rhythms from SCN slices in vitro persist indefinitely (Patton & Hastings, 2018). Taken together, these data suggest that mammalian circadian timing system is distributed, but the SCN still remains atop the hierarchy.

The Circuitry of Mammalian Circadian Timekeeping:

Anatomy of the SCN: Discrete regions of the SCN may mediate specific functions, which may map onto neurotransmitter identity of neurons and/or neuroanatomy. The SCN is not a homogenous tissue nor an entirely oscillatory one (Jobst and Allen 2002). Comprised of ~10000, mostly GABAergic neurons, with distinct subgroups based on neuropeptide expression, it is organized classically into an afferent retinorecipient ventral core and an efferent dorsal shell (Patton and Hastings 2018; Herzog et al 2017; Evans and Gorman 2016). Vasoactive Intestinal Polypeptide (VIP) neurons, especially prominent in the retinorecipient SCN core, are thought to lead to increased network synchrony, with knockout of the peptide or its receptor leading to desynchronized SCN neurons. Notably restoration of synchrony is possible in VIP negative SCN slices with a VIP positive SCN graft (Maywood et al. 2011). This fixing is not mediated by

restored electrical connections though. Use of a mesh that prevents electrical connections between the slice and graft still allows for restoration, but only if it sized to still allow VIP through (Maywood et al. 2011; Herzog et al. 2017). In contrast, GABA has been proposed to oppose synchrony within the SCN adding "jitter" into rhythms (Herzog et al. 2017), though this is complicated by findings that GABA can promote synchrony in some cases and the way that the role of GABA can change with changing photoperiod (Evans and Gorman 2016). Arginine Vasopressin (AVP) associated with the efferent shell has been traditional thought to only play a weak role on coupling (Evans and Gorman; Herzog et al 2017; Hasting and Patton 2018). However, recent work using novel transgenic animals has shown that AVP may play a much greater role in inter-SCN synchrony than previously appreciated (Shan et al. 2020). Neuromedin S (NMS) neurons, comprising about 40% of the SCN, play a disproportionate role in determining the SCN's ensemble period as seen by various strategies of creating chimeric SCNs as well as conditional expression of tetanus toxin in these cells (Herzog et al. 2017). The properties of the SCN then are at least partially explained by the SCN's neuroanatomy. Strict regional and neuropeptidergic identity are not fully explanatory of SCN function, however.

Structural Caveats: Understanding of the structural organization of the SCN is only a model. There are afferent connections in the SCN shell and efferent outputs from the core (Hastings et al., 2018). Heterogeneous subpopulation within the SCN, probably allow the plasticity needed to adjust to variable inputs and produce a coherent timing program (Hastings et al., 2018). Phased dispersed subpopulations change the magnitude of their phase differences with different photoperiods, and are thus hypothesized as one of the ways the SCN may encode day length. Knocking out the NMS peptide has no effect on SCN function (Herzog et al., 2017). Moreover, despite NMS neurons disproportionate regional contribution, there also does not appear to be

populations of SCN neurons that are just, for example, the "pacemaker". In chimeric SCNs with both WT neurons with normal periods, and mutant neurons with altered periods, the emergent ensemble period appears to be an average of the number of each type of neuron present in the circuitry (Herzog et al., 2017; Low-Zeddies & Takahashi, 2001). Furthermore, circadian outputs rely idiosyncratically on neural and humoral outputs. The SCN location in neural space is not even fully necessary. In SCN lesioned animals, placement of fetal SCN transplant in the third ventricle or with a semipermeable membrane can reestablish behavioral rhythms without neural connections (Lehman et al., 1987; LeSauter et al., 1996; Silver et al., 1990) endocrine rhythms though are not restored by this process (Meyer-Bernstein et al., 1999). Thus, while neuroanatomical organization of the SCN is useful for a general understanding of function, it does not fully account for all SCN features and a strict focus on anatomy may distract from the properties of the SCN that only emerge at the network level.

Network Effects: It is only through intercellular coupling that phase coherence, circadian amplitude, and period synchrony seen in global behavior emerge as properties of the neural network (Hastings et al., 2018; Herzog et al., 2017; Patton & Hastings, 2018). For example, blockade of electrical firing by tetrodotoxin (TTX) desynchronizes tissue level rhythms; both in phase and period (Welsh et al., 1995). It importantly does not, however, abolish cell autonomous clocks— upon washout and the reemergence of synchrony, behavioral rhythmicity does not resume to where it was upon application of TTX but instead is where would be project to be if TTX weren't administered at all (Schwartz et al., 2011; Welsh et al., 1995). Robust circadian organization in traits such as locomotor activity are an output of the aforementioned oscillators in the SCN but time is not kept at a network level. Oscillatory neurons within the SCN maintain autonomous timekeeping, but have weak, low amplitude rhythms with different periods when

isolated, and phasing (Hastings et al., 2018; Herzog et al., 2017; Patton & Hastings, 2018). Hence the SCN is synchronizer and pacemaker, but its proper functioning is not required for endogenous timekeeping, which occurs at the level of cell.

The Molecular Circadian Clock

Overview of the Organization of the Circadian TTFL: At the cellular level this internalized representation of time is accomplished using a transcriptional-translational feedback loop organized into a primary negative feedback loop, and stabilizing accessory loops (Cox & Takahashi, 2019). The genes of these loops, known as clock genes, are pleiotropic transcription factors and thereby impose timing on the rest of the genome (Evans & Gorman, 2016) and are in turn modulated by the external environment in the SCN via calcium signaling via both direct modulation of clock genes through calcium response elements (Herzog et al., 2017) and indirectly through CAMKII/ERK/cAMP signaling (Herzog et al., 2017). The main loop consists of the constitutively expressed clock gene, *clock* or its paralog *npas2* (DeBruyne et al., 2006) whose protein complexes with the rhythmically expressed protein of *bmal1*, also known as *arntl* or *mop3*, or its paralog *bmal2*. This heterodimer then promotes the transcription of the paralogs *period 1, period 2, period 3* and *cryptochrome 1* and *cryptochrome 2*, hereafter known as *per* and *cry,* through E box enhancer elements (Cox & Takahashi, 2019). *Per3* is so far shown to have only a minor role in the circadian system, and its protein product is much shorter than that of its paralogs, lacking a critical PAS domain needed for dimerization (Bae et al., 2001). PER1/PER2 and CRY1/CRY2 form heterodimers before translocating back to the nucleus inhibiting *bmal1/2* and thereby inhibiting their own production (Cox & Takahashi, 2019). Eventually these complexes degrade through binding with CASEIN KINASE 1δ and CASEIN KINASE 1ε, disinhibiting *bmal1/2* and reinitiating the transcriptional activation loop. This

negative feedback loop takes about ~24 hrs to complete and is thought to be the molecular representation of circadian time (Mohawk et al., 2012).

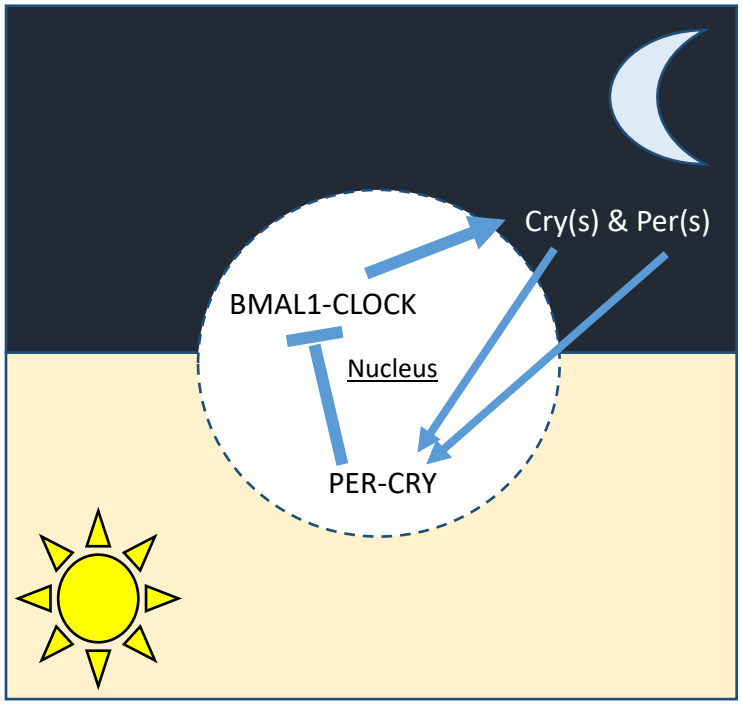

Figure 3: Diagram of the basic circadian TTFL
As it is organized in a negative feedback loop in time and cellular space.

The cellular circadian oscillation is stabilized against by perturbation by accessory feedback loops Two major loops have been identified beyond the BMAL/CLOCK→PER/CRY negative feedback loop. First is *ror-alpha/beta* and *rev-erb alpha/beta,* nuclear receptors whose ligands' transcription is driven by *bmal*. These ligands compete for binding between the two types of receptors which then competitively bind directly to the *bmal* promoter upregulating or down regulating transcription respectively (Cox & Takahashi, 2019; Preitner et al., 2002; Sato et al., 2004). The second loop composed of NIFL3, whose transcription/translation is regulated by the REV-ERBs and RORs, and DBP, regulated by BMAL and CLOCK. NIFL3 and DBP binds to

the D-box elements in the promotors of *rev-erb alpha/beta, ror-alpha/beta*, as well as *per1/2* and *cry1/2* (Cox & Takahashi, 2019; Ueda et al., 2005). Together this main loop and accessory loops drive precise cell autonomous circadian rhythms.

Epigenetic Role in Timekeeping: Epigenetic factors also play a role in circadian timekeeping. Epigenetics at the histone, DNA, and protein level have been shown to provide additional levels of control of biological timing, altering the accessibility of the different binding sites, changing the rate of translation, and speeding up or slowing down the rate of translation (Sahar & Sassone-Corsi, 2013). Global DNA methylation in particular has been shown to change over the course of the day in a circadian fashion altering the generation of the many non-clock gene transcription factors that none the less influence the core clock (Azzi et al., 2014). Recent work has shown that region specific DNA methylation changes may help the SCN to reorganize in response to light and changes clock gene expression when mice are exposed to altered T cycles (22 h instead of 24 h days) (Azzi et al., 2014; Azzi et al., 2017). At the level of histones, one of the core clock genes, *clock*, is a histone acetyltransferase that upregulated the expression of its binding partner *bmal* (Doi et al., 2006). Ubiquitination is a major player in degradation timing of the negative arm of the feedback loop (Stojkovic et al., 2014). RNA methylation of the m6A site can influence the pace of the circadian clock (J.-M. Fustin et al., 2013; Fustin et al., 2018). This is still a very active area of research, where the relative contributions of these various levels of regulation are as of yet unclear, but certainly play a role (Sahar & Sassone-Corsi, 2013). In contrast, the hierarchical contribution of clock genes and their nonredundant paralogs is much better understood.

Sex Differences in Circadian Timing

Brief note on terminology: Gender and sex are separable things. Gender is a sociological phenomenon, much like race, whereas sex is based in the interaction of several biological features including chromosomes and hormones. In clinical studies, the two are confounded both by uncareful use of language, on the part of researchers, and the ways in which sociological groups' biology can be altered by societal expectation and treatment (Silver, 2018). Although there are men who were assigned female at birth, women who were assigned male, nonbinary individuals who were assigned either, and intersexual individuals who fall across the gender spectrum that do not fit neatly in the categories of male and female or men and women, I will use male and female when referring to nonhuman animals, whose sexes were known for certain, and men and women when discussing humans, as in most cases sex was not confirmed and these studies only reported binary gender. The scope of the below review then must be understood as very general, and depending on the specific topic, it may or may not capture the variations of discordance of gender and assigned sex.

The importance of understanding sex differences: Sex differences can have critical implications. Recent work by Zucker and Prendergast (2020) has documented differences in the pharmokinetics of drugs across sex, with implications for adverse reactions to medication (Zucker & Prendergast, 2020). Much like the rest of neuroscience and biology in general (Beery & Zucker, 2011; Prendergast et al., 2014; Woitowich et al., 2020; Zucker & Beery, 2010), in chronobiology much of focus has remained on male animals in rodent studies due to unfounded fears about females increasing variability (Beery, 2018; Smarr et al., 2017). And yet sex differences in circadian biology are of clear clinical import.

Sex Differences and the Circadian system, a clinical perspective: The interfaces between sex and biological timekeeping are surveyable. Before the age of 40, women on average wake up earlier than men (Duffy et al., 2011; Fischer et al., 2017) and their intrinsic circadian period is shorter (Duffy et al., 2011). Women have higher amplitude melatonin rhythms and lower amplitude core body temperature than men. The timing of which occurs earlier relative to sleep onset, intriguing given the different prevalence of sleep disorders in women compared to men (Cain et al., 2010). Women are increased risk of insomnia compared to men, and self-report worse sleep quality despite objectively sleeping better based on sleep metrics (Bixler et al., 2009; Mong et al., 2011). Of course, some caution must be taken in this conclusion as these metrics may simply fail to capture aspects of sleep that worsen quality. Beyond just sleep, sex affects circadian rhythms across several different metrics of biological functioning. Following circadian misalignment, energy regulation is altered across sex, with men exhibiting more cravings for energy dense and savory foods, and women exhibiting changes in their energy homeostasis with alterations in hormones that gate hunger and satiety (Qian et al., 2019). Breast cancer risks are increased in women following circadian misalignment due to interactions between clock genes (Clock, Per2, Cry2) and the estrogen receptor (Gery et al., 2007; Liu et al., 2017; Mahoney, 2010; Xiang et al., 2008; Yang et al., 2009; Zhu et al., 2011). Women are at greater risk of seasonal affective disorder then men (Lyall et al., 2018) and mood disorders in general (Mong et al., 2011), both of which are influenced by circadian function (Logan & McClung, 2019). Women's fecundity can even be lowered by the circadian system as it plays an intrinsic role in gating the luteninzing hormone surge (Beymer et al., 2016; Joye & Evans, 2021; Kriegsfeld & Silver, 2006; Mackinnon & Bulmer, 1974; Mahoney, 2010). Understanding sex differences in the circadian system, then is crucial for better understanding of human health.

Anatomical and Physiological Differences: Basic features of the circadian system vary by sex (Krizo & Mintz, 2015). Sex differences in the morphological features and volume of the SCN are widespread (Bailey & Silver, 2014) and have been reported in rats (Güldner, 1982, 1983, 1984; Robinson et al., 1986), gerbils (Collado et al., 1995), and even humans (Hofman et al., 1996). When adjusted for brain size, the SCN is 14% smaller in men than in women (Hofman et al., 1996; Joye & Evans, 2021), but structural differences in humans are complicated, some features like cell number, density and diameter do not differ by sex, but shape does and this may reflect differences in organization (Joye & Evans, 2021). The amount of VIP expressing neurons in the SCN has also been shown to be sexually dimorphic both in rhythm and expression within the SCN (Bailey & Silver, 2014). AVP neurons in contrast, do not differ in humans (Hofman et al., 1996; Joye & Evans, 2021; Swaab et al., 1985) or rats (Krajnak et al., 1998; Mahoney et al., 2009). Innervation by AVP and VIP regions onto other brain regions controlling reproduction are sexually dimorphic (Horvath et al., 1998; Rood et al., 2013). Anatomical differences reflect physiological differences. Kuljis and colleague have demonstrated sex-based difference in the electrical activity (Kuljis et al., 2013). A review by Joye and Evans (2021) documents all these differences in far greater detail (Joye & Evans, 2021).

Behavioral Differences: This sexual diphenism extends to behavioral rhythms. Circadian period is generally only slightly different depending on rodent species (Joye & Evans, 2021). In rats and hamsters, females have shorter periods than male counterpart (Davis et al., 1983; Schull et al., 1989). In some studies mice have no difference in period across sex (Blattner & Mahoney, 2012; Iwahana et al., 2008; Kuljis et al., 2013), but in some they do (Feillet et al., 2016). Female mice, hamsters, and rats exhibit higher variability in activity onset than their male counterparts (Kuljis et al., 2013; Morin et al., 1977; Takahashi & Menaker, 1980; Wollnik & Turek, 1988).

Davis and colleagues demonstrated that male hamsters exhibit larger phase delays than females in early subjective night, can entrain to longer T cycles, and have more stable entrainment (Davis et al., 1983). Female golden hamsters have been shown to have a 4 day estrous cycle which modifies their activity onset, an effect known as scalloping (Fitzgerald & Zucker, 1976). This finding has been replicated in rats (Wollnik & Turek, 1988), but in mice it is less clear. Some groups have reported that C57Bl6 mice do not appear to exhibit scalloping though (Kuljis et al., 2013) others, however, report scalloping in wheel running activity (Nakamura et al., 2016). Differences may be due to strain, diet or housing condition (Joye & Evans, 2021). Total activity levels are higher in female hamsters rats, mice, and gerbils than males (Blattner & Mahoney, 2012; Brockman et al., 2011; Duffy et al., 1999; Iwahana et al., 2008; Roper, 1976; Stowie & Glass, 2015). Both mice and hamsters exhibit sex differences in the phase angle of entrainment, though it can depend on age (Davis et al., 1983; Stowie & Glass, 2015). When the circadian system is perturbed, male and female rodents responded differently (Joye & Evans, 2021).Upon delivery of a light pulse in the delay region of the PRC, female hamsters exhibit smaller phase delays than males (Davis et al., 1983). Whereas female mice have larger phase delays than males (Blattner & Mahoney, 2012; Brockman et al., 2011). See Joye and Evans (2021) for further discussion.

Taken together these results suggest the circadian system is intrinsically sexually differentiated.

Hormones: The above differences in almost all case can be influenced by the effects of hormones (Joye & Evans, 2021). Diphenism in circadian period between the sexes for example can be changed by the altering of gonadal hormones, causing differences to emerge where previously there were none (Iwahana et al., 2008). In general hormones can have effects on two

different levels. The first is organizational. Here the hormone is involved in setting up the system: altering gene expression, morphology, etc. Once this developmental organizational period has passed, the system is generally permanently altered no matter what hormone is later administered. Hormones can also play an activational role. In comparison to organizational effects, activational effects require the continuous presence of the circulating hormone. Both levels of hormonal control can influence the circadian system (Joye & Evans, 2021; Yan & Silver, 2016).

Activational Hormone Effects on Circadian Rhythms: Much of the investigation into sex differences in the circadian system has focused on the role of activational hormone effects, that is effects driven by the presence and absence of the circulating hormones, but results have varied with sex. Daan and colleagues showed that castration of mice lengthens their free running period and changes the distribution of activity over their active periods, by decreasing activity at the start of their active period and increasing activity at the end of their activity period, These changes are rescued with testosterone replacement, (Daan et al., 1975). This result has been replicated in male mice (Iwahana et al., 2008). Morin and fellows showed estradiol shortens circadian period in blinded, and ovariectomized hamsters, demonstrating a similar activational effect (Morin et al., 1977). In contrast to males, this result is not replicated in female mice (Iwahana et al., 2008). Moreover, in mice, androgen receptor expression in the SCN is sexually dimorphic with the SCN core exhibiting much higher androgen receptor in male mice than their female conspecifics. Castration of male mice reduces this expression to intact female levels and hormone replacement caused intact male level of AR expression in both gonadectomized male and female mice demonstrating this difference is under activational control of testosterone

(Iwahana et al., 2008). The activational effects of hormones on the circadian system thus exist, but vary by species.

Organization Effects of Hormones on Circadian Rhythms: Organizational effects of hormones, effects in driven by having hormones at a specific time of development, have also been reported the mammalian circadian timing system. The ability of golden meadow hamsters to exhibit changes to circadian period with estrogen is organizational. Intact male hamsters and male hamsters castrated in adulthood do not respond to estradiol whereas estradiol shorten circadian period in intact females. When males are gonadectomized within 24 hours of birth they respond to estradiol like intact females(Zucker et al., 1980). In mice, male and female conspecific exhibit differential estrogen receptor expression in the SCN shell, but surgical removal of the gonads does not abolish this difference. Suggesting this is a sex difference is under organizational control (Vida et al., 2008). Moreover, estrogen replacement differentially affects the levels of the type subtype of Estrogen receptor (ER). ER-alpha levels are unaffected, but ER-beta levels are reduced five-fold in female mice and two-fold in males (Vida et al., 2008; Yan & Silver, 2016) demonstrating a difference between activational and organizational effects between the two hormones receptors (ER). Hormones, then play an organizational role in circadian rhythms as well.

Connection between Clock genes and Sex Hormones: It is still unclear if sex differences systematically exist in the expression and function of clock genes. *Per2* has been shown to regulate the expression estrogen receptor α, suggesting it might serve as the interface between the Circadian TTFL and sex hormones (Gery et al., 2007). Estrogen receptor β expression likewise is regulated by *Per1* and CLOCK:BMAL (Cai et al., 2008). Moreover, two studies in rats have shown a role of estradiol in the expression of four genes important for circadian

function, but this role appears to be tissue specific. Following estradiol treatment mCry1 but not mCry2 was increased in the cerebral cortex but not the SCN. Meanwhile mCry2 levels decreased in the SCN but not the cortex (Nakamura et al., 2001). There was no effect of estradiol treatment on two other orthologs mPer1 and mPer2, in the cerebral cortex or SCN. In peripheral tissue, estrodial treatment increased the expression of mPer1 in the liver and kidneys, but not the uterus. There was no effect of estradiol treatment on mPer2 expression in the liver, kidney, or uterus (Nakamura et al., 2005). Though later work on isolated uterus form Per2::LUC mice did show alterations of Per2 rhythms with estradiol treatment (Nakamura et al., 2008). These results do not appear to be followed upon or replicated in other species, however. Karatsoreos and colleagues also have shown that gonadectomy and androgen replacement alter the induction mPer1 and mPer2 by light pulse in the SCN of male mice, but the timing of this light pulse matters (Karatsoreos et al., 2011). At circadian time 13.5 there was no effect of castration or replacement by nonaromatizable androgen dihydrotestosterone (DHT) on mPer1 expression in the SCN post light pulse. At the same time point however, mPer2 expression was significantly lowered in the SCN by castration, and this lowering was rescued by DHT. By contrast at circadian time 21, castration significantly increased mPer1 expression in the SCN following a light pulse, and DHT replacement restored expression to intact levels. The expression of mPer2 in the SCN at this timepoint was unaffected by castration or DHT replacement (Karatsoreos et al., 2011) In summary, little is known about how clock genes and sex hormones interface, but period 2 may place a special role.

Models of Circadian Disruption and Analysis of Circadian Rhythms:

The communication and analysis of data in chronobiology has some idiosyncrasies which warrant special attention. The actogram, a raster plot of activity counts introduced by Johnson in

1926 allows a clear presentation of chronobiological organization over the hours in a day (the abscissa) and longitudinally over many days (the ordinate), but has limitations. With this tool visual identification of entrainment, free running— the organization of the endogenous clock unentertained, phase shifts, changes in activity duration (α), and the descent into arrhythmia are easily identifiable. A standard workflow for the evaluation of circadian rhythms is to first depict the behavior of interest on an actogram. The actogram, however, is idiographic. From actograms alone, group level analysis can be difficult, requiring subjective qualitative assessment. Moreover, features of the waveform: phase, period, and power are not easily quantifiable. Thus the actogram, while useful, is limited.

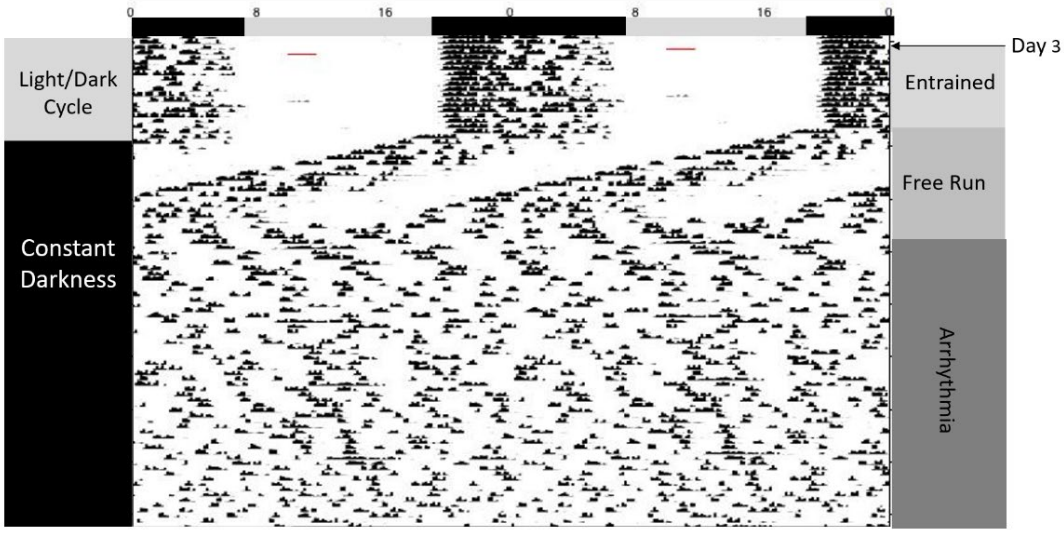

Figure 4: Representative Actogram

A double plotted actogram demonstrating three states of rhythmicity: entrainment, free-run, and arrhythmia across both a light-dark cycle and constant conditions. The x-axis depicts a duplication of 24 hours and the y-axis separate days. Tick marks correspond with running wheel turns and their amplitude represents number of wheel turns a minute. The period of light and dark, grey and black respectively are labeled across the top with their corresponding hour and lighting conditions and rhythm state are labeled to either side.

Fourier Based Quantification: Quantifiable features of the waveform need to be abstracted and this is the common next analysis step after production of actograms. The common statistical tool the ANOVA or parametric variation of it are not suitable for the detection rhythmicity (Refinetti et al., 2007). Fourier based techniques are often applied, based on the insight by Fourier that any time series can be decomposed into summations of different sin waves. Elaboration on this insight allowed later scientists to create periodograms depicting the relative spectral energy contribution of each sin wave composing the time series and statistical significance tests for them (Refinetti et al., 2007). Still this techniques is not without its issue (Refinetti et al., 2007). It is generally out performed by the Enfield/χ^2 periodogram in the analysis of rhythmicity (Refinetti et al., 2007), which is in turn is very slightly out performed by the Lomb-Scarge periodogram, which is better suited for data drop out (Ruf, 1999). Both techniques are vulnerable to artifacts, detecting harmonics that don't actual exist in the data (Refinetti et al., 2007). Lomb-Scargle periodograms additionally can underestimate the strength of the circadian component and have small spurious and erroneous peaks and offset of activity. Onsets and offsets of activity are still often called by hand and phase shifts quantified from projected onsets (Refinetti et al., 2007), but new techniques are emerging to change this approach, though they have yet to be widely accepted (Leise, 2013; Leise & Harrington, 2011). Regardless, a number of distinct procedures, all based on Fourier based methods are the standard to address the quantification limitation of the actogram.

Strategies of Clock Disruption: In the pursuit of understanding the circadian clock, the chronobiology field has made a general strategy of perturbing the clock through various means and asking either: how the remaining timing systems does or does not compensate for it; and how downstream systems like metabolism or immune response are affected. The 3 most common

clock disruption strategies are: (1) using simulated jet lag or phase shifts to temporarily perturb the clock and in special cases break it by driving it toward a phase singularity (Winfree, 2001), (2) chemical/electrolytic lesioning of pacemaker tissue (Stephan & Zucker, 1972), or (3) use of genomic tools to inhibit or overexpress molecular components of the circadian clock (Cox & Takahashi, 2019).

Strategy 1: Simulated Jet Lag and Disruptive Phase shifts. A high amplitude advance or delay can temporarily disrupt CRs. The circadian clock is limited in how rapidly it can shift both in humans and rodents, an experience relevant to many travelers known as jet lag (Gibson et al., 2010). In this simulated jet lag strategy phase advances are frequently used because they are more difficult for the system to adjust to than phase delays (Davidson et al., 2009; Reddy et al., 2002; Yamaguchi et al., 2013). This advance leaves the system out of synchrony. It takes about 8 days for a murine SCN to reentrain to its external environment after simulated jet lag (a 6h phase advance) (Davidson et al., 2009) and peripheral tissues resynchronize with the SCN at different rates. Interestingly disruption of AVP through knockout of its receptors is protective against jet lag (Yamaguchi et al., 2013) and the clock gene *cry1* seems to play a role in the inertia of reentrainment (Reddy et al., 2002). Regardless this strategy has shown that chronic jet lag is associated with a host of negative health outcomes (Davidson et al., 2009).

Abrupt phase advances can also cause enduring disturbances to CRs. While phase shifts are often caused by a brief exposure to light, when the circadian system is not expecting it, a long enough exposure to constant light will lead to arrhythmia (Daan & Pittendrigh, 1976). Moreover, Arthur Winfree first showed it was possible to drive drosophila ecclosion rhythms to a phase singularity by providing conflicting phase shifts at the right intervals (Winfree, 2001) and work by others have shown that the same process is possible in Siberian hamsters (Ruby et al. 2004).

Functionally this manifests as circadian arrhythmia with suppressed clock gene transcription rhythms (Grone et al., 2011) and is an arrhythmia that functionally distinct from that of a SCN lesion (Fernandez et al., 2014). This disruptive phase shift model has been used to great effect in studying the role of competent circadian rhythms in seasonality, immune function, and ultradian rhythms, among others (Prendergast, Beery, et al., 2012; Prendergast et al., 2015; Prendergast, Cisse, et al., 2012), but thus far has been limited to hamsters.

Strategy 2: Lesion Studies. Lesion studies have played a major role in working out the location of the circadian clock. Richter classically showed that other endocrine tissues are not the superordinate clock through careful lesion studies (Richter, 1965). Later work showed that bilateral electric lesions of the SCN resulted in a complete loss of endocrine, behavioral, physiological rhythms (Moore & Eichler, 1972; Stephan & Zucker, 1972) implicating the SCN as the superordinate pacemaker. Further experiments cemented this observation by showing: the persistence of rhythms within the SCN, but not outside it, when it was electrically isolated but not destroyed (Inouye & Kawamura, 1979); the restoration of behavioral rhythmicity in lesioned hamsters following transplant of circadian competent fetal SCN tissue with the period of the transplanted tissue graft rather than the shorted period of the lesioned hamster's mutated genomic background (Ralph et al., 1990); and that even in *cry1*$^{-/-}$/*cry2*$^{-/-}$ mice with no peripheral ability to generate endogenous rhythms via the circadian TTFL, transplant of WT fetal SCN restored rhythmicity (Sujino et al., 2003). Early reports suggested that post SCN lesion circadian gene expression damped after 2-7 cycle, independent of whether the measurement was taken *in vivo* or through *ex vivo* culturing of peripheral tissue (Akhtar et al., 2002; Hara et al., 2001; Sakamoto et al., 1998; Terazono et al., 2003; Yamazaki et al., 2000), but later results challenged these findings both *ex vivo* (Yoo et al., 2004) or *in vivo* (Tahara et al., 2012). Some of the

difference between these and prior studies may come from the reporter system used, whereas as both (Yoo et al., 2004) and (Tahara et al., 2012) used luciferase reporters on the *per2* gene, previous work used the *per1* gene (Yamazaki et al., 2000), which unlike *per2* only show sustained rhythmic oscillations in the SCN not the periphery (Yamazaki et al., 2000; Yoo et al., 2004). Nevertheless, using mice with a knockin of a lucerifase reporter attached to the *per2* gene, Yoo and colleagues (2004) demonstrated circadian rhythmicity for greater than 20 cycles in culture peripheral organs from SCN lesioned mice, albeit dampened. Tahara et al. 2012 extended this finding to *in vivo* mice, demonstrating the persistence of *per2* lucerifase rhythms in the liver, kidney, submandibular glands of ~50% of behaviorally arrhythmic SCN lesioned animals. Why only half the animals showed peripheral rhythmicity is unclear, but it may indicate that the thresholds for maintenance of clock gene rhythms in periphery and behavioral/endocrine outputs differ.

Interestingly it also appears that an absent SCN is less deleterious to system functioning than a malfunctioning one. SCN lesioned hamster do not have the same deficits in spatial and recognition memory as a SCN made malfunctional (Fernandez et al., 2014). Hence while they have limitations, lesion studies are a potent way of perturbing the circadian clock to study its function.

Strategy 3: Genomic Manipulation of TTFL genes. Lastly, each of the major clock genes has been knocked out and the resultant effect on circadian period, phase, and power quantified in both a 12:12 light-dark cycle, and constant condition as well as various combinations of genes to understand the various roles that each clock gene and its orthologs plays in the maintenance of biological time. The effect of genomic ablation of each of the six core clock genes (*bmal*, *clock*,

cry1, *cry2, per1*, and *per2*) on behavioral circadian rhythmicity in constant darkness has been investigated (Ripperger et al., 2011).

Bmal1$^{-/-}$, and functionally *Bmal2*$^{-/-}$ mice (Shi et al., 2010), of unreported sex go arrhythmic immediately (Bunger et al., 2000). *Clock* $^{-/-}$ mice of both sexes exhibit .5 hour shorter circadian locomotor rhythms, but do not go arrhythmic (DeBruyne et al., 2006). *Cry1*$^{-/-}$ and *Cry2*$^{-/-}$ mice demonstrate 1 hour shorter and 1 hour longer endogenous periods respectively, but no loss of circadian rhythmicity in constant conditions when knocked out separately, at least for the up to 3-week analysis window (Van Der Horst et al., 1999; Vitaterna et al., 1999). *Per1* mice either male or of unreported sex exhibited 0.5-1 hour shorter circadian periods, but remained rhythmic (Bae et al., 2001; Cermakian et al., 2001; Zheng et al., 2001). Finally, *per2* mice persist in their rhythmicity for at least a couple cycles before going arrhythmic (Bae et al., 2001; Zheng et al., 1999). With the exception of *per2* and *bmal,* though only because *bmal* also regulates its ortholog (Shi et al., 2010), both orthologs of a clock gene have to be knocked out to in order to ablate the clock (Cox & Takahashi, 2019). These genomic ablations have revealed the indispensable roles of *bmal* and *per2* to clock function, they are the only core clock genes whose ablation leads to arrhythmia. It is only through double knockout that other clock gene mutant animals exhibit circadian arrhythmia (Ripperger et al., 2011). Thus, *per2* and *bmal1* are uniquely indispensable among other clock genes.

This genomic ablation strategy has not been without its limitation. The standard workflow has been to investigate the effect of these knockouts in constant darkness for ~ 3-4 weeks (Izumo et al., 2014; Siepka & Takahashi, 2005; Siepka et al., 2007). Yet redundancy dynamics of clock genes are not fully understood. Van der hoost and colleagues showed that mice with *cry1* knocked out, but one copy of *cry2* exhibited a delayed onset of arrhythmicity, whereas mice with

cry2 knocked out but one copy of *cry1* maintained endogenous circadian rhythms (Van Der Horst et al., 1999). And Oster and fellows showed that loss of rhythmicity in *per2* mutant mice could be rescued with knockout of *cry2*, but not *cry1* (Oster et al., 2002). Moreover, the contribution of sex is unknown. Of the foundational studies investigating the phenotype of clock gene knockouts in constant darkness, only (DeBruyne et al., 2006), but did not specifically discuss if any role of sex was investigated. Using the search terms "sex" and "clock gene" and "mice or mouse" in Pubmed yields only 29 results. Other than the publication that forms chapter 3, only in one case, is a specific sex difference in the basic circadian functioning reported. On a completely different, background, *clock* mutant mice exhibit a sex difference in the circadian period of their body temperature rhythms, that is undiminished by gonadectomy (Ochi et al., 2003). Other reports document sex differences in the influence on clock genes in noncircadian traits (Easton et al., 2003), circadian locomotor activity in field conditions (Daan et al., 2011) or extra-SCN temporal organization (Li et al., 2015). Therefore, the standard genomic ablation is limited in its ability to address longer term stability of the clock and potential sex-based differences in clock function.

Included among any consideration of the genomic mechanism mediating circadian rhythms should be a consideration of the epigenomic mechanisms. Indeed, in addition to clock genes, epigenomic processes also participate in circadian clock function. investigation of chromatin remodeling has shed light on how the basic circadian TTFL interfaces with the genome over the course of the day (Koike et al., 2012).In addition, particular attention has been paid to epigenomic modification as it relates to circadian control of metabolism and interaction with cancer, but less focus has been paid to basic clock function (Sahar & Sassone-Corsi, 2013). Of particular prominence, in what is known about the way epigenomics affects circadian clock

function, are the methyltrransferase MLL1, the deacetlyase SIRT1, and CLOCK in its role as a histone acetyltransferase. MLL1 has been shown to be circadian in its expression and its knockout in mouse embryonic fibroblasts has been shown to drastically diminish the circadian patterning and relative abundance of mDBP, and mPer2 (Katada & Sassone-Corsi, 2010). *Sirt1* KO in mouse embryonic fiberblasts and NIH 3T# cells abolishes BMAL Luciferase reporter activity and alters the mRNA expression of several clock genes (Asher et al., 2008). CLOCK as a histone acetyltransferase, acetylates its binding partner BMAL1 allowing the binding of CRY1 to help mediated transcriptional repression and contributes to further control by influencing its sumolyation (Cardone et al., 2005; Hirayama et al., 2007). Importantly arrhythmic *bmal* KO mouse embryonic fibroblasts can only be rescued with *bmal* transfection if that *bmal* has the capacity to be acetylated by clock, mutant *bmal* that lacked these acetylation site failed to rescue rhythmicity when transfected (Hirayama et al., 2007). Recent work on DNA methylation also holds some promise to understanding clock function and seems to play a dynamic role in setting circadian period in the SCN (Azzi et al., 2014; Azzi et al., 2017).

In addition to DNA, RNA is also subject to epigenetic modification and several lines of evidence indicate that RNA epigenetics also participate in clock function. The inhabitation of RNA methylation via 3-deazaadenosine (DAA) has been shown to lengthen circadian period in cell culture, ex vivo scn slice, in the locomotor activity of three male mice whose brains were infused with it (J.-M. Fustin et al., 2013), the mechanism of this lengthen seems to be through m6A's regulation of isoforms of Casein Kinase 1 Delta (CK1δ), particularly the CK1δ isoform, CK1δ2 which phosphorylates PER2 in a way which slows its degradation and thereby lengthen circadian period, in contrast with the other isoform CK1δ1 whose phosphorylation of PER2 speeds its degradation, shortening circadian period. While much of the work was performed in

cell culture, the authors showed that male mice (n=6) with a deletion of m6A locus on the *ck1δ* have elongated circadian periods (Fustin et al., 2018) but the role of RNA methylation still need to be further explored. A Pubmed search using the terms “RNA methylation”, “Circadian”, or “Mice or Mouse” yielded only 59 results of which the only relevant papers were the two attributable to Fustin and colleagues (J. M. Fustin et al., 2013; Fustin et al., 2018), a paper on histone methylation (Etchegaray et al., 2006) and a paper on micro RNAs (Aten et al., 2018). Taken together these data suggest that epigenetics mediate circadian function, but the extent is not well understood.

Finally, an important note on the conventions with the field of chronobiology that guide how the roles of clock genes are elaborated. Convenience dictates that full light-dark cycles be used for many studies of circadian biology. But investigations of how the circadian system responds to endogenous or exogenous stimuli requires examination under conditions of continuous darkness. Only under constant darkness can one examine the core features of a pacemaker: its ability to generate self-sustained period, and exhibit phase resetting responses to zeitgeber inputs. Both of these processes are masked under a light dark cycle. And it is only in DD that the circadian system can be observed in the absence of the robust masking effects of light. Light-dark cycles overtly drive rhythms even in the absence of a functional circadian clock. Under a light dark cycle, every single known clock gene mutant mouse exhibits robust circadian rhythms in locomotor activity (Ripperger et al., 2011). But transfer of mice to constant darkness immediately indicates that these behavioral rhythms do not fully explain the phenotype of the gene. For example, during the intervals over which they have been monitored *cry1* mice all free run indicating that cry1 is not essential for the long-term maintenance of circadian rhythms (Van Der Horst et al., 1999). In contrast per2 mice freerun for a variable number of cycles before

decaying into arrhythmia supporting the view that per2 is essential for maintenance of circadian rhythms, and that in its absence of per2 the circadian clock is a rapidly dampening oscillator (Zheng et al., 1999). Finally, bmal1 mice immediately become arrhythmic suggesting that it is indispensable for timing a single cycle of rhythmic activity in constant darkness (Bunger et al., 2000). By unmasking behavior in constant darkness, we gain a more refined understanding of the roles of individual genomic elements.

Summary of Circadian Considerations

The previous sections reviewed the basic features of the circadian system: its organization; neural substrates and molecular underpinnings, and a broad overview of sex differences in circadian organization and function. Several key insights should be taken away. These serve as cross cutting themes of this dissertation and feature as foundational context for chapters 3, 4, 5, and 6. First, sex differences in the circadian system are well established, but the mechanisms that generate them are poorly understood. Second, the *per2* gene plays a special role in maintaining the integrity of the circadian TTFL: in common with *Bmal1*, it is the only TTFL gene that is mandatory for long-term retention of circadian rhythmicity in DD; but unlike *Bmal1* ablation of *per2* does not yield an immediate loss of circadian rhythmicity. Specifically, the *per2* mutant is characterized by a rapidly dampening circadian system. Unlike *Bmal1* mice which possess a nonfunctional circadian system, *per2* mutants exhibits a system which decays into disfunction, which I propose to be useful for investigations of how environmental variables perturb the circadian network. Thus, manipulating *per2* affords an opportunity to understand how environmental and biological variables affect the circadian system. Third, in general there is a

shortage of investigation into how sex impacts the retention of circadian rhythmicity in DD. Chapters 3-4 of this dissertation will describe novel research that focuses on these issues.

Thirdly, epigenetic influences such as acetylation and methylation of the DNA template in core TTFL genes in circadian system have been described, but how epigenetic processes impact circadian transcriptional activity have not been reported. Chapter 6 addresses this question using a mouse model of RNA methylation. Further investigation into all these features then could yield important insights into the mammalian circadian system, and constitute the focus of different chapters in this thesis.

Finally, daily intervals are but one temporal scale over which behavior is structured. A final point of inquiry in this dissertation examines how sex, clock genes, and methylation affect biological oscillations that structures behavior on the scale of hours. A brief perspective follows.

Ultradian Timing System in Mammals:

Rhythmic behavioral structure in the 1-6 hour range —dubbed ultradian that is *ultra* (above/higher frequency than) *dian* (a day)— has been observed in scores of physiological and behavioral measures: sleep, locomotion, body temperature, gene expression and the endocrine system, (among others), but is poorly understood (Prendergast & Zucker, 2016). Common voles serve as one of the best behavioral models of the system, exhibiting robust ultradian rhythms (URs) in their feeding behavior. These rhythms are not derived from the circadian system or an 'hourglass' interval timer, that is reset by environmental cues. They persist in the absence of a functional clock or feedback from food, water, or sleep to drive the system (Gerkema & van der Leest, 1991). Suggesting they are generated by an endogenous oscillator and yet these rhythms are not synchronized to any known geoperiodicites (Prendergast & Zucker, 2016). Indeed work in other rodents have replicated that these URs persists despite ablation of the circadian system

with clock gene knockout, or chemical lesion and appear more prominently in FFT and LSP periodograms (Prendergast & Zucker, 2016). Nor is it just a coincidental pattern, a long standing finding is that in rhesus macques with hypothalamic lesions that prevent normal gonadotrophin release, gonadotrophin releasing hormone when administered in a 1 hr physiological ultradian pulsatile pattern, but not a continuous one, can restore sustained gonadatrophin release (Belchetz et al., 1978). Work by Smarr and colleagues has linked changes in this structure to having predictive power in pregnancy and Huntington's disease (Smarr et al. 2016; Smarr et al. 2017; Smarr et al. 2019) (Smarr et al., 2019; Smarr et al., 2016). Many studies have also reported observed differences in this UR structure based on sex and photoperiod in multiple species (Prendergast, Beery, et al., 2012; Prendergast, Cisse, et al., 2012; B. J. Prendergast & Irving Zucker, 2012; Scannapieco et al., 2009; Wollnik & Turek, 1988). Taken together, the available data suggest that ultradian oscillators exist and are of significance.

The Substrates of Ultradian Rhythms: The neural and molecular underpinings of ultradian organization, though, is currently undetermined. The leading hypothesis is that a circadian independent oscillator or oscillators is driving this system similar to how the circadian system works (Prendergast & Zucker, 2016). Grant and colleagues have proposed a coupled hormone oscillator which organizes hormone pulsatility across different tissues and generates ultradian body temperature rhythms (Grant et al., 2018). Developmental biologists have demonstrated that gene driven ultradian rhythmicity exists (Isomura & Kageyama, 2014). Meanwhile, Blum and colleagues have shown what once was consider a methamphetamine dependent and SCN independent circadian oscillator can be tuned to ultradian frequencies with dopamine. Knockout of the dopamine transporter *Slc6a3* alters UR period length in DD. Methamphetamine (a dopamine agonist) can alter the URs of *bmal* knockout mice. Importantly striatal dopamine

fluctuates in concert with the URs in these mice (Blum et al., 2014). These findings in conjunction with lesion studies of the dopaminergic, striatal circuitry, particularly the arcuate nucleus has led to the proposal that dopamine driven ultradian pacemaker is located somewhere in the circuitry of the nucleus acumbens, ventral tegemental area, and arcuate nucleus. This is supported by both laboratory and clinical findings of opioids also altering URs (this circuitry also contains plentiful opioid receptors) (Prendergast & Zucker, 2016). As well as evidence that shows orexin knockout mice have altered locomotor and body temperature URs but have not lost the capacity for ultradian patterning (Miyata et al., 2016) because the arcuate nucleus is one of the major target of orexinergic neurons (Burdakov et al., 2003). It is unclear, though, if URs generated by a dopamine based oscillator are the same as those seen in the pulsatile expression of hormones and speculated to work as coupled oscillators (Bourguignon & Storch, 2017). There is some potential evidence of linkage. Gonadotrophic releasing hormone (GnRH) which is released in a pulsatile fashion from GnRH neuron terminals at the portal vessels of the median eminence, an area at the ventral surface of the arcuate nucleus (Bourguignon & Storch, 2017). The lutenizing hormone surges driven by this pulsatilty however, are highly sexually dimorphic, leading some to suggest that a lack of sex differences reported in the UR of murine locomotor activity precludes this connection (Bourguignon & Storch, 2017). Sex differences in the URs of locomotor activity of hamsters and rats have already been demonstrated (Prendergast, Cisse, et al., 2012; Wollnik & Dohler, 1986; Wollnik & Turek, 1988). They may very well exist in mice as well. Given the systematic neglect of female mice in neuroscience (Prendergast et al., 2014), this is far from concrete evidence. Regardless while the substrates of ultradian organization have not been proven, good neural and mechanism candidates exist.

Difficulties with Evaluating Ultradian Oscillator Candidates: Resolving the neural basis of URs is far from simple however, because comparatively little is still known about their properties. The neglect of UR research compared to CRs is severe (Prendergast & Zucker, 2016). Indeed it has become common parlance amongst researchers to refer to this ultradian behavioral organization as the output of a clock but even this designation remains controversial. In fact, some have questioned whether a periodic oscillator generates URs, instead suggesting ultradian structure may emerge from stochastic events of an aperiodic oscillator that merely has a high probability of varying on an ultradian period (Goh et al., 2019). This is inconsistent with existing evidence (Blum et al., 2014; Grant et al., 2018), but because of the state of uncertainty around URs, is not as of yet completely refutable.

Quantification Problems: URs have proven more difficult to quantify than their circadian counterparts. In order to go from behavioral observation to testable hypotheses in chronobiology, it is necessary to dissect time series down to their essential components: phase, period, and spectral power. These units of measure are essential to be able to tell if a treatment group has had an effect or even if oscillator driven rhythmicity is occurring. In the past, the circadian field has relied on Fourier based method i.e. fitting or breaking down time series to/into sine waves. Most ultradian quantification to date have also been performed using these methodologies (Blum et al., 2014; Dowse et al., 2010; Prendergast, Cisse, et al., 2012). Leise and colleagues, however, have argued that these methods fail to capture true ultradian rhythms, even in synthetic (i.e., computer-generated) data, where the UR features are known and the noise is low. Taken together, theoretical and empirical lines of inquiry suggest that Fourier based methods are not well-suited for the quantification of these rhythms for two major reasons: 1. the apparent high degree of nonstationarity of URs, their frequency content is not constant over time, which is an

important assumption of the Fourier-based methods in use. And 2. the need for a high degree of time-frequency resolution. Most URs of interest fall in the 1-6 hour range, overlapping with many of the circadian harmonics at 6 hrs, 4 hrs, 3 hrs, 2 hrs, 1 hrs, etc (Leise, 2013; Leise & Harrington, 2011).

Wavelet Analysis: Leise and colleagues, instead, have advocated the use of the continuous wavelet transform (CWT) using an analytic wavelet, which properly identifies URs of their synthetic time series, is known for its ability to resolve nonstationarity, and has generated reasonable quantifications of individual records from real animals. While initially daunting, wavelet analysis is not so different from the commonly used Fourier transform, or the intermediate Gabor transform. Instead of using a sine waves, wavelet analysis use a waveform that only oscillates for a short interval such -1 to 1 and is otherwise zero hence the wavelet. The idea is to slide the wavelet across the time series cross-correlating as it is slid, because over short intervals the time series should be more stationary and then, because there may be signals of different scales in the time series, resize the wavelet in a systematic way and do the process all over again (Leise, 2013; Leise & Harrington, 2011). The result of the CWT is a large data matrix of cross correlation/fit value at each time point at each scale this is known as a scalograms which can be graphed as the approximate equivalent of a spectrogram i.e. approximate period vs time. These spectrograms are a lot like actograms under widespread use in the chronobiology field: they provide a lot of information about individual animals, but are idiographic, and need to be further distilled in order to provide information about anything more than one individual animal. Up to this point, this has been a major limitation of the CWT approach: the output has been limited to individual case analyses, and thus has been most useful at a descriptive level. Efforts are underway. Guzman and fellows has shown how fractals may be used to enhance the wavelet

analysis of URs in Japanese quails (Guzman et al., 2017). Work by Smarr and colleagues has applied techniques called wavelet coherence to look at pairwise phase comparisons to great effect, and software does exist to apply the wavelet method to chronobiology see WAVECLOCK, WAVOS, and more recently through Actimetrics's popular ClockLab (Grant et al., 2018; Harang et al., 2012; Price et al., 2008; Smarr et al., 2019; Smarr et al., 2017; Smarr et al., 2016), but these methods use the Morlet wavelet which due to negative frequency leakage is not as accurate at approximating the instantaneous frequency of the underlying time series as the strictly analytic Morse wavelet and are still optimized for studying a single animal (Leise, 2013; Leise & Harrington, 2011) (Blessing & Ootsuka, 2016; Goh et al., 2019; Grant et al., 2018; Smarr et al., 2019; Smarr et al., 2017; Smarr et al., 2016; Wu et al., 2018). For group level analysis of ultradian rhythms the tools do not yet exist for their quantification.

Summary of Ultradian Considerations:

URs are an ubiquitous but understudied aspect of chronobiology. Our ignorance about their role in biology and behavior and how they respond to environmental variables can be connected, at least in part, to a lack of appropriate and standardized chronobiological tools for their quantification. Further development of wavelet analytical tools may hold promise for the systematic investigation of URs, which may permit robust experimental designs that allow group-level analyses. A chapter in this thesis (Chapter 4), will focus on addressing this methodological shortcoming.

Chapter 2: Materials and Methods Common to Many Experiments

Photoperiod manipulations and Housing. Animal housing rooms or soundproof light-tight boxes were illuminated with overhead fluorescent lighting (~400 lux at the level of the cage lid). Programmed room timers were used to control photoperiod of each room. When required experiments were performed concurrently across different housing rooms with comparable lighting cycles. Cage location in the room was chosen randomly. At all times mice had ad libitum access to standard rodent diet (Irradiated Teklad Global 18% Rodent Diet 2918, Envigo RMS) and filtered drinking water. In some experiments, animals were transferred to constant darkness (DD). Under these conditions, animal husbandry in DD was facilitated via dim handheld red illumination (<1 lux), otherwise DD mice were exposed to complete darkness. The integrity of experimental LD cycles and DD treatments was continuously monitored and verified by dataloggers (HOBO, UX90, Onset Comp). All procedures related to animal use were approved by the University of Chicago Institutional Animal Care and Use Committee.

Activity monitoring and telemetry. Mice were housed in polypropylene cages equipped with either 7" steel running wheels (RW) or passive infrared motion detectors (PIR), as described in detail in other reports (Kampf-Lassin et al., 2011; Prendergast, Cisse, et al., 2012). Activity was collected using Clocklab Acquisition software (Actimetrics; Evanston, IL, USA). Constant darkness health checks were performed with dim-red, hand held flashlights

Circadian Activity Measures. Activity (PIR and RW) data were visualized and analyzed using Clocklab (Actimetrics). Characterization and quantitative evaluation of circadian chronotypes in mice were performed via methodology described previously for this mutant (Albrecht et al., 2001; Zheng et al., 1999): double-plotted activity records were scored by one experimenter (I.Z.), blind to sex, photoperiod, genotype, and surgical manipulations. Circadian

arrhythmia for the purposes of this analysis manifested as activity occurring randomly around the clock; distinct intervals of activity and rest were no longer evident, and the effect persisted for multiple days. The beginning and end of intervals of free-running activity and arrhythmicity were similarly determined, and were verified via quantification of the amplitude of the circadian peak in the Fourier transform (FFT) and Lomb-Scargle Periodogram (LSP) performed on a 10-day epoch of activity either preceding or following the chronotype state change.

Additional quantification of circadian phenotypes included determination of phase angles of entrainment in LD, free running circadian period in DD, and total activity counts, and were performed using Clocklab 6 software. Daily activity onsets in LD were obtained directly from Clocklab's 'onset/offset' feature, with manual corrections performed by an experimenter blind to file identity. Total daily activity counts in LD were derived from Clocklab over a 10 day interval and aggregated in Matlab. Circadian period was calculated using a Lomb-Scargle Periodogram analyses (LSP) on 10 days of DD activity data (Ruf, 1999; Tackenberg & Hughey, 2021). A fast Fourier transform (FFT) power spectrum with a Blackson and Harris window was used to determine rhythmic power in Clocklab 6, also using 10 days of data.

Pre-processing. Post-collection data quality assessment was performed in MatLab: infrequent data dropouts (transcription errors, corrupted data points; encoded as 'NaN') were substituted with values equal to a 10-minute moving average. In instances where this failed, values were substituted with zero. To remove the influence of outlier data points in the time series, any value exceeding 4x the standard deviation of the time series was replaced with a value equal to 4x the standard deviation of the time series.

Parsing. Locomotor activity data from each mouse were first separated into light or dark phase components (diurnal parsing) or inactive and active component (conditional parsing).

Parsing was performed prior to wavelet transformations, Light (inactive) and dark (active) phase activity data were then each individually subjected to the continuous wavelet transform, which produced scalogram matrices for each record.

Wavelet analyses. Wavelet scalograms were generated according to methods previously described (Leise, 2013; Leise & Harrington, 2011) using JLAB software with MATLAB. Briefly, wavelet matrices were calculated using activity data sampled at 1 min, with outliers (values greater than 4 * the Standard Deviation of each time series) replaced with an interpolated moving mean and NaN replaced with zeroes. A generalized Morse wavelet of the strictly analytic airy family ($\gamma = 3$; to avoid negative frequency leakage) was utilized; time-frequency resolution was toggled to a β value of 10. To manage edge effects periodic boundary extension was performed by trimming of 1.5 × the longest period measured (as previously recommended).

Time series data were evaluated using wavelet analyses, which quantify rhythms in multiple period bands (i.e., ultradian and circadian). When applied to time series data, wavelets identify harmonics, remove trends and noise, and compensate for non-stationarity; the latter is especially useful in more accurately resolving UR components. For additional background and a focused discussion of the merits and limitations of wavelet-based time series analyses in the measurement of behavioral rhythmicity, see reviews (Leise, 2013; Leise, 2015, 2017; Leise & Harrington, 2011). We identified a generalized Morse wavelet of $\gamma=3$ and $\beta=10$ to provide optimal time-frequency resolution for our experimental data (i.e., C57BL6/J mice, recorded via passive infrared motion detectors), but results were stable for β'= 6-12. The generalized Morse (Airy wavelet; $\gamma=3$) was chosen over the Morlet wavelet due to its strict analytic nature (Lilly & Olhede, 2012). Analyses were performed using the Jlab Matlab package and with modified versions of code generously provided by T. Leise (Department of Mathematics, Amherst

College). A wavelet sized for 1 to 6.5 h was used to perform an analytic continuous wavelet transform on time series data using jLab package (Matlab). To generate UR measures for each individual animal, treatment group and phase of the light:dark cycle, locomotor activity data obtained from each phase of the long day cycle (i.e., light phase and dark phase) were each passed through the wavelet operation separately for each mouse.

Normalization and signal averaging. Edge effects were managed by using a periodic boundary extension and removing 1.5 × the greatest period estimated (see (Leise, 2013; Leise & Harrington, 2011) for justification and further discussion). Scalograms were collated by treatment as appropriate for each experiment. The magnitude of each matrix was summed and divided by the total number of matrix cells, providing an average power for each activity record; each scalogram matrix was subsequently normalized by dividing by this average total power.

The complex magnitude of each matrix was then summed to a single cell and divided by the total number of matrix cells to compute an average total power from each individual time series record. Because photoperiod was manipulated in Experiment 3, this average was calculated for photoperiod for all groups based on the total number of cells in the 12L:12D photoperiod; this permitted direct comparisons of magnitude across the different photoperiod treatment groups, by compensating for the different numbers of data bins in light and dark phase of different length. Next, to minimize individual differences in locomotor activity levels, the complex magnitude of each scalogram matrix was normalized by dividing by its average total power. Finally, to correct for edge distortion and to avoid biasing, the ends of each time series were extended periodically, and the resultant data were trimmed from either side of the scalogram matrix at 1.5 times the maximum value of the assessed period range (6.5 h), as recommended elsewhere (Leise & Harrington, 2011). The scalogram matrices were averaged within each treatment group to

compute a scalogram that best approximated the true matrix for the group. Ergodicity and stationarity were assumed for each grouping.

Variance estimates and group-wise differences. To facilitate comparisons of UR power distributions among treatment groups, each mouse's normalized scalogram matrix was averaged across the time dimension into a power-period plot, which computes the average continuous wavelet transform power at each scale and its corresponding approximate ultradian period (designated as τ' [tau-prime], to distinguish UR period [i.e., τ'] from CR period [τ]). These power-period plots (e.g., Fig. 1A6were sorted and combined into average plots for each treatment group. To generate measures of variability around the group mean, individual values of power distribution across period were grouped and bootstrapped 2000 times to calculate 95% confidence intervals (using the bootci function in MatLab). Significant differences between groups were inferred to exist at UR periods where 95% CIs did not overlap.

Wavelet ridge extraction. Power (signal) exists at all frequencies, and the continuous wavelet transform analysis described above permitted evaluation of changes in the distribution of this power across all frequencies. We also determined whether experimental manipulations affected the ultradian frequencies at which maximal power occurred by utilizing wavelet ridge analyses to identify these values. In the continuous wavelet transform, the maximum wavelet ridge at each time point approximates the true frequency component, in this case the output of an ultradian clock[s]) in the data, even in the presence of harmonic, e.g., circadian contamination. The wavelet ridge is defined as the maximum cross-correlation between time series and wavelet and approximates the instantaneous frequency (=1/'τ) at every wavelet scale and time coordinate in the magnitude of the wavelet transform (Leise, 2013; Leise, 2015; Leise & Harrington, 2011; Lilly & Olhede, 2010).

A full continuous wavelet transform window is characterized by a fragmented maximum wavelet ridge (e.g., scalogram), indicating the presence of multiple ultradian components in the locomotor activity time series data. A discrete wavelet transform, described below, was used to apply multiple band pass filters and decompose locomotor activity time series data into a sum of wavelets or period bands. The results of the discrete wavelet transform analyses technique guided a re-windowing and reanalysis of the data. Locomotor activity time series for each subject were parsed by circadian phase and again passed through the continuous wavelet transform with the analysis restricted to one of 3 period windows, corresponding to the 3 period bands of the discrete wavelet transform that contributed most to the UR waveform: a short UR period, from .53 h – 1.07 h [designated 'tau-prime' short, or τ'_s]; a medium-duration period from 1.07 h – 2.13 h [τ'_m]; and a longer period from 2.13 h – 4.26 h [τ'_l]. Continuous wavelet transform analyses were computed separately for each period band and then normalized. Maximum wavelet power within each of these bands was used to characterize short, intermediate, and long-duration UR periods for each mouse.

Discrete wavelet transform and data smoothing. To aid in interpreting the fragmented wavelet ridge observed, we adopted a technique recommended in the supplementary methods of (Leise & Harrington, 2011), the modified discrete wavelet transform was employed to decompose the time series to the 10^{th} detail level into coefficients describing period between, $2^j\Delta t \rightarrow 2^{j+1}\Delta t$ where j is the coefficient detail level and Δt is the sampling interval. Edge effects were managed by extending end periodically and clipping 1.5 times the maximum period accessed (2048 minutes) which was clipped from each end. The energy contribution of each band was then quantified. Variance of the total time series can be described by the equation $\sigma^2 = \left(\frac{1}{N}\|V_J\|^2 - \underline{x}^2\right) + \frac{1}{N}\sum_{j=1}^{J}\|W_j\|^2$ where $\left(\frac{1}{N}\|V_J\|^2 - \underline{x}^2\right) + \frac{1}{N}$ describes the variance

attributable to the J level scale coefficient and $\frac{1}{N}\sum_{j=1}^{J}\|W_j\|^2$ is the variance of the wavelet. Neglecting the variance of the scale coefficient, energy was defined (as described by Leise and Harrington 2011) (Leise & Harrington, 2011) as the variance of the wavelet coefficients: $\frac{1}{N}\sum_{j=1}^{J}\|W_j\|^2$ and we expressed it as each individual wavelet coefficient level divided by the total energy i.e. $percent\ total\ energy = \frac{\|W_j\|^2}{\sum_{j=1}^{10}\|W_j\|^2}$. With this calculation, a large degree of noise occurred in very low period bands (d_1-d_4: 2-4 min, 4-8 min, 8-16 min, and 16-32 min), masking the contributions of the ultradian and circadian components of interest. This is likely an artifact of sampling. Data sampling was performed at 1 min intervals. Over a full-length (10 d) timeseries, whereas circadian rhythmicity is clearly visible, this d_1-d_4 modulation does not differ greatly between filled bins in circadian active vs. inactive states, but rather manifests in the density of bins next to each other with counts. This density modulation led to a high degree of variability and thus a high degree of *percent total energy* in details d_1-d_4, obscuring the true ultradian and circadian signal. If this account is correct, then applying a moving average filter of 30 min would be sufficient to eliminate this high-frequency variance signal. Indeed, this was the case. Thus, to improve signal-to-noise ratio in the energy decomposition analysis, a moving average with a window of 30 min was first performed on each time series and then the modified discrete wavelet transform was run. Note that this moving average filter was applied to data only for the process of performing the decomposition evaluation. The continuous wavelet transform and discrete wavelet transform analyses performed to determine UR power and period and were performed on the unfiltered raw time series data.

Genotyping. Genotyping of all mice bred in our vivarium was done using primers from the Jackson Lab Website and using specification for the Platinum Taq Polymerase (Life

Technologies, Invitrogen catalog number: 10966-018). For each individual PCR reaction: 16.65 uL of DNAase free H2O, 2.5 uL of 10X PCR Buffer with no $MgCl_2$, 0.75 uL 50mN $MgCl_2$, 0.5 uL 10mM dNTP mix, 0.5 uL of each primer, and 0.1 uL of Taq were added to a master mix and thoroughly mixed by pipetting up and down. 22 uL of master mix were aliquoted and added to 3 uL of DNA derived via QIAGEN DNeasy Blood and Tissue Kits (Catalog number: 69504 and 69506) or from HotShot (Truett et al., 2000) from tail clips collected at the conclusion of the studies.

Statistics. Mean values of activity onset, onset variance, circadian period and total activity counts were evaluated using ANOVA; the F statistic is robust to violations of sample size inequality or normality (Lindman, 1974). In some instance of heteroscedasticity or clearly nonparametric distribution of the data, use of the ANOVA was replaced with either more specialized ANOVAs (i.e. Brown-Forsythe) or comparable nonparametric tests (Kruskal-Wallis) To control for alpha inflation and Type I error, pairwise comparisons were performed using two-tailed t-tests or Mann-Whitney U-tests where justified by a significant omnibus F or H statistic, except in instances of a priori planned comparisons. Survival analyses were performed by generating Kaplan-Meier survival plots followed by logrank post-hoc tests. All statistical comparisons were performed using Graphpad Prism Software, or StatView software (SAS), except in some cases of non-parametric Fisher's exact tests, which were performed using an online calculator (available at https://www.socscistatistics.com). Differences were considered significant if $P<0.05$.

Chapter 3: Spontaneous Recovery of Circadian Organization in Mice Lacking a Core Component of the Molecular Clockwork

Introduction

Circadian rhythms in vertebrate physiology and behavior are generated by a molecular cascade in which transcription of the 'clock genes' *Period* (*Per*) *1* and *2* and *Cryptochrome* (*Cry*) *1* and *2* are driven by the CLOCK:BMAL1 complex. PER and CRY heterodimerize, translocate to the nucleus, and repress the transcription of *Clock* and *Bmal1,* thus inhibiting their own production. Accessory circadian feedback loops, including *Ror* and *Rev-erb* genes, add stability and redundancy to the circadian genomic network (Mohawk et al., 2012). Together, these clock gene interactions create an autoregulatory transcriptional-translational feedback loop with a circadian period (tau; τ) of ~24 h (Ko & Takahashi, 2006; Mohawk et al., 2012; Panda et al., 2002; Storch et al., 2002).

PER2 is critical for the integrity of the organismal circadian network: mutant mice (*mPer2*^{Brdm1}) with a functional deletion of the mPER2 protein dimerization PAS domain initially exhibit an extremely short free-running circadian period in constant darkness (DD) and become behaviorally circadian arrhythmic (Zheng et al., 1999); mice with a null mutation in the mPER2 gene (*mPer2*^{ldc}) exhibit a similar DD arrhythmia phenotype (Bae et al., 2001). In both *mPer2*^{Brdm1} and *mPer2*^{ldc} mutants, the persistence of circadian rhythmicity in constant conditions varies from a few days to several weeks. In humans, hPer2 single nucleotide polymorphisms are associated with changes in circadian period τ (Chang et al., 2019), and an early chronotype (Jones et al., 2016), and phosphorylation of hPER2 is linked to a short τ and heritable circadian sleep disorders (Toh et al., 2001). Studies of *Per2*$^{m/m}$ animals have assessed the impact of this gene on reproductive and maternal behavior (Pilorz & Steinlechner, 2008) and documented how

gonadal hormones affect Per2 expression (Nakamura et al., 2005; Nakamura et al., 2008). Of particular note: ovarian hormone secretion was disrupted in 9-12 month old *Per2*$^{m/m}$ mice: 4-day estrous cycles occurred significantly less often than in WT mice (Pilorz & Steinlechner, 2008) and estradiol applied to explanted cultures from ovariectomized PER2::LUC knockin mice shortened the period of rhythmic PER2::LUC expression in uterus but not SCN (Nakamura et al., 2008). In general, the importance of circadian rhythms in modulating hormones of the reproductive system has been reviewed by (Kriegsfeld, 2013) and (Bailey & Silver, 2014). However, despite these studies, widespread evidence of sex differences in circadian biology (Yan & Silver, 2016), and a strong female bias in the prevalence of sleep disorders (Krishnan & Collop, 2006), the role of PER2 in the generation of circadian rhythms has not been specifically examined in female mice. We thus examined the role of gonadal sex on the circadian phenotype of *mPer2*-mutant mice in constant conditions. The outcomes revealed an unexpected and striking sex difference in the dependence on PER2 for the maintenance of circadian rhythmicity.

Materials and Methods

Experiments. Experiment 1 consisted of a pilot study to characterize sex differences in the necessity of mPER2 for the maintenance of circadian rhythmicity. Experiment 2a replicated Experiment 1 and included multiple assays of locomotor activity (passive infrared and running wheels); Experiment 2b examined the long-term persistence of circadian arrhythmicity in constant darkness. Experiment 3 examined the contribution of gonadal hormones toward the circadian behavioral phenotype in *mPer2* mutant mice.

Animals. Adult female and male *Per2* mutant mice (*Per2*$^{m/m}$: B6.Cg-*Per2*^{tm1Brd} *Tyr*$^{c\text{-}Brd}$/J, JAX#: 003819) and control mice (WT: C57BL/6J [JAX#: 000664] or B6(Cg)-Tyr$^{c\text{-}2J}$/J [JAX#: 000058], see below) were obtained from Jackson Laboratory (Bar Harbor, ME, USA). Mice of

both sexes were single housed in conventional cages with wirebar lids, and without microisolater filters in a 12L:12D photocycle of approximately 150-200 lux until the housing room was switched to continuous darkness (DD). Each experiment was performed within a single room. Cage location in the room was chosen randomly. At all times mice had *ad libitum* access to standard rodent diet (Irradiated Teklad Global 18% Rodent Diet 2918, Envigo RMS) and filtered drinking water. Animal husbandry in DD was facilitated via dim handheld red illumination (<1 lux), otherwise DD mice were exposed to complete darkness. Cage changing was performed at two-week intervals. All mice were acclimated to running wheel or PIR cages for at least one week prior to data collection. The integrity of experimental LD cycles and DD treatments was continuously monitored and verified by dataloggers (HOBO,UX90, Onset Comp). Estrous cycles of females were not monitored. All experimental procedures complied with the ARRIVE guidelines. All procedures related to animal use were approved by the University of Chicago Institutional Animal Care and Use Committee.

For experiment 1, mice were ordered directly from JAX and upon arrival were placed under PIR sensors and exposed to 12L:12D (LD) for 21 days before subsequent transfer to DD for behavioral data collection (*Per2*$^{m/m}$: B6.Cg-*Per2*^{tm1Brd} *Tyr*$^{c\text{-}Brd}$/J, JAX#: 003819 [albino]; WT: C57BL/6J, JAX#: 000664 [black]); mice in this experiment (*Per2*$^{m/m}$: n=5 females, n=5 males; WT: n=7 females, n=7 males) were 2 months of age when transferred to DD. One male *Per2*$^{m/m}$ mouse died 2 weeks into experiment 2 and was excluded from all analyses. Another mouse Mice in experiment 2 were the offspring of homozygous *Per2*$^{m/m}$ breeding pairs (*Per2*$^{m/m}$: B6.Cg-*Per2*^{tm1Brd} *Tyr*$^{c\text{-}Brd}$/J, JAX#: 003819 [albino]) or WT breeding pairs (B6(Cg)-Tyr$^{c\text{-}2J}$/J, JAX#: 000058 [albino]); mice in this experiment (*Per2*$^{m/m}$: n=20 females, n=19 males; WT: n=20 females, n=17 males) were 2-5 months of age when transferred to DD. Mice in experiment 3

were the offspring of heterozygous breeding pairs, heterozygous-homozygous breeding pairs, and homozygous breeding pairs, all of which were derived within three generations from heterozygous mice (B6.Cg-*Per2*^{tm1Brd} *Tyr*$^{c\text{-}Brd}$/J, JAX#: 003819; heterozygous for the *Per2*$^{m/m}$ and the Tyr$^{C\text{-}Brd}$ mutations) supplied directly from JAX out of cryopreserved stock (8 of 39 *Per2*$^{m/m}$ mice, and 3 of 14 WT mice in experiment 3 exhibited an albino phenotype, the remainder were black). Mice in experiment 3 (*Per2*$^{m/m}$: n=20 females, n=19 males; WT: n=9 females, n=5 males) were 8-12 months of age when transferred to DD and 6-10 months of age when gonadectomized. Offspring were group housed by sex at weaning and singly-housed in adulthood shortly before experiments began. Initial sample sizes were designed to be >10 per group to permit sufficiently-powered non-parametric tests on the incidence circadian arrhythmia.

At the conclusion of the experiments homozygous WT and *Per2*$^{m/m}$ genotypes were confirmed in all mice by PCR using the protocol described for this genotype by JAX (see below). Mice in experiment 1, in which experimental animals were delivered directly from JAX, were not genotyped. Heterozygous mice were not included in any analyses.

Activity monitoring and telemetry. Mice were housed in polypropylene cages equipped with either 7” steel running wheels (RW) or passive infrared motion detectors (PIR), as described in detail in other reports (Kampf-Lassin et al., 2011; Prendergast, Cisse, et al., 2012). Activity was collected using Clocklab Acquisition software (Actimetrics; Evanston, IL, USA).

Circadian Activity Measures. Activity (PIR and RW) data were visualized and analyzed using Clocklab (Actimetrics). Actograms and FFT vector graphics were generated in Clocklab v2.5.3; all quantitative analyses were performed using Clocklab 6. Characterization and quantitative evaluation of circadian chronotypes in mice were performed via methodology described previously for this mutant (Albrecht et al., 2001; Zheng et al., 1999): double-plotted

activity records were scored by one experimenter (I.Z.), blind to sex, genotype and surgical manipulations. Circadian arrhythmia for the purposes of this analysis manifested as activity occurring randomly around the clock; distinct intervals of activity and rest were no longer evident, and the effect persisted for multiple days. The beginning and end of intervals of free-running activity and arrhythmicity were similarly determined, and were verified via quantification of the amplitude of the circadian peak in the Fourier transform (FFT) performed on a 10-day epoch of activity either preceding or following the chronotype state change.

Additional quantification of circadian phenotypes included determination of phase angles of entrainment in LD, free running circadian period in DD, and total activity counts, and were performed using Clocklab 6 software. Daily activity onsets in LD were obtained directly from Clocklab's 'onset/offset' feature, with manual corrections performed by an experimenter blind to file identity. Total daily activity counts in LD were derived from Clocklab over a 10 day interval and aggregated in Matlab 2018b. Circadian period was calculated using a Lomb-Scargle Periodogram analyses (LSP) on 10 days of DD activity data (Ruf, 1999; Tackenberg & Hughey, 2021). A fast Fourier transform (FFT) power spectrum with a Blackson and Harris window was used to determine rhythmic power in Clocklab 6, also using 10 days of data. Among WT and *Per2*$^{m/m}$ mice that did not exhibit circadian arrhythmia, LSP and FFT were computed on data from experimental dates yoked to mean (+/- 1 day) onsets of arrhythmia (ARR) and recovery (FR2) in arrhythmic mice to control for age and duration of exposure to DD. In experiments 2 and 3, initial chronotypes (FR1) were evaluated beginning 10 days after transfer to DD. In a small number of cases, equipment malfunction caused missing data for the proscribed 10 day chronotype evaluation window, and in these instances the chronotype analysis window was delayed by the minimum number of days required to obtain 10 successive days of data. In one

instance, a male's recovery from circadian arrhythmia occurred during an interval of channel malfunction; in this case the date of circadian recovery was assigned to the day on which the data collection resumed.

Wavelet analyses. Wavelet scalograms were generated according to methods previously described (Leise, 2013; Leise & Harrington, 2011) using JLAB software with MATLAB 2018b. Briefly, wavelet matrices were calculated using activity data sampled at 1 min, with outliers (values greater than 4 * the Standard Deviation of each time series) replaced with an interpolated moving mean and NaN replaced with zeroes. A generalized Morse wavelet of the strictly analytic airy family ($\gamma = 3$; to avoid negative frequency leakage) was utilized; time-frequency resolution was toggled to a β value of 10. To manage edge effects periodic boundary extension was performed by trimming of 1.5 × the longest period measured (as previously recommended). For aid of comparison scalograms were normalized across all individuals in all experiments by dividing each by its average total power. Once normalized the average value of every three time points in the wavelet matrix was found. This did not result in any visually detectable difference, but greatly reduced the graphical memory required to generate the scalograms.

Surgical procedures. Mice were randomly assigned to either a gonadectomy or sham-operation control group in experiment 3. Gonadectomy was performed under 3-4% isoflurane/O_2 gas anesthesia. In males, a ventral midline incision was made, testicular blood vessels were ligated and cauterized, and the testes removed. In females, after a dorsal midline incision, ovarian blood vessels were ligated and cauterized, and the ovaries were removed. Incisions were closed with non-reabsorbable vinyl sutures and cutaneous wound clips. Topical antibiotic ointment was applied to the wound site. Analgesic buprenorphine was administered immediately after surgery and every 12 h for the next 48 h. Animals were allowed 2 months to recover prior

to behavioral experiments. Surgical condition was confirmed in all mice at the conclusion of the study via necropsy.

Genotyping. Only homozygous WT or homozygous *Per2*$^{m/m}$ mice were included in these analyses (a priori criterion). Genotyping of all mice bred in our vivarium was done using primers from the Jackson Lab Website [5' → 3': Common Forward (TTC CAC TCT GTG GGT TTT GG), Wild Type Reverse (AAA GGG CCT CTG TGT GAT TG), and Mutant Reverse (GCC AGA GGC CAC TTG TGT AG)] and using specification for the Platinum Taq Polymerase (Life Technologies, Invitrogen catalog number: 10966-018). For each individual PCR reaction: 16.65 uL of DNAase free H2O, 2.5 uL of 10X PCR Buffer with no $MgCl_2$, 0.75 uL 50mN $MgCl_2$, 0.5 uL 10mM dNTP mix, 0.5 uL of each primer, and 0.1 uL of Taq were added to a master mix and thoroughly mixed by pipetting up and down. 22 uL of master mix were aliquoted and added to 3 uL of DNA derived via QIAGEN DNeasy Blood and Tissue Kits (Catalog number: 69504 and 69506) in experiment 2 or from HotShot (Truett et al., 2000) in experiment 3, from tail clips collected at the conclusion of the studies. We used the following PCR Protocol on a thermocycler: (1) 94 C for 2 minutes, (2) 94 C for 20 seconds, (3) 65 C for 15 seconds, with a -0.5 C decrease with each cycle, (4) 68 C for 10 seconds, (5) repeat steps (2-4) 10 times, (6) 94 C for 15 seconds, (7) 60 C for 15 seconds, (8) 72 C for 10 seconds, (9) Repeat (6-8) 38 times, (10) 72 C for 2 minutes, (11) 10 C for 2 minutes, (12) End. 7-8 uL of the resultant PCR products, and a 100 Bp to 2000 Bp Ladder (Thermofisher catalog # 15628050) for reference were mixed with 1.4-1.5 uL of loading dye (Thermo Scientific catalog number: R0611), loaded on a 2% agrarose gel with 2.5uL of Ethidium Bromide (stock solution: 10mg/mL), and visualized. Resultant bands (amplicon sizes) per Jackson Lab Website were as follows: mutant (m/m) = ~200 bp,

heterozygote (m/+) = ~200 bp and 297 bp, and wild type (+/+) = 297 bp. Genotyping identified a total of 5 heterozygous mice (experiment 3: n=5), all of which were excluded from the analyses.

Statistics. Mean values of activity onset, onset variance, circadian period and total activity counts were evaluated using ANOVA; the F statistic is robust to violations of sample size inequality or normality (Lindman, 1974).To control for alpha inflation and Type I error, pairwise comparisons were performed using two-tailed t-tests where justified by a significant omnibus F statistic, except in instances of a priori planned comparisons. Paired, two-tailed t-tests were used to evaluate changes in FFT power within groups over two or more time points. Survival analyses were performed by generating Kaplan-Meier survival plots of the latency to arrhythmia onset in DD of *Per2*$^{m/m}$ mice, followed by logrank post-hoc tests. All statistical comparisons were performed using StatView software (SAS), except in cases of non-parametric Fisher's exact tests, which were performed using an online calculator (available at https://www.socscistatistics.com). Differences were considered significant if $P<0.05$.

Results and Discussion

Experiment 1: Sex differences in the necessity of mPer2 for expression of circadian rhythms.

To examine the circadian role of *mPer2* in female and male mice, activity rhythms of mice homozygous for the *Per2*^{Brdm1} mutation (*Per2*$^{m/m}$ mice; females, n=5; males, n=5) and of wild-type (WT) controls (females, n=7; males, n=7) were monitored using passive infrared detectors (Fig. 1A-D). WT mice became active ~30 min before dark onset, whereas *mPer2* mutants began activity several hours earlier (ANOVA: $F_{1,20}=51.8$, $P<0.0001$; Fig. 1E). In addition, entrainment to the LD cycle was considerably less stable in mutant compared to WT mice ($F_{1,20}=20.9$, $P<0.0005$; Fig. 1F).

Following transfer to DD mutant mice exhibited free-running locomotor activity rhythms with very short circadian periods (τ_{DD}; *Per2*$^{m/m}$: 22.46 ±0.09 h, n=10; WT: 23.83 ±0.04 h, n=14 [mean ±SEM]; ANOVA: $F_{1,20}$=341.2, P<0.0001; Fig. 1G). Moreover, whereas in WT mice τ_{DD} was comparable between males and females (t_{12} = 1.43, P>0.15), among *Per2*$^{m/m}$ mice τ_{DD} was significantly shorter in females (t_8 = 3.11, P<0.02; Fig. 1G).

Prolonged exposure to DD revealed an additional sex difference in the *Per2*$^{m/m}$ chronotype. As expected, the short τ_{DD} expressed by *Per2*$^{m/m}$ mice was followed by a loss of the circadian rhythm of locomotor activity (Fig. 5D). Unexpectedly, however, whereas 4 of 5 female mutants became arrhythmic during the first 6 weeks in DD, all 5 male mutants maintained robust free-running rhythms in constant darkness (Fisher's Exact Test: P<0.05; Fig. 5C). To quantify changes in power of the circadian rhythm, as has been reported previously for this mutant (Zheng et al., 2001; Zheng et al., 1999), a fast Fourier transform (FFT) was performed on activity during weeks 1-2 and weeks 5-6 in DD (Fig. 5H). FFT power remained relatively higher over these intervals in WT mice and *Per2*$^{m/m}$ males, but decreased by nearly an order of magnitude in arrhythmic female mutants (Fig. 5H; t_3 = 5.67, P=0.011), confirming a striking loss of circadian power. Based on visual examination of activity records, the latency to exhibit circadian arrhythmia varied from 14 to 29 days in *Per2*$^{m/m}$ females (e.g., Fig. 5D). Arrhythmic female mice also exhibited a marked increase in FFT power in the ultradian range (Fig. 5D; (Zheng et al., 2001)).

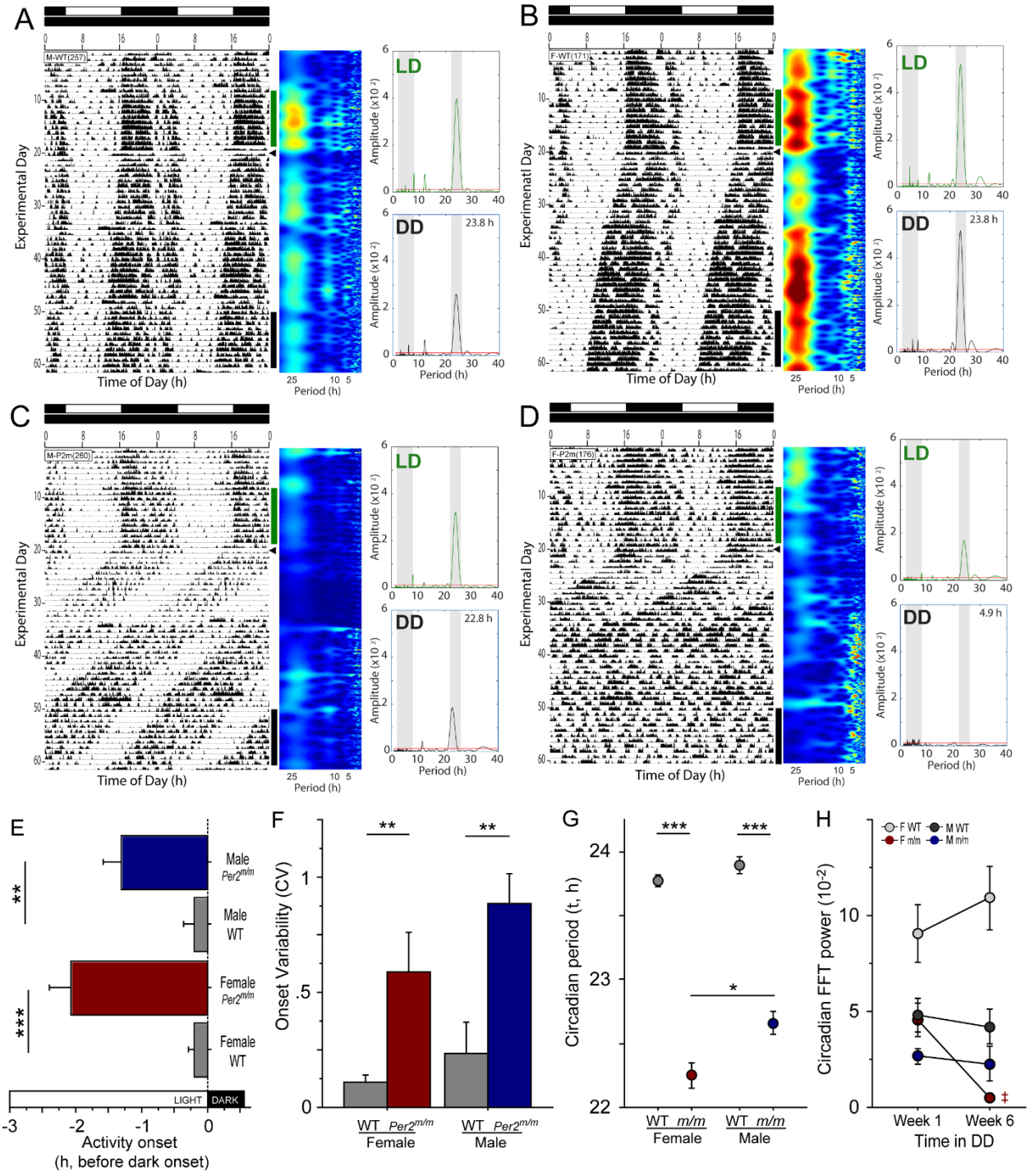

Figure 5: Sex differences in circadian behavior of *Per2*$^{m/m}$ mice

Representative double plotted actograms of (A) WT male, (B) WT female, (C) *Per2*$^{m/m}$ male, and (D) *Per2*$^{m/m}$ female mice housed in a 12L:12D (LD) photocycle (shown at the top of each raster plot) for 3 weeks, then transferred to continuous darkness (DD; arrowhead indicates time of transfer) for 6 weeks. Home cage locomotor activity was monitored continuously using

Figure 5 continued: passive infrared (PIR) motion detectors. Abscissae indicate circadian time, successive days descend from the top, and vertical bars indicate 10-day epochs of LD (green) and DD (black) activity subjected to Lomb-Scargle periodogram (LSP) analyses. To the right of each actogram, scalograms depict rhythmic power across circadian (CR) and ultradian (UR) period ranges (1-28 h), determined by continuous analytic wavelet transform. (E) Phase analysis: phase angle (timing) of activity onset in LD. Red bars indicate female mutant mice, blue male mutant mice, and grey WT animals. (F) Stability analysis: circadian variability (SD of successive activity onsets) in LD. (G) Periodogram analysis: free-running circadian period (τ) during initial exposure to DD as determined by LSP. (H) Fourier analysis: relative power derived from the peak value in the circadian range (22-26 h) of the Fourier transform (FFT). LSP analyses identified comparable decrements in power in *Per2*$^{m/m}$ females (week 1-2: 183.0 ±21, week 5-6: 26.4 ±10 [mean PN value ±SEM]; $P<0.004$, paired t-test). *P<0.05, ***0.001; ‡ P<0.05 vs. week 1-2 value, within group.

Experiment 2a: The role of Per2$^{m/m}$ in circadian function does not depend on the method of measurement

Two aspects of the *Per2*$^{m/m}$ chronotype support the inference that mPER2 is a core component of the mammalian circadian pacemaker: *Per2*$^{m/m}$ mice exhibit a markedly shortened period length, and a loss of circadian rhythmicity in constant conditions (Albrecht et al., 2001; Bae et al., 2001; Zheng et al., 2001). Each of these *Per2*$^{m/m}$ chronotypes was sexually differentiated (cf. Fig. 1G-H). To our knowledge, circadian arrhythmia in mPER2 mutants has only been documented in males (or in mice of unspecified sex; e.g., of the 8 *Per2* studies cited in this report, 5 employed males and 3 did not specify sex), and primarily using cages equipped with running wheels, which provide feedback onto the circadian system (Reebs & Mrosovsky, 1989) but also alter pacemaker period (Edgar et al., 1991) and amplitude (Schroeder et al., 2012). To interrogate whether the persistence of free-running rhythms in DD in male *Per2*$^{m/m}$ mice was a consequence of the absence of running wheels, female and male *Per2*$^{m/m}$ and WT mice were housed with or without wheels and transferred from 12L:12D to DD (Fig. 6A-E). Again, τ_{DD} was shorter in *Per2*$^{m/m}$ than WT mice (genotype: $F_{1,71}=175.5$, P<0.0001; Fig. 6F), and shorter in female than male mutants ($t_{36} = 2.39$, P<0.025; Fig. 6F). Running wheel access did not impact

the development of circadian arrhythmia: 9 of 18 *Per2*$^{m/m}$ mice (50%) housed with wheels and 13 of 21 housed without wheels (62%) became arrhythmic over the first 6 weeks in DD (χ^2=0.56, P>0.4; thus data were pooled across wheel access groups). Sex, however, markedly affected the development of circadian arrhythmicity: consistent with data from experiment 1, 16 of 20 (80%) female mutants exhibited arrhythmia whereas only 5 of 19 (26%) male mutants became arrhythmic during the first 6 weeks in DD (Fisher's exact test: P<0.005). Mice remained in DD for an additional 12 weeks, during which time the remaining 4 *Per2*$^{m/m}$ females, and an additional 7 *Per2*$^{m/m}$ males, became arrhythmic. In total, 12 of 19 (63%) male and 20 of 20 (100%) female mutants exhibited circadian arrhythmia over the course of 18 weeks in DD (Fisher's exact test: P<0.004). Survival analysis indicated a striking sex difference in the emergence of the arrhythmic chronotype (χ^2=15.3, P<0.001, Logrank test; Fig. 6G), with a mean (± SD) latency to arrhythmia of 36.3 ± 19 days in females versus 52.1 ± 24 days in males (t_{30}=2.06, P<0.05). To further characterize rhythmic and arrhythmic chronotypes, activity during the two weeks immediately after the transition from rhythmicity to arrhythmicity was evaluated, again using FFT: in both sexes the loss of behavioral circadian rhythmicity was characterized by a log-scale reduction in FFT power (female *Per2*$^{m/m}$: t_{18}=3.70, P<0.005; male *Per2*$^{m/m}$: t_{11}=4.71, P<0.001; FFT power did not decrease significantly over a yoked interval in female WT mice (t_{19}=1.33, P>0.15) but did decrease among male WTs (t_{16}=2.63; P=0.018; Fig. 6H) and a redistribution of rhythmic power into ultradian frequency bands (Fig. 6A-E); Lomb-Scargle periodogram analyses identified comparable decreases in rhythmic power in *Per2*$^{m/m}$ mice (females: t_{18}=4.21, P<0.001; males: t_{11}=4.71, P<0.001) and no significant decreases in rhythmic power in WT mice (females: t_{19}=1.69, P>0.10; males: t_{16}=2.06, P>0.05). Lastly, the onset of circadian arrhythmia did not bear any obvious relation to identifiable external stimuli: all mice

were housed in the same room for the entire experiment, and DD treatment was initiated on the same calendar date, yet behavioral arrhythmia among 32 mice (20 F, 12 M) began on 22 unique days over an 87-day interval, and the onset of arrhythmicity did not appear to occur at an obvious phase of the circadian cycle.

Despite the widespread use of *Per2* mutants in chronobiology research, this sex difference has not been reported previously. In earlier reports (Zheng et al., 2001; Zheng et al., 1999), 100% of $Per2^{Brdm1}$ mice were reported to exhibit arrhythmicity after 2-18 days in DD. Such rapid and global development of arrhythmia in the $Per2^{Bdrm1}$ mutant, combined with the lack of examination and analysis by sex, likely prevented the recognition of this categorical sex difference in the dependence of circadian rhythmicity in DD on PER2. $Per2^{m/m}$ mice in the present report (bearing the $Per2^{Bdrm1}$ mutation) were first generated on a B6;129S background (Zheng et al., 1999), but then backcrossed for 5-6 generations with C57 mice, and are therefore 97–98% C57BL/6 (Wang et al., 2009) (Additional information at http://www.informatics.jax.org). Genetic background may impact chronotype expression in a trait-specific manner; for example, $Per2^{ldc}$ mutants crossed to a C57BL/6 background exhibited a short τ (~22 h), but not the rapid-onset circadian arrhythmicity typical of the $Per2^{ldc}$ mutation (Bae et al., 2001; Xu et al., 2007); however, behavior in DD was only examined for 14-18 days, which, on a B6 background, may be too short an interval for the arrhythmic chronotype to emerge (cf. Fig. 6G). The present data would be consistent with the conjecture that genomic background delays the onset of arrhythmicity in *Per2* mutants, unmasking a previously-unrecognized categorical sex difference in the dependence on *Per2* for circadian rhythmicity in constant darkness.

The *Per2*$^{m/m}$ mutation interacts with biological sex to generate a sexually-differentiated circadian phenotype. Arrhythmia in *Per2* mutants manifests synchronously in at least 2 circadian traits (spontaneous locomotor activity and wheel running), suggesting that the entire circadian network is arrhythmic. These data underscore the well-established critical role of PER2 in the generation and maintenance of circadian rhythms (Bae et al., 2001; Zheng et al., 2001), but indicate that compensation for the absence of a functional PER2 protein is considerably more robust in males.

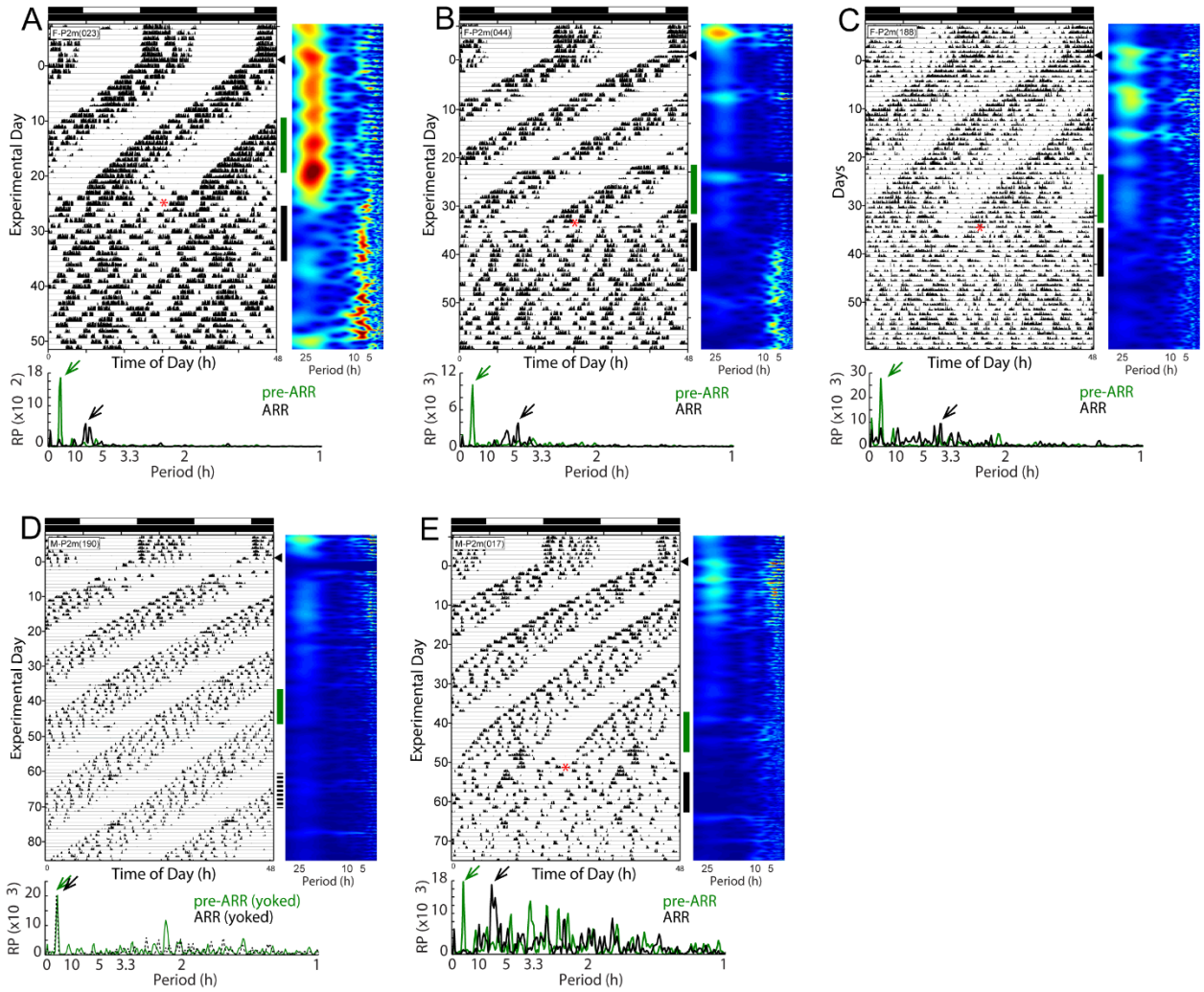

Figure 6: Uniform loss of circadian rhythms in female but not male *Per2*$^{m/m}$ mice

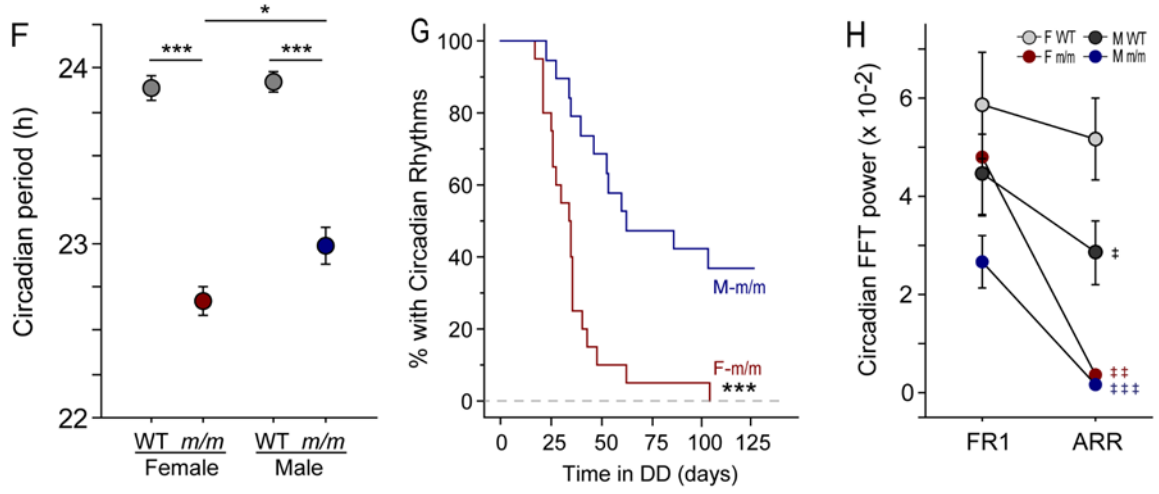

Figure 6 continued: Double-plotted actograms of representative (A-C) female and (D-E) male *Per2*$^{m/m}$ mice housed in LD and transferred to DD (arrowhead, conventions as in Fig. 1). Home cage locomotor activity was monitored continuously using running wheels (RW; A,B,D, E) or PIR motion detectors (C). Vertical green bars alongside activity data indicate 10-day intervals just prior to the onset of circadian arrhythmia (pre-ARR; green) and just after arrhythmia onset (ARR; black) subjected to FFT analyses, which appear beneath each actogram (arrowheads indicate peak FFT value. The mouse in panel D did not exhibit arrhythmicity; instead, activity was analyzed during a yoked interval of FR activity (dashed line). (F) Periodogram analysis: free-running circadian period (τ) among male and female WT and *Per2*$^{m/m}$ mice during initial exposure to DD as determined by Lomb-Scargle periodogram. (G) Survival analysis: Kaplan-Meier survival plot evaluating the emergence of circadian arrhythmia in DD among male and female *Per2*$^{m/m}$ mice (12/19 male and 20/20 female *Per2*$^{m/m}$ mice exhibited arrhythmia in DD). (H) Fourier analysis: relative power in the circadian range (20-26 h) of the FFT prior to (FR1) and after (ARR) the onset of circadian arrhythmia in male and female *Per2*$^{m/m}$ mice, confirming the arrhythmia classification. *P<0.05, ***0.001. ‡P<0.05, ‡ ‡ P<0.01, ‡ ‡ ‡ 0.001 vs. FR1 value.

Experiment 2b: Per2$^{m/m}$ mice spontaneously recover circadian rhythmicity

Surprisingly, *Per2*$^{m/m}$ mice did not remain arrhythmic indefinitely in DD. Instead, the majority of circadian-arrhythmic mutants spontaneously recovered coherent, free-running circadian rhythms in DD when behavioral chronotyping was extended longer than in previous studies (Fig. 7A-D). Females were categorically superior to males in re-establishing behavioral circadian rhythms: 19 of 20 (95%) *Per2*$^{m/m}$ females, but only 4 of 12 (33%) males, recovered

free-running rhythms after a bout of arrhythmicity (Fisher's exact test: $P<0.0005$). Spontaneous recovery of circadian rhythmicity also occurred more rapidly in females: the mean latency to recovery (i.e., the duration of circadian arrhythmia) was 38.6 ± 16 days in females and 69.5 ± 15 days in males ($t_{21}= 3.6$, $P<0.005$; F range: 12-69 days; M range: 51-85 days; Fig. 7E). As with the induction of arrhythmia, the recovery of circadian rhythmicity occurred in mice housed with (11 of 18; 61%) and without (12 of 21; 57%) running wheels and was not linked to any obvious external stimuli: in 23 mice, circadian rhythms re-appeared on 18 different days over an 83-day interval; rhythm re-emergence did not consistently occur at any specific time of day. Circadian rhythmicity re-emerged as abruptly as it disintegrated: in the modal phenotype a consolidated inactive phase emerged via a reduction in activity levels over 1-2 circadian cycles (e.g., Fig. 7B). In neither sex did the latency to arrhythmia predict arrhythmia duration ($P>0.8$, both comparisons). Circadian period or power (FFT or LSP) during the rhythmic interval in DD did not predict the latency to ($P>0.05$, all comparisons), or persistence of ($P>0.05$, all comparisons), arrhythmia in DD, nor did circadian power during the arrhythmic interval of DD predict the duration of arrhythmia ($P>0.3$, all comparisons).

Finally, the reconstituted circadian rhythm differed from that exhibited prior to the development of arrhythmia. FFT power increased 8-14 fold during the transition from arrhythmicity to free-running circadian recovery (FR2); restoring in females and males, respectively, 74% and 82% of power that had been present in the FFT of the initial (FR1) free-running rhythm (Fig. 7F). In addition, a consistent feature of the reconstituted circadian pacemaker was its shorter τ: in every individual that exhibited circadian recovery τ_{FR2} was shorter than τ_{FR1} (females: $t_{17} =6.86$, $P<0.001$; males: $t_3 =6.11$, $P<0.01$; Fig. 7G). Indeed, 6 female mice with reconstituted circadian rhythms exhibited a second bout of arrhythmicity,

followed by yet another recovery of coherent free-running rhythmicity (FR3), and in each of these individuals $\tau_{FR3} < \tau_{FR2} < \tau_{FR1}$ (Fig. 7G).

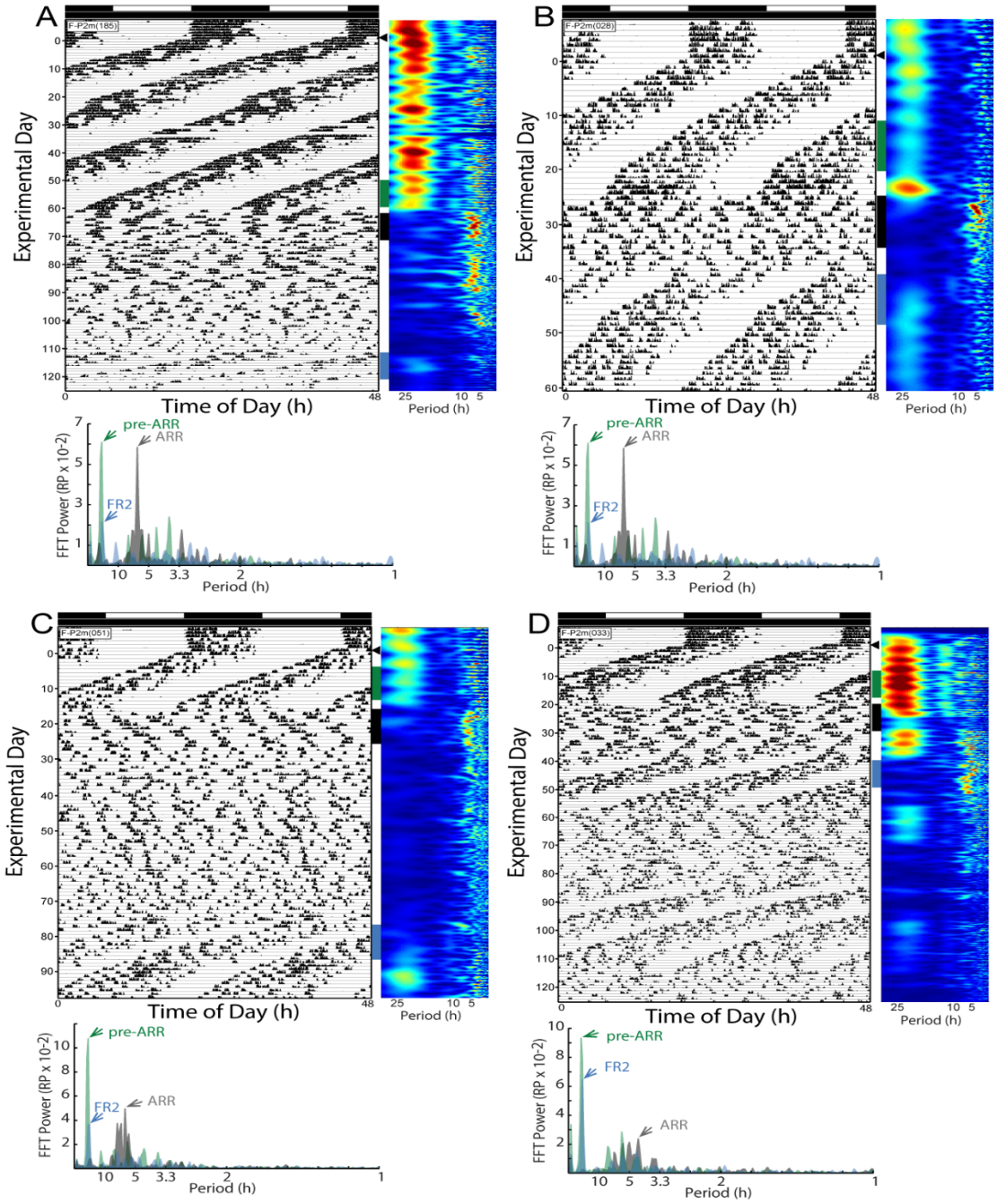

Figure 7: Spontaneous recovery of circadian rhythms in *Per2*$^{m/m}$ mice

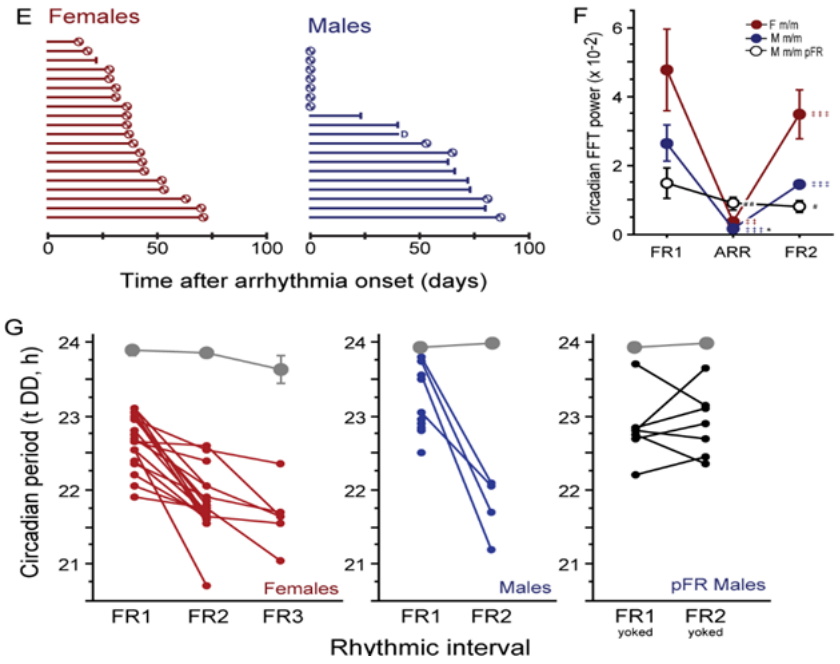

Figure 7, continued: Representative double-plotted RW actograms of female mice that exhibited circadian arrhythmia in DD and subsequently recovered free-running rhythms. Mice in panels A-C exhibited a single bout of arrhythmia, weeks to months in duration; the mouse in panel D exhibited multiple bouts of arrhythmia and recovery of rhythmicity. Vertical bars indicate free-running locomotor activity occurring just prior to arrhythmia (pre-ARR; green), during arrhythmia (ARR; black) and following recovery of circadian rhythmicity (FR2; blue); these intervals were subjected to FFT analyses, shown beneath each actogram. (E) Idiographic recovery plots: horizontal bars indicate the number of days elapsed between the onset of circadian arrhythmia and either the recovery of free-running circadian rhythms (circles) or the end of the experiment (bars). One mouse died prior to the end of the experiment (indicated as "D"); 7 of 19 male *Per2*$^{m/m}$ mice did not exhibit arrhythmia. (F) Fourier analysis: relative power in the circadian range (20-26 h) of the FFT prior to (FR1) and after (ARR) the onset of circadian arrhythmia, and after recovery of free-running (FR2) circadian activity rhythms, confirming the FR2 classification. *Per2*$^{m/m}$ males that did not exhibit arrhythmicity are designated 'persistent free-running' [pFR] mice. Due to the small number of males that recovered rhythms, we performed a supplemental LSP analysis to confirm this pattern. LSP confirmed increases, albeit more modest, in power in *Per2*$^{m/m}$ mice that recovered circadian rhythms (females: t_{18}=4.85, P<0.001; males: t_3=2.75, P=0.071); LSP power increased 3.4-7.9 fold during the transition from ARR to FR2, restoring in females and males, respectively, 58% and 56% of power that had been present in the LSP of the initial (FR1) free-running rhythm. (G) Periodogram analysis: circadian period (τ) of the initial episode of free-running circadian locomotor activity in DD (FR1) and of the free-running circadian rhythm after recovery from circadian arrhythmia (FR2). Note: 15 of 19 females exhibiting FR2 exhibited a second bout of arrhythmia; and 5 of these 15 females exhibited a subsequent cycle of recovery (indicated as FR3). In Panel F: *P<.05 vs. female value; #P<.05, ##P<.01 vs. all other groups at same timepoint; ‡‡P<.01, ‡‡‡ .001 vs. previous timepoint, within group.

Experiment 3: Gonadectomy promotes circadian arrhythmia in male Per2$^{m/m}$ mice

Prior investigations have revealed marked activational influences of circulating gonadal hormones, in particular androgens, on the circadian system, notably on the consolidation and amplitude of circadian locomotor activity (Daan et al., 1975; Iwahana et al., 2008; Yan & Silver, 2016). In light of the prominent sex differences described here, we examined the effects of gonadal hormones on DD-induced circadian arrhythmia in *Per2*$^{m/m}$ mice. Adult mice in 12L:12D were surgically gonadectomized (females: OVx, males: GDx) or sham-operated (n=9-10/group), and after recovery from surgery all mice were transferred to DD for >100 days and monitored with running wheels. As expected (Bailey & Silver, 2014; Iwahana et al., 2008; Yan & Silver, 2016), gonadectomy markedly reduced locomotor activity ($F_{1,45} = 9.14$, $P<0.005$; Fig. S1A), with significant effects in *Per2*$^{m/m}$ females ($t_{18} = 2.24$, $P<0.05$), but not in *Per2*$^{m/m}$ males ($t_{17} = 0.51$, $P>0.6$). Upon transfer to DD, *Per2*$^{m/m}$ mice also exhibited the expected short τ ($F_{1,45} = 8.68$, $P<0.01$; Fig. 8A-D); although τ during the initial interval of exposure to DD did not differ between male and female *Per2*$^{m/m}$ mice ($t_{17}=0.076$, $P>0.9$). GDx did not affect τ in WT mice of either sex (F: $t_7 = 0.86$, $P>.40$; M: $t_3 = 1.67$, $P>.15$).

WT mice, regardless of surgical treatment did not exhibit circadian arrhythmia (Fig. 33C-F). As before, the vast majority of gonad-intact female mutants exhibited arrhythmia (9 of 10), whereas fewer than half (4 of 9) of the intact mutant males did so (90% vs. 44%; Fisher's exact test: P=.057; Fig. 8E). Ovariectomy (OVx) did not meaningfully alter the likelihood of arrhythmia in female *Per2*$^{m/m}$ mice: 8 of 10 OVx females exhibited at least one bout of circadian arrhythmia in DD (Fisher's exact test: P>0.9 vs. sham-operated females; Fig. 8E). In *Per2*$^{m/m}$ males, castration (GDx) caused a striking increase in circadian arrhythmia: 9 of 10 GDx males

exhibited arrhythmia in DD (Fisher's exact test: P=0.057 vs. sham-males; Fig. 8E)—an incidence comparable to that of sham- and OVx females (Fisher's exact test: P>0.9, both comparisons; Fig. 4E). Overall, arrhythmia in 30 animals occurred on 25 unique days.

Survival analyses indicated that, among gonad-intact mice, sex again significantly impacted the development of circadian arrhythmia (τ^2=4.07, P<0.05), and among males, GDx markedly altered the emergence of arrhythmia over time (τ^2=4.13, P<0.05; Fig. 8F). Gonad-intact males also tended to differ from OVx-females (τ^2=3.44, P=0.06), but circadian arrhythmia evolved comparably in DD among all other groups (P>0.60, all comparisons; Fig. 8F). Circadian arrhythmia occurred more rapidly in this study compared to the previous experiment, and the mean latency to arrhythmia did not differ between the 4 intact males (35.8 ± 12 d) and 9 intact females (40.3 ± 5 d; t_{11} = 0.41, P>0.6) that became arrhythmic. Taken together this pattern of results suggests that the sex difference in circadian arrhythmia in the *Per2*$^{m/m}$ mouse is mediated in part by concurrent effects of male gonadal hormones and that ovarian hormones are not required for high rates of expression of arrhythmia in females.

As in the prior experiment, many (20 of 38; 53%) arrhythmic *Per2*$^{m/m}$ mice also exhibited spontaneous recovery from circadian arrhythmia (Fig. 8G). Recovery was evident in 78% (7 of 9) and 75% (6 of 8) of intact and OVx females, respectively. Just 50% (2 of 4) of intact males that exhibited arrhythmia recovered, and 56% (5 of 9) arrhythmic GDx males recovered. These 20 recoveries occurred on 15 unique days. Sample sizes were not sufficient to permit statistically powerful categorical analyses of the incidence of recovery, but the patterns suggest: (1) again an increased likelihood of spontaneous recovery in females, (2) no obvious augmentation of recovery in GDx males, and (3) no effect of OVx on recovery in females (Fig. 8G). Circulating male gonadal hormones may play a role in the induction of arrhythmia, but not circadian

recovery, whereas circulating female gonadal hormones are not mandatory for either. Organizational effects of gonadal hormones in both sexes may be implicated in the latter. Whether male and female gonadal hormones act via androgen or estrogen receptors in the mediation of these phenomena requires further investigation (Vida et al., 2008; Yan & Silver, 2016).

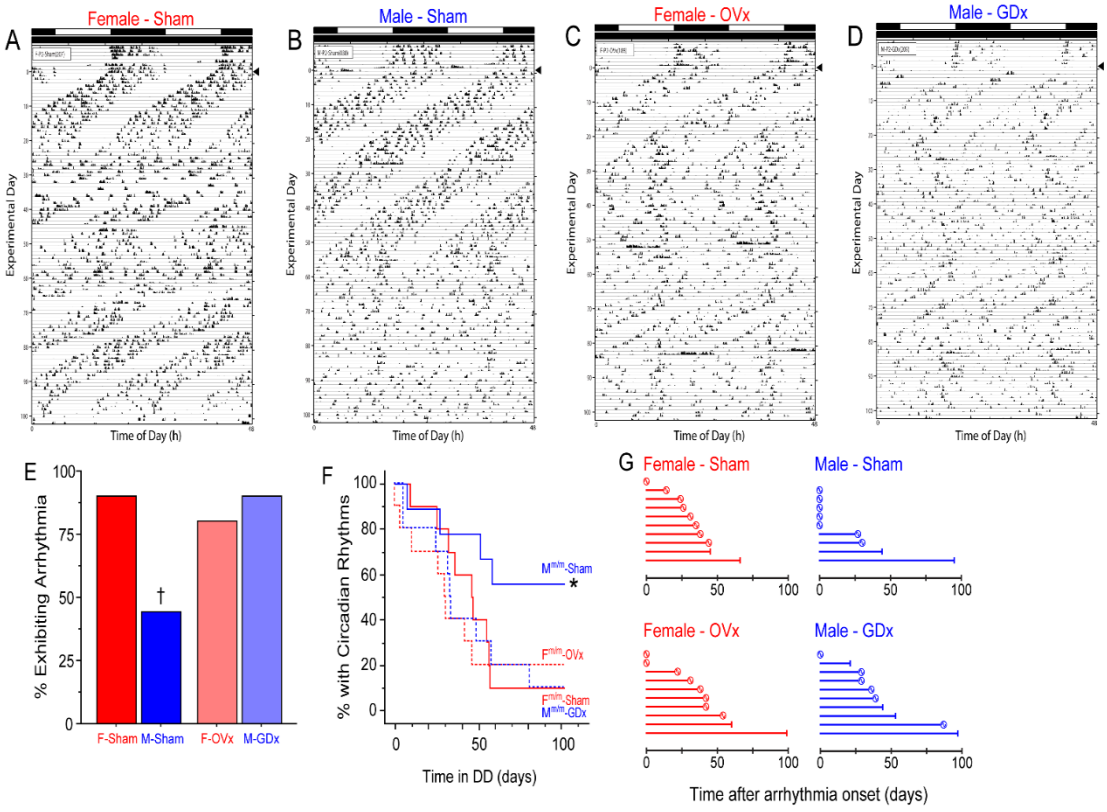

Figure 8: Castration promotes circadian arrhythmicity in *Per2*$^{m/m}$ males

Representative double-plotted RW actograms of female and male *Per2*$^{m/m}$ mice that were sham operated (female: panel A; male: panel B) or gonadectomized (ovariectomized [OVx] female: panel C; orchiectomized [GDx] male: panel D), and maintained in DD for >100 days (transfer from LD to DD indicated by arrowhead; actogram conventions as in Fig. 1). See Fig. S1 for representative actograms of WT control mice, which did not exhibit circadian arrhythmia. (E) Percentage of *Per2*$^{m/m}$ mice of each sex and surgical condition that exhibited circadian arrhythmia in DD. (F) Survival analysis: Kaplan-Meier survival plot evaluating the emergence of circadian arrhythmia in DD among male and female WT and *Per2*$^{m/m}$ mice (G) Idiographic recovery plots: horizontal bars indicate the number of days elapsed between the onset of circadian arrhythmia and either the recovery of free-running circadian rhythms (circles) or the

Figure 8, continued: end of the experiment (vertical bars). Recovery of free-running circadian rhythms was evident in 7 of 9 sham-females, in 2 of 4 sham-males, in 6 of 8 OVx females and in 5 of 9 GDx males.

General Discussion

Mice lacking a functional copy of the *Per2* gene exhibited an atypical pattern of entrainment and largely failed to sustain circadian rhythms in multiple measures of general locomotor activity (RW activity, PIR activity) in constant darkness, confirming and extending the critical role for PER2 in the molecular transcription and translation feedback loop (TTFL) that comprises the circadian pacemaker. The $Per2^{m/m}$ circadian phenotype was exaggerated in female mice: two core features of the $Per2^{m/m}$ chronotype—shortened circadian period and loss of circadian rhythmicity in DD— were markedly enhanced in females compared to males. Females were far more likely to become arrhythmic in DD, and circadian arrhythmia occurred many weeks earlier in females than males. Moreover, once circadian arrhythmia emerged, most (8 of 12) males remained in this state; in contrast, nearly all (19 of 20) females recovered from circadian arrhythmicity, re-establishing coherent free-running circadian rhythms. Indeed, several (5 of 19) female mice repeated this arrhythmia/recovery cycle multiple times. Whereas many males can sustain circadian rhythms in behavior without a functional PER2 protein, few females can. The data identify an unstable state of equilibrium in the absence of a functional PER2 protein, characterized by sequential fluctuations between transient states of coherent circadian rhythmicity and arrhythmicity.

Restoration of rhythmicity in Per2 mutant mice was previously reported (Abraham et al., 2006; Steinlechner et al., 2002). Double mutant Per2/Cry1 mice exhibited loss of circadian rhythms in wheel running activity in DD and the emergence of robust ultradian rhythms. Exposure to high intensity constant illumination (LL) restored circadian rhythms with a much

shorter period (Abraham et al., 2006). We also observed emergence of strong ultradian rhythms in association with DD arrhythmicity, but circadian reinstatement occurred in DD in the absence of light signals. Whether the relay of timing information from ultradian rhythms to the suprachiasmatic nuclei is critical for reestablishment of circadian rhythms, as posited by (Abraham et al., 2006) remains to be verified. (Steinlechner et al., 2002) reported rapid development of arrhythmicity in *Per2*$^{m/m}$ mice held in DD; subsequently, under constant light, these mice exhibited robust circadian activity and body temperature rhythms with short period lengths, an outcome consistent with the original description of this mutant model, in which a 6 h light pulse immediately restored circadian rhythmicity in 100% of mice (Zheng et al., 1999). Collectively, these findings suggest that residual, potentially-unstable, clock function in *Per2*$^{m/m}$ mice supports coherent circadian rhythms in DD as well as in LL, with interspersed circadian arrhythmicity.

PER2 plays a prominent role in the generation of cellular circadian rhythms (Bae et al., 2001; Zheng et al., 2001; Zheng et al., 1999); mice with loss-of-function mutations in the *Per2* gene (e.g., *Per2*^{Brdm1} and *Per2*^{ldc}) exhibit two essential chronotypes in DD: a short τ (22-23 h) and ubiquitous loss of circadian rhythmicity (Bae et al., 2001; Zheng et al., 1999). The present data identify quantitative and categorical sex differences in each of these chronotypes: females exhibited a much shorter τ, and all females lost circadian rhythmicity, but only approximately half of all males did. PER2 is indispensable for the generation of circadian rhythms in peripheral circadian oscillators, but network dynamics within the SCN introduce compensation or redundancy that allow persistent circadian rhythmic output by the SCN in the absence of a functional mPER2, and thus transient rhythmicity in *Per2*$^{m/m}$ fibroblasts in DD (Liu et al., 2007). As in other reports, circadian arrhythmicity did not occur immediately upon transfer to DD;

instead *Per2*$^{m/m}$ mice exhibited free-running rhythms that lasted from 12 days to 18 weeks, supporting previous conclusions that the *Per2*^{Brdm1} mutant has a partially functional clock (Albrecht et al., 2001; Zhang et al., 2019; Zheng et al., 2001). *mPer1* mRNA rhythms were attenuated but not eliminated in *Per2*^{Brdm1} mice (Zheng et al., 1999), suggesting that residual levels of mPER1 provided only partial compensation for the absence of mPER2, which may account for the rapid onset, but not instantaneous, arrhythmicity in DD. As compared to prior reports in B6;129 hybrid *Per2* mutants, rhythmicity was sustained by *Per2*$^{m/m}$ mice for much longer intervals in DD, although arrhythmia onset occurred somewhat earlier in experiment 3 (Fig. 8) compared to the previous experiment (Fig. 7); regardless, in many males, the circadian pacemaker remained functionally robust for months, and perhaps indefinitely (Fig. 6G). Given that the PERIOD ortholog *mPer3* does not compensate for *mPer2* deficiency (Bae et al., 2001), the present results suggest that in the *Per2*$^{m/m}$ mutant, severely dampened mPER1 rhythms may afford a more potent compensation for the absence of mPER2 in the substantial population of males that exhibit persistent free running rhythms in DD. A similar degree of compensation is categorically absent in females.

Circadian arrhythmicity was not permanent; rather, free-running locomotor activity rhythms spontaneously re-emerged in arrhythmic mice (Fig. 7A-D). It was not possible to determine, from activity records alone, whether the loss and subsequent gain of circadian rhythmicity merely reflected a transient uncoupling of the circadian pacemaker from output pathway(s) that mediate overt rhythmicity, or if the pacemaker was arrested during behavioral arrhythmicity. Activity onset of FR2 (the second, recovered, free-running rhythm) did not resume at the same time of day that activity onset of FR1 had last been expressed, which would be predicted if the circadian pacemaker had become arrested at the end of FR1 and subsequently restarted in FR2.

Alternatively, if the circadian pacemaker had continued to keep time during the interval of behavioral arrhythmia, then the phase of the restored rhythm ought to be predictable by extrapolation of the phase of the rhythm prior to the loss of rhythmicity. However, because τFR1 often lengthened in the days leading up to arrhythmicity, it was not possible to clearly extrapolate onset phase between FR1 and FR2. Further complicating such an extrapolation, τ changed markedly in mice that recovered from arrhythmia. Further characterization of this novel model of circadian instability (e.g., via longitudinal evaluation of the molecular TTFL within the SCN) may afford direct insight into whether the circadian pacemaker continues to oscillate during the interval of arrhythmia.

The propensity of most female and many male *Per2*$^{m/m}$ mice to fluctuate between states of coherent circadian rhythmicity and arrhythmicity has not been reported previously, likely because the 18 weeks of recording employed herein is, to our knowledge, the longest interval over which mice bearing mutations in any of the core circadian clock genes have been continuously monitored. Similar long-term monitoring of behavior has been performed in rodents and primates bearing SCN lesions, with no evidence of functional rhythm recovery (Mosko & Moore, 1978). In contrast, spontaneous recovery of circadian pacemaker expression was pervasive in *Per2*$^{m/m}$ mice, occurring in 95% of females and 33% of males, indicating that the state of circadian arrhythmia induced by the *Per2*^{Brdm1} mutation is not permanent. This categorical difference suggests that circadian disruptions induced by genomic mutation may not be isomorphic with those induced by chemical or physical lesions of the anatomical pacemaker. During transient arrhythmicity, molecular circadian rhythms may be eliminated at the level of individual SCN oscillatory neurons; alternatively, cells within the SCN may continue to oscillate individually during transient arrhythmia, but become transiently uncoupled (desynchronized)

from one another at a cellular (Ohta et al., 2005) or network (Evans et al., 2013) level, or uncoupled from SCN output pathways. Irrespective of such formal features, the present data indicate that compensation among molecular elements of the circadian TTFL is more robust than previously described. Moreover, these data suggest that compensation for the absence of a functional PER2 protein is strongly sexually-differentiated and mediated, at a minimum, by effects of gonadal hormones. Indeed, the effects of orchidectomy and ovariectomy on arrhythmia in DD are consistent with several reports indicating robust effects of GDx relative to OVx in adult mice (Daan et al., 1975; Iwahana et al., 2008; Morin et al., 1977; Yan & Silver, 2016). The relative importance of androgen and estrogen receptors in mediating effects of gonadal hormones on arrhythmia in *Per2*$^{m/m}$ mice remains to be determined, however.

Per2$^{m/m}$ females undergo reproductive aging faster than males (Pilorz & Steinlechner, 2008) and we do not know how longterm DD effects estrous cycling. Given the impact of female reproductive hormones on circadian rhythms in general and *Per2* in particular (Nakamura et al., 2005; Nakamura et al., 2008), processes associated with reproductive aging may contribute to the sex difference in arrhythmia identified here or in part mask the effect of loss of estrous cycling (Pilorz et al., 2020). Pilorz & Steinlechner (2008) identified reproductive senescence in female *Per2*$^{m/m}$ mice as beginning sometime after 6 months of age, as 9-12 month old *Per2*$^{m/m}$ females had reduced fertility compared to WT controls. Aging also decreased overall levels of locomotor activity in acyclic female *Per2*$^{m/m}$ mice, but a similar effect of aging was observed in WT controls; however, the phase angle of entrainment to the LD cycle was comparable in aged and young *Per2*$^{m/m}$ mice (Pilorz et al., 2009). In experiment 2, some female *Per2*$^{m/m}$ mice would have entered this window of reproductive senescence during exposure to DD, whereas in experiment 3, female *Per2*$^{m/m}$ had already aged well into, if not beyond, this window before being subjected

to DD. The comparable rates of arrhythmia observed among females in experiments 2 and 3 (100% and 90%, respectively), and the arrhythmia observed in male mice (albeit a lower incidence), together argue against aging of the reproductive system *per se* playing a categorical role in DD-induced arrhythmia. However, the different latencies to arrhythmia onset documented across the two experiments may indeed be related to such aging. The effects of long-term DD on estrous cycles of *Per2*$^{m/m}$ mice are not known. The lack of an effect of ovariectomy on arrhythmia in experiment 3 may be related to the relatively advanced age of female mice in this study; although effects of OVx on overall activity were still evident. The circadian instability in *Per2*$^{m/m}$ mice characterized here may offer a useful model for further investigations of the role of aging and hormones on circadian biology and behavior.

Behavioral genomic assays used in recent decades to identify circadian clock genes in mice typically examine free-running locomotor activity for ≤ 21 days in DD (Siepka & Takahashi, 2005; Siepka et al., 2007). Assays of this length are inherently biased towards genes that markedly alter τ, and induce a rapid loss of circadian rhythmicity (Siepka et al., 2007). The identification here of circadian chronotypes which emerge only after much longer intervals of exposure to DD, indicate that such assays are less robust in identifying genes that regulate the circadian system, or in a sexually-differentiated manner. Moreover, even core molecular components of the circadian TTFL likely have more complex roles than currently recognized.

What is occurring at a molecular level is unclear. One prior paper, in a Per2/Rev-erbα double knockout previously documented such a recovery, suggesting that part of the feedback loop is not playing a role (Schmutz et al., 2010), but ascribed it to a potential increase in *Bmal1* expression. Perhaps the most promising potential explanation comes from work by Oster and colleagues which showed that double knockout of *Cry2* and *Per2* prevents arrhythmia at least in

short term constant darkness (Oster et al., 2002). This effect was not present in other of the knockout combinations of *Per2, Per1, Cry1,* and *Cry2,* suggesting that perhaps in these *Per2* mutant mice, *Cry2* suppression could lead to recovery. Further testing, however, is needed to know for certain.

Chapter 4: Wavelet Analyses of Behavioral Ultradian Rhythms in Male and Female C57BL/6 Mice

Introduction

Biological rhythmicity is a fundamental property of all living systems (Bloch et al., 2013; Edgar et al., 2012) with implications for many fields of biology (Bloch et al., 2013; Evans & Gorman, 2016; Ramp et al., 2015; Riede et al., 2017; Spoelstra et al., 2016; Turek, 2016; G. Z. Wang et al., 2015). Circadian rhythms (CRs), which evolved to anticipate regularly-recurring cycles tied to the ~24 h rotation of the earth about its axis, have been studied extensively, and their relevance to regulatory biology and human health is well-established (Evans & Davidson, 2013; Savvidis & Koutsilieris, 2012; Stevenson et al., 2015; Walker et al., 2020; Zheng et al., 2020).

In contrast, intradaily (1-6 h) ultradian rhythms (URs) are relatively understudied (Grant et al., 2018; Prendergast & Zucker, 2016). This is surprising, given that the influence of URs on physiology and behavior appears as pervasive as that of CRs: URs manifest in countless behavioral and physiological processes important for homeostasis (e.g., food consumption, water intake, sleep, body temperature, metabolic gene expression, hormone secretion, among others) in diverse species (Aviram et al., 2021; Blessing & Ootsuka, 2016; Bloch et al., 2013; Bourguignon & Storch, 2017; Prendergast & Zucker, 2016; Stavreva et al., 2009; van der Veen & Gerkema, 2017). Changes in the temporal properties of URs have also been associated with major life history events (e.g., ovulation, pregnancy, lactation; (Prendergast, Cisse, et al., 2012; Smarr et al., 2016)) and with the progression of disease (Smarr et al., 2019). Ultradian patterns of hormone release are required to elicit normal pituitary activity (Belchetz et al., 1978) and gene transcription (McMaster et al., 2011; Stavreva et al., 2009). And finally, URs are sexually

differentiated [14], exhibiting phenotypic plasticity in response to endogenous (Painson & Tannenbaum, 1991) and exogenous changes in gonadal hormones rats (Wollnik & Turek, 1988), hamsters (Prendergast, Cisse, et al., 2012; Wang et al., 2014), mice (Smarr et al., 2017); gonadectomy: (Daan et al., 1975; Wollnik & Dohler, 1986)). Sex- and hormone-mediated changes in URs also manifest more prominently in specific phases of the circadian cycle (Daan et al., 1975; Prendergast, Cisse, et al., 2012; Smarr et al., 2017; Wang et al., 2014; Wollnik & Dohler, 1986; Wollnik & Turek, 1988). Despite these many commonalities, the mechanisms by which sex, gonadal hormones and the circadian system interact to modify the UR waveform are not fully characterized.

Several differences between URs and CRs present obstacles to more extensive investigation. First, URs are not linked to any known astrophysical periodicity (e.g., planetary rotation or orbit), and thus there is no *a priori* expected period value for any given UR. Indeed, URs exhibit complex waveforms, often with more than one ultradian periodicity expressed depending on the time of day, thus the specification of a single period is not always applicable to URs. Second, neural substrates of URs have proven difficult to localize, and it is unclear whether individual URs are controlled by distinct substrates (Bourguignon & Storch, 2017; Grant et al., 2018; Miyata et al., 2016; Prendergast & Zucker, 2016; Wu et al., 2018). Third, URs appear to change over the circadian cycle, but any role of the circadian system in the generation and expression of URs is likely complex: an intact circadian oscillator is not required for the expression of URs, for example, and URs persist following physical (Blum et al., 2014; Gerkema et al., 1993; Gerkema et al., 1990; Gerkema & van der Leest, 1991), chemical (Blum et al., 2014) and genomic (Abraham et al., 2006; Bunger et al., 2000; Vitaterna et al., 1994; Zheng et al., 2001; Zheng et al., 1999) manipulations of the circadian pacemaker, yet circadian transitions between locomotor

activity and rest robustly modulate the UR waveform (Smarr et al., 2017); URs exhibit remarkable plasticity as the circadian system entrains to seasonal changes in photoperiod: under short (winter) photoperiods nocturnal locomotor activity URs of mice (Refinetti, 2002), hamsters (Prendergast, Cisse, et al., 2012), and rats (Siebert & Wollnik, 1991) become more prominent. In the field, when extremely long and short photoperiods prevail, arctic species (e.g., reindeer, ptarmigan) largely abandon CRs in favor of robust URs (Appenroth et al., 2021; Bloch et al., 2013; van Oort et al., 2007), challenging the hegemony of circadian rhythmicity (Hazlerigg & Tyler, 2019).

A final and critical dissimilarity is that URs must be quantified differently than CRs. Individuals commonly exhibit multiple URs simultaneously (e.g., locomotor activity, hormone pulsatility) (Bourguignon & Storch, 2017; Grant et al., 2018), with a broader normative period range than CRs, that tend to co-occur around circadian harmonics. URs are extremely non-stationary, varying in period/phase, waveform, and amplitude from cycle to cycle (Refinetti et al., 2007). Harmonics, non-stationarity, and multiple periodicities each pose substantial challenges to Fourier-based methods that are typically used to extract quantitative metrics (period/phase, power) from CRs, and thus these quantitative methods are not ideal for measuring URs (Leise, 2017).

The continuous wavelet transform surmounts many of these obstacles and provides a desirable alternative technique for quantification, by generating a scalogram (a spectrogram-like representation of the underlying signal (Leise, 2013)) which is robust to non-stationarity and has time-frequency resolution sufficient to accurately identify URs even in the face of circadian harmonic contamination (Leise, 2013; Leise & Harrington, 2011). Continuous wavelet transform scalograms are highly informative but, in common with circadian actograms, are also highly

individualistic. The presence of multiple UR periods within individual scalograms, together with the modulation of URs over circadian timescales, precludes simply collapsing UR scalograms across many individuals to develop measures of central tendency and perform group-level parametric statistical analyses. Consequently, wavelet-derived information on URs is often idiographic, restricted to representative-animal illustrations, (Blum et al., 2014; Goh et al., 2019; Leise & Harrington, 2011; Miyata et al., 2016; Wu et al., 2018), or systems level analyses (Smarr et al., 2019). Given the emerging interest in ultradian biology over the past decade (Appenroth et al., 2021; Aviram et al., 2021; Bloch et al., 2013; Blum et al., 2014; Grant et al., 2020; Grant et al., 2018; Hazlerigg & Tyler, 2019; Miyata et al., 2016; Prendergast et al., 2015; Smarr et al., 2016; van Rosmalen & Hut, 2021; Wu et al., 2018), resolving such limitations may provide useful new research methods for the field.

Here we report and extensively validate, using *in silico* models with known ultradian periods, straightforward modifications to wavelet analysis procedures which address many of the challenges posed by URs. Reduction of the complex wavelet scalogram into discrete estimates of power (across periods) and period (within objectively-defined power bands) permitted aggregation of data across individual subjects for group-level analyses. Additional experiments evaluated the accuracy, repeatability, and precision of these analytical methods *in vivo*, by quantifying URs of female and male mice following genomic, hormonal and environmental manipulations previously reported to alter URs. The approaches described here supplement existing wavelet methods and permit novel analyses of CR and UR interactions.

General Methods

Animals and housing. Male and female mice for all experiments were obtained from Jackson Laboratory (Bar Harbor, ME, USA). WT mice were on backgrounds of (C57BL/6J [JAX Catalog

#: 000664; black coat color] or B6(Cg)-Tyrc-2J/J [JAX Catalog #: 000058; albino color]). Mutant mice in Experiment 1 homozygous for the *Per2*^{Brdm1} mutation [JAX Catalog #: 003819] were ordered directly from Jackson Labs (Riggle et al., 2022). Mice were housed in an intermediate-duration photoperiod that provided 12 h light and 12 h darkness each day (12L:12D; 'intermediate days'), with the exception of Experiment 3 (see *Photoperiod manipulations*). Experiments were performed on adult mice; see specific *Experiments* for ages and sample sizes. Estrous cycles of females were not monitored. Mice were housed in polypropylene cages (28 × 17 × 12 cm) on irradiated corncob bedding (Irradiated 1/8" Corn Cobs, Envigo, Indianapolis, IN, USA). Ambient temperature and relative humidity were monitored and maintained at 20 ±0.5°C and 53 ±2%, respectively. Food (Teklad Global 18% Protein Rodent Diet 2918, Envigo); filtered tap water and cotton nesting material were continuously available in the cages. All experimental procedures conformed to the NIH Guidelines for the Care and Use of Laboratory Animals and were approved by the Institutional Animal Care and Use Committee of the University of Chicago.

Locomotor activity monitoring. In all experiments, home cage locomotor activity was continuously monitored with passive infrared motion detectors mounted outside the cage, ~22 cm above the cage floor. Motion detectors registered locomotor activity via closure of an electronic relay, recorded by a computer running Clocklab software (Actimetrics; Evanston, IL, USA). Cumulative locomotor activity counts were binned at 1 min intervals. URs and CRs were quantified from 10 day epochs of locomotor activity (described below).

Photoperiod manipulations. Animal housing rooms were illuminated with overhead fluorescent lighting (~400 lux at the level of the cage lid). Digital timers controlled lights to deliver one of 3 static lighting cycles (photoperiods): Mice were maintained in one of three

different photoperiods: 12L:12D (an intermediate photoperiod), 16L:8D (a long photoperiod), and 8L:16D (a short photoperiod). Increases and decreases in photoperiod duration were accomplished by symmetrical expansion and compression, respectively, of the light phase (i.e., the midpoint of the light phase always remained the same). *Per2*^{Brdm1} mutant mice used in Experiment 1.3 were also exposed to continuous darkness and a 2L:2D photocycle. Mouse husbandry in constant darkness was facilitated via dim handheld red illumination (<1 lux), otherwise mice were maintained in complete darkness.

Circadian locomotor activity analyses. Circadian entrainment was confirmed via qualitative analysis of double-plotted actograms (Fig. 4A), which were generated in Clocklab software (v. 2.56; Actimetrics, Evanston, IL, USA). Fourier-based quantitative evaluation of CRs was performed using a Lomb-Scargle periodogram analysis in MatLab (Mathworks), which estimates a frequency spectrum by using a least-squared method of fitting the locomotor activity time series to a series of sinusoids**.** The Lomb-Scargle periodogram is a common and well-established analytical technique for the evaluation of rhythmic circadian signals (Refinetti et al., 2007; Tackenberg & Hughey, 2021).

Pre-processing. Post-collection data quality assessment was performed in MatLab: infrequent data dropouts (transcription errors, corrupted data points; encoded as 'NaN') were substituted with values equal to a 10 minute moving average. In instances where this failed, values were substituted with zero. To remove the influence of outlier data points in the time series, any value exceeding 4x the standard deviation of the time series was replaced with a value equal to 4x the standard deviation of the time series. On occasion, larger, multi-day data dropouts occurred because of passive infrared sensor malfunction on a channel, in which case that channel was excluded from the affected 10 day analysis window. Final sample sizes are reported in the each

experimental section below and in figure legends. In mice exposed to short days, a computer failure during the week 6 data collection interval resulted in one day of incomplete data for all animals. In order to obtain a complete 10 days of data for this analysis interval, data collection was extended by one additional day, and the data from the day of the computer failure was excised.

Parsing. Locomotor activity data from each mouse were first separated into light or dark phase components (diurnal parsing). Parsing was performed prior to wavelet transformations, and did not generate artifacts or spurious ultradian periods to emerge from the analysis, as confirmed via simulations (see *Experiment 1.1*, and Fig. 10A-C). Light and dark phase activity data were then each individually subjected to the continuous wavelet transform, which produced scalogram matrices for each record.

Wavelet Analyses. Time series data were evaluated using wavelet analyses, which quantify rhythms in multiple period bands (i.e., ultradian and circadian). When applied to time series data, wavelets identify harmonics, remove trends and noise, and compensate for non-stationarity; the latter is especially useful in more accurately resolving UR components. For additional background and a focused discussion of the merits and limitations of wavelet-based time series analyses in the measurement of behavioral rhythmicity, see reviews (Leise, 2013; Leise, 2015, 2017; Leise & Harrington, 2011). We identified a generalized Morse wavelet of $\gamma=3$ and $\beta=10$ to provide optimal time-frequency resolution for our experimental data (i.e., C57BL6/J mice, recorded via passive infrared motion detectors), but results were stable for $\beta'= 6\text{-}12$. The generalized Morse (Airy wavelet; $\gamma=3$) was chosen over the Morlet wavelet due to its strict analytic nature (Lilly & Olhede, 2012). Analyses were performed using the Jlab Matlab package and with modified versions of code generously provided by T. Leise (Department of

Mathematics, Amherst College). A wavelet sized for 1 to 6.5 h was used to perform an analytic continuous wavelet transform on time series data using jLab package (Matlab). To generate UR measures for each individual animal, treatment group and phase of the light:dark cycle, locomotor activity data obtained from each phase of the long day cycle (i.e., light phase and dark phase) were each passed through the wavelet operation separately (Fig. 9A1) for each mouse as described in Fig. 9.

Normalization and signal averaging. Edge effects were managed by using a periodic boundary extension and removing 1.5 × the greatest period estimated (see (Leise, 2013; Leise & Harrington, 2011) for justification and further discussion) (Fig. 9A1). Scalograms were collated by treatment (*photoperiod*: 16L:8D, 12L:12D, 8L:16D; *sex*: female, male; *surgical treatment*: OVx, GDx, sham-OVx, sham-GDx; *duration of photoperiod treatment*: 6 weeks, 8 weeks, 10 weeks; *circadian phase*: light phase, dark phase) as appropriate for each experiment. The magnitude of each matrix was summed and divided by the total number of matrix cells, providing an average power for each activity record; each scalogram matrix was subsequently normalized by dividing by this average total power (Fig. 9A1).

The complex magnitude of each matrix was then summed to a single cell and divided by the total number of matrix cells to compute an average total power from each individual time series record. Because photoperiod was manipulated in Experiment 3, this average was calculated for photoperiod for all groups based on the total number of cells in the 12L:12D photoperiod; this permitted direct comparisons of magnitude across the different photoperiod treatment groups, by compensating for the different numbers of data bins in light and dark phase of different length. Next, to minimize individual differences in locomotor activity levels, the complex magnitude of each scalogram matrix was normalized by dividing by its average total power. Finally, to correct

for edge distortion and to avoid biasing, the ends of each time series were extended periodically, and the resultant data were trimmed from either side of the scalogram matrix at 1.5 times the maximum value of the assessed period range (6.5 h), as recommended elsewhere (Leise & Harrington, 2011) (Fig. 9A). The scalogram matrices were averaged within each treatment group to compute a scalogram that best approximated the true matrix for the group (Fig. 9A3). Ergodicity and stationarity were assumed for each grouping.

Variance estimates and group-wise differences. To facilitate comparisons of UR power distributions among treatment groups, each mouse's normalized scalogram matrix was averaged across the time dimension into a power-period plot, which computes the average continuous wavelet transform power at each scale and its corresponding approximate ultradian period (designated as τ' [tau-prime], to distinguish UR period [i.e., τ'] from CR period [τ]; Fig. 1A4). These power-period plots (e.g., Fig. 9A6) were sorted and combined into average plots for each treatment group. To generate measures of variability around the group mean, individual values of power distribution across period were grouped and bootstrapped 2000 times to calculate 95% confidence intervals (using the bootci function in MatLab; Fig. 1A5). Significant differences between groups were inferred to exist at UR periods where 95% CIs did not overlap.

Wavelet ridge extraction. Power (signal) exists at all frequencies, and the continuous wavelet transform analysis described above permitted evaluation of changes in the distribution of this power across all frequencies. We also determined whether experimental manipulations affected the ultradian frequencies at which maximal power occurred by utilizing wavelet ridge analyses to identify these values. In the continuous wavelet transform, the maximum wavelet ridge at each time point approximates the true frequency component, in this case the output of an ultradian clock[s]) in the data, even in the presence of harmonic, e.g., circadian contamination. The

wavelet ridge is defined as the maximum cross-correlation between time series and wavelet and approximates the instantaneous frequency (=1/'τ) at every wavelet scale and time coordinate in the magnitude of the wavelet transform (Leise, 2013; Leise, 2015; Leise & Harrington, 2011; Lilly & Olhede, 2010).

The initial continuous wavelet transform window was characterized by a fragmented maximum wavelet ridge (e.g., scalogram in Fig. 12B), indicating the presence of multiple ultradian components in the locomotor activity time series data. A discrete wavelet transform, described below, was used to apply multiple band pass filters and decompose locomotor activity time series data into a sum of wavelets or period bands (Fig. 9B1). The detailed methodology along with validation of the windowing procedure are described in Experiment 1.2 and Fig. 2. The results of the discrete wavelet transform analyses technique guided a re-windowing and reanalysis of the data. Locomotor activity time series for each subject were parsed by circadian phase (Fig. 9) and again passed through the continuous wavelet transform with the analysis restricted to one of 3 period windows (Fig. 9B3), corresponding to the 3 period bands of the discrete wavelet transform that contributed most to the UR waveform: a short UR period, from .53 h – 1.07 h [designated 'tau-prime' short, or τ'_s]; a medium-duration period from 1.07 h – 2.13 h [τ'_m]; and a longer period from 2.13 h – 4.26 h [τ'_l] (Fig. 1B2; Fig.4F). Continuous wavelet transform analyses were computed separately for each period band and then normalized (Fig. 1B3). Maximum wavelet power within each of these bands was used to characterize short, intermediate, and long-duration UR periods for each mouse (Fig. 9B4, 9B5).

Discrete wavelet transform and data smoothing. To aid in interpreting the fragmented wavelet ridge observed, we adopted a technique recommended in the supplementary methods of (Leise & Harrington, 2011), the modified discrete wavelet transform was employed to

decompose the time series to the 10th detail level into coefficients describing period between, $2^j\Delta t \rightarrow 2^{j+1}\Delta t$ where j is the coefficient detail level and Δt is the sampling interval. Edge effects were managed by extending end periodically and clipping 1.5 times the maximum period accessed (2048 minutes) which was clipped from each end. The energy contribution of each band was then quantified. Variance of the total time series can be described by the equation $\sigma^2 = \left(\frac{1}{N}\|V_J\|^2 - \underline{x}^2\right) + \frac{1}{N}\sum_{j=1}^{J}\|W_j\|^2$ where $\left(\frac{1}{N}\|V_J\|^2 - \underline{x}^2\right) + \frac{1}{N}$ describes the variance attributable to the J level scale coefficient and $\frac{1}{N}\sum_{j=1}^{J}\|W_j\|^2$ is the variance of the wavelet. Neglecting the variance of the scale coefficient, energy was defined (as described by Leise and Harrington 2011) (Leise & Harrington, 2011) as the variance of the wavelet coefficients: $\frac{1}{N}\sum_{j=1}^{J}\|W_j\|^2$ and we expressed it as each individual wavelet coefficient level divided by the total energy i.e. $percent\ total\ energy = \frac{\|W_j\|^2}{\sum_{j=1}^{10}\|W_j\|^2}$. With this calculation, a large degree of noise occurred in very low period bands (d_1-d_4: 2-4 min, 4-8 min, 8-16 min, and 16-32 min), masking the contributions of the ultradian and circadian components of interest. This is likely an artifact of sampling. Data sampling was performed at 1 min intervals. Over a full-length (10 d) timeseries, whereas circadian rhythmicity is clearly visible, this d_1-d_4 modulation does not differ greatly between filled bins in circadian active vs. inactive states, but rather manifests in the density of bins next to each other with counts (see Fig. 9B for a visual example). This density modulation led to a high degree of variability and thus a high degree of *percent total energy* in details d_1-d_4, obscuring the true ultradian and circadian signal. If this account is correct, then applying a moving average filter of 30 min would be sufficient to eliminate this high-frequency variance signal. Indeed, this was the case. Thus, to improve signal-to-noise ratio in the energy decomposition analysis, a moving average with a window of 30 min was first performed on each

time series and then the modified discrete wavelet transform was run. Note that this moving average filter was applied to data only for the process of performing the decomposition evaluation. The continuous wavelet transform and discrete wavelet transform analyses performed to determine UR power and period and were performed on the unfiltered raw time series data.

Additional details of the wavelet analyses used in these experiments, including all simulations and validation steps appear in Experiments 1.1 – 1.3, and in Figs. 9-11. Code files (Matlab) used in analyses are available online (URLs in *Data Availability Statement*).

Additional statistical analyses. Lomb-Scargle periodogram power values (PN values) appeared non-normally distributed and were $\log_{10}$-transformed prior to analyses. ANOVA was used to assess group differences and pairwise comparisons were evaluated with two-tailed t-tests when warranted by a significant F statistic. Note that locomotor activity data from 12L:12D analyzed in Experiment 2 were also included in the ANOVA model for Experiment 4 to permit comparisons among all three photoperiods. Statistical analyses were performed using Statview v5 (SAS Institute) on a PC. Differences were considered significant if $P \leq .05$.

Experiment 1. Validation of the analytic workflow

Because aspects of the data reduction and analyses are novel, we created a model of locomotor activity (see Locomotor Activity Model and Simulation Data, below, and *Supplementary Material*) and performed simulation experiments to validate the precision, accuracy and sensitivity of the quantitative procedures. The order of operations in the analytic pipeline were also validated via simulation experiments (Figs. 1 and 2), which are described below.

Experiment 1.1: Validation of a diurnal parsing procedure in the presence and absence of circadian modulation of the UR waveform.

Rationale: Because UR period, complexity and power may vary across the circadian cycle, evaluation of URs without regard for time-of-day may fail to capture important features of the UR waveform. To directly examine this circadian modulation, we analyzed diurnal activity data from the light and dark phases separately. Specifically, locomotor activity data generated during the part of the day when the room lights were on and when the room lights were off, were each extracted from the locomotor activity record time series, and were concatenated into separate 'parsed' records consisting of light-phase only or dark-phase only data. These parsed records were then evaluated via the continuous wavelet transform and/or discrete wavelet transform as described in Figs. 1 and 2. The simulations conducted in Experiment 1.1 evaluated: (1) the accuracy and precision of this procedure by comparing its handling of parsed vs. non-parsed data, and (2) the effect of performing the diurnal parsing prior to versus after the wavelet transform was performed. In order to ensure that the diurnal splicing procedure itself did not generate systematic differences in UR period or power, we assessed the precision of the procedure by evaluating simulated activity data, generated *in silico*, which contained URs with defined ultradian periods and which varied in period between the light and dark phases (circadian modulated) or remained at a fixed period over the circadian cycle (circadian unmodulated).

Locomotor Activity Model and Simulation Data: A model comprised of 10 days of locomotor activity was created to mimic actual mouse activity data in amplitude and variance (except for aspects that were experimentally manipulated as described below; Fig. 10A). The locomotor activity model was set to have a robust CR with a period of 24 h, either 2 or 4 URs with known periods, and a variable but reasonable amount of background noise. URs were

randomly selected, with the condition that records were always adulterated with both 'long' (2.13 – 4.26 h) and short (1.07 – 2.13 h) URs. For full details of the mathematical operations used to generate locomotor activity by this model, see *Supplementary Material: Locomotor Activity Model and Simulation Data*.

The model was then used to generate three treatment groups (n=10 simulated subjects / group; Fig. 2A). In one experimental group ('CR modulated'), UR period was modulated by circadian phase: long- and intermediate-period URs inserted into the light phase time series had different periods than the long- and intermediate-period URs that were interpolated into the dark phase of the time series (Fig. 2B). In a second group ('CR unmodulated'), URs were not modulated by circadian phase: within each locomotor activity record, identical long- and intermediate-period URs were interpolated into both the light and dark phases (Fig. 2B). Importantly the modulated and unmodulated groups were generated at the same time using the same dark phase URs, so that the only differences between them was in the period of the light phase URs. Finally, a control group ('no UR'), was created by taking the 10 modulated versions of the artificial activity records and scrambling the data within each "day" and "night" (i.e., light and dark phases, respectively) such that the circadian structure was preserved but all ultradian structure was randomly shuffled (Fig. 10B). To complete the simulation, the creation of the three UR treatment groups (CR modulated, CR unmodulated, or no UR; n=10 records / group) was performed 100 times with different, random-selected long- and intermediate-duration URs. Using these datasets, we then performed the quantitative analyses of UR period and power (as outlined in Fig.1) for each of the 1000 total simulations.

In performing these analyses we also evaluated whether the analysis stage at which the diurnal parsing procedure was performed affected the accuracy and precision of the resulting

power and period measurements. Thus, the diurnal parsing procedure (concatenation into light-phase only and dark-phase only records) was performed: (1) before the data were analyzed by the continuous wavelet transform (Fig. 2C), (2) after the data were analyzed by the continuous wavelet transform (Fig. 10D), or (3) not at all (i.e., the data remained unparsed at all stages of analysis; Fig. 10D). Following the wavelet transform, all matrices were normalized, with their edges trimmed before collapsing across time (experimental days) to generate two-dimensional period-power plots, which permitted evaluation of the effects of modulation and parsing on the accuracy and precision of the continuous wavelet transform analysis. Simulations were performed across a range of β' values (4-12) and results remained stable although, as expected, higher β' values improved frequency resolution.

Experiment 1.2: Segmentation of the ultradian frequency spectrum.

Rationale: URs do not resonate with any known geophysical periodicity, thus there is no *a priori* expectation that UR power should occur at a single period (cf. CRs). Specification of just a single UR period, therefore, likely fails to capture the polyrhythmic nature of URs. Indeed, individuals exhibit URs in multiple traits, which may manifest as power at multiple periodicities. Accurate characterization of the UR spectrum should capture this waveform complexity. Wavelet transforms are well-suited for quantifying UR power simultaneously at multiple periodicities: peak ridge power in the continuous wavelet transform matrix approximates the instantaneous period of the UR (Leise, 2013; Leise, 2015; Leise & Harrington, 2011; Lilly & Olhede, 2010, 2012), but at many times of day, peak scalogram power may occur at multiple periodicities (Fig 9A; Figs. 12B, 12C). Segmenting these fragmented scalograms into multiple period bands would permit quantification of peak UR periods therein. Simply identifying the few highest peaks in the scalogram is inadequate in this regard, as it introduces biases due to

clustered peaks and difficulties distinguishing among multiple peaks within a cluster. Ideally, segmentation of the UR domain should not be arbitrary (e.g., period bands of 2 h, or a similar convenient integer), but rather should be objectively driven, informed by the actual distribution of where power lies in the ultradian domain. The wavelet ridge extraction (described above) offers a suitable method for objective segmentation of the ultradian domain into period 'bands'.

Quantitative Procedures and Workflow: Locomotor activity time series were decomposed with the modified discrete wavelet transform (discrete wavelet transform) from the 1st to the 10th detail of the discrete wavelet transform (defined by $2^j\Delta t \rightarrow 2^{j+1}\Delta t$, where j is the detail level and Δt is the sampling interval). This resulted in the generation of period bands (termed 'details' in the discrete wavelet transform) ranging from 2-4 min through 17-34 h; the latter of which contained the fundamental circadian component (see *Methods: Wavelet ridge extraction*). Spectral decomposition was performed using a symlet wavelet (also termed a Daubechies least asymmetric wavelet) with 6 vanishing moments (Fig. 9B1), following procedures and considerations for this analysis as it applies to behavioral time series data described in detail in Leise & Harrington (2011). In order to impartially characterize the relative contribution of each detail – and thus generate an unbiased estimate of the relative importance of each detail to the overall rhythmic structure of the locomotor activity waveform— we calculated the energy (i.e., variance) explained by each normalized wavelet detail energy as described in Discrete Wavelet Transform and Data Smoothing and (Leise & Harrington, 2011). The distribution of power generated by this analysis of variance permitted the specification of period bands in the UR domain guided not by arbitrary concepts, but rather by the operational limit of the data sampling interval (i.e., 1 min bins).

Data: First, in order to specify the distribution of rhythmic power *in vivo*, we used locomotor activity records (10 days, 1 min bins) obtained from male (n=20) and female (n=20) mice housed in 12L:12D. For the initial discrete wavelet transform symlet analysis, locomotor activity data contained only endogenously-generated URs (i.e., simulated URs were not added; Figs. 1B1-1B2). The resulting power distribution clearly identified three detail bands which explained a substantial proportion of the variance in spectral power (a short UR period, from .53 h – 1.07 h [designated 'tau-prime' short, or τ'_s]; a medium-duration period from 1.07 h – 2.13 h [τ'_m]; and a longer period from 2.13 h – 4.26 h [τ'_l]; Fig. 9B4). These bands were used thereafter to objectively segment the ultradian domain and specify UR periods using continuous wavelet transform (Fig. 9B3-9B5).

Next, simulation data from Experiment 1, comprised of locomotor activity records created with circadian-modulated (n=2000) and -unmodulated (n=2000) UR periods (cf. Fig. 2A, 2B) were again passed through the continuous wavelet transform, with each analysis limited to 2 of the 3 period windows specified above (τ'_m and τ'_l , which corresponded to the UR periods with which the simulated data were created). Each continuous wavelet transform analysis computed the maximum ridge value, the mean scale, and the period corresponding to that scale value for each individual record. Continuous wavelet transform analyses were computed separately for each period band as in Fig. 9B3-5, and normalized. The period at which scalogram matrix cross-correlational power was maximal was used to define the instantaneous period in a given τ-band. Linear regression analyses were calculated to evaluate the accuracy and precision of the wavelet ridge procedure in recovering interpolated UR values.

Experiment 1.3: In vivo validity.

Rationale: This experiment sought to determine whether the wavelet workflow described above was capable of detecting and adequately characterizing rhythmic power not merely in period-recovery simulations, but in locomotor activity data generated by actual mice. In order to possess *in vivo* validity, the wavelet workflow should be capable of quantifying functionally significant overt behavior.

Circadian rhythms in vertebrate physiology and behavior are generated by transcriptional-translational feedback loops of circadian clock genes and their protein products. One element of this feedback loop, *Period 2* (and its protein product, PER2) is critical for the integrity of the organismal circadian network: germline mutant mice with a functional deletion of the mPER2 protein dimerization PAS domain (*mPer2*^{Brdm1}; *Per2*$^{m/m}$ mice) entrain to 24 h L:D cycles, but upon transfer to constant darkness (constant darkness) exhibit an extremely short free-running circadian period (~22-23 h), and subsequently become behaviorally circadian arrhythmic (Zheng et al., 1999). Moreover, *Per2*$^{m/m}$ mice have been characterized as exhibiting robust increases in ultradian rhythm power after the loss of circadian rhythmicity in constant darkness (Abe et al., 2002; Bae et al., 2001; Riggle et al., 2022; Zheng et al., 2001; Zheng et al., 1999)). We used *Per2*$^{m/m}$ mice to evaluate the ability of the continuous wavelet transform analysis described above to detect: (1) changes in circadian period upon transfer from long day to constant darkness, (2) the loss of circadian rhythmicity following prolonged exposure to constant darkness, and (3) the emergence of power in the ultradian domain following the loss of circadian rhythms, and in doing so further characterize the ecological validity of the analytic workflow used here.

Animals and data collection: This experiment used mutant (*Per2*$^{m/m}$: B6.Cg-*Per2*^{tm1Brd} *Tyr*$^{c-Brd}$/J, JAX#: 003819 [albino]) and WT (C57BL/6J, JAX#: 000664 [black]) mice ordered directly from the Jackson Laboratories (Bar Harbor, ME, USA). Female mice (*Per2*$^{m/m}$: n=5; WT: n=7;

~5 weeks of age) were singly-housed in 12L:12D under passive infrared motion sensors. A more extensive analysis of data from these mice has been reported elsewhere. The data described here (in Experiment 1.3) are a re-analysis of locomotor activity records from *Per2*$^{m/m}$ mice that were previously reported in a study of sex differences in circadian behavior (Riggle et al., 2022); the data are used here solely for the purposes of validating the accuracy and precision of the continuous wavelet transform ability in measuring period and power in a model of circadian arrhythmia. Mice were kept in 12L:12D for 21 days to establish a baseline of entrained locomotor activity and were then transferred to constant darkness. Locomotor activity data were analyzed using the continuous wavelet transform analytic pipeline described in Experiment 1.1 and illustrated in Figs. 9A and 9B. Specifically, (1) locomotor activity records were diurnally parsed, and light-phase and dark-phase data were concatenated and subjected to the continuous wavelet transform to generate scalograms and power distribution plots (Fig. 9A), and (2) diurnally-parsed data were band-pass filtered into short-, intermediate- and long-duration TAU' windows and subjected to the continuous wavelet transform to identify peak instantaneous UR period within each window (Fig. 9A).

Experiment 2. Circadian and sex differences in UR period and power

Methods. Male (n=20) and female (n=20) mice (4 weeks of age) were singly housed in 12L:12D upon arrival in the laboratory. Following <1 week of adaptation, passive infrared motion detectors were mounted above the cages and home cage locomotor activity data collection began (= *week 0*). Locomotor activity during the 10 days immediately preceding the end of *week 6* (on *day 42* of the study) were exported as a time series for behavioral analyses via the continuous wavelet transform analytic workflows described and validated in *Experiment 1*.

Additionally, in an effort to replicate the *week 6* data and to evaluate the stability and precision of quantitative measures of UR parameters generated by the continuous wavelet transform, identical continuous wavelet transform measures were repeated on the same mice two weeks later (beginning on *week 8*). Due to loss of data from channel dropouts, final sample sizes were: week 6; 18 females and 17 males; week 8: 18 females and 16 males. After the week 8-10 measurement interval, photoperiod manipulations began (*Experiment 3*).

Experiment 3. Effects of circadian entrainment to long and short photoperiods on URs

Methods. Following 10 weeks of exposure to 12L:12D in *Experiment 2*, male (n=20) and female (n=20) mice were subjected to a sequence of increasing and decreasing day lengths as follows: mice were transferred from 12L:12D (intermediate day) to 16L:8D (long days), where they remained for 6 weeks; mice then were transferred to 8L:16D (short days), where they remained for 10 weeks. As in previous analyses, 10 days of locomotor activity data were collected and analyzed via continuous wavelet transform. In long days and short days, locomotor activity was examined after 6 weeks and in short days replicated again twice over 4 more additional weeks. Final sample size in each condition was as follows: long day (week 6: 19 F and 19 M), short day (20 F and 20 M).

Experiment 4. Effects of gonadectomy on URs

Methods. A separate cohort of 4 week old male and female mice, ordered from Jackson Labs, were subjected to surgical gonadectomy (males: orchidectomy [GDx, n=17]; females: ovariectomy [OVx; n=7]) or were sham-operated (sham-GDx [n=15]; sham-OVx [n=7]). Gonadectomy was performed under 3-4% isoflurane/O_2 gas anesthesia. In males, a ventral midline incision was made, testicular blood vessels were ligated and cauterized, and testes

removed. In females, after a dorsal midline incision, ovarian blood vessels were ligated and cauterized, and the ovaries were removed. Incisions were closed with non-resorbable vinyl sutures and cutaneous wound clips. Topical antibiotic ointment was applied to the wound site. Analgesic buprenorphine was administered immediately after surgery and every 12 h for the next 48 h. The sham procedure replicated the GDx or OVx procedure, except tissues were not ligated or removed. Animals were allowed 7 weeks to recover, after which time locomotor activity data were collected for 4 weeks via home-cage passive infrared motion detectors. Surgical condition was confirmed in all mice at the end of the study via necropsy.

Results

Experiment 1.1: Validation of the analytic workflow – circadian modulation and parsing.

In order to validate the analytic workflow (Fig. 9), simulated locomotor activity records were created so as to contain a naturalistic waveform of circadian activity interpolated with known ultradian periods (τ) (see Fig. 10A for representative records; see supplementary methods for details of activity simulation). Each record contained a medium-duration (τ'_m) and a longer-duration (τ'_l) UR, the periods of which either remained fixed over the entire circadian cycle (unmodulated), or varied systematically between circadian phases (modulated; Fig. 10B). Light phase and dark phase activity were separated (parsed) for ultradian power structure and ridge period analyses either prior to ('pre-parsed') or after (post-parsed') performing each wavelet analysis. In pre-parsed records, ultradian power structure plots contained clear, high-amplitude peaks in scalogram power that corresponded closely to the interpolated τ'_m and τ'_l, and differed between the light and dark phases (i.e., were circadian-modulated; Fig. 10C). In contrast, when the same activity records were either parsed *after* the analyses (post-parsed) or not parsed at all

(unparsed), power structure waveforms were distorted: UR spectral power was reduced, peaks appeared less distinct, and they occurred at values that did not as closely match the interpolated URs (Fig. 10D). Diurnal parsing after performing the analyses also created sharp crepuscular discontinuities (edges) in the wavelet matrix, readily visualized by comparing post-parsed and pre-parsed scalograms (inset plots in Figs. 10C, 10D). These near-instantaneous shifts in power are unlikely to reflect actual changes in URs over time *in vivo* as daily activity onsets and offsets are not generally discrete transitions when measured with passive infrared detectors. Finally, power structure analyses of unparsed data also yielded multiple peaks that approximated the interpolated UR periods; however, outside of an *in silico* period-recovery paradigm, it would not be possible to determine which phase of the circadian cycle each individual UR was occurring in.

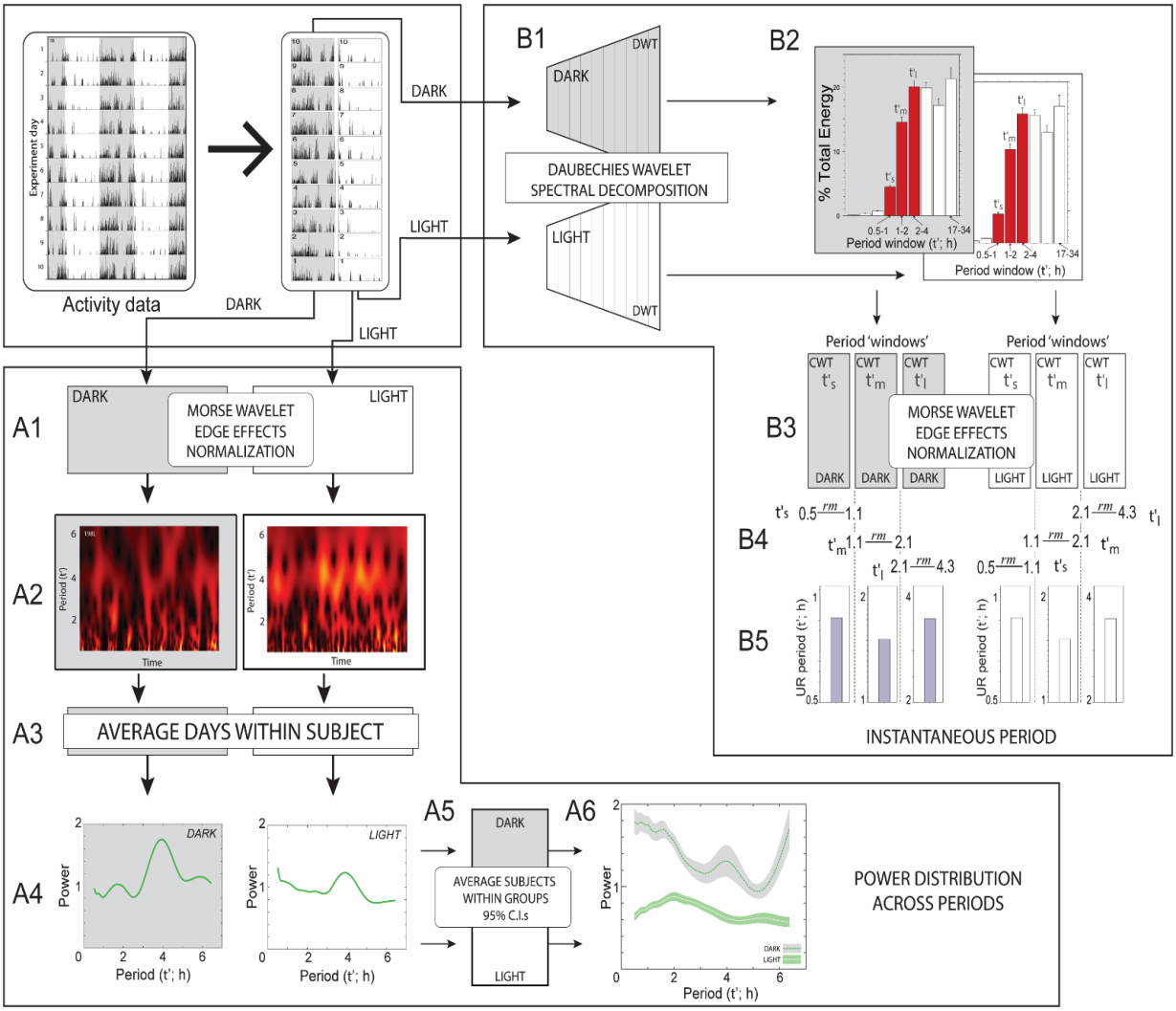

Figure 9. Ultradian Power structure and ridge period analysis workflow.

Examples of double-plotted locomotor activity records (actograms) from mice in a 12:12 photocycle are depicted in the top panel, followed by schematic illustrations of two wavelet-based calculations for measurement of ultradian power and period. (A) Quantification of the distribution of wavelet power across ultradian periods. Locomotor activity records (data time series binned at 1 min intervals) were parsed into dark phase (grey) and light phase (white) components (diurnal parsing), which were then concatenated within photocycle to generate dark phase only and light phase only time series consisting of 10 consecutive phases. [A1] Phase-specific time series were then convolved with a generalized Morse analytic wavelet ($\gamma = 3$, $\beta = 10$) across a period range of 0.5 to 6.5 h, edge effects were managed, the resultant matrices were normalized by their average total matrix value, and their magnitudes were found. [A2] Idiographic analyses permitted evaluation of individual, representative scalograms, depicting dark and light phase specific wavelet matrix cross correlation. [A3] Next, the magnitude of the normalized matrices were averaged across time, which allowed calculation of average period across power collapsed over experimental days for a given subject. [A4-A5] These values were

Figure 9, continued: then combined within treatment group to generate mean power values at periods across the ultradian domain and bootstrapped to generate 95% confidence intervals. [A6] Individual dark and light phase power vs. period traces, prior to bootstrapping, for the 3 actograms depicted in the top panel. (B) Measurement of peak period within ultradian time bands. Actograms were parsed and concatenated into light and dark phase components as in panel A. [B1] Spectral decomposition was performed on locomotor activity records of 40 mice (17 F, 18M) using a symlet 6 Daubechies wavelet identified 9 period bands spanning ultradian and circadian domains, 3 of which were empirically determined to contain high levels of ultradian power; these 3 period bands (τ'_s, τ'_m , τ'_m ; dark grey shading) defined windows for subsequent period measurements. [B3] Diurnally-parsed time series were convolved with a generalized Morse analytic wavelet ($\gamma = 3$, $\beta = 10$; continuous wavelet transform) separately within each of the period ranges ('windows') defined by the spectral decomposition, edge effects were managed, the resultant matrices were normalized by their average total matrix value, and their magnitudes were found. The dashed arrow indicates common continuous wavelet transform-based convolution operation that was performed (separately) for calculating power distributions and for calculating period within each window. [B4] Ultradian periods were identified as the average of the approximate periods corresponding to the maximum wavelet value over time, i.e. the relative maximum (*rm*) value within each window, or the 'wavelet ridge'. [B5] Individual period measures within each ultradian window for the 3 actograms depicted in the top panel (note axis is on log scale).

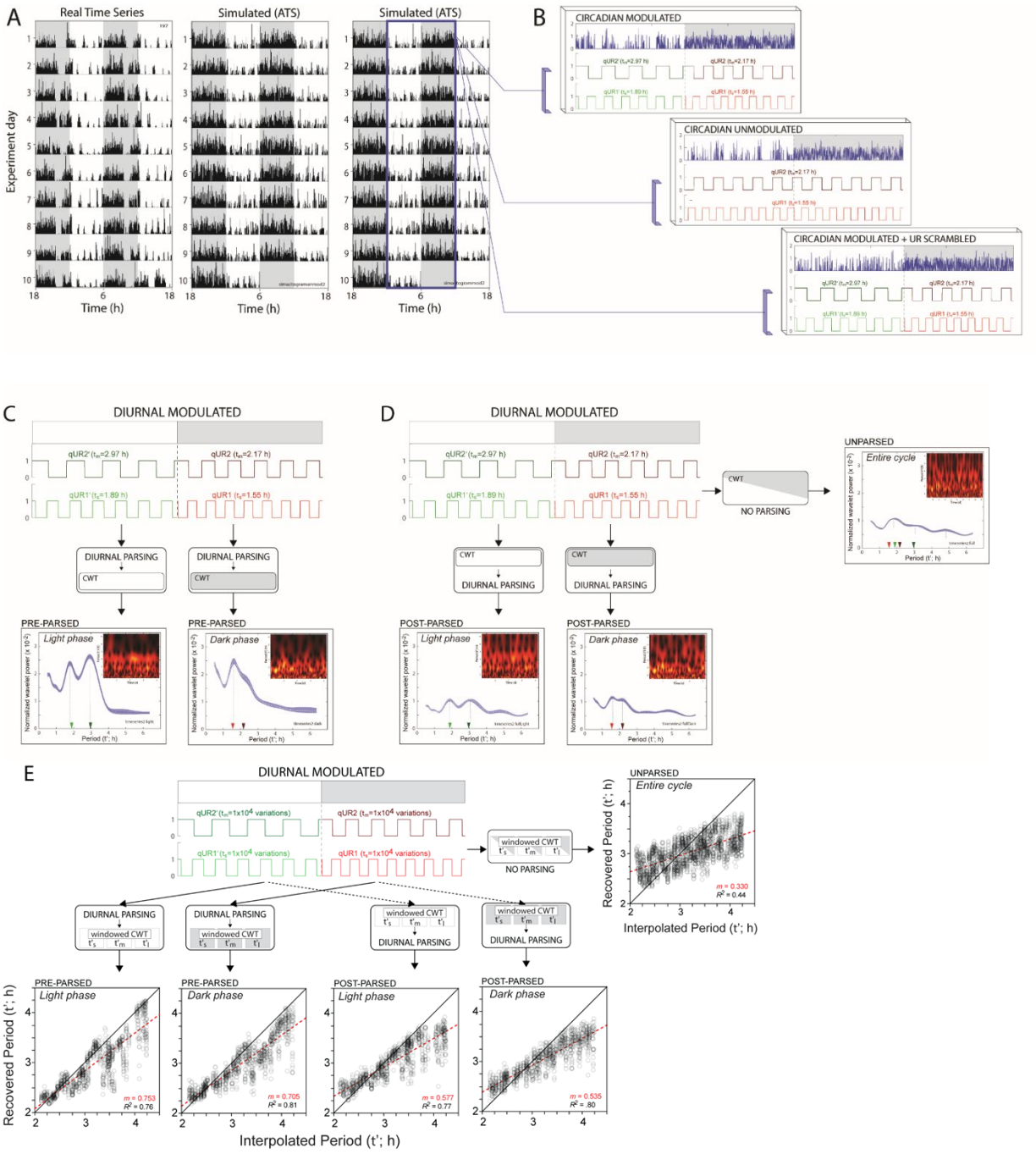

Figure 10. Validation of analyses using synthetic behavior containing known ultradian periods.

(A) Representative double-plotted actograms depicting 10 days of locomotor activity (in a 12L:12D photocycle, collected via passive infrared sensors) of a real C57BL6J mouse (left), and in two synthetic actograms (simulated activity record) generated by a computational model of locomotor activity with circadian parameters, and adulterated with known ultradian rhythm components. (B) Circadian locomotor activity records each contained randomly-selected UR periods in the τ'_m and τ'_l bands. In *circadian modulated* records, the period of each UR periods

Figure 10, continued: differed consistently between the light and the dark phases of the circadian cycle (top panel); in *circadian unmodulated* records, each UR period remained constant regardless of circadian phase (middle panel). Finally, in a control group, circadian-modulated UR periods were generated, but reordered randomly ('scrambled') within each circadian phase such that circadian structure and power were preserved, but all ultradian power was random across periods (bottom panel). (C,D) Effects of diurnal parsing on the power-period distribution. Power-period distributions were calculated as described in Fig. 1A. Diurnal parsing was performed by separating and concatenating Simulated activity records into records consisting of light phase only or dark phase only activity either *prior to* continuous wavelet transform analyses (pre-parsed) or *after* performing the continuous wavelet transform analyses (post-parsed). Analysis of unparsed records are depicted as a control comparison. Below each parsing schematic is depicted a power-period plot composed of the average of 10 Simulated activity records created with modulated UR periods with a known average value (as indicated above square-wave UR schematics), and with bootstrapped ±95% confidence intervals. Vertical lines descend from peak values in the power-period distribution plots. Inset plots depict a representative scalogram of one simulated activity record in each group. Inverted arrowheads along the abscissae identify expected UR period values for each circadian phase. Note the greater normalized wavelet power and in most cases more distinct peaks after pre-parsing of simulated activity records. (E) Effects of diurnal parsing on UR period measurement. UR periods for the τ'_m, τ'_l bands were calculated as described in Fig. 1B. Simulated activity records were either pre-parsed or post-parsed, as in panels C and D. Regression plots depict UR period values in the τ'_l band (abscissa) vs. τ'_l values obtained via continuous wavelet transform analysis (ordinate) for the light and dark phases of pre-parsed or post-parsed simulated activity records. Analyses of unparsed records are also depicted. For each period-recovery analysis, 1000 simulated activity records were each created with 2 randomly-selected, circadian-modulated UR periods; τ'_m and τ'_m were calculated as the maximum wavelet ridge value for each window. Solid black line indicates ideal period recovery (slope (*m*) = 1.0), and dashed red line indicates regression slope obtained for each parsing scheme in each circadian phase. Regressions in panel E depict only τ'_l values (period range: 2.13-4.26 h); similar outcomes were obtained for τ'_m URs.

Experiment 1.2: Segmentation of the ultradian frequency spectrum

A spectral decomposition analysis using a discrete wavelet transform identified 3 period bands (τ' bands) that contained a disproportionate amount of the total variance in the ultradian domain: (1) a short UR band, from 0.53 h – 1.07 h [designated 'tau-prime short', or τ'_s], (2) an intermediate-duration UR band, from 1.07 h – 2.13 h [τ'_m], (3) a longer UR band, from 2.13 h – 4.26 h [τ'_l]) (Fig. 10E). Note that the circadian period band (discrete wavelet transform detail

i=10) also contained a substantial portion of the spectral variance. In addition, these three bands (which contain periods from 0.53 h – 4.26 h; discrete wavelet transform details 5-7), exclude information from power at periods of 8 h and 12 h, and thereby avoid artifacts arising from the interval between light-dark transitions in long (16L:8D), intermediate (12L:12D), and short (8:16D) photoperiods.

Instantaneous period in each of these three τ'-bands was measured in activity records from Experiment 1.1, and a period-recovery analysis was performed to evaluate accuracy and precision of the period estimates. Simulated locomotor activity time series data, adulterated with modulated or unmodulated URs, were passed through the continuous wavelet transform limited to either the τ'_m or the τ'_l band. As in Experiment. 1.1, data were either pre-parsed or post-parsed. Peak scalogram power defined instantaneous UR period for a given τ'-band. Period-recovery analyses indicated that measures of instantaneous period in pre-parsed records were strongly and positively correlated with the periods of interpolated URs (regression coefficients: light phase = 0.753; dark phase = 0.705; $p<0.0001$; Fig. 10F). Post-parsing yielded substantially lower regression coefficients (light phase = 0.577; dark phase = 0.535; $p<0.0001$; Fig. 10E; Table 1).

In sum, simulation results from Experiments 1.1 and 1.2 indicate that power structure and ridge period calculations reliably recover the expected UR power and period values from a complex artificial activity waveform. Post-parsed and pre-parsed data yielded UR peaks with period and phase accuracy, although peaks generated by pre-parsed data were generally higher in amplitude and thus more precise. Post-parsed data also exhibited sharp crepuscular discontinuities in the wavelet matrix, which are unlikely to correspond to actual activity and thus may constitute artifacts. Period measures in the decomposed τ'_m and τ'_l bands were also more

accurate when locomotor activity records were pre-parsed. Taken together, the simulation data indicate that power structure and ridge period calculations: (1) accurately quantify the distribution of rhythmic power in complex (non-stationary, multiple periods) ultradian activity records, (2) permit specification of UR power and period features to specific circadian phases via parsing, (3) yield more accurate and precise results when parsing is performed prior to wavelet analyses.

Experiment 1.3: in vivo validation.

Among WT mice housed in 12L:12D, power structure analyses identified a clear circadian period at 24 h (Fig. 11A). Following transfer to constant darkness, power in the circadian domain remained ~24 h in WT mice (Fig. 11A) but exhibited a period of ~22-23 h in *Per2*$^{m/m}$ mice (see Methods for more details), as previously reported (Fig. 3B; (Riggle et al., 2022; Zheng et al., 1999)). Subsequently, 4 of 5 *Per2*$^{m/m}$ mice exhibited circadian arrhythmicity in constant darkness; this was accompanied by a broad spectrum reduction in power in the circadian waveform (Fig. 11B). An increase in UR power (~2-6 h; Fig. 11B) was commonly associated with circadian arrhythmia, an observation consistent with prior reports of disinhibition of URs in arrhythmic mutant mice (Bunger et al., 2000; Zheng et al., 2001; Zheng et al., 1999). In contrast, WT mice retained circadian rhythms in constant darkness and exhibited no obvious changes in CR or UR power as compared to their measures during early exposure to constant darkness (Fig. 11A). Finally, ridge period analyses were performed on locomotor activity sampled from intervals during which distinct chronotypes (free-run, arrhythmicity). τ'_1 values were calculated for each mouse and aggregated within genotype groups: τ'_1 was similar in WT and *Per2*$^{m/m}$ mice while free-running in constant darkness, but was significantly longer in *Per2*$^{m/m}$ mice after they became circadian arrhythmic (Fig. 11C).

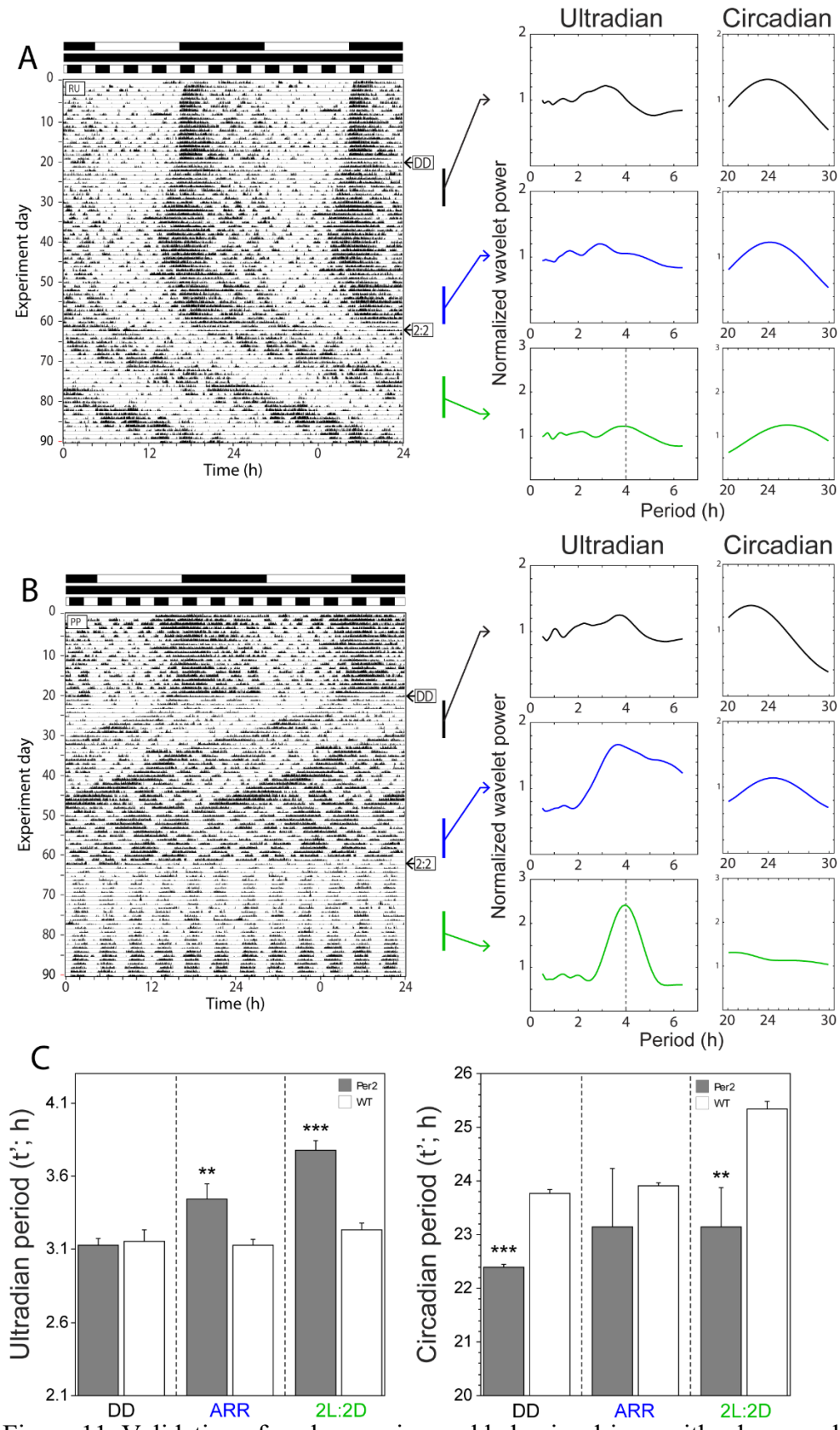

Figure 11. Validation of analyses using real behavior driven with a known ultradian period.

Figure 11, continued: Representative double-plotted actograms of (A) a WT female mouse and (B) a homozygous *Per2*^{Bdrm1} mutant (*Per2*$^{m/m}$) female mouse housed in a 12L:12D light cycle, then in constant darkness (indicated by → "DD"), and finally in a 2L:2D light:dark cycle (indicated by → "2:2"). Black and white bars along the abscissae indicate intervals of darkness and light, respectively. Black (early DD, when wildtype and *Per2*$^{m/m}$ were both free running) , blue (late DD when *Per2*$^{m/m}$ mice were arrhythmic and wildtype mice remained free running), and green (during exposure to 2L:2D) vertical bars indicate 10 day intervals of locomotor activity that were subjected to wavelet analyses, the results of which appear to the right of each corresponding interval. Separate power plots depict ultradian (.5-6.5 h) and circadian (20-30 h) analysis windows for each of the analyzed epochs. Continuous wavelet transform and power-period plots were calculated as described in Fig. 1A. (C,D) Mean +/- SEM ultradian (τ'_1 band) and circadian (20-30 h band) period of female WT mice (n=7) and *Per2*$^{m/m}$ mice that exhibited circadian arrhythmia in constant darkness (n=4). UR periods (maximum wavelet ridge values) were calculated as described in Fig. 1B. * $p<0.05$ ** $p<0.01$ *** $p<0.001$ vs WT value

Mice were then exposed to a high-frequency T-cycle (photocycle) (2L:2D; period = 4 h;) for several weeks. WT mice continued to exhibit free-running locomotor activity in 2L:2D, with a period > 24 h, with some evidence of masking effects imposed by the T-cycle (Fig. 11A). *Per2*$^{m/m}$ mice, in contrast, exhibited strong masking responses to 2L:2D, with high levels of locomotor activity and rest aligned with the dark and light phases, respectively. Thus, *Per2*$^{m/m}$ mice manifested a behavioral UR with a known periodicity, driven by the T-cycle. We then evaluated whether power structure and ridge period analyses could accurately quantify this environmentally-driven behavioral UR. Power structure plots of *Per2*$^{m/m}$ mice contained clear and prominent maxima at periods approximating 4 h, and ridge period measures in the τ'_1 band also indicated that activity occurred with a period near 4 h (mean +/- SEM = 3.77 +/-0.07).

In summary, Experiment 1 provided convergent evidence validating the accuracy and precision of wavelet-based analyses for the measurement of ultradian power distribution and period in mice. We next sought to extend these analyses to evaluate URs in mice exposed to

environmental and hormonal manipulations previously reported to modulate the UR waveform in diverse mammalian models. Thus, Experiments 2-4 employed power structure and ridge period analyses to quantify group-level effects of sex (Experiment 2), circadian entrainment (Experiment 3), and gonadectomy (Experiment 4) on UR power and period.

Experiment 2. Circadian and sex differences in UR period and power

Circadian rhythms: Male (n=20) and female (n=20) mice housed in 12L:12D exhibited normal nocturnal circadian rhythms in locomotor activity, with intermittent active bouts during the light phase (Fig. 12A). After the exclusion of broken channels, the Lomb-Scargle periodogram identified the presence of 24 h rhythm in all individuals, indicative of entrainment to the photocycle. Circadian power was greater in females than males (Fig. 34 (see appendix) $F_{1,33}$=4.55, p<0.05; cf. (Iwahana et al., 2008; Yan & Silver, 2016)).

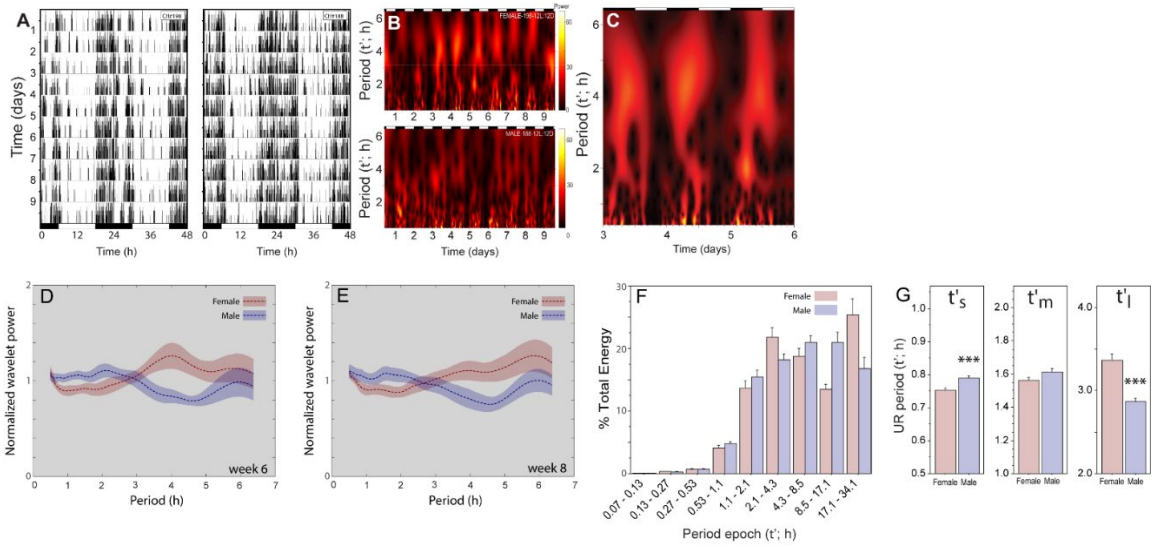

Figure 12. Sex differences in ultradian power and period.

(A) Representative double-plotted locomotor activity records of female (left) and male (right) C57BL6/J mice housed in a 12L:12D photocycle over 10 days as measured with passive infrared recording devices in the home cage. Black and white bars along the abscissae indicate intervals of darkness and light, respectively. (B) Scalograms depicting the scaled cross-correlation value of the Morse wavelet (continuous wavelet transform; β =10; γ=3; UR analysis

Figure 12, continued: window: 0.5 – 6.5 h) for the 10 day time series of locomotor activity in panel A. Magnitude scale bar references panels B &C. (C) Re-depiction of 72 h from the scalogram in panel B permits visualization of relatively higher cross-correlations (i.e., power) present at multiple ultradian periods simultaneously. (D) Average cross-correlational power at each scale-approximated period derived from the continuous wavelet transform on a time series consisting of locomotor activity during 10 consecutive dark phases in 12L:12D (pre-parsed). Separate power curves are depicted for male (blue) and female (red) mice; the curves depict mean ± 95% confidence intervals (Cis) generated by bootstrapping male and female groupings of these curves (Bootstrapped: 2000x ; 18 females and 17 males). (E) Power/period curve generated by continuous wavelet transform of 10 days of dark phase locomotor activity data as in panel D from the same mice as depicted in panel D, two weeks later (i.e., on *week 8* in 12L:12D; 18 females and 16 males). (F) Mean +SEM percent of total spectral energy explained by each detail level of wavelet coefficients for the time series consisting of locomotor activity over 10 consecutive days in 12L:12D of female and male mice. Abscissa indicates period of details 2-10 (in h). Details 5, 6 and 7 encompass intervals defined as short, medium and long UR periods (τ'_s, τ'_m, τ'_l, respectively). (G) Mean (+ SEM) ultradian periods (τ') of pre-parsed dark phase locomotor activity data within each of the 3 UR analysis intervals identified in panel F (short τ'[τ'_s: 0.53 – 1.1 h], medium τ' [τ'_m : 1.1 – 2.1 h], and long τ' [τ'_l : 2.1 – 4.3 h]), and via continuous wavelet transform methods described in Fig. 1B.

Ultradian rhythms: URs were next evaluated using power and period analyses described in Fig. 1 and validated in Experiments 1.1 - 1.3. Locomotor activity (10 days) were pre-parsed into dark phase and light phase records prior to all analyses.

UR power distribution. Scalograms identified multiple regions of high cross-correlation in the ultradian band (Fig. 12B); diurnal variations in UR power and period were also common (Fig. 4C). During the dark phase, power structure plots revealed a non-uniform power distribution across the ultradian spectrum for both sexes. In females, power peaked at ~4.0 h and was lower across a range of shorter periods (τ': 1.0 – 3.5 h; Fig. 12D). In males, power was highest in a similar range of shorter periods (τ': ~1.0 – 3.0 h) with a conspicuous decrease in the ~4.0 h range (Male (n=18) and Female n=17); Fig. 12D). Sex differences in the distribution of rhythmic power were identified via non-overlapping 95% CIs: power was greater in males from

~0.75 h to ~2.25 h and in females from ~3 h to ~5 h. power structure analyses performed 2 weeks later (*week 8* in 12L:12D) yielded strikingly similar results (Fig. 12E), indicating that power distribution across ultradian periods is relatively stable and reliable over time, within and between sexes.

During the light phase, power structure plots were similar in males and females (Fig. 35A). Power peaked at ~3.0 h, with lower power values preceding and following the peak. Light phase period-power relations were also similar on *weeks 6* and *8* (Fig. 35B).

UR period. Fragmented wavelet scalograms were decomposed using a symlet wavelet (as described in Experiment 1.2) to identify the distribution of spectral energy across the UR domain. Males and females both exhibited substantial power in the τ'_s, τ'_m, and τ'_l bands (encompassing 0.53 - 1.07 h; 1.07 - 2.13 h and 2.13 h- 4.26 h; Fig. 12F). As in Experiment 1 these bands were analyzed individually by extrapolating UR period from the maximum value of the continuous wavelet transform scalogram within each band. τ'_l was significantly longer in females than males in the dark phase (Fig 12G; $p<0.0001$), but not in the light (Fig. 35C; $p>0.30$; sex x phase interaction: $F_{1,66}=21.7$, $p<0.0001$); small but significant sex differences were also evident in dark phase τ'_s ($p<0.005$; Fig. 12G). Light phase UR period did not differ between males and females in any period band ($p>0.30$, all comparisons). Overall, UR period was significantly longer during the light phase compared to the dark phase in the τ'_s band ($F_{1,66}=178.4$, $p<0.0001$) and in the τ'_m band ($F_{1,66}=15.0$, $p<0.0005$), and among males in the τ'_l band ($p<0.05$) (Fig. 12G vs. Fig. 35C).

Period measures obtained 2 weeks later yielded similar, phase-specific effects of sex on τ'_l (sex x phase interaction: $F_{1,64}=29.0$, $p<0.0001$), τ'_s ($p<0.005$), and no evidence of sex differences in light phase UR period ($p>0.05$, all τ' bands). Period measures from *week 6* also positively

correlated with those obtained two weeks later (*week* 8: τ'_s slope = 0.82, $p<0.0001$; τ'_m slope = 0.45, $p<0.0005$; τ'_1 slope = 0.73, $p<0.0001$), indicating reliability and stability over time.

In sum, dark phase UR power was distributed across shorter periods in males compared to females, but light phase power was distributed similarly in both sexes. During the active phase τ'_s and τ'_m were longer in males, and τ'_1 was longer in females. Overall, UR periods were also longer in the rest (light) phase. Taken together, power structure and ridge period analyses exhibited a precision sufficient to identify multiple sex differences in UR power and period which confirm and extend prior studies of sex differences in ultradian behavior patterns (Daan et al., 1975; Prendergast, Cisse, et al., 2012; Prendergast & Zucker, 2016; Smarr et al., 2017; Wang et al., 2014; Wollnik & Dohler, 1986; Wollnik & Turek, 1988).

Experiment 3. Effects of circadian entrainment to long and short photoperiods on URs.

We next examined whether the entrainment state of the circadian pacemaker modulates URs by exposing all mice to a series of different experimental day lengths: intermediate- (12L:12D), long- (16L:8D) and short-duration (8L:16D) photoperiods. Lomb-Scargle periodogram *a*nalyses first confirmed that mice exhibited typical nocturnal patterns of circadian entrainment to the respective experimental photoperiods (Figs. 35A-35F). Peak values in the periodogram were greater in females than males ($F_{1.107}=24.3$; $p<0.0001$; Fig. 34G). Circadian rhythm power was comparable in all photoperiods among females ($p>0.30$, all comparisons), but among males, power was greater in long days than short days ($p<0.05$; Fig. 34G).

UR power distribution. Entrainment to long and short photocycles systematically altered UR power in both females and males (Fig. 13A, 13B). In the dark phase, overall UR power was greater in long days than in intermediate days, and greater in intermediate days compared to

short days; sex differences in the distribution of UR power were maintained in all photoperiods (Fig. 13C-13E). Photoperiod also conspicuously reshaped power structure waveforms. In long days, power was concentrated at ~4 h in both sexes, whereas in short days peak UR power shifted to higher (>5 h) periods. In all photocycles, males exhibited greater high-frequency UR power (τ'<2 h) than females. Conversely, light phase UR power was greatest in short days, and decreased monotonically with longer day lengths (Fig. 36A-C). In short days, light phase power also shifted towards shorter periods (1-3 h) and away from longer periods (Fig. 36C). Regardless of day length, however, females and males exhibited remarkably similar distributions of light phase UR power (Fig. S3).

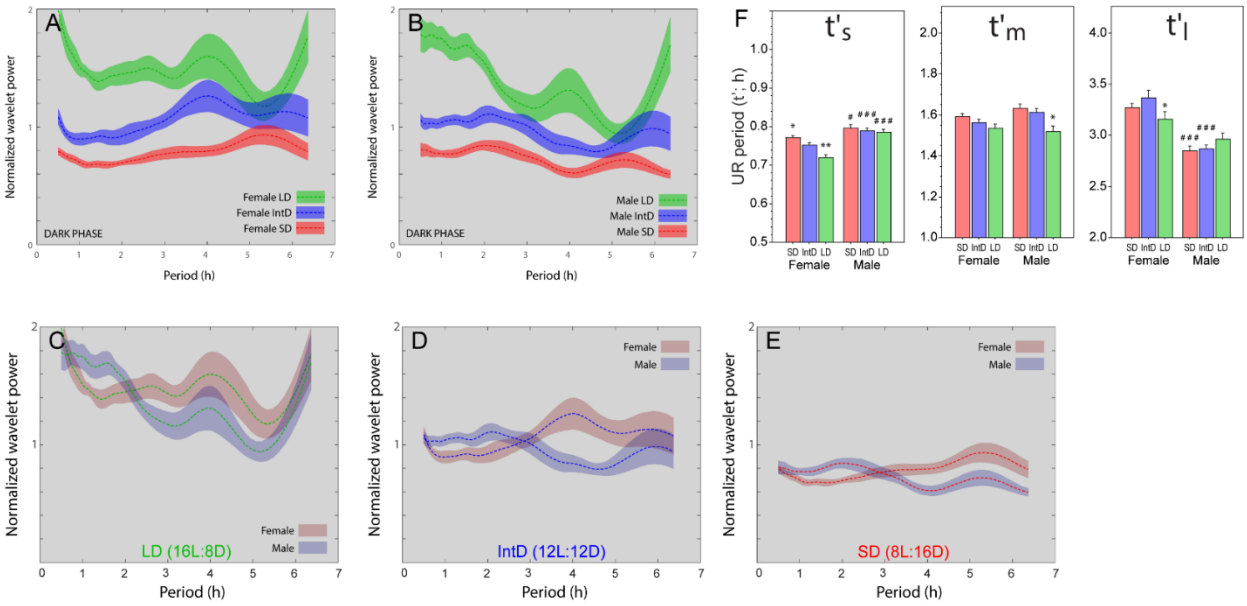

Figure 13. Photoperiodic modulation of ultradian power and period.

Power-period plots (±95% CI) calculated by continuous wavelet transform of 10 days of pre-parsed dark phase locomotor activity data from (A) female (long day: n=19, intermediate day: n=18, short day: n=20) and (B) male (long day: n=19, intermediate day: n=17, short day: n=20) mice after adaptation to 16L:8D (green), 12L:12D (blue) or 8L:16D (red) photoperiods. See Figure S2 for confirmation of circadian entrainment. (C-E) Re-depiction of dark phase power/ period curves from panels A and B to permit direct comparisons of male and female mice in (C) 16L:8D, (D) 12L:12D, and (E) 8L:16D. (F) Mean (± SEM) instantaneous ultradian periods (τ') of pre-parsed dark phase locomotor activity data in the τ' in the τ'_s, τ'_m and τ'_l period analysis

Figure 13, continued: bands. *:*p<0.05, **p<0.01 ***p<0.001 vs.IntD value within sex; #p<0.05, ###p<0.001 vs. females within DL*

UR period. UR period depended on the interaction of photoperiod and sex, in a circadian phase-specific manner (τ'_s: $F_{2,214}=3.97$, $p<0.05$; τ'_m: $F_{2,214}=3.18$, $p<0.05$; τ'_l: $F_{2,214}=3.58$, $p<0.05$; Fig 5F). In the dark phase τ'_s of females lengthened as day length decreased ($p<0.05$, all comparisons), but male τ'_s did not ($p>0.30$, all comparisons); τ'_m was shortest in long days in both sexes ($p<0.05$ vs short day values, both comparisons; Fig 13F). Photoperiod was largely without effect on τ'_l. Finally, in most instances, τ'_s was longer in males and τ'_l was longer in females (Fig 13F). In the light phase, sex differences were largely absent across most photoperiods and τ' bands (Fig. 36D).

<u>*Longitudinal evaluation in short days*</u>. Power structure of dark phase URs on *week 6* was similar to that on *weeks 8* and *10* (Fig. 37D), and a similar pattern of results obtained for light phase locomotor activity data, with the exception of an increase in longer-period (~5-6 h) power on *week 10* in both sexes (Fig. 37). Similarly, there was no main effect of week in short days ($F_{2,228}=2.2$, $p>0.10$, all ANOVAs) and no interaction effect of week x sex x phase ($F_{2,228}=.52$, $p>0.50$, all ANOVAs) on UR period in any of the 3 period bands.

<u>*Diurnal rhythms in UR power*</u>. Direct juxtaposition of dark and light phase period-power plots identified striking diurnal modulation of power structure distributions (Fig. 38). In long days, dark phase power exceeded light phase power across the entire UR period domain (Fig. 38A), this diurnal modulation of UR power was greatly attenuated in intermediate days (Fig. 35B, E), and reversed in short days (Fig. 35C, F).

In sum, day length affected ultradian period and power, and exerted opposite effects in the dark and light phases. In both sexes, the incremental decrease in day length attenuated dark phase UR power and augmented light phase UR power. Together, power structure and ridge period analyses identified consistent patterns of power and period modulation by photoperiod in male and female mice.

Experiment 4: Effects of gonadectomy on URs

This experiment tested the hypothesis that sex differences in UR power and period are maintained by concurrent gonadal hormone secretion (i.e., activational effects).

UR power distribution. As in Experiment 2, gonad-intact females exhibited lower dark phase UR power than intact males across a range of shorter (1.5 – 3 h) periods (Fig. 14A), but power in the 3 – 5 h range was not significantly greater than that of males (cf. Fig. 14D). OVx caused minor increases and decreases to dark phase UR power, in narrow bands around 2 and 4 h, respectively (Fig. 6B), and GDx increased power between 0.5 – 1 h, and decreased power from 2.5 – 3.5 h (Fig. 14C). Light phase power again peaked between 3-4 h and was largely comparable in females and males, (Fig. 14E; cf. Fig. 34). OVx did not affect light phase UR power (Fig. 6F), but GDx flattened the power distribution: increasing power in periods <2 h and decreasing power in periods > 2.5 h (Fig. 14G).

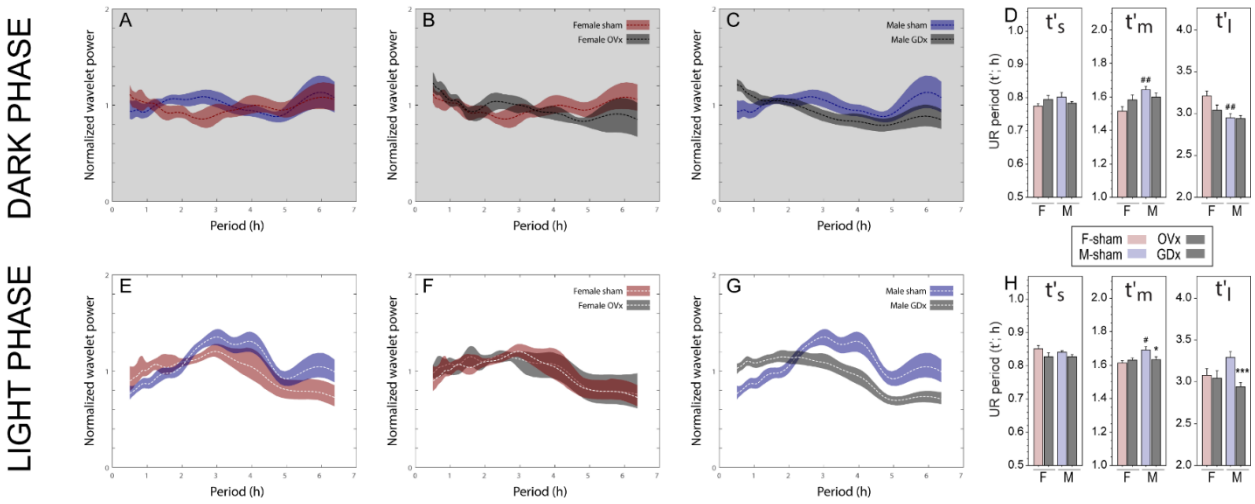

Figure 14. Effects of gonadal hormones on ultradian power and period.

Power-period plots (±95% CI) calculated by continuous wavelet transform of 10 days of pre-parsed dark phase and light phase locomotor activity records from (A, E) sham-operated female (n=7) and male mice (n=15), (B, F) ovariectomized (OVx; n=7)) and sham-operated female (n=7) mice, and (C, G) orchidectomized (GDx; n =17) and sham-operated male (n=15) mice. (D, H) Mean (± SEM) instantaneous ultradian periods (τ') of pre-parsed dark phase and light phase locomotor activity data in the τ' in the τ'_s, τ'_m and τ'_l period analysis bands. *$p<0.05$, ***$p<0.001$ vs. sham-value within sex; #$p<0.05$, ##$p<0.01$ vs. females, within surgical condition.*

UR period. As in Experiment 2, τ'_l depended on sex in a phase-specific manner, and this relation depended on gonadal status (sex x surgery x phase interaction: $F_{1,84}=7.10$, $p<0.001$; Fig. 14D, 14H). Neither dark phase nor light phase τ'_l was affected by OVx ($p>0.50$, both comparisons), but GDx caused a decrease in light phase τ'_l of ~ 20 min ($p<0.0005$) without affecting dark phase τ'_l ($p>0.80$). Sex and gonadal condition also interacted to affect τ'_m ($F_{1,84}=7.80$, $p<0.01$): GDx caused a small but significant decrease in light phase τ'_m ($p<0.05$; Fig. 14H).

Effects of sex on UR period among intact mice in Experiment 4 were similar to those obtained in Experiment 2, despite a smaller female sample size. Specifically, the effect of sex on τ'_l depended on circadian phase (sex x phase interaction: $F_{1,40}=12.0$, $p<0.005$). In addition, light phase period was greater than dark phase period in the τ'_s ($F_{1,40}=24.3$, $p<0.0001$) and τ'_m

($F_{1,40}$=9.73, p<0.005) bands, and among males (p<0.0005) but not females (p>0.10) in the τ'_1 band.

In sum, many effects observed in Experiment 2 also materialized in the longer and shorter photoperiods of Experiment 4: intact males exhibited similar power structure waveforms; dark phase UR periods were longer in males in the shorter period bands, and longer in females in the τ'_1 band; and in females light phase period was greater than dark phase period in every ultradian τ' band. GDx shortened period in select τ' bands, but OVx was largely without effect on ridge periods. The smaller number of female mice in Experiment 4 was associated with greater variability in power structure analyses, but did not obviously increase variability in the ridge period analyses. The male UR period chronotype is also dependent on gonadal hormones in specific period bands. Taken together, the results indicate that in males gonadal hormones exert a more potent effect on the distribution of UR power in the light phase than during the dark phase.

Discussion

Here we report simple-to-implement modifications to wavelet analyses that permit quantification of period and power in ultradian behavioral rhythms. These analyses build on the application of the generalized Morse and Daubechies wavelets to biological rhythms (Blum et al., 2014; Goh et al., 2019; Grant et al., 2020; Guzman et al., 2017; Leise, 2015; Leise & Harrington, 2011; Miyata et al., 2016; Smarr et al., 2017; Smarr et al., 2016; van Rosmalen & Hut, 2021) and extend their utility by allowing: (1) measurement of URs during distinct phases of the circadian cycle, (2) specification of peak period values within discrete bands of the UR spectrum, and (3) aggregation across individuals within treatment groups (Fig. 1). The accuracy and precision of these procedures were validated using *in silico* and *in vivo* models with known ultradian periods in Experiments 1.1 – 1.3. In subsequent experiments, application of these

modified wavelet analyses to mouse locomotor activity records demonstrated that core UR metrics (power structure and ridge period) were repeatable within individuals and treatment groups (Fig. 12D, 12E, 34A,, 37) and across experiments (intact mice in Experiment 2 vs. Experiment 4; light vs. dark phase in Experiments 2 & 3 vs. 4). These procedures thus provide novel analytical tools for the experimental study of URs and permit quantification and description of URs without the limitations inherent in qualitative and/or idiographic analyses of scalograms.

To rigorously probe the sensitivity of these techniques in quantifying URs, we first developed a computational model of mouse circadian locomotor activity, using actual mouse activity as a guide. The model treated the likelihood of a mouse's locomotor activity in any given minute as a probabilistic event whose occurrence and amplitude are modulated by the phase state of known circadian and ultradian parameters. Locomotor activity, however, could still randomly occur at high amplitudes or not occur at all, regardless of phase state. Thus by design, this model attempted to replicated the variability inherent in URs (and, to a much lesser degree, in CRs) in order to remain agnostic to recent conjectures that the variability of URs is not the result of external factors distorting the rhythmic output of an oscillator, but rather may reflect stochastic episodic events which happen to occur in an ultradian range (Blessing & Ootsuka, 2016; Goh et al., 2019). The computational model thus made minimal assumptions (see Supplementary Methods for a full model description), but nevertheless had a high degree of face validity with actual mouse locomotor activity (cf. Fig. 10A vs. Fig. 12A). This model was then used to generate multiple simulated subjects in treatment groups that had shared CR temporal properties common to all groups, but unique URs in each record, generating complex activity waveforms upon which the precision and accuracy of the analyses could be tested. Importantly, in some

individuals and groups the interpolated UR periods were designed to vary over the circadian cycle, and in others UR period remained the same across the light and dark cycles. Overall, the analyses recovered UR period with remarkable fidelity: peaks in power structure plots were in the expected period locations (Experiment 2, Fig. 10C, 10D) specific to each circadian phase; ridge period measures were likewise accurate (Fig. 10F). URs vary over the circadian cycle, and the analysis techniques described here validate a method for quantifying active and rest phase URs separately (Table. 1).

We next evaluated the accuracy of power structure and ridge period analyses on locomotor activity data from actual mice in which real behavioral URs were experimentally introduced. We took advantage of behavioral plasticity exhibited by *Per2*$^{m/m}$ mice which, under prolonged exposure to constant darkness, exhibit short-period free-running CRs, followed by circadian arrhythmicity which coincides with an emergence of ultradian power (Bae et al., 2001; Riggle et al., 2022; Zheng et al., 1999). Power structure clearly documented circadian periods of 22-23 h in female *Per2*$^{m/m}$ mice, the eventual loss of CR power, and an emergence of UR power (Fig. 11B; see also (Riggle et al., 2022)). *Per2*$^{m/m}$ mice also possess the remarkable capacity to synchronize locomotor activity with high-frequency, i.e., non-circadian, light:dark cycles (Bae et al., 2001; Zheng et al., 1999), and in the present study ~4 h ultradian rhythms were exhibited by mice in the 2L:2D photocycle (Fig. 11B). Power structure plots and period measures also clearly indicated power distributions peaking at ~4 h and period measures of ~3.8 h, respectively, both closely matching the behavioral UR imposed by the experimental 4 h T-cycle. This outcome extends the utility of the present analyses beyond simulation data, indicating an ability to accurately and precisely quantify true behavioral URs despite the vicissitudes inherent in real locomotor activity data (Fig 11B).

This analytic approach was applied to quantify changes in URs in response to genomic, environmental, and endocrine factors previously reported to modulate the ultradian waveform. Consistent with observations in numerous and diverse species (Hagenauer et al., 2011; Heldmaier et al., 1989; Prendergast, Cisse, et al., 2012; Prendergast et al., 2013; B. J. Prendergast & I. Zucker, 2012; Siebert & Wollnik, 1991; Smarr et al., 2019; Wang et al., 2014; Wollnik & Dohler, 1986; Wollnik & Turek, 1988), C57BL6/J mice exhibited multiple sex differences in UR power structure and period under a 12L:12D photocycle. In the active phase, UR power was more prominently distributed across shorter periods in males, and among longer periods in females, whereas in the light phase UR power structure was largely indistinguishable between the sexes. Decreasing day length caused a stepwise reduction in dark phase UR power and a corresponding accretion of light phase UR power, but the overall sexually diphenic pattern in wavelet power distribution was maintained. UR measures were stable when reevaluated over multiple 2-week intervals both in intermediate- and short days (animals were not kept in long days for a long enough interval for URs to be similarly re-evaluated at 2 week intervals). In a separate experiment, UR sex differences were influenced by gonadal hormones in a circadian phase dependent manner (Fig. 6). OVx yielded only minor changes in dark and light phase UR power distributions, but castration of males caused a striking shift in the distribution of UR power towards shorter periods. Many small but significant sex and photoperiod effects were evident in τ'_s and τ'_m periods, but a robust sex difference was consistently observed in τ'_l period during the active phase, which was notably longer in females across multiple measurement intervals across two experiments. Entrainment of the circadian system to short photoperiods or OVx eliminated this sex difference, indicating potential convergence among gonadal hormones

and the circadian system's processing of environmental information in the modulation of behavioral URs.

A clear circadian influence on the ultradian waveform was evident across all experiments. The loss of circadian coherence in arrhythmic *Per2*$^{m/m}$ mice gave rise to an increase in UR power, but did not result in a narrow period peak similar to that seen in the 2L:2D light-dark cycle. Circadian phase also strikingly modulated UR power and period (Fig. 38). For example, sex differences in URs were more prominent in the dark phase (Fig. 12 & Fig. 14), and photoperiod exerted opposite effects on light phase and dark phase UR power (Fig. 13). Whether this reflects a sexual diphenism in the ultradian system *per se* or a refraction of well-established circadian sex differences onto URs (Yan & Silver, 2016) requires further dissection. Diurnal modulation of UR power and/or period is evident in both sexes of numerous species, including other mouse strains (BALB/c (Smarr et al., 2017; Smarr et al., 2016)), hamsters (B. J. Prendergast & I. Zucker, 2012), rats (Wollnik & Dohler, 1986), common and tundra voles (van Rosmalen & Hut, 2021), and several arctic vertebrates (Appenroth et al., 2021; Bloch et al., 2013; van Oort et al., 2007). The present data extend these observations to C57 mice and quantify the influence of circadian phase on URs in finer detail. URs persist despite diverse insults to the circadian pacemaker (Abraham et al., 2006; Blum et al., 2014; Bunger et al., 2000; Gerkema et al., 1993; Gerkema et al., 1990; Gerkema & van der Leest, 1991; Vitaterna et al., 1994; Zheng et al., 2001; Zheng et al., 1999), supporting the hypothesis that a functional circadian system is not required for the expression of URs (Prendergast & Zucker, 2016); however, the present data contribute to a substantial body of work which collectively indicates that the circadian system is nonetheless sufficient to impose temporal structure on URs: circadian phase *per se* modifies UR power and period, as does circadian entrainment to long and short

days. The significance of circadian regulation of URs has been reviewed elsewhere (Bloch et al., 2013): UR flexibility may be adaptive when energetic demands compel high amplitude bouts of foraging activity during the rest phase, as has been reported in locomotor and thermoregulatory rhythms of mice (Hut et al., 2011), common voles and tundra voles, under conditions of food scarcity (van Rosmalen & Hut, 2021). Moreover, conditions where circadian environmental cues may be less prominent or less relevant to an individual's short-term survival (e.g., arctic latitudes, lactation) may also favor disinhibition of URs (Appenroth et al., 2021; Bloch et al., 2013; Prendergast, Cisse, et al., 2012; van Oort et al., 2007). In addition, the emergence of prominent, longer-period dark phase URs reported here in short days bears a strong resemblance to UR waveform changes reported in CD-1 mice (Refinetti, 2002), hamsters (Heldmaier et al., 1989; B. J. Prendergast & I. Zucker, 2012), LEW/Ztm rats (Siebert & Wollnik, 1991), and reindeer (van Oort et al., 2007) in response to winter cues, the ecological significance of which may be linked to energetic challenges in seasonal environments, where longer URs may permit longer consolidated rest periods and thereby conserve energy.

It is unclear the molecular mechanics by which circadian clocks and ultradian clocks interact, but the proposed circuitry of the ultradian clock lies spatially adjacent to the SCN in the hypothalamus (Prendergast & Zucker, 2016), so their association may be one at the electrical/neuropeptide level.

Conclusions:

This report describes and validates a set of novel modifications to wavelet analyses that permit quantification of power structure and ridge period with time-frequency resolution that permits precise, accurate, and repeatable measures of UR period and power even in the face of the circadian harmonic contamination and nonstationarity inherent in URs. Using both simulated

and real locomotor activity data, this analytic workflow quantified URs with known features (i.e., UR periods and 2L:2D masking URs) with high accuracy and precision. It permitted derivation of normalized data from the continuous wavelet transform matrix of each individual subject, which was subsequently aggregated into treatment groups, a practice which allows group-level quantitative analyses not possible with an idiographic approach limited to , qualitative evaluations of individual scalograms.

Finally, one important result of applying the wavelet analyses to actual data belies previous notions of the ultradian system as highly variable (Blessing & Ootsuka, 2016; Goh et al., 2019); indeed, although variable in response to experimental manipulations, the power structure and the multimodal periods measured here were stable across time within individuals and across studies. The specification of circadian modulation of UR period and power was notably superior and free of distortions when time series were parsed before the wavelet transform was performed (Figs. 10C, 10D), and the results from all three *in vivo* studies suggest that ultradian power structure in mouse locomotor activity more closely resembles a system with circadian-modulated rather than circadian-unmodulated URs (Fig. 14, Fig. 38). Additionally, separating the UR domain into several empirically-defined period bands permitted quantification of multiple URs, rather than just a single 'peak' UR. Ultimately, this may better characterize the fragmented multimodal scalogram, and thus circumvent a fundamental challenge to the study of URs. Finally, continuous wavelet transform-based measures of UR period and power in several instances confirmed and extended measures obtained independently in prior reports using other quantitative approaches in other species. The approach offers novel and robust analytical tools for the investigation of URs, which may permit accurate and precise disentanglement of the complex waveforms generated by interacting ultradian and circadian clocks.

Chapter 5: Effects of Photic Environmental Cues on Circadian Network Organization in Male and Female Per2 Mutant Mice

Introduction:

Inbred mice carrying a functional knockout of the Period 2 gene become circadian arrhythmic in conditions of sustained constant darkness, with variable latencies (Riggle et al., 2022; Zheng et al., 1999). With prolonged exposure, some arrhythmic mice can even begin to spontaneously recover rhythmicity—a phenomenon that has yet to be reported on a non-Per2 mutant background. The manifestation of this arrhythmicity and recovery is sexually differentiated, and circulating androgens appear to prevent arrhythmia in some male mice, but do not cause either arrhythmia or recovery. Moreover, sex does not explain all the variability seen in the latency to arrhythmia; some as yet to be discovered mechanism is at play (Chapter 4; (Riggle et al., 2022)). The labile circadian system of the *Per2*$^{m/m}$ mouse thus affords opportunities to understand how environmental and biological factors converge to impact the circadian clock.

Circadian rhythms in behavior are an emergent property of different levels of biological organization. Most cells in the mammalian body have a molecular clock derived from a transcription-translational negative feedback loop of several clock genes in which the CLOCK-BMAL (1 & 2) heterodimer drives the transcription and translation of PERIOD (1 & 2) and CRYPTOCHROME(1 & 2) which in turn heterodimerize and inhibit the transcription and translation of CLOCK and BMAL (1&2)(Mohawk et al., 2012). These cell-based clocks, however, are synchronized by tissue -level oscillators which are in turn are synchronized by a superordinate oscillator in the superchiasmatic nucleus of hypothalamus (Herzog et al., 2017; Mohawk et al., 2012; Patton & Hastings, 2018). Circadian arrhythmia and recovery may result from changes any or all of these levels. The variability and months-long duration over which

arrhythmia and recovery manifest poses a major challenge to easy molecular dissection or chronic recordings which might address the level of organization at which loss of rhythmicity and recovery are occurring. Another approach then is to investigate (1) how the initial system state might alter the latency to arrhythmia and propensity toward recovery and (2) the stability of the phenomena.

Photoperiod entrainment has enduring effects on the circadian system which persist long after mice are placed into constant darkness. Prior work (Evans et al., 2013) has demonstrated that the coupling state of the SCN is markedly impacted by entrainment to long and short photoperiods. Rhythms of clock gene expression in the core and shell of the mouse SCN are typically in phase with one another, but following entrainment to very long day lengths (20L:4D), these rhythms become out of phase by 6+ h. These phase relations are evident via luciferase reporting in vitro, and are present immediately following excision of the SCN from the mouse. Restoration of normal (12L-like) phase relations happens gradually, over many days in vitro. In vivo, mice housed in 20L show a compressed alpha upon release into DD, but behavioral effects at the organismal level were not documented beyond a week or so into DD, so the persistence of VLD effects in the circadian system remains unknown. Similarly, work (Gorman et al., 1997) demonstrated (in vivo) a gradual expansion of nocturnal locomotor activity of Siberian hamsters following transfer from long (15L) to short (10L) days, but exposure to very long days (18L) delayed, and in many cases prevented, this alpha decompression. This photoperiodic reorganization does not similarly impact peripheral clock gene rhythms(Evans et al., 2015). This very long day manipulation provides a ready tool for altering the properties of the circadian network in the SCN without as readily altering the periphery. We hypothesized, then, that if arrhythmia (ARR), recovery or both reflected changes in the state of the central

circadian system, then exposure to photoperiods that alter circadian network coupling would affect features of the Per2 chronotype during subsequent exposure to DD. Moreover, that if VLD alters either ARR or recovery then it would be unlikely that changes to peripheral circadian network drive the phenomena, since VLD does not affect peripheral and central coupling (Evans et al., 2015).

In addition, the *Per2*$^{m/m}$ mutant phenomena (i.e., sexually differentiated ARR and recovery) has only been elaborated following transfer of mice from 12L:12D to constant darkness (Riggle et al., 2022). Under such conditions, we identified wide individual differences in many aspects of the Per2 chronotype: (1) the latency to ARR, (2) the incidence of arrhythmia, and (3) the incidence of recovery. These chronotypes may reflect traits that are stable over time within individuals; alternatively, they may instead reflect stochastic processes and thus individual variability merely reflects an underlying difference in probability of rhythmicity. If the former hypothesis is true, then an individual's chronotype during an interval of exposure to constant darkness should be predictive of its behavior during a subsequent interval of DD (and thus the phenotype can be said to be repeatable).

Thus, the aims of this experiment were twofold: First, to investigate how circadian entrainment might impact the constant darkness behavioral organization of *Per2*$^{m/m}$ mice, we allowed male and female animals to entrain to a very short (VSD: 4L:20D), intermediate (IntD: 12L:12D), or very long photoperiod (VLD: 20L:4D) and then placed animals in constant darkness for 110 days. Secondly, to test the repeatability and the stability of arrhythmia incidence, latency, and recovery as traits, mice that were housed in DD were subsequently re-entrained to VSD, IntD, and VLD days for another 30 days, after which time all mice were again

returned to DD for 110 days. Results shed new light on the underlying mechanics of *Per2*$^{m/m}$ circadian organization in constant darkness.

Materials and Methods:

Animals. Adult female (n= 27) and male (n=30), *Per2* mutant mice (*Per2*$^{m/m}$: B6.Cg-*Per2*^{tm1Brd} *Tyr*$^{c\text{-}Brd}$/J, JAX#: 003819) were bred in a mouse colony from homozygous breeding pairs. Experiments were performed on adult mice (170-257 days at the start of the experiment and 425-512 days at the end of the experiment). Estrous cycles of females were not monitored. Mice were housed in polypropylene cages (28 × 17 × 12 cm) on irradiated corncob bedding (Irradiated 1/8" Corn Cobs, Envigo, Indianapolis, IN, USA). Ambient temperature and relative humidity were monitored and maintained at 20 ±0.5°C and 53 ±2%, respectively. Food (Teklad Global 18% Protein Rodent Diet 2918, Envigo); filtered tap water and cotton nesting material were continuously available in the cages. All experimental procedures conformed to the NIH Guidelines for the Care and Use of Laboratory Animals and were approved by the Institutional Animal Care and Use Committee of the University of Chicago. Mouse husbandry in constant darkness was facilitated via dim handheld red illumination (<1 lux), otherwise mice were maintained in complete darkness.

Locomotor activity monitoring. Home cage locomotor activity was continuously monitored with passive infrared motion detectors mounted outside the cage, ~22 cm above the cage floor. Motion detectors registered locomotor activity via closure of an electronic relay, recorded by a computer running Clocklab software (Actimetrics; Evanston, IL, USA). Cumulative locomotor activity counts were binned at 1 min intervals. CRs were quantified from 10-day epochs of locomotor activity (described below).

Photoperiod manipulations. Animal housing rooms or soundproof light-tight boxes were illuminated with overhead fluorescent lighting (~400 lux at the level of the cage lid). Digital timers controlled lights to deliver one of 3 static lighting cycles (photoperiods): Mice were maintained in one of three different photoperiods: 12L:12D (IntD, an intermediate photoperiod), 20L:4D (VLD, a long photoperiod), and 4L:20D (VSD, a short photoperiod). Increases and decreases in photoperiod duration were accomplished by symmetrical expansion and compression, respectively, of the light phase (i.e., the endpoint of the light phase always remained the same). After entrainment to IntD, VLD, and VSD for >4 weeks, mice were transferred to DD for 110 days. During this interval (termed, 'DD1') the *per2* behavioral phenomena of ARR and recovery were monitored. After DD1 was completed, mice were returned to full light-dark cycles for 30 days of circadian re-entrainment as follows: mice that were in VLD prior to DD1 were re-entrained to VSD. Mice which were in VSD prior to DD1 were re-entrained to VLD. Finally, mice in IntD prior to DD1 were re-entrained to IntD. After 30 days of re-entrainment, all mice were again transferred to DD for another 110 days. As before, the *per2* behavioral phenomena of ARR and recovery were examined during this interval (termed, 'DD2').

Circadian Activity Measures. Characterization and quantitative evaluation of circadian chronotypes in mice were performed via methodology described previously for this mutant (Albrecht et al., 2001; Zheng et al., 1999): double-plotted activity records were scored by one experimenter (I.Z.), blind to sex, photoperiodic manipulations. Circadian arrhythmia for the purposes of this analysis manifested as activity occurring randomly around the clock; distinct intervals of activity and rest were no longer evident, and the effect persisted for multiple days. The beginning and end of intervals of free-running activity and arrhythmicity were similarly

determined, and were verified via quantification of the amplitude of the circadian peak in the Lomb-Scargle Periodogram (LSP) performed on a 10-day epoch of activity either preceding or following the chronotype state change.

Genotyping. Homozygous *Per2*$^{m/m}$ mice were included in these analyses. Genotyping of all mice bred in our vivarium was done using primers from the Jackson Lab Website [5' → 3': Common Forward (TTC CAC TCT GTG GGT TTT GG), Wild Type Reverse (AAA GGG CCT CTG TGT GAT TG), and Mutant Reverse (GCC AGA GGC CAC TTG TGT AG)] and using specification for the Platinum Taq Polymerase (Life Technologies, Invitrogen catalog number: 10966-018). For each individual PCR reaction: 16.65 uL of DNAase free H2O, 2.5 uL of 10X PCR Buffer with no $MgCl_2$, 0.75 uL 50mN $MgCl_2$, 0.5 uL 10mM dNTP mix, 0.5 uL of each primer, and 0.1 uL of Taq were added to a master mix and thoroughly mixed by pipetting up and down. 22 uL of master mix were aliquoted and added to 3 uL of DNA derived via HotShot (Truett et al., 2000) in experiment 3, from tail clips collected at the conclusion of the studies. We used the following PCR Protocol on a thermocycler: (1) 94 C for 2 minutes, (2) 94 C for 20 seconds, (3) 65 C for 15 seconds, with a -0.5 C decrease with each cycle, (4) 68 C for 10 seconds, (5) repeat steps (2-4) 10 times, (6) 94 C for 15 seconds, (7) 60 C for 15 seconds, (8) 72 C for 10 seconds, (9) Repeat (6-8) 38 times, (10) 72 C for 2 minutes, (11) 10 C for 2 minutes, (12) End. 7-8 uL of the resultant PCR products, and a 100 Bp to 2000 Bp Ladder (Thermofisher catalog # 15628050) for reference were mixed with 1.4-1.5 uL of loading dye (Thermo Scientific catalog number: R0611), loaded on a 2% agrarose gel with 2.5uL of Ethidium Bromide (stock solution: 10mg/mL), and visualized. Resultant bands (amplicon sizes) per Jackson Lab Website were as follows: mutant (m/m) = ~200 bp, heterozygote (m/+) = ~200 bp and 297 bp, and wild type (+/+) = 297 bp.

Statistics. Fisher Exact Tests, or in the case of 3x2 comparisons, Chi^2 test were used for categorical comparison DD chronotypes. Survival analyses were performed by generating Kaplan-Meier survival plots of the latency to arrhythmia onset in DD of *Per2*$^{m/m}$ mice, followed by logrank post-hoc tests. When appropriate two-way ANOVAs, one-way ANOVAs, Kruskal Wallis tests were used to compare latency to arrhythmia. All statistical comparisons were done using Graphpad Prism Software. Results were considered significant below $p = 0.05$.

Results:

Experiment 1: Effect of Photoperiod

We first sought to assess the effect of photoperiod on arrhythmia and recovery. Although the primary goal of this experiment was to examine effects of prior circadian entrainment on the mPer2 chronotype, we were well aware of the existence of sex differences in many mPer2 circadian traits. Thus, in the initial analyses below, we evaluated effects of photoperiod by collapsing across both sexes and by evaluating effects separately for each sex.

Incidence of arrhythmia: Collapsed across sex, in DD1: 7 of 19 VSD mice (36.8%), 7 of 20 IntD mice (35%), and 9 of 18 VLD mice (50%) went arrhythmic, and in DD2: 8 of 17 VSD mice (47%), 9 of 19 IntD mice (47.4%) and 6 of 17 VLD mice (35%); statistically, none of these incidences differed between photoperiod groups either in DD1 (Fig. 15A) or in DD2 (Fig. 15B; Fisher's exact tests: $p>0.35$, all comparisons; Table 1). When sexes were evaluated separately, there was no effect of photoperiod within females alone (Fisher's Exact Tests: $p>0.62$, all comparisons) or within males alone (Fisher's Exact Tests: $p>0.35$, all comparisons) in either DD1 (Fig. 15C) or DD2 (Fig. 15D; Table 1)

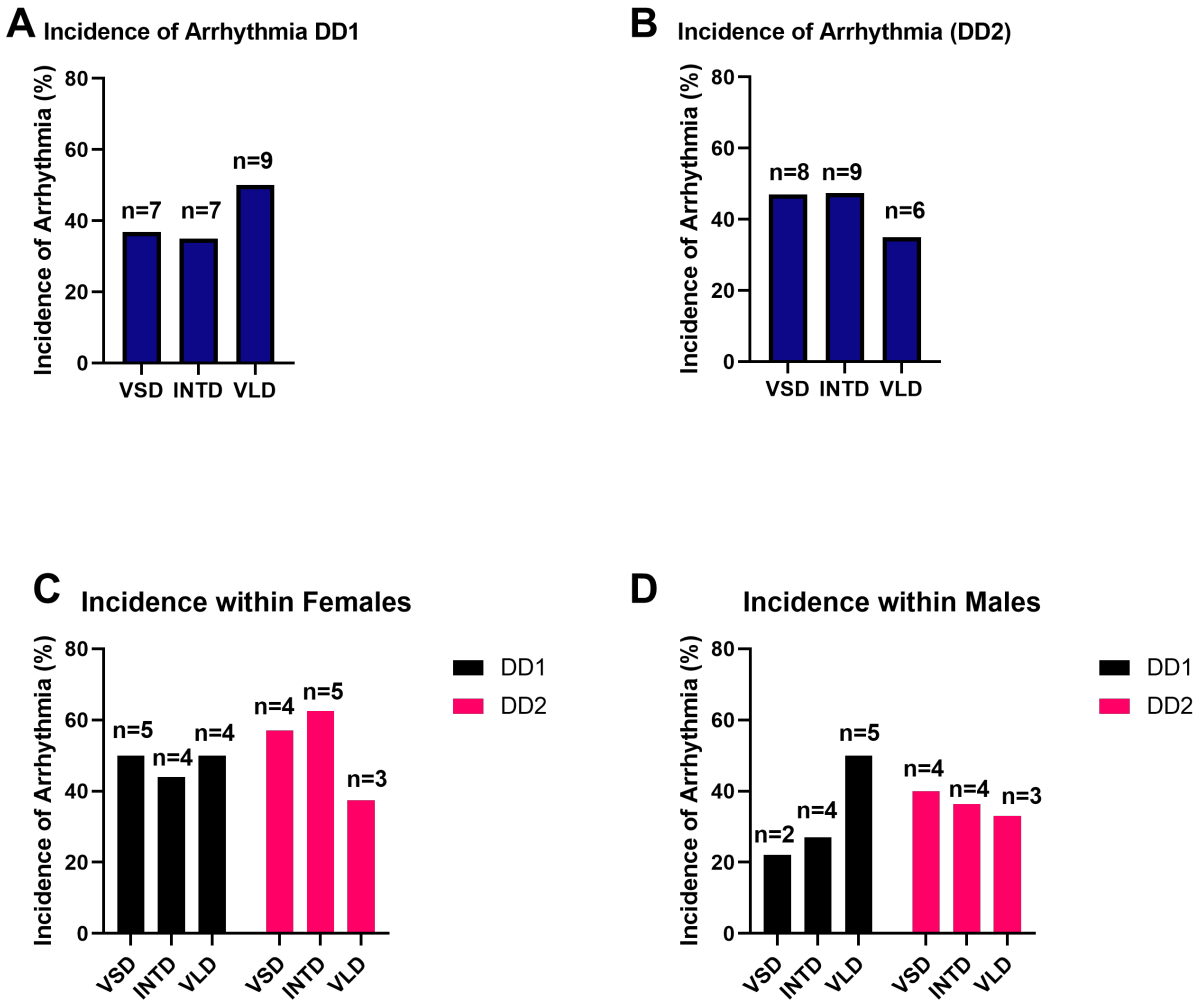

Figure 15: Incidence of arrhythmia collapsed across sex.

Graphs depict the percent of male and female mice who went arrhythmic in an 110 day interval of constant darkness after exposure to VSD (4L:20D), IntD(12L:12D), or VLD (20L:4D). Numbers over bars correspond to number animal exhibit arrhythmia in each treatment group (A) Percent incidence of arrhythmia collapsed across sex in DD1. (B) Percent incidence of arrhythmia collapsed across sex in DD2. [DD1: VSD (19 mice), IntD (20 mice), VLD (18 mice) and DD2: VSD (17 mice), IntD (19 mice), VLD (17 mice)]. (C) Percent incidence within females. (D) Percent incidence within males DD1: [Int (12L:12D: 11 males and 9 females), VLD (20L:4D: 11 males and 9 females), VSD (4L:20D: 9 males and 10 females)] and DD2: [Int (12L:12D: 11 males and 9 females), VLD (20L:4D: 9 males and 8 females), VSD (4L:20D: 10 males and 7 females)].

Table 1: Incidence of Arrhythmia by Photoperiod.

Comparison:	**Statistic:**
DD1: IntD vs VSD	Fisher's exact test: $p > 0.99$
DD1: IntD vs VLD	Fisher's exact test: $p = 0.51$
DD1: VSD vs VLD	Fisher's exact test: $p = 0.51$
DD2: IntD vs VSD	Fisher's exact test: $p > 0.99$
DD2: IntD vs VLD	Fisher's exact test: $p = 0.52$
DD2: VSD vs VLD	Fisher's exact test: $p = 0.73$
DD1 Females: IntD vs VSD	Fisher's exact test: $p > 0.99$
DD1 Females: IntD vs VLD	Fisher's exact test: $p > 0.99$
DD1 Females: VSD vs VLD	Fisher's exact test: $p > 0.99$
DD2 Females: IntD vs VSD	Fisher's exact test: $p > 0.99$
DD2 Females: IntD vs VLD	Fisher's exact test: $p = 0.62$
DD2 Females: VSD vs VLD	Fisher's exact test: $p = 0.62$
DD1 Males: IntD vs VSD	Fisher's exact test: $p > 0.99$
DD1 Males: IntD vs VLD	Fisher's exact test: $p = 0.39$
DD1 Males: VSD vs VLD	Fisher's exact test: $p = 0.35$
DD2 Males: IntD vs VSD	Fisher's exact test: $p > 0.99$
DD2 Males: IntD vs VLD	Fisher's exact test: $p > 0.99$
DD2 Males: VSD vs VLD	Fisher's exact test: $p > 0.99$

Emergence of arrhythmia: There also was no effect of photoperiod on the emergence of arrhythmia in DD1 (Fig. 16A; all χ^2s < 1.4; $p > 0.23$, all comparisons) or in DD2 (Fig. 16B; χ^2s <0.23; $p > 0.63$), all comparisons) when collapsed across sex. Survival analyses also indicated that photoperiod did not affect emergence of ARR within females in DD1 (Fig. 19C; $\chi^2 < 0.15$; $p > 0.70$, all comparisons) or in DD2 (Fig. 19D; χ^2 <0.50; $p > 0.48$, all comparisons), and was also without effect in males in DD1 (Fig. 19E; χ^2s <1.7; p >0.18) or in DD2 (Fig. 19F; $\chi^2 < 0.05$; $p > 0.83$, all comparisons).

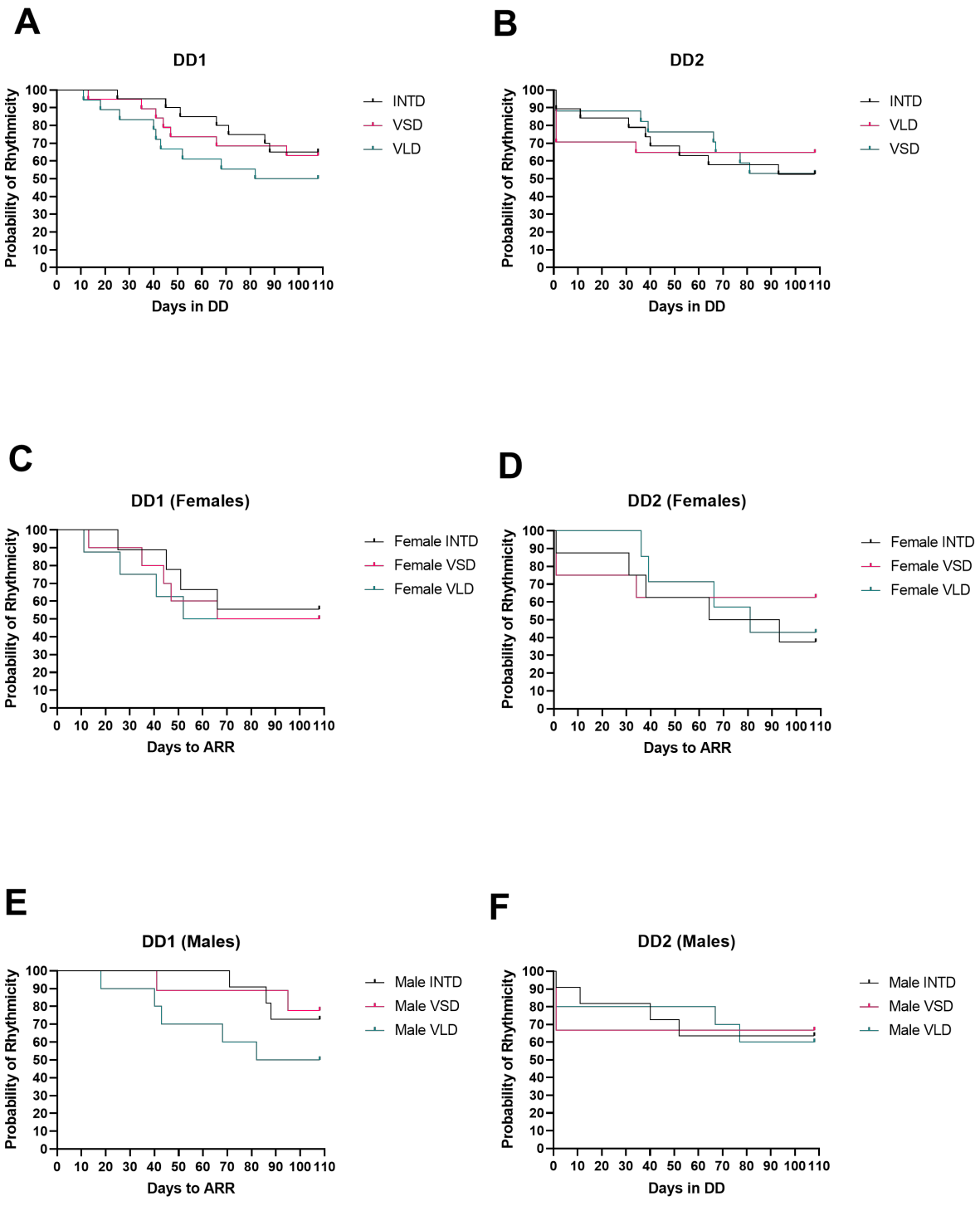

Figure 16: Effect of photoperiod on the emergence of arrhythmia

Graphs depict the Kaplan-Meier survival curves of rhythmicity in male and female *Per2*$^{m/m}$ mutant mice in DD1 or DD2 after exposure to VSD (4L:20D), IntD(12L:12D), or VLD

Figure 16, continued: (20L:4D). Logrank (Mantel-Cox) tests were used to test for significance. (A) Survival of rhythmicity in DD1 split by photoperiod. (B Survival of rhythmicity in DD1 split by photoperiod. (C) Female survival of rhythmicity in DD1 split by photoperiod. (D) Female survival of rhythmicity in DD2 split by photoperiod. (E) male of rhythmicity in DD1 split by photoperiod. (F) male survival of rhythmicity in DD2 split by photoperiod. DD1: [Int (12L:12D: 11 males and 9 females), VLD (20L:4D: 11 males and 9 females), VSD (4L:20D: 9 males and 10 females)] and DD2: [Int (12L:12D: 11 males and 9 females), VLD (20L:4D: 9 males and 8 females), VSD (4L:20D: 10 males and 7 females)].

Latency to arrhythmia: In DD1 there was no main effect of photoperiod on latency to arrhythmia (Fig. 20A; $F_{2,17}$=2.35, p = 0.13) nor was the interaction of sex and photoperiod significant ($F_{2,17}$ = 0.33, p = 0.72). Within sex, standard deviations did not appear equal between groups, thus pairwise comparison were done using the Welch's t-test. Amongst females there was no significant effect of photoperiod (Welch's t-test: q > 0.29, all comparisons) nor was there within males (Welch's t-test: q > 0.10, all comparisons). In DD2, the data failed Spearman's test for heteroscedasticity but was normally distributed and therefore was analyzed using the one-way Brown-Forsythe and Welch ANOVAs. In this analysis, collapsing across sex yielded effect of photoperiod in both the Brown-Forsythe and Welch ANOVAs ($F_{2,17.39}$ = 4.140, p <0.05; $W_{2,12.83}$ = 6.592, p <0.05). Latency to arrhythmia after IntD and VSD did not significantly differ, but latency to arrhythmia after VLD, is significantly shorter compared to both 4L:20D ($t_{9.905}$ = 3.130, p <0.05) and IntD ($t_{11.77}$= 2.625, p <0.05; Fig. 20B). When evaluated separately, however, there was no effect of photoperiod within females ($F_{2.0, 8.6}$ =2.67, p > 0.13) or within males ($F_{2.0, 4.8}$ =1.53, p > 0.31).

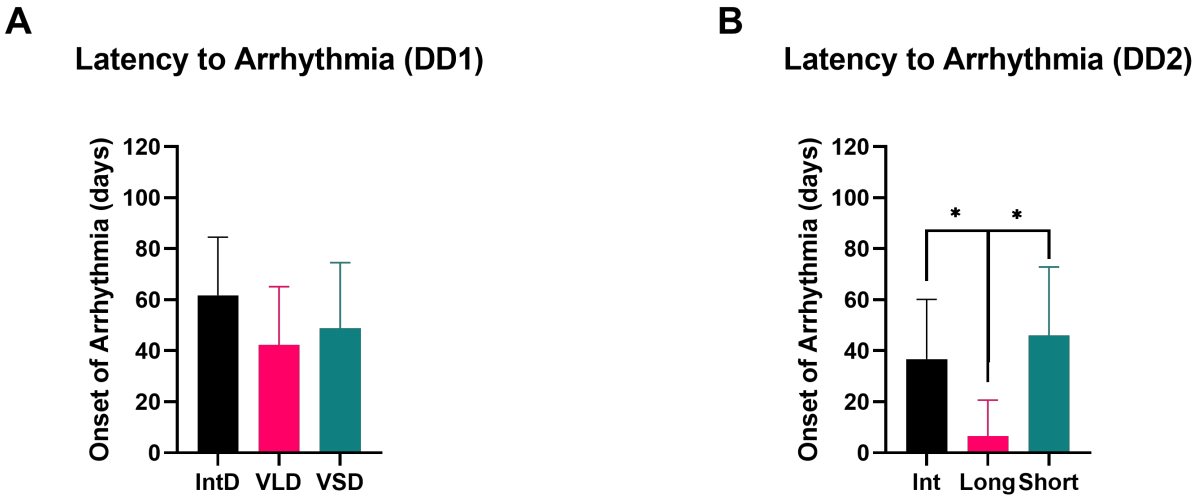

Figure 17: Effect of photoperiod on latency to arrhythmia

(A) Mean (+95% CIs) numbers of days to onset of arrhythmia to mice in DD1 after each photoperiod housing conditions. (B) Mean (+95% CIs) numbers of days to onset of arrhythmia DD2 after each photoperiod housing conditions.

Spontaneous Recovery: In total, 22 mice went ARR (as well as survived to the end of DD) and 13 recovered in DD1 (4 of 9 males, and 9 of 13 females). In DD2, 23 mice went ARR and 18 recovered. (10 of 11 males, and 8 of 12 females). There was no difference in incidence of recovery among photoperiod in either DD1 or DD2 (Fisher's exact tests: $p > 0.29$, all comparisons).

Experiment 2: Repeatability and Stability of Phenomena

Across most traits in Experiment 1, values for DD2 were comparable to those obtained in DD1. However, these values were aggregated across all individuals in a treatment group, and the thus the above analyses do not afford insights into whether individual mice behaved comparably in DD1 and DD2. Thus, Experiment 2 examined the question of whether aspects of arrhythmia and recovery were repeatable and stable traits across successive intervals of exposure to DD. We

examined this both at the level of each individual mouse and the population of mice. Similar to Experiment 1, to remain agnostic about collapsing across sex, below we report analyses separately for each sex as well as collapsed across both; in addition, to remain agnostic about photoperiod, we likewise report aggregate and photoperiod-specific results.

Arrhythmia: Fig. 18 summarizes the repeatability of ARR among *Per2*$^{m/m}$ mutant mice in Experiment 2. Of the 57 mice exposed to DD1, 23 (40.4%) exhibited ARR, and 34 (59.6%) did not. Four mice did not survive until the end of DD2, and thus their data are not eligible for fair consideration in any subsequent measures of repeatability. Thus, of the 20 eligible mice that exhibited ARR in DD1, 10 (50%) also exhibited ARR in DD2, and 10 (50%) did not. Conversely, of the 33 eligible mice that did not exhibit ARR in DD1, 13 (39.4%) exhibited ARR in DD2 and 20 (60.6%) did not. To answer whether DD1 chronotype predicts the DD2 chronotype, we compared the chance of randomly selecting an arrhythmic animal from the pool of Per2 mutant mice in DD1 (23 of 57; 40.4%) versus animals that were subject to a screening procedure (i.e., DD1) and then filtered based on that outcome (i.e., ARR in DD1) them from a pool of *Per2*$^{m/m}$ mutant mice, Within the DD1-ARR mice, 10 of 20 go ARR in DD2 (50%). Selecting only the mice that go ARR in DD1, improves chances above random selection by 9.6%, a nonsignificant increase (χ^2 =0.56, p = 0.45). Thus, an animal going ARR in DD1 does not predict it going ARR in DD2.

It was possible that, while being arrhythmic in DD1 did not predict being arrhythmic in DD2, failure to go ARR (NON-ARR) was predictive of NON-ARR in DD2. Therefore, using the same procedure, we compared the chance of randomly being NON-ARR in DD1 (34 of 57; 59.6%) to the probability of being NON-ARR in DD2 given the animal was NON-ARR in DD1. Of the 34 NON-ARR mice, 20 were NON-ARR in DD2 (58.8%), thus there was no significant difference

between the two ($\chi^2 = 0.01$, $p = 0.92$) and NON-ARR in DD1 does not predict NON-ARR in DD2.

Overall, of the 53 eligible animals, 30 showed concordant chronotypes in DD1 and DD2 (56.6%) and 23 (43.4%) did not (Fig. 18A). However, 21 of 30 males were concordant whereas only 9 of 23 females were ($\chi^2 = 5.05$, $p = 0.02$).

Quantitative parameters were evaluated next. Among the mice that exhibited ARR in DD1 and DD2, we examined how well the latency to arrhythmia in DD1 predicted the latency to arrhythmia in DD2. We fit a simple linear regression to the data, but the residual plot exhibited a clear parabolic pattern, thus fit a nonlinear model instead. A centered 2nd order polynomial fit the fully collapsed dataset well (n=10, r^2=0.84; Fig. 18B). When split by sex, a similar pattern emerged (males: n = 6; r^2=0.98, Fig. 21C; females: n = 4; r^2=0.99, Fig. 18D). Analyses of IntD mice alone also indicated a significant fit by a 2nd order poly (n=5; r^2 =0.76).

Recovery: In total, 13 of 22 mice (59%) who went ARR in DD1 recovered and 41% did not. Of these only 9 animals went arrhythmic again and survived to the end of DD2. Of these 9 animals, 6 (66.6%) exhibited concordance in whether recovered or failed to recover.

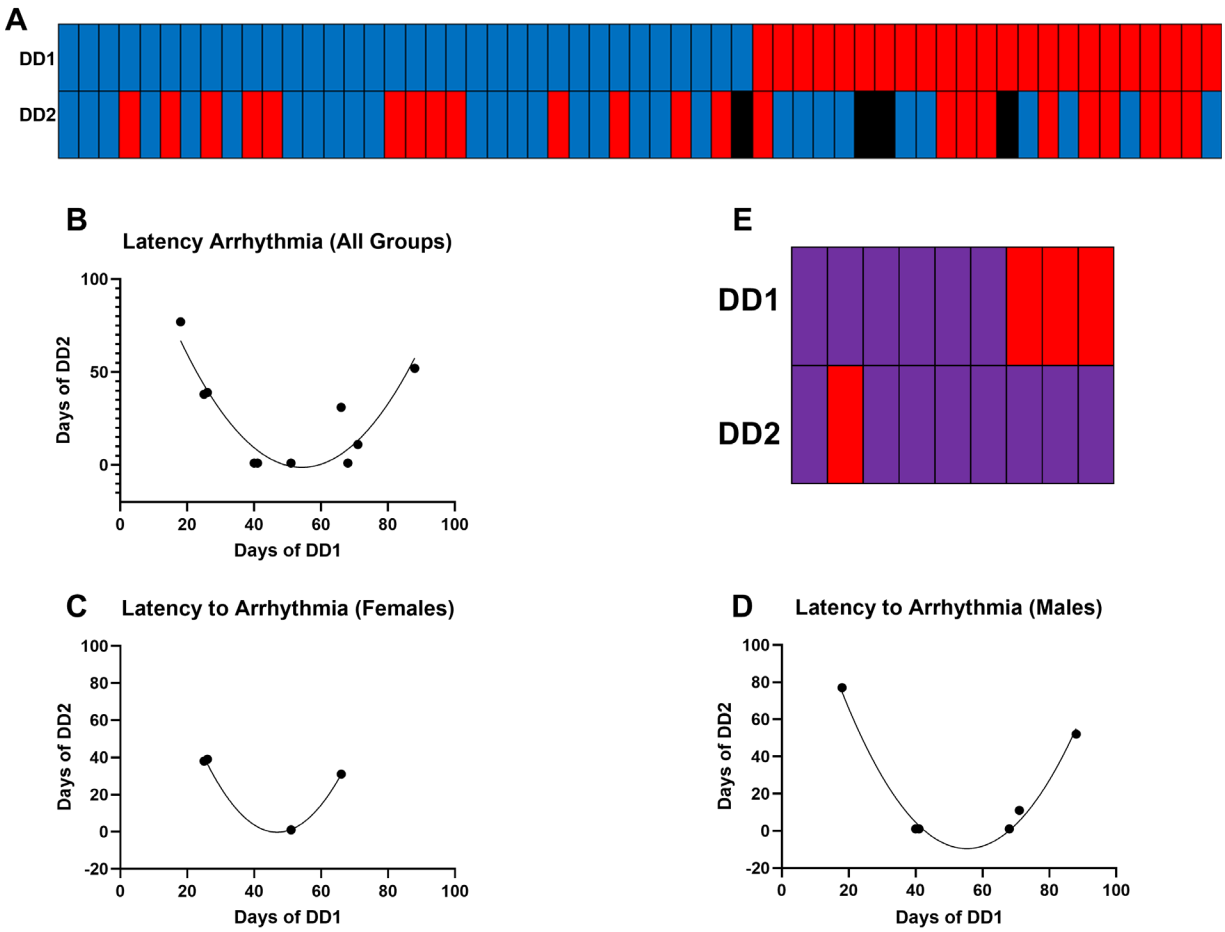

Figure 18: Repeatability of the phenomena

(A) Piano Plot of arrhythmia across both DD1 and DD2. Each color cell represents an animal and whether it went arrhythmic (Red) or free-ran the entire interval. (B) Centered 2nd order polynomial regression of latency to arrhythmia in DD1 vs. DD2, collapsed across sex and photoperiod. (C) Centered 2nd order polynomial regression of latency to arrhythmia in DD1 vs. DD2 in female animals. (D) Centered 2nd order polynomial regression of latency to arrhythmia in DD1 vs. DD2 in male animals. (E) Piano plot of circadian recovery in DD1 or DD2. Color cells represent an animal whether it recovered rhythmicity (purple) or stayed arrhythmic the entire DD interval (red).

Finally, we also wanted to compare quantitative measures of arrhythmia in DD1 vs DD2.

Incidence of Arrhythmia: None of the comparison in incidence to arrhythmia were significant between DD1 and DD2 (Table 2).

Table 2: Incidence of arrhythmia (DD1 vs DD2)

Incidence of Arrhythmia:	**Animal Numbers:**	**Statistic:**
DD1 vs. DD2, all animals	23 of 57 mice (40.4%) vs. 22 of 50 mice (44%)	χ^2=0.15, p = 0.70
Males: DD1 vs. DD2	11 of 31 mice (35.5%) vs. 11 of 30 mice (36.7%)	χ^2=0.01, p = 0.92
Females: DD1 vs. DD2	13 of 27 (48.1%) vs. 12 of 22 mice (54.5%)	χ^2=0.20, p = 0.66
VSD: DD1 vs DD2	9 of 18 mice (50%) vs. 5 of 16 mice (31.3%)	Fisher's exact test, p = 0.32
IntD: DD1 vs DD2	7 of 20 mice (35%) vs. 9 of 19 (47.4%) mice	Fisher's exact test, p = 0.52
VLD: DD1 vs DD2	7 of 19 (36.8%) mice vs. 8 of 17 (47.1%) mice	Fisher's exact test, p =0.74

Emergence of arrhythmia: Using survival analyses to compare the development of ARR over time yielded no statistically significant differences in emergence of arrhythmia between DD1 and DD2 (Table 3).

Table 3: Emergence of arrhythmia (DD1 vs. DD2)

Emergence of Arrhythmia:	**Statistic:**
DD1 vs. DD2, all animals	χ^2=0.39, p = 0.53
Males: DD1 vs. DD2	χ^2 < 0.01 p = 0.97
Females: DD1 vs. DD2	χ^2=0.54, p = 0.46
VSD: DD1 vs. DD2	χ^2=0.25, p = 0.62
IntD: DD1 vs. DD2	χ^2=1.03, p = 0.31
VLD: DD1 vs. DD2	χ^2=0.36 p = 0.55

Latency to arrhythmia: We found no significant effects of two-way repeated measures ANOVAs of the latency of arrhythmia which did not assume sphericity and used the Geisser-Greenhouse correction, and thus did not examine pairwise comparisons (Table 4).

Table 4: Latency to arrhythmia (DD1 vs. DD2)

Interval of DD	$F_{2,4}$ =0.27, p = 0.77
Sex x Photoperiod	$F_{2,4}$ = 0.23, p = 0.81
Sex	$F_{1,2}$ = 2.78, p = 0.24
Photoperiod	$F_{1.720, 3.439}$ = 2.17, p = 0.24

Supplementary Analyses: Sex Differences in Arrhythmia and Recovery

Since the sex difference in chronotype between male and female *Per2*$^{m/m}$ mutants was such a prominent feature of Chapter 3 (Riggle et al., 2022), I also examined sex differences in chronotypes of *Per2*$^{m/m}$ mutants in DD1 and DD2, specifically whether male and female *Per2*$^{m/m}$

mutants differed in the incidence of arrhythmia, population level emergence of arrhythmia, latency to arrhythmia, or rate of spontaneous recovery after entrainment to the various light-dark cycles.

Incidence of arrhythmia: The incidence of arrhythmia did not differ significantly between male and female mice in any photoperiod, or in either interval of DD (Fig.19A & B). However, across most photoperiods and in most DD intervals, the incidence of ARR in females was consistently greater than that exhibited by males: VSD-DD1: 5 of 10 females ARR (50%), and 2 of 9 males (22%) ARR; VSD-DD2: 4 of 7 females (57%) ARR and 4 of 10 males (40%) ARR. IntD- DD1: 4 out of 9 females (44%) ARR and 3 out of 11 males (27%) ARR; IntD-DD2: 5 of 8 females (62.5%) ARR, and 4 of 11 males (36.4%) ARR. Finally, VLD-DD1: 4 out 8 females (50%) ARR, and 5 out of 10 males (50%) ARR, VLD-DD2: 3 out of 8 females (37.5%) ARR, and 3 out of 9 males (33%) ARR. The sample sizes of this experiment were substantially lower for each sex than experiment 3, and none of these differences were statistically significant, Nevertheless, it is noteworthy that, similar to the findings of Chapter 3, quantitatively nearly twice as many females exhibited ARR as compared to males in IntD. This observation also appeared to be the case following VSD as well. Notably, the incidence of ARR was quantitatively much more similar in males and females following pre-exposure to VLD.

The most notable difference between Chapter 3 and this chapter, however, lay in the overall incidence of ARR in *Per2*$^{m/m}$ mutant mice in general, which was substantially lower than expected based on Chapter 3. Here, the incidence of ARR in males ranged from 22% to 50%; whereas the incidence of ARR in females ranged from 37.5% to 62.5%. In contrast, across the 3 studies in Experiment 3 the incidence of ARR in females ranged from 80% to 100%, and in

males from 0% to 63% (note, the 0% value was from Study 1 in Chapter 3, which only lasted 60 days; most other DD intervals for assessing ARR in per2 mice ranged from 90 – 110 days.

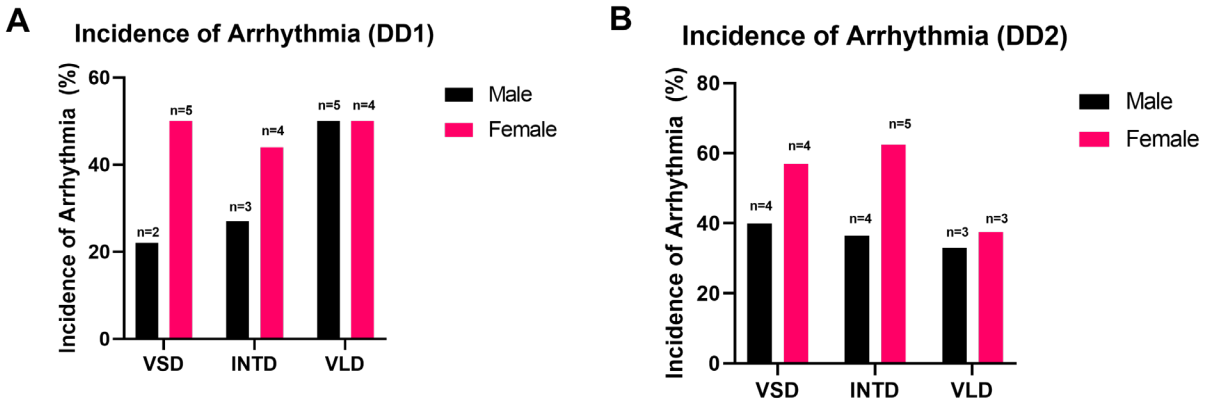

Figure 19: Incidence of arrhythmia across sex by photoperiod

Graphs depict the percent of male and female mice who went arrhythmic in an 110 day Interval of constant darkness after exposure to VSD (4L:20D), IntD(12L:12D), or VLD (20L:4D).This experiment was done twice such that there were two Intervals of DD (DD1 and DD2), though whereas the 12L:12D was repeated in the same animals, animals previously exposed to long day were subsequently exposed to short day and vice versa. Number of animals who went arrhythmic is denoted above each bar. (A) Percent incidence of Arrhythmia in DD1 [SD: 10 Females and 9 Males; IntD: 9 females and 11 males; VLD: 8 Females and 10 males]. (B) Percent incidence of Arrhythmia in DD2 [SD: 7 females and 10 Males; IntD: 9 Females and 11 males; VLD: 8 Females and 9 Males].

Emergence of arrhythmia: There was also no statistically significant difference in the emergence of arrhythmia between male and female mice after any photoperiod ($\chi 2 < 1.71$, $p > 0.19$, all comparisons). However, the pattern of emergence of arrhythmia following entrainment to VSD (Fig. 20A) and IntD (Fig. 20C) resembled that observed in Chapter 3 with females having a lower probability of arrhythmia much earlier than males. This pattern, however, was not as apparent after VLD Fig. 20E) or following any photoperiod in DD2 (Fig. 20B, D, F).

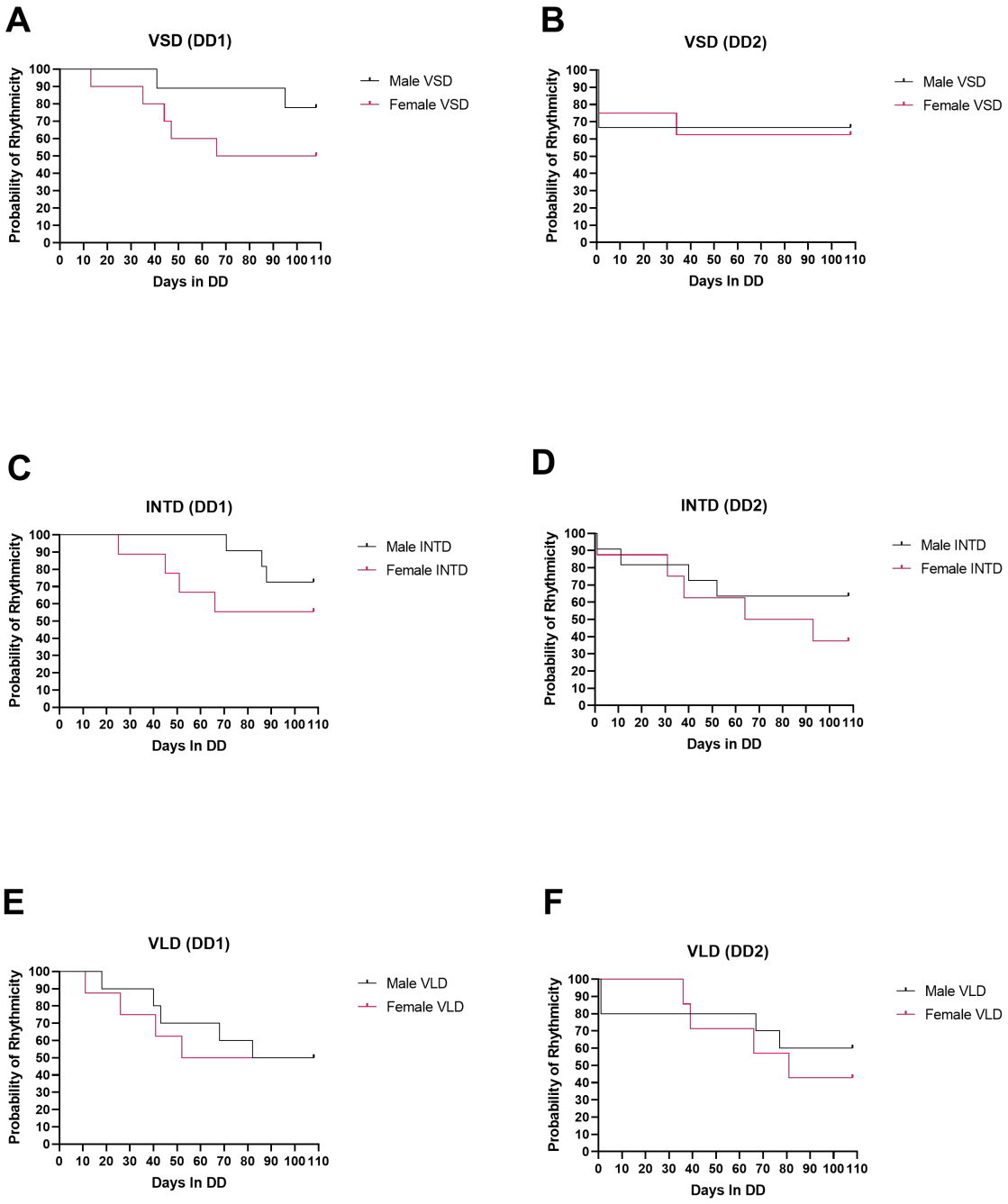

Figure 20: Emergence of arrhythmia across sex by photoperiod

Graphs depict the Kaplan-Meier survival curves of rhythmicity in male and female *Per2*$^{m/m}$ mutant mice in DD1 or DD2 after exposure to VSD (4L:20D), IntD (12L:12D), or VLD (20L:4D). Logrank (Mantel-Cox) tests were used to test for significance. (A) male and female Figure 20, continued: survival of rhythmicity in DD1 post VSD. (B) male and female survival of rhythmicity in DD2 post VSD. (C) male and female survival of rhythmicity in DD1 post IntD. (D) male and female survival of rhythmicity in DD2 post IntD. (E) male and female survival of

Figure 20, continued: rhythmicity in DD1 post VLD. (F) male and female survival of rhythmicity in DD2 post VLD. DD1: [Int (12L:12D: 11 males and 9 females), VLD (20L:4D: 11 males and 9 females), VSD (4L:20D: 9 males and 10 females)] and DD2: [Int (12L:12D: 11 males and 9 females), VLD (20L:4D: 9 males and 8 females), VSD (4L:20D: 10 males and 7females)].

Latency to arrhythmia: In DD1 there was a main effect of sex on the latency to arrhythmia in (sex: $F_{1,17}$=8.33, p<0.05; Fig 17A). In VSD and VLD, males and females did not differ in this measure (t-tests: q>0.28, both comparisons), but in IntD, males trended toward having longer latency than females (t-test: q = 0.08). In DD2, heteroscedasticity prevented significance testing via the two-way ANOVA, but we found no statistically significant difference of treatment ($F_{5,11.8}$ = 0.14, p, = 0.14; Fig 17B).

Recovery: There was no significant effect of sex on circadian arrhythmia in either DD1 or DD2 (Fisher's exact tests: p>0.52, all comparisons). Notably, though, in Chapter 3 we reported incidence of recovery in males that ranged from 33% to 50% and in females from 75% to 95%. Overall, comparable rates were observed here. In DD1, the pattern of recovery resembled that observed in Chapter 3: 33% to 50% of males exhibited recovery and 60% to 75% of females did so (Fig. 21C). In DD2, rates of recovery remained high in females, however, males exhibited the prevalence of recovery now ranged from 75% to 100% (Fig. 21D).

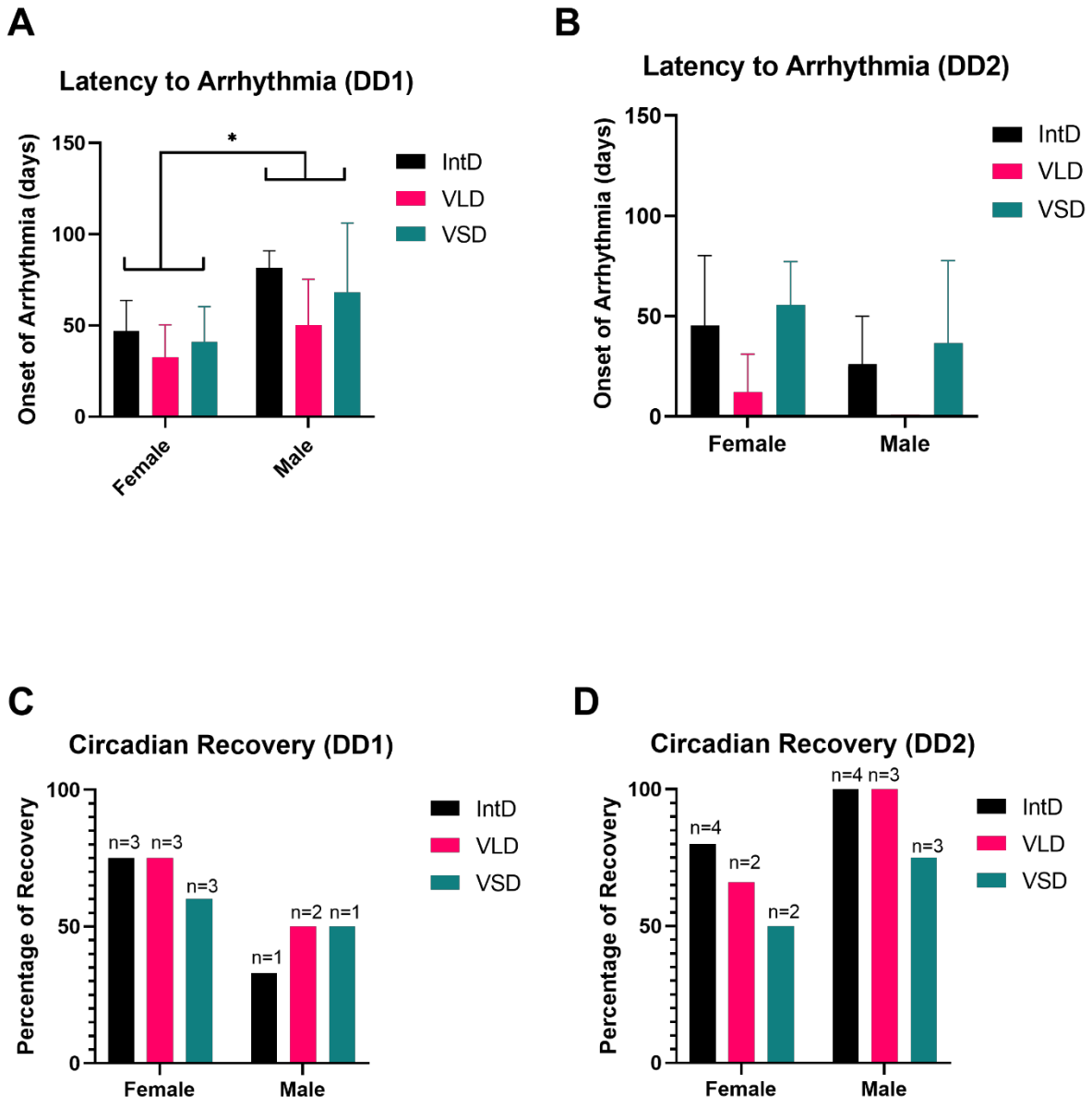

Figure 21: Latency Arrhythmia and Circadian Recovery

(A) Mean (+95% CIs) numbers of days to onset of Arrhythmia by sex and photoperiod of mice that went arrhythmic in DD1. (B) Mean (+95% CIs) numbers of days to onset of Arrhythmia by sex and photoperiod of mice that went arrhythmic in DD2. Comparison by two-way ANOVA. (C) Percentage of arrhythmic animals that exhibited recovery in DD1. (D) Percentage of arrhythmic animals that exhibited recovery in DD2. Number of animals who recovered rhythmicity is denoted above each bar. DD1: [Int (3 males and 4 females), VLD (4 males and 4 females), VSD (2 males and 5 females)] and DD2: [Int (4 males and 5 females), VLD 3 males and 3 females), VSD (4 males and 4 females)]). *$p<0.05$

Discussion:

These experiments sought to investigate (1) whether alteration of circadian network properties via photoperiod could influence the manifestation of arrhythmia and spontaneous recovery in male and female *Per2*$^{m/m}$ mutant mice and (2) whether aspects of the *Per2*$^{m/m}$ chronotype were repeatable and stable within both mice themselves and at the level of the population.

Photoperiod significantly affected the latency to arrhythmia, but only in the second interval of constant darkness. In DD2, VLD mice exhibited a more rapid onset of ARR as compared to mice in other photoperiod groups. This outcome suggests that the VLD photoperiod accelerated the onset of ARR—an outcome that would be consistent with the hypothesis that circadian network organization—to the extent that it can be manipulated via the VLD treatment—impacts aspects of the *per2* DD arrhythmia chronotype. However, this effect was isolated to the DD2 interval. In DD1, latency was unaffected by photoperiod, and none of the other metrics used to evaluate the *per2* chronotype generated evidence of a photoperiod effect: neither incidence (% ARR), nor emergence (survival analyses) nor recovery (resumption of circadian rhythms) were augmented by prior exposure to VLD. Taken together, the results are not compatible with the hypothesis that photoperiod-induced circadian entrainment exerts an influence on arrhythmia in DD.

Exposure to VLD exerts enduring effects on the mouse circadian system. Termed ‘aftereffects’, WT mice exhibit a prolonged decrease in circadian period (accelerated circadian clock) in DD following prior entrainment to VLD (Evans et al., 2013). One possible explanation for the present data is that the *per2* gene is required for photoperiod to exert such aftereffects. Albrecht et al. (2001) have hypothesized that the Per1 and Per2 genes may each play separate

and specific roles in the 'dual oscillator' model of circadian entrainment (Albrecht et al., 2001; Daan & Pittendrigh, 1976). Circadian aftereffects require changes in oscillator-oscillator coupling interactions (Evans et al., 2005; Evans & Gorman, 2016; Gorman & Zucker, 1997). If *Per2*$^{m/m}$ mutants lack (or have a functional decrement in) one of the component oscillators in the circadian system, then perhaps the network-altering effects of VLD are not as prominent in *Per2*$^{m/m}$ mutant mice as they would be in WT mice. If this were the case, then this study may not have engaged VLD aftereffects as fully as we had originally anticipated. Further analyses could test this hypothesis by examining *Per2*$^{m/m}$ mutant mice for the signature aftereffects of VLD, specifically, a short tau in DD. If aftereffects are not present in VLD-exposed *Per2*$^{m/m}$ mutant mice, this outcome may be a serendipitous finding: that the *per2* gene is essential for circadian aftereffects.

The second experiment evaluated repeatability. Although the *Per2*$^{m/m}$ mutant chronotype was largely not repeatable, the data was consistent with these traits being stable at the population level. The overall incidence in arrhythmia did not change between DD1 and DD2, no matter how the data was parsed. Likewise, emergence of arrhythmia did not significantly differ between DD1 and DD2. Finally, we found no main effect of interval in either latency to arrhythmia or recovery. We did find main effects of sex and photoperiod in latency to arrhythmia that only occurred in one interval of DD. It is unclear if these represent a real effect. The main effect of sex is in line with previous results from Chapter 3. It is unclear though, why it would disappear. The effect of photoperiod may more likely represent the difficult of the system in adjusting to the switch a maximally expanded activity duration in constant darkness to greatly compressed activity duration in VLD, consistent with the VLD seemingly driving the effect of latency. These effects disappeared in a repeated measures two-way ANOVA, but that may be the

masking of the difference by the interval without a significant effect. Overall, it appears that incidence of arrhythmia and emergence are categorically stable, latency to arrhythmia may not be, and latency to recovery is potentially stable, though the very small sample of animals that recovered in both rounds, may make this metric unreliable. Ultimately, though, via multiple trait measures and via multiple ways of conceptualizing repeatability (correlations, predictability, considering repeatability of the ARR phenotype separately from that of the FR phenotype, examining concordance), DD1 phenotypes did not predict DD2 phenotypes in per2 mice. This outcome indicates that a propensity to exhibit ARR in DD is not a stable, recurring trait in a given *Per2*$^{m/m}$ mutant mouse. Instead, it may arise form stochastic (probabilistic-based) processes, of unknown origins and sources.

Otherwise put, individual *Per2*$^{m/m}$ mutant mice may simply have a set probability of exhibiting ARR. If so, is this probability modifiable by exteroceptive or interoceptive stimuli? The data from Chapter 3 suggest that this is indeed the case: sex exerts a profound effect on whether a *Per2*$^{m/m}$ mutant mouse will become ARR in DD. This study (Chapter 5) was underpowered with regard to examining a sex difference, and few-to-none of the sex comparisons were significant, but a similar overall sex-biased pattern or ARR emerged in most groups, especially in IntD group, which is most comparable to the Chapter 3 experiments (i.e., 12L:12D → DD).

A most remarkable pattern emerged in the data form this experiment, which is worthy of commentary. In Chapter 5, the overall incidence of arrhythmia appears to be categorically different in this study than in prior reports. In Study 2 of Chapter 3, 100% of females and 63% of males exhibited ARR. In this study (Chapter 5), ARR occurred approximately half as frequently. Remarkably (as noted in the previous paragraph) the pattern of ARR was still comparable in

males and females, however, this pattern manifested against a background of markedly reduced rates of overall ARR. The reasons for this are unclear. The age (5-9 months) at the start of DD1 was comparable to that of prior studies in Chapter 3. Genetic drift is a possible explanation, as this can occur in all breeding colonies. On some genetic backgrounds not all *Per2*$^{m/m}$ mutant mice exhibit ARR (Xu et al., 2007). However, it is unlikely that genetic background change could have occurred in our breeding colony in the interval between when experiments for Chapters 3 and 5 were performed. Mice used in Chapter 5 were born from the same lab breeding colony in Rooms 207/208 of the BPSB, and were, on average, born only 3 months before/after from those used in experiment 3 of Chapter 3. In fact, experiment 3 of Chapter 3 was run concurrently with Chapter 5 studies, which not only renders genetic drift unlikely, but also somewhat reduces the likelihood that these differences are explainable by an environmental factor occurring in the lab/building. Unpublished results from multiple studies of *Per2*$^{m/m}$ mutant mice derived from the colony after this experiment's conclusion, furthermore, also appear to exhibit high rates of arrhythmia. Locomotor activity records [not depicted] were noticeably sparser in appearance than those that were obtained in previous experiments. This outcome could potentially affect the scoring by the blind experimenter. Another possible explanation for this divergence in incidence of arrhythmia may be related to infradian (~3 month) rhythms in locomotor activity levels that have been reported in lab mice (Pernold et al., 2021).

Taken together, the data indicate that photoperiodic induction of circadian network organization does not alter arrhythmia in DD in *Per2*$^{m/m}$ mutants mice. Nor does the behavior of a mouse during an initial interval of DD predict its behavior during a later interval.

Chapter 6: Sex Differences in the Effects of RNA Methylation on Behavioral Circadian and Ultradian Rhythms in *Ythdf1* Knockout Mice

Introduction:

Sex differences in biology and neuroscience are systematically understudied due in part to exclusion of female rodents from studies and or lack of documentation of sex in many foundational studies, based in the mistaken belief that female animals are more variable due to states like estrous (Prendergast et al., 2014; Smarr et al., 2017). This systematic neglect can have clear clinical consequences (Zucker & Prendergast, 2020). Thus, there is an abundant and urgent need to detail and document sex differences in basic biology.

Recent work suggests that the core mechanics of circadian rhythms are more sexually differentiated than previously appreciated (Riggle et al., 2022). Daily circadian timekeeping is molecularly represented in almost every cell of the mammalian body, by the transcription and translation of several core clock genes organized in a negative feedback loop. This core loop is further supported and enhanced by additional loops and multiple levels of epigenetic regulation (Cox & Takahashi, 2019). Many aspects of mammalian behavior and physiology are circadian regulated measurements range from 10-50% of the genome (Turek, 2016; Zhang et al., 2014) depending on tissue— see also (Koike et al., 2012). These daily rhythms are also vital for human health (Evans et al., 2013; Walker et al., 2020).

Sex differences in circadian rhythms are widespread (Bailey & Silver, 2014; Davis et al., 1983; Elderbrock et al., 2020; Krizo & Mintz, 2015; Kuljis et al., 2013; Zucker et al., 1980). Anatomically and behaviorally, circadian features differ across sex (Bailey & Silver, 2014; Davis et al., 1983; Elderbrock et al., 2020; Güldner, 1982; Iwahana et al., 2008; Krizo & Mintz, 2015;

Kuljis et al., 2013; Riggle et al., 2022; Yan & Silver, 2016; Zucker et al., 1980). These differences can appear subtle in a circadian intact system, but become more prominent with genomic or surgical disruption (Kuljis et al., 2013). Much of the investigation into circadian sex difference has focused the role of gonadal hormones and their receptors, as well as the contribution of sex chromosomes. Across different species, following the surgical removal of gonads, differences in many circadian traits (i.e. activity levels) become less prominent, suggesting that gonadal hormones in the circadian system in part, maintain differences between the sexes in adulthood (Iwahana et al., 2008; Joye & Evans, 2021; Kuljis et al., 2013). Some connections have been drawn between these hormones and the basic core molecular machinery of the circadian clock (Cai et al., 2008; Gery et al., 2007; Karatsoreos et al., 2011; Nakamura et al., 2005; Nakamura et al., 2001), but until recently there was no evidence that the core molecular machinery was sexually differentiated (Riggle et al., 2022); Chapter 3). However, it is remarkable to note the high level of variance documented in this study. Given the highly inbred background suggests other sources of variability. One such source might be epigenetic.

The transcription and translation of genes are under regulation— the chromatin state can affect how readily a gene is transcribed into mRNA as can the presence of chemical markers on the DNA itself. Once transcribed into mRNA, addition and removal of chemical markers (i.e methyl groups) can further affect whether a given mRNA is translated into protein. This type of transcriptional regulation is referred to as epigenomic ('on top of the genome') (Sahar & Sassone-Corsi, 2013).

It is becoming increasingly clear that epigenetic regulation is a fundamental part of clock function (Sahar & Sassone-Corsi, 2013). One of the core clock genes, the aptly named *clock,* is a histone acetlyltransferase (Doi et al., 2006). Global DNA methylation is rhythmic on the

circadian scale (Azzi et al., 2014). Region specific DNA methylation changes may allow the superordinate mammalian circadian pacemaker in the hypothalamus, the suprachiasmatic nucleus (SCN) to reorganize in response to light and change clock gene expression (Azzi et al., 2014; Azzi et al., 2017). RNA too can be a site of regulation, over 163 different types of RNA modification have been identified to date with important impacts on RNA function (Lewis et al., 2017) One of these, N6-methyladenosine (m6A) is the most abundant and conserved internal cotranscriptional modification in eukaryotic RNAs(Jiang et al., 2021), has been prominently implicated in circadian biology. The clock genes, *Per1*, *Per2*, *Per3*, *Bmal*, and *Clock* have prominent m6A sites in their transcripts and silencing m6A methylation through inhibition of the methylase *Mettl3* is sufficient to lengthen the period of the circadian clock, (J.-M. Fustin et al., 2013). In part, this methylation method of action seems to be through regulation of Casein Kinase 1 Delta (CK1δ) function and thereby the stability of PERIOD2, elongating the clock's period (Fustin et al., 2018) in line with previous reports connecting CK1δ to *Per2* stability (Lee et al., 2009).

RNA methylation at the m6A site is read by a host of different proteins with different downstream functions (Jiang et al., 2021). One such recognition protein is YTHDF1, recognizes the presence or absence of methylation at m6A sites and interacts with ribosomes and initiation factors of the translation machinery to increase protein synthesis (X. Wang et al., 2015) and has been shown to have an important role in learning and memory (Shi et al., 2018), a process known to be circadian regulated (Gerstner & Yin, 2010; Ruby et al., 2008; Smarr et al., 2014). Given the important role of epigenetics in CRs and the relevance of CRs to processes known to be affected by YTHDF1-mediated identification of RNA methylation, we hypothesized that manipulations of YTHDF-1 activity would alter the expression of behavioral rhythmicity. Therefore, this

experiment tested the hypothesis that YTHDF1 affects the expression of circadian and ultradian rhythms in behavior, using male and female mice with a functional mutation in YTHDF1. Note however, that YTHDF1 has the ability to bind many different mRNAs, thus manipulation of YTHDF1 1 does not alter the regulation of specific transcripts. Rather the present experiment was designed simply to examine the hypothesis that epigenetic regulation of RNA, as a general cellular transcriptional mechanism, plays some role in circadian and ultradian rhythms.

Materials and Methods:

Animals. Adult female and male *Ythdf1* knockout (KO), heterozygote (HET), and control mice (WT) on a C57BL/6J [JAX#: 000664] were bred from heterozygotes breeding pairs derived from lines that were created as described by (Shi et al., 2018). Mice of both sexes were single housed in conventional cages with wirebar lids, and without microisolater filters in a 12L:12D photocycle of approximately 150-200 lux until the housing room was switched to continuous darkness (DD). Experiments were performed concurrently across two different housing rooms with comparable lighting cycles. Cage location in the room was chosen randomly. At all times mice had ad libitum access to standard rodent diet (Irradiated Teklad Global 18% Rodent Diet 2918, Envigo RMS) and filtered drinking water. Animal husbandry in DD was facilitated via dim handheld red illumination (<1 lux), otherwise DD mice were exposed to complete darkness. Cage changing was performed at two-week intervals. All mice were acclimated to running wheel or PIR cages for at least one week prior to data collection. The integrity of experimental LD cycles and DD treatments was continuously monitored and verified by dataloggers (HOBO, UX90, Onset Comp). Estrous cycles of females were not monitored. Prior to the experiment (3 males: 1 WT, 1 HET, 1 KO; and 8 females: 2 WTs, 3 KOs, 3 HETs) were exposed to a rotarod

test. The remaining animals were naïve. All were transferred from one animal facility to another 2 months prior to the circadian rhythm monitoring evaluated here. At the beginning of experiments animals were between 9-15.5 months of age and between 13-19 months of age at the end of the experiment. All procedures related to animal use were approved by the University of Chicago Institutional Animal Care and Use Committee.

Photoperiod manipulations. Mice were housed in LD for 5-9 weeks, during which time data for LD analyses were obtained as described below. Mice were 274-464 days of age during the interval of behavioral data collection in LD. Mice were then transferred to DD (as described below) where they were maintained for 10 days, during which time data for DD analyses were obtained as described below. Mice were 284-474 days of age during the interval of behavioral data collection in DD. Finally, mice were re-entrained to a LD cycle for 30 days and released into DD for 2 days before being subjected to a 20 minute light pulse at projected Zeitgeber time 15 (pZT15)

Sexing and Genotyping. All animals' genotypes were confirmed before and after the experiments. Animals were visually sexed and these calls were confirmed with sexing primers from Jackson Labs: Y Forward (5′-AAAGGAATTCTGGAGGCTGG-3′), Y Reverse (5′-AAAGGAATTCTGGAGGCTGG-3′), X Forward (5′-GACTAGGTTCATAGGCACTGG-3′), X Reverse (5′-CCGCCAAAACTCCTTCTCTAC-3′). *Ythdf1* (5′-GTGTATGAGGTGGTCAGCAT-3′) and primer R1 (5′- CTTGTTGAGGGAGTCACTGT-3′). Genotyping was done using specification for the Platinum Taq Polymerase (Life Technologies, Invitrogen catalog number: 10966-018). For each individual PCR reaction: 16.65 uL of DNAase free H2O, 2.5 uL of 10X PCR Buffer with no $MgCl_2$, 0.75 uL 50mN $MgCl_2$, 0.5 uL 10mM dNTP mix, 0.5 uL of each primer, and 0.1 uL of Taq were added to a master mix and thoroughly

mixed by pipetting up and down. 22 uL of master mix were aliquoted and added to 3 uL of DNA derived from HotShot (Truett et al., 2000) from tail clips collected at the conclusion of the studies. For *Ythdf1* primers, 3x the amount of $MgCl_2$ was used with a commensurate amount removed from the water. Upon completion of the study a subset of the animals (n=30) were taken and used for another experiment. In a few instances records of which animal was which was lost with this transfer. Any animal whose providence was unclear was excluded. The number of animals analyzed were (17 HET Females, 16 HET Males, 11 KO Females, 15 KO Males, 4 WT Females, and 5 WT Males).

Activity monitoring and telemetry. Mice were housed in polypropylene cages equipped with passive infrared motion detectors (PIR), as described in detail in other reports (Kampf-Lassin et al., 2011; Prendergast, Cisse, et al., 2012). Activity was collected using Clocklab Acquisition software (Actimetrics; Evanston, IL, USA).

Circadian Activity Measures. Activity (PIR) data were visualized and analyzed using Clocklab (Actimetrics). Circadian period was calculated using a Lomb-Scargle Periodogram analyses (LSP) on 10 days of LD and DD activity data (Ruf, 1999; Tackenberg & Hughey, 2021). Additional quantification of circadian phenotypes included determination of phase angles of entrainment in LD and DD, free running circadian period in DD, and total activity counts, and were performed using Clocklab 6 software. Daily activity onsets in LD were obtained directly from Clocklab's 'onset/offsets' feature, with manual corrections performed by an experimenter blind to file identity. Total daily activity counts in LD and DD were derived from Clocklab over a 10 day interval and aggregated in Matlab 2021.

Light Pulse and Phase Delay. To test the response to circadian disruption animals released into DD for 2 days and then were given a 20-minute light pulse at zeitgeiber time 15, animals

were returned to DD for 10 days. The magnitude of the phase shift was measured by determining the displacement between activity onset on the second day in DD and the activity onset predicted by a line fitted to 6 postpulse onsets excluding the first 3 postpulse days to avoid transients. Animals were allowed 30 days to re-entrain to a LD cycle, before being released again into DD for two days and subjected to another light pulse likely at zeitgeber time 21, but exact records were lost. For the purposes of this dissertation, data was not analyzed.

Ultradian rhythm analyses. Ultradian rhythms in behavior under the LD cycle and under the DD cycle were examined using wavelet-based time series analyses as developed and described in detail in Chapter 4. Modifications to this workflow were implemented for the collection and analyses of URs in DD. Because DD data cannot be segregated/parsed by light-phase and dark-phase (as in Chapter 4), behavioral data were parsed using a projected theoretical light on:off adjusted for each animal's circadian period (τ). τ was determined via the Lomb-Scargle periodogram. Using this τ, the time of lights on and off projected as if it followed an animal's free running τ. This ensured an equally sized analysis window for each of analysis and retained the discrete parsing of the data into an interval in which an animal is very active and an interval in which it is relatively less active. Actograms were viewed to confirm that DD induced expansion of the interval of heightened activity, termed the active phase (α), did not expand so much as to compromise the validity of a 12 h window.

Statistics. For many measures below, the distributions of data failed tests of normality, which are a common (although not mandatory) assumption underlying clear interpretations of the F statistic. In these cases, the Kruskal-Wallis H statistic was calculated, which is analogous to an omnibus F statistic in an ANOVA. In the event of a significant H, pairwise comparisons were performed using Mann-Whitney U tests. Because an overarching motivation in these

experiments is the study of sex differences in circadian biology, we examined data in statistical models that separated males and females, as well as in a model that incorporated both sexes. K-W tests as performed here do not permit 2x3 factorial designs, therefore to accomplish this, the data were evaluated as two separate 1x3 designs, with 3 'genotypes' (M-WT, M-HET, M-KO) for males, and 3 genotypes for females (F-WT, F-HET, F-KO), and also as a larger, 1x6 design, with 6 'treatment groups'. Graphpad Prism software was used to run all statistical test. Significance was set at $p<0.05$

Results:

In order to investigate the role of *ythdf1* on biological rhythms in male and female mice, we evaluated the impact of full (Homozygous mice; "KO") or partial (heterozygous mice; "HET") *ythdf1* knockout in comparison to mice with two functional copies of the gene (wild-type mice; "WT"), on basic circadian traits in a 12L:12D light dark cycle and in constant darkness (DD), both within and between sex.

Circadian Period: In females, genotype significantly altered circadian period ($H(2) =6.66$, $p=0.04$), whereas in males there was no effect of genotype ($H(2)=0.24$, $p=0.89$; Fig. 22A), and overall, there was a main effect of treatment group on τDD ($H(5) =12.02$, $p<0.03$; Fig. 19B. KO and HET females tended to have shorter tauDD than WT females (KO: $U = 12$, $p = 0.08$; HET: $U = 18$, $p = 0.05$); KO females also trended toward shorter τDD than female HETs ($U = 53.50$, $p = 0.06$). Circadian period in DD (τDD) did not differ between WT male and female mice ($U = 7.5$, $p = 0.59$). In HET mice, τDD was longer in male than female mice ($U=69$, $p = 0.01$); the same was true of KO mice ($U=38$, $p = 0.031$).

Periodogram (LSP) Amplitude in LD: Among females, genotype significantly affected LSP amplitude, ($H(2)=13.69$; $p<0.01$); while in males, this effect only trended toward significance

(H(2) = 8.201; p=0.08); the overall in the 1x6 analysis, treatment group also significantly affected LSP amplitude (H(5) =23, p<0.01; Fig. 22B). In females, circadian amplitude was reduced in both KOs and HETs relative to WTs (KO: U = 0, p < 0.01; HET: U = 17; p < 0.05). Amplitude was also lower in KOs relative to HETs (U=36, p < 0.01). In males, LSP amplitude tended to also be lower in KO relative to WT mice (U = 11, p = 0.08) and again was lower in KOs relative to HETs (U = 59, p < 0.03).

Finally, among WT mice, LSP amplitude was greater in females compared to males (U = 1, p = 0.03). However, no such difference was observed in either KO (U = 57, p = 0.29) or HET (U = 103, p = 0.25).

Periodogram (LSP) Amplitude in DD: Genotype significantly affected amplitude in females (H(2) = 11.67; p<0.01); and in the overall 1x6 analysis, treatment group significantly affected LSP amplitude (H = 21.29; p < 0.01; Fig. 19 D) but there was no effect of genotype in males (H(2) = 4.127; p = 0.13). In females, LSP amplitude was again lower in KOs and HETs as compared to WTs (KO: U = 0; p < 0.01 ; HET:U = 13; p = 0.02), and though KOS tended toward having lower amplitude than HETs (U = 52; p = 0.05). In males, amplitude did not differ WTs and either other genotype (p > 0.23, both comparisons), but as in females, KOs trended toward lower LSP amplitude than HETs (U = 66, p = 0.06). Among WT mice, females tended to have a greater amplitude than males (U = 2; p = 0.06), and in KOs and HETs, there were no differences in LSP amplitude between the sexes (p>.10, both comparisons).

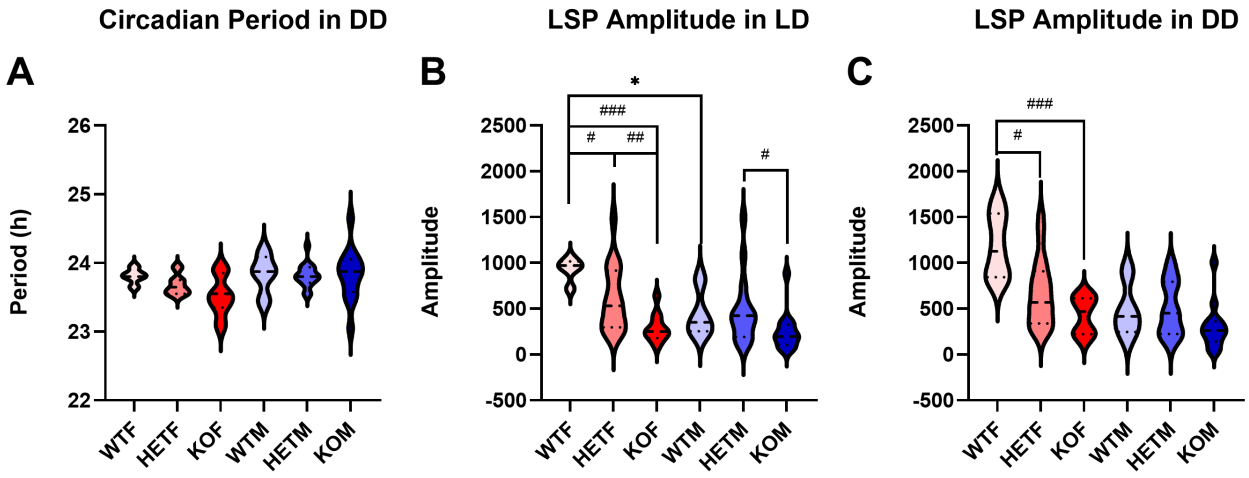

Figure 22: Circadian period and amplitude across sex and genotype

Violin plots locomotor activity structure from mice housed for 10 days under passive infrared recording devices in the home cage. (A) Circadian peak period in constant darkness (DD) between 24 ± 2 h. (B) Lomb-scargle periodogram (LSP) amplitude of circadian peak period in LD. (C) LSP amplitude of amplitude of circadian peak period in DD. (HET [females = 17; males = 16], KO [females = 11; males =14], WT [females = 5; males = 4]). *p<0.05 between sex, #p<0.05, ##p<0.01, ###p<0.001 between genotypes.

LD Locomotor Activity: Dark (active) phase. We documented no significant effect of genotype on dark phase locomotor activity in females ($H(2) = 4.8$; $p = 0.09$) or males ($H(2) = 3.29$; $p = 0.19$), but the overall 1x6 analysis, treatment group did significantly affected dark phase locomotor activity($H(5) = 16.90$, $p = 0.04$, Fig. 23A). Amongst females, KOs trended toward having less locomotor activity than WTs ($U = 10$, $p = 0.08$), and HETs ($U = 43$, $p = 0.08$), but WTs did not have different dark phase locomotor activity than HETs ($p = 0.44$). In males, KOs had comparable locomotor activity levels to WTs, as did HETs ($p > 0.45$, both comparisons), but HETs trended toward having more dark phase locomotor activity than KOs (U

= 54, p = 0.08). Across WTs, female mice had more dark phase locomotor activity than males (U = 0, p = 0.02). In HETs and KOs, however, there were no difference in dark phase locomotor activity between males and females (p > 0.14, both comparisons).

LD Locomotor Activity: Light (rest) phase. There was no effect of genotype in females (H(2) = 3.633, p = 0.16) or males on locomotor activity (H(2) = 2.45, p =0.29), nor was there an effect of treatment group on locomotor activity (H(5) = 7.13, p = 0.21; Fig. 23B).

DD Locomotor Activity: Circadian Active phase. Genotype in females (H(2) =9.372; p<0.01); and the overall 1x6 analysis, treatment group significantly affected active phase locomotor activity (H(5) =15.09, p = 0.01; Fig. 23C), but there was no effect in males (H(2) = 1.556; p = 0.46). Amongst females, KOs had less locomotor activity than WTs (U = 4, p < 0.01), but there was no difference between HET female and KO female locomotor activity (U = 79, p = 0.98). HETs had less locomotor activity than WTs (U = 4, p < 0.01) though. In males, there were no differences in active phase locomotor activity between any genotype (p>0.19, all comparisons).

DD Locomotor Activity: Circadian Rest phase. While there was no effect of genotype in females (H(2) = 3.6; p = 0.16) or males (H(2) =2.45; p=0.25); and in the overall 1x6 analysis, treatment group significantly affected locomotor activity (H(5) = 19.11, p<0.01; Fig. 23D). Across females and males, there was no difference in activity between genotypes (p>0.09, both comparisons). Within WTs, there was no difference in locomotor activity between males and females (U = 3, p = 0.11). In HETs, females trended toward activity than males (U = 78, p = 0.06). Amongst KOs, females had more locomotor activity than male mice (U =17, p < 0.01).

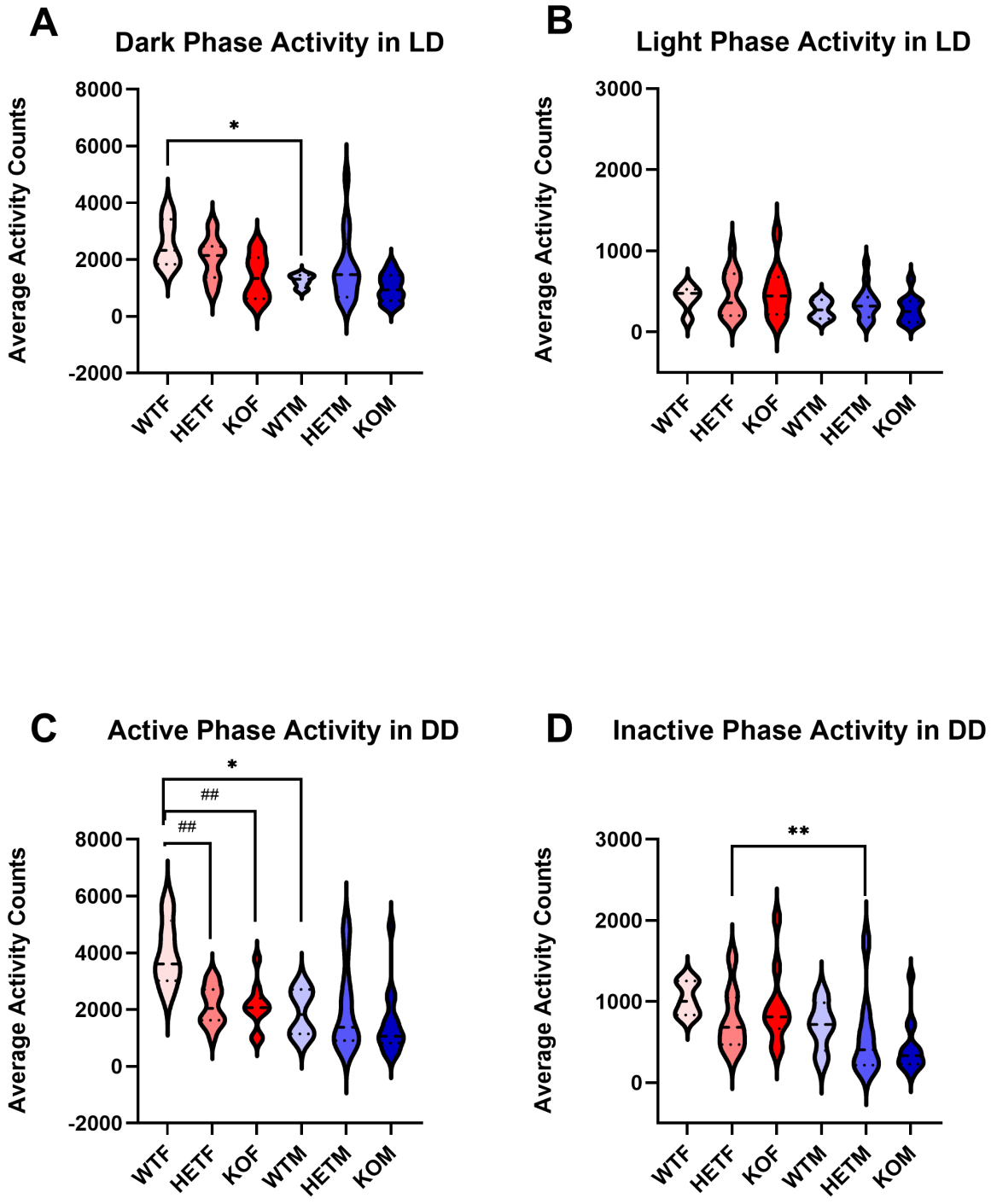

Figure 23: Activity counts across sex and genotype

Violin plots of average activity counts over 10 days. For the DD interval, active and inactive phase were calculating the projected onsets using the LSP calculated circadian period across the sex and genotype pairs. (A) Light phase average total activity counts in LD. (B) Dark phase average total activity counts in DD. (C) Inactive phase average activity counts from DD. (D)

Figure 23, continued: Active phase average total activity counts in DD. (LD: (HET [females = 15; males = 15], KO [females = 10; males =12], WT [females = 5; males = 4]) DD: (HET [females = 17; males = 16], KO [females = 10; males =14], WT [females = 5; males = 4]). *p<0.05, **p<0.01 between sex. ##p<0.01 between genotype.

LD cycle: Phase Angle of Entrainment. Genotype's effect in females ($H(2) = 5.01$; $p = 0.08$) on phase angle of entrainment trended toward significant, but the effect of genotype in males ($H(2) = 0.02$, $p = 0.99$), and in the overall 1x6 analysis were not significant ($H(5) = 6.08$, $p = 0.30$; Fig. 24A) .

LD cycle: Onset variability. There was no effect of genotype within female ($H(2) = 2.68$, $p = 0.26$) or males ($H(2) = 1$, $p = 0.61$) treatment group on LD onset variability ($H(5) = 6.21$, $p = 0.29$; Fig. 24B).

DD: Onset Variability. Genotype in females ($H(2) = 0.25$; $p = 4.13$), and the effect of genotype in males ($H(2) = 0.04$; $p=0.98$) on onset variability were not significant, but the overall 1x6 analysis, treatment group significantly affected LSP amplitude ($H = 22.64$, $p < 0.01$; Fig. 24C). In females and males, there was no difference across genotype ($p > 0.1148$, all comparisons). Within WTs, there was no difference in onsets between male and female mice ($U = 5$, $p = 0.29$). Amongst both HETs and KOs, females had more variable onsets than males (HET: $U = 46$, $p < 0.01$; KO: $U = 15$, $p < 0.01$).

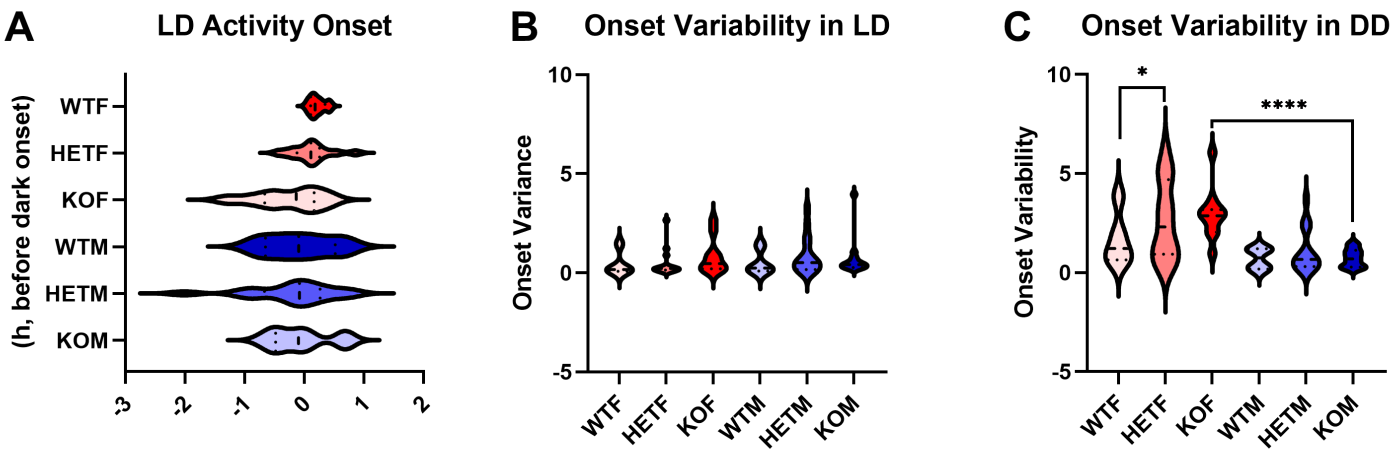

Figure 24: Average onset and onset variability across sex and genotype

Violin plots of average onset and onset variability over 10 days. (A) LD activity onset, reflecting the phase angle of entrainment. (B) Variability of daily onset of activity in LD. (C) Variability of daily onset of activity in DD. (LD: (HET [females = 14; males = 16], KO [females = 10; males =13], WT [females = 5; males = 4]); DD: (HET [females = 15; males = 16], KO [females = 11; males =14], WT [females = 5; males = 4])). *p<0.05, ***p<0.001, ****p<0.0001 between sex

Ultradian Rhythms

URs were examined in male and female *ythdf* mutant mice via procedures similar to those described in detail in chapter 4, with modifications for DD described above (see Methods). Instantaneous period and power distribution were examined.

Dark phase UR period. There was no effect of genotype in females ($H(2) = 1.25$, $p = 0.54$) or males ($H(2) = 1.54$, $p = 0.46$) on τ's, but there was a main effect of treatment group on τ's ($H = 14.2$, $p = 0.01$; Fig. 25A). Within sex, there was no difference in τ's between genotypes ($p > 0.24$, all comparisons). However, in WTs and KOs, males had longer τ's than females (WT: $U = 0$, $p = 0.02$; KOs: $U = 30$, $p = 0.02$), and tended to in HETS ($U = 77$, $p = 0.09$). There was no effect of genotype in females ($H(2) = 0.16$, $p = 0.92$), or males ($H(2) = 3.46$; $p = 0.18$) on τ'm,

nor was there one of treatment group (H(5) = 4.70, p = 0.45; Fig. 25B. In neither females (H(2) = 1.20, p = 0.54) or males (H(2) = 1.20, p = 0.54) did genotype affect t'l), but treatment group did affect dark phase τ'l (H = 19.82, p = 0.01; Fig. 25C). Amongst females and males, τ'l did not differ across genotype (p>0.24, both comparisons). In both WTs and HETs, females had longer τ'l than males (WT: U = 0, p = 0.02; HET: U = 36, p < 0.01). Across KOs though, τ'l did not differ across sex (U = 51, p = 0.28).

Light phase UR period. Neither τ's, τ'm nor τ'l differed significantly by treatment group in the light phase (H(5)< 7.77, p>0.17, all comparisons; not illustrated)

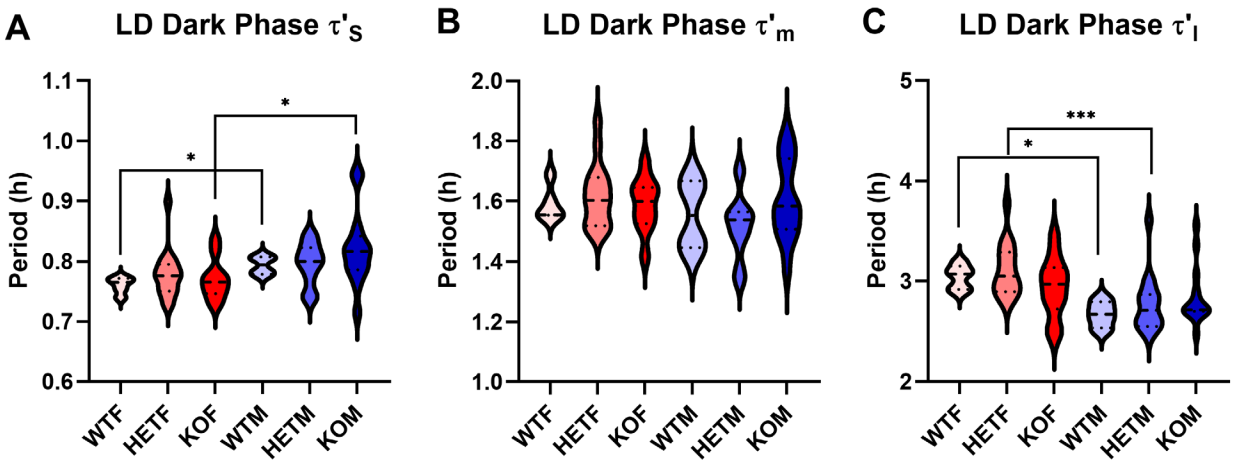

Figure 25: Ultradian period in LD

Violin plots of ultradian period (τ') in the short (.53 -1.07 h) and long (2.13 - 4.26 h) analysis window as accessed using wavelet ridge maximum analysis on 10 days of locomotor activity across treatment group. (A) Dark phase ultradian period in the τ's window in LD. (B) Dark phase ultradian period in the τ'm window in LD. (C) Dark phase ultradian period in the τ'l window in LD. (D) Light phase ultradian period in the τ's window in LD.

Active Phase τ' in DD. τ's tended toward a significant effect of treatment group (H(5) = 11.03, p >0.05, 26A) but the effect of genotype within either males (H(2) = 2.55, p = 0.28) or females (H(2) = 0.3842, p = 0.8252) and τ'm were comparable across all treatment groups (H(5)

= 4.70, p > 0.45; Fig. 26B). However, there was a main effect of treatment group on τ'l (H(5) = 21.10, p < 0.01; Fig. 26C). Within females (H(2) = 3.91, p = 0.14) and males (H(2) = 1.22, p = 0.54) there was no effect of genotype on τ'l, and it did not differ across genotype in either sex (p>0.09, all comparisons). In WT mice, DDt'l was comparable among M and F (U = 3, p =0.11), but in KOs and HETs, females had longer τ'l than males (KO: U = 36, p = 0.046; HET: U=40, p = 0.0006).

Inactive Phase τ' in DD. There was no effect of treatment group on either τ's, τ'm, or τ'l in the inactive phase of DD (H(5) < 8.192, p>0.15, all comparisons).

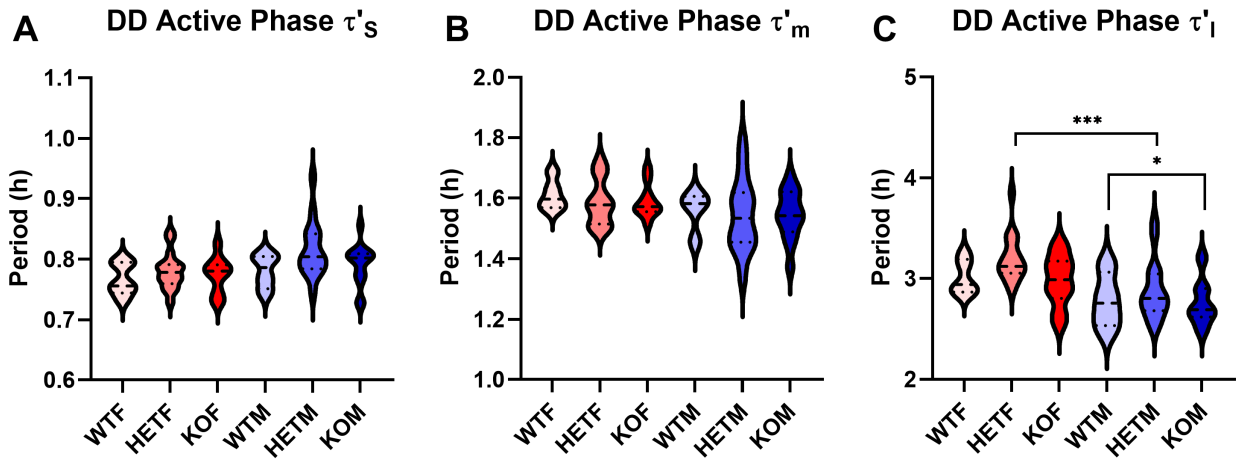

Figure 26: Ultradian period in DD

Violin plots of ultradian period (τ') in the short (.53 -1.07 h) and long (2.13 - 4.26 h) analysis window as accessed using wavelet ridge maximum analysis on 10 days of locomotor activity across treatment group. (A) Active phase ultradian period in the τ's window in LD. (B) Active phase ultradian period in the τ'm window in LD. (C) Active phase ultradian period in the τ'l window in LD. (D) Light phase ultradian period in the τ's window in LD. (E) Light phase ultradian period in the τ'm window in LD. (F) Light phase ultradian period in the τ'l window in LD. (HET [females = 17; males = 16], KO [females = 11; males =14], WT [females = 5; males = 4]). *p<0.05, ***p<0.001 between sex

Ultradian Power Structure in LD and DD. In a LD cycle, dark phase UR power of WT and KO mice differed and over a short range of periods (from ~1.3-1.7 h; Fig. 27A). Power structure was comparable between HET and KO males (Fig. 27C & E). Similarly, in females, dark phase UR power of WT and KO mice differed and over a short range of longer periods (~3.2-3.8: Fig 27B), and HETs had more ultradian power than KOs for longer periods (~3.0-4.0 h; Fig. 27C) but HETs and WTs were comparable (Fig. 27D). In the light phase, there were no obvious effects of genotype on UR power distributions (Fig. 28).

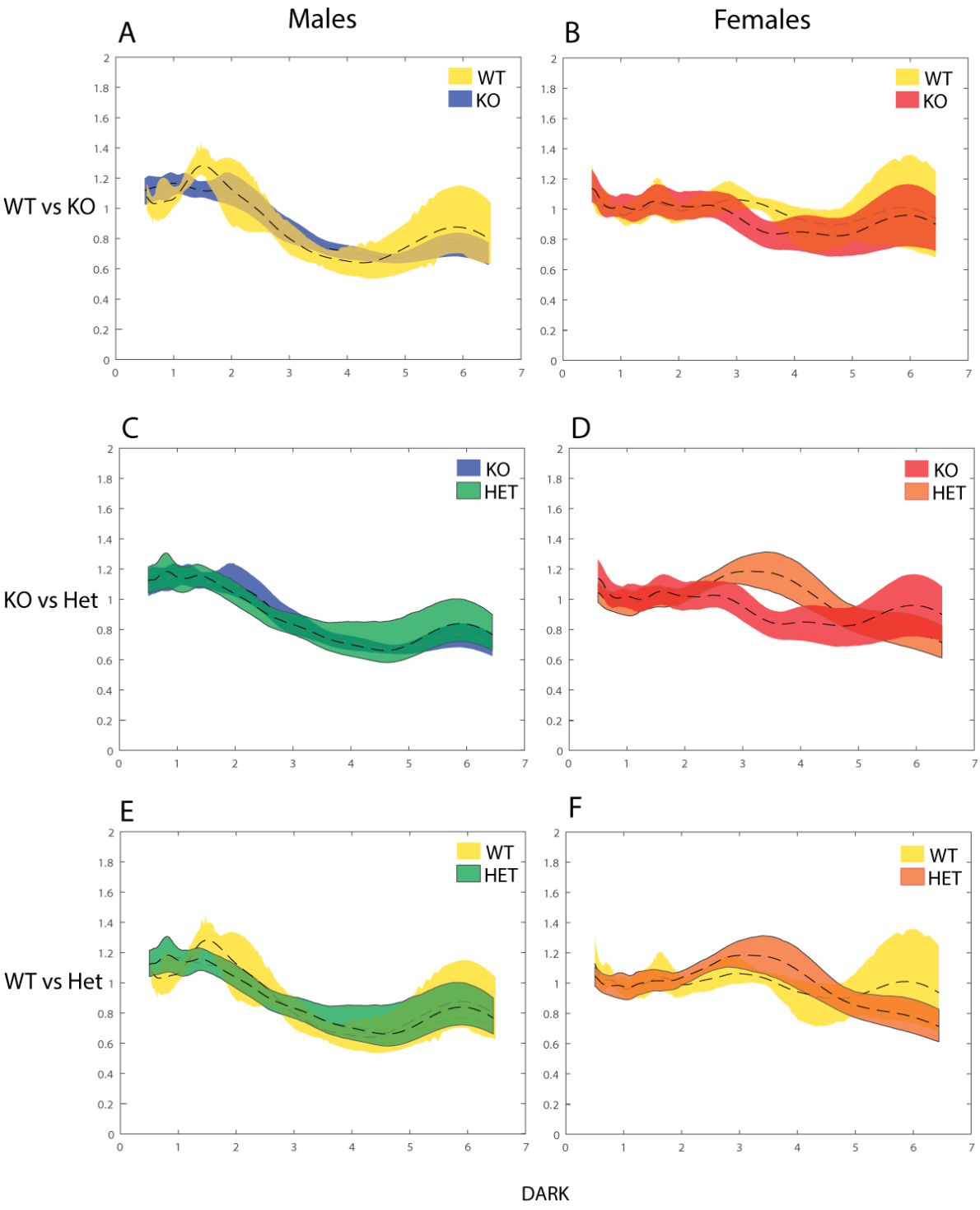

Figure 27: Dark phase ultradian power structure in 12L:12D

Ultradian power structure across period (τ') over a (.5 – 6.5 h) analysis window in LD. Average cross-correlational power at each scale-approximated period derived from the continuous wavelet transform on a time series consisting of locomotor activity during 10 consecutive dark or light phases in 12L:12D (A) Male KO and WT ultradian power structure in the dark phase. (B)

Figure 27, continued: Female KO and WT ultradian power structure in the dark phase. (C) Male KO and HET ultradian power structure in the dark phase. (D) Female KO and HET ultradian power structure in the dark phase. (E) Male HET and WT ultradian power structure in the dark phase. (F) Female HET and WT ultradian power structure in the dark phase. (Separate power curves within males: WT (yellow), HET (green), and KO (blue) and within females: WT (yellow), HET (orange), KO (red); the curves depict mean ± 95% confidence intervals (CIs) generated by bootstrapping male and female genotype groupings of these curves (Bootstrapped: 2000x ; (HET [females = 17; males = 16], KO [females = 11; males =14], WT [females = 5; males = 4]).

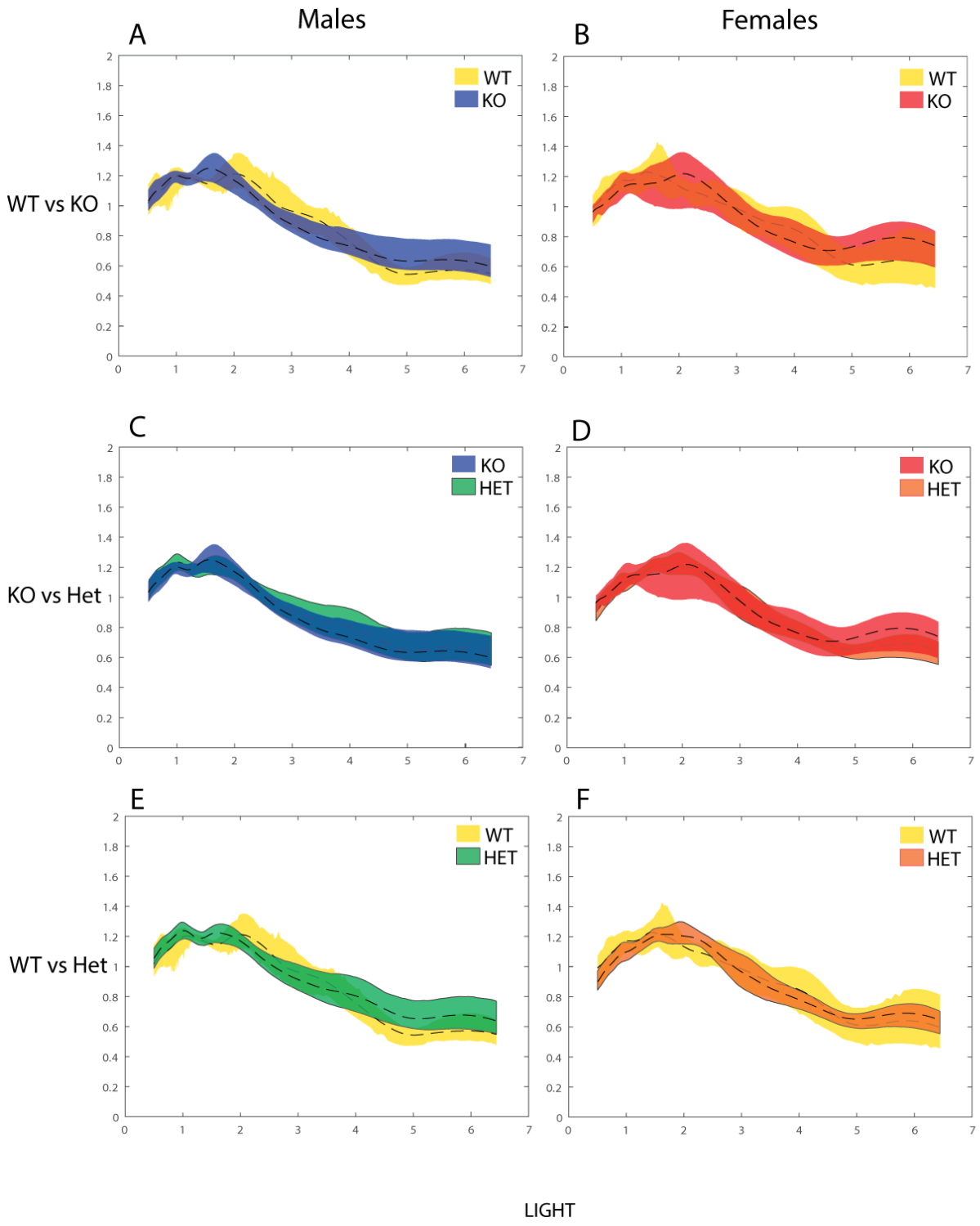

Figure 28: Light phase ultradian power structure in 12L:12D

Ultradian power structure across period (τ') over a (.5 – 6.5 h) analysis window in LD. Average cross-correlational power at each scale-approximated period derived from the continuous

Figure 28, continued: wavelet transform on a time series consisting of locomotor activity during 10 consecutive dark or light phases in 12L:12D. (A) Male KO and WT ultradian power structure in the light phase. (B) Female KO and WT ultradian power structure in the light phase. (C) Male KO and HET ultradian power structure in the light phase. (D) Female KO and HET ultradian power structure in the light phase. (E) Male KO and HET ultradian power structure in the light phase. (F) Female KO and HET ultradian power structure in the light phase. Separate power curves are depicted within males: WT (yellow), HET (green), and KO (blue) and within females: WT (yellow), HET (orange), KO (red); the curves depict mean ± 95% confidence intervals (CIs) generated by bootstrapping male and female genotype groupings of these curves (Bootstrapped: 2000x; (HET [females = 17; males = 16], KO [females = 11; males =14], WT [females = 5; males = 4]).

Comparing sexes, in WT mice, dark phase power was greater in males than females in a range of shorter periods (~1.0-1.5 h) and was greater in females than males in longer periods (~3.0-4.0 h; Fig. 29A). In HET mice, power was greater in females than males in longer periods (~2.5-4.5 h h; Fig. 29C). KOs were comparable across sex (29E). In the light phase, there were no obvious effects of genotype on UR power distributions (Fig. 29B, D, F).

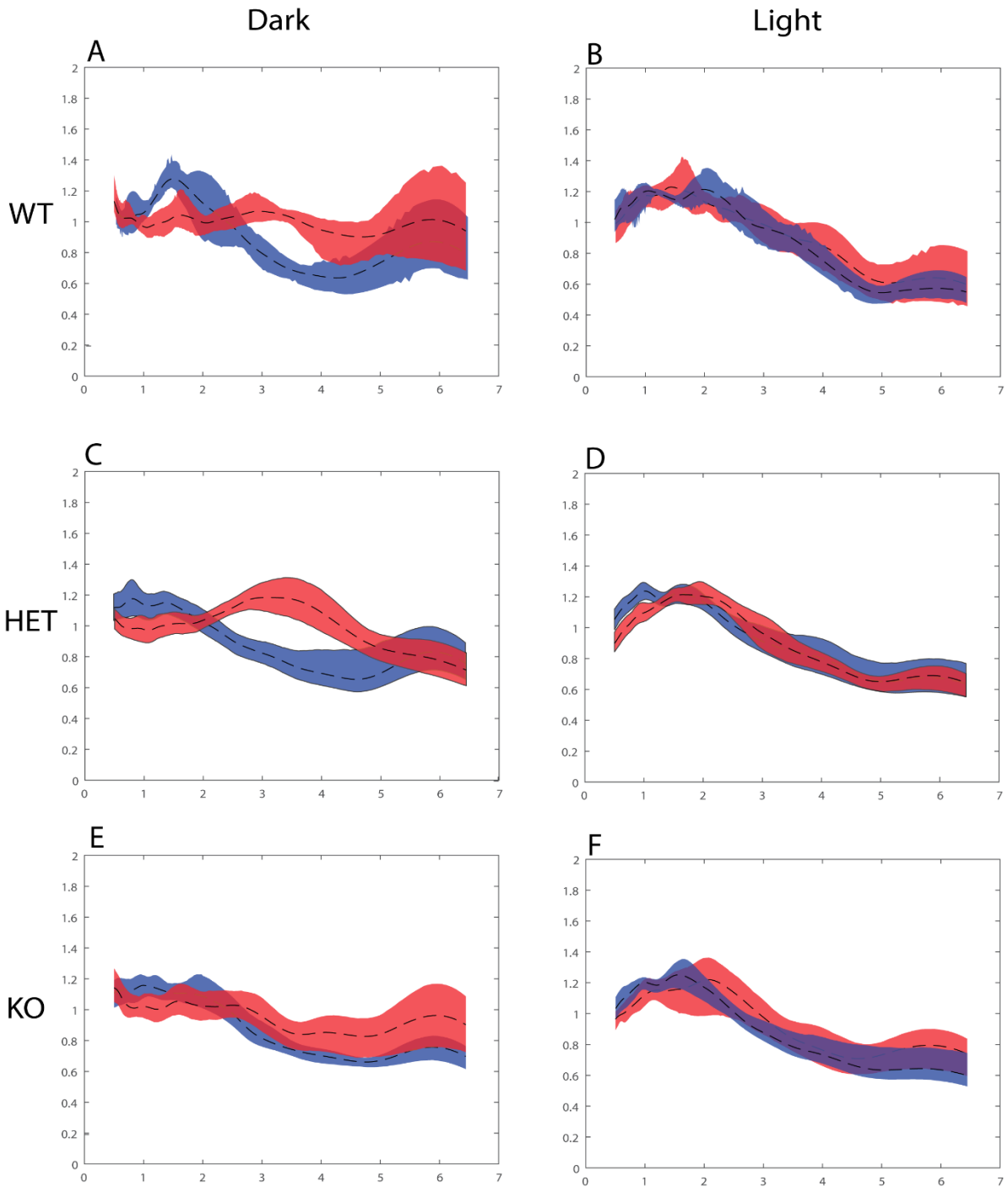

Figure 29: Male and female ultradian power structure in 12L:12D

Ultradian power structure across period (τ') over a (.5 – 6.5 h) analysis window in LD. Average cross-correlational power at each scale-approximated period derived from the continuous wavelet transform on a time series consisting of locomotor activity during 10 consecutive dark or light phases in 12L:12D. (A) WT male and female ultradian power structure in the dark phase. (B) WT male and female ultradian power structure in the light phase. (C) HET

Figure 29, continued: male and female ultradian power structure in the dark phase. (D) HET male and female ultradian power structure in the light phase. (E) KO male and female ultradian power structure in the dark phase. (F) KO male and female ultradian power structure in the light phase. Separate power curves are depicted for male (blue) and female (red) mice; the curves depict mean ± 95% confidence intervals (CIs) generated by bootstrapping male and female genotype groupings of these curves (Bootstrapped: 2000x ; (HET [females = 17; males = 16], KO [females = 11; males =14], WT [females = 5; males = 4]).

In DD, during the active phase, power structure of KO mice resembled that of WT and HET mice in both males and females (Fig. 30A-D). However, while WT and HET males were comparable (Fig. 30E), HET females exhibited an increase in wavelet power distributed across a band of URs from ~3.5 to 4.5 h compared to WTs (Fig. 30F). During the rest phase, UR power of WT and KO mice did not noticeably differ with the exception of a small increase in UR power across a narrow band of short periods in males (Fig. 31A). Otherwise, no effects of genotype on rest phase UR power in DD were evident (Fig. 31).

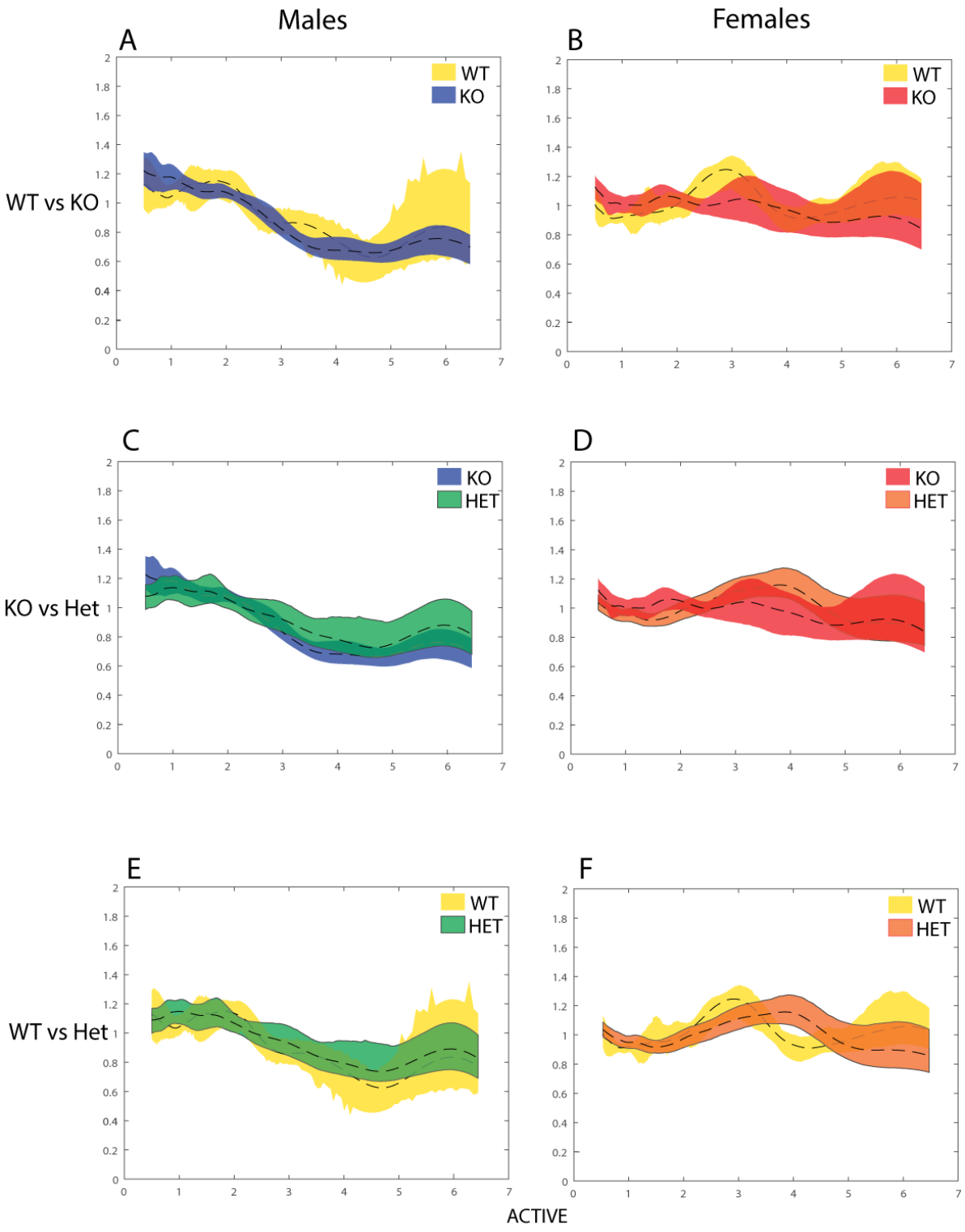

Figure 30: Active phase ultradian power structure in DD

Ultradian power structure across period (τ') over a (.5 – 6.5 h) analysis window in DD. Average cross-correlational power at each scale-approximated period derived from the continuous

Figure 30, continued: wavelet transform on a time series consisting of locomotor activity during 10 consecutive active or inactive phases in DD. (A) Male KO and WT ultradian power structure in the active phase. (B) Female KO and WT ultradian power structure in the active phase. (C) Male KO and HET ultradian power structure in the active phase. (D) Female KO and HET ultradian power structure in the active phase. (E) Male HET and WT ultradian power structure in the active phase. (F) Female HET and WT ultradian power structure in the active phase. (Separate power curves are depicted within males: WT (yellow), HET (green), and KO (blue) and within females: WT (yellow), HET (orange), KO (red); the curves depict mean ± 95% confidence intervals (CIs) generated by bootstrapping male and female genotype groupings of these curves (Bootstrapped: 2000x ; (HET [females = 17; males = 16], KO [females = 11; males =14], WT [females = 5; males = 4]).

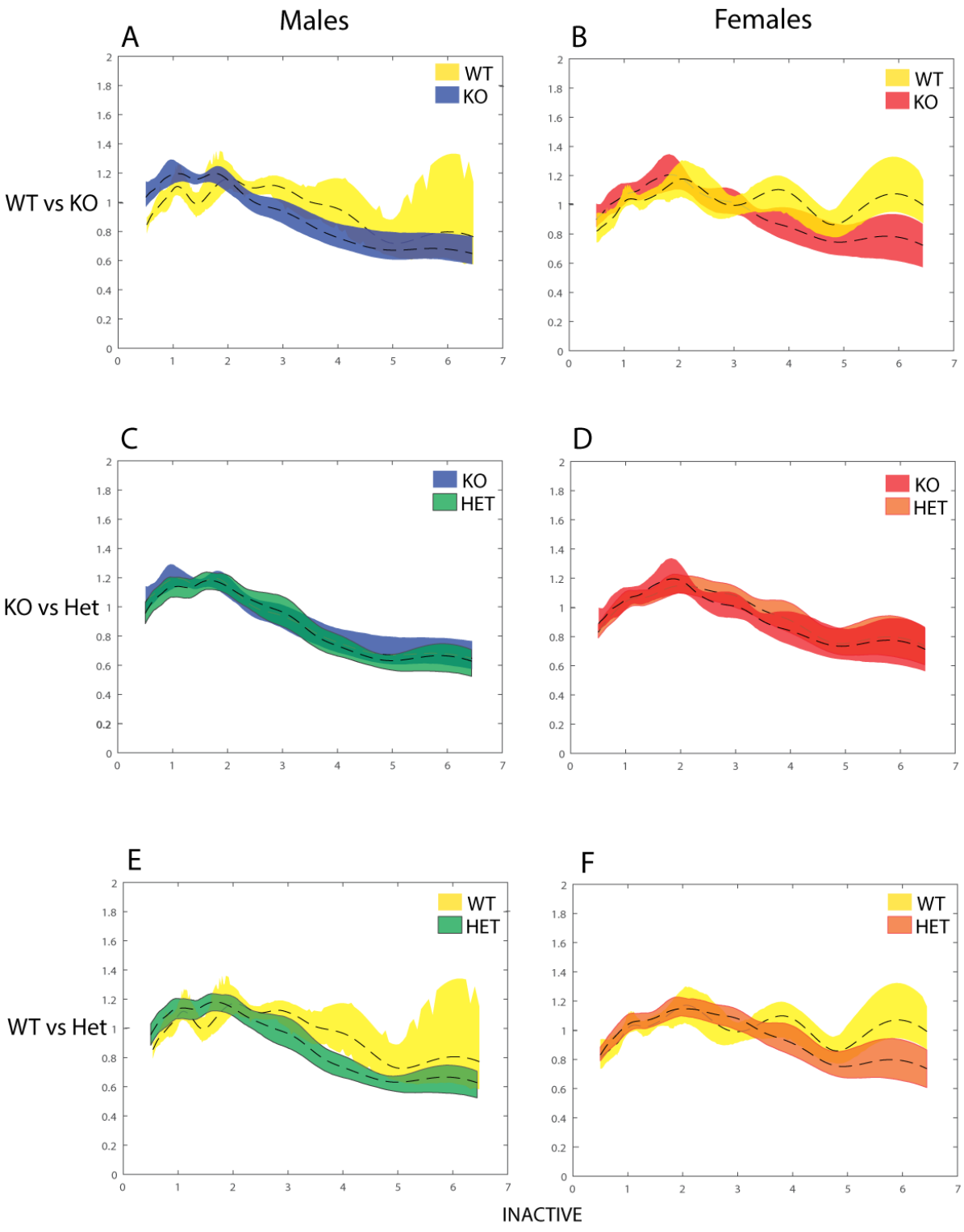

Figure 31: Inactive phase ultradian power structure in DD

Figure 31, continued: Ultradian power structure across period (τ') over a (.5 – 6.5 h) analysis window in DD. Average cross-correlational power at each scale-approximated period derived from the continuous wavelet transform on a time series consisting of locomotor activity during 10 consecutive active or inactive phases in DD. (A) Male KO and WT ultradian power structure in the inactive phase. (B) Female KO and WT HET ultradian power structure in the inactive phase. (C) Male KO and HET ultradian power structure in the inactive phase. (D) Female KO and HET ultradian power structure in the inactive phase. (E) Male HET and KO ultradian power structure in the inactive phase. (F) Female HET and KO ultradian power structure in the inactive phase. Separate power curves are depicted within males: WT (yellow), HET (green), and KO (blue) and within females: WT (yellow), HET (orange), KO (red); the curves depict mean ± 95% confidence intervals (CIs) generated by bootstrapping male and female genotype groupings of these curves (Bootstrapped: 2000x ; (HET [females = 17; males = 16], KO [females = 11; males =14], WT [females = 5; males = 4]).

Comparing sexes, in WT mice, similar to the dark-phase of LD, active phase power was greater in males than females in a range of shorter periods (~1.0-1.5 h) and was greater in females than males in distinct regions of a range of longer periods (spanning from 2- 5 h; Fig 32 A). A similar pattern of sex differences in the active phase of DD was evident in HET and KO mice, although the magnitude of the sex difference appeared to diminish from WT > HET > KO (Fig. 32 C, D). In the rest phase, there were no obvious effects of sex on UR power distributions (Fig. 32).

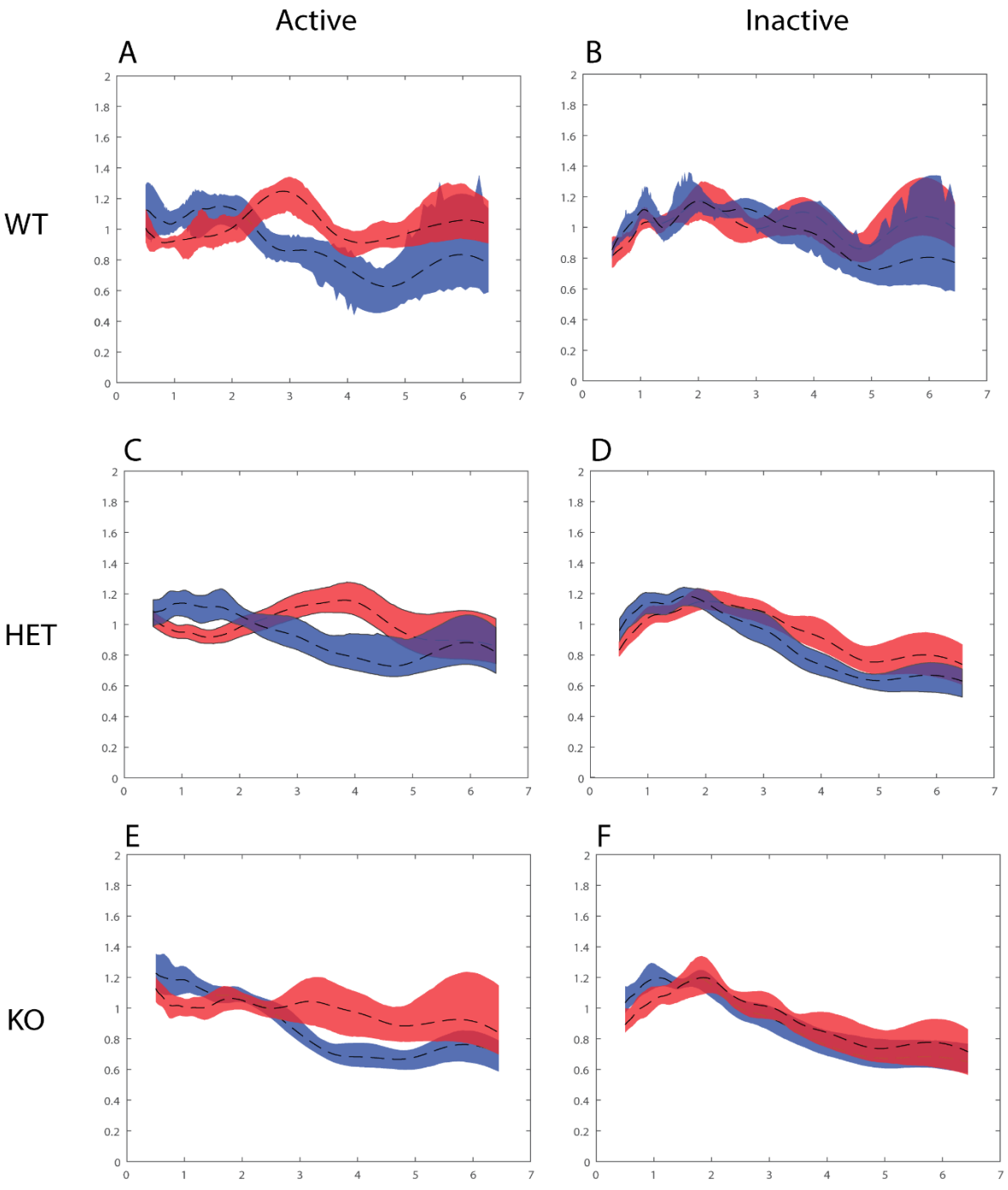

Figure 32: Male and female ultradian power structure in DD

Ultradian power structure across period (τ') over a (.5 – 6.5 h) analysis window in DD. Average cross-correlational power at each scale-approximated period derived from the continuous wavelet transform on a time series consisting of locomotor activity during 10 consecutive active

Figure 32, continued: or inactive phases in DD. (A) WT male and female ultradian power structure in the active phase. (B) WT male and female ultradian power structure in the inactive phase. (C) HET male and female ultradian power structure in the active phase. (D) HET male and female ultradian power structure in the inactive phase. (E) KO male and female ultradian power structure in the active phase. (F) KO male and female ultradian power structure in the inactive phase. (Separate power curves are depicted for male (blue) and female (red) mice; the curves depict mean ± 95% confidence intervals (CIs) generated by bootstrapping male and female genotype groupings of these curves (Bootstrapped: 2000x ; (HET [females = 17; males = 16], KO [females = 11; males =14], WT [females = 5; males = 4]).

Discussion:

The results described here are largely consistent with prior reports. In the circadian system, WT females showed greater activity (Iwahana et al., 2008; Kuljis et al., 2013; Stowie & Glass, 2015) and LSP amplitude in a 12L:12D light-dark cycle than their male counterparts (Fig. 22B). There also was no difference in circadian period between WT males and female (Iwahana et al., 2008; Kuljis et al., 2013). We did not identify a sex difference in onset variability or phase angle of entrainment, which have been previously reported in mice (Kuljis et al., 2013; Stowie & Glass, 2015), although these may be due to the difference in use of locomotor monitoring medium (running wheel vs PIR (Mather, 1981; Sherwin, 1998), the age of the animals (Stowie & Glass, 2015) and/or the relatively small number of WT mice reported here.

In the ultradian system we likewise replicated WT sex differences in ultradian power structure (Fig. 12 vs Fig. 29) and period in both the τ's and τ'l bands (Fig. 12 vs. Fig. 25) which we had first characterized in Chapter 4. Power structure was remarkably similar in both the directionality of the difference and distribution of power across period: males exhibited greater dark phase power in a band of short periods (~1-2 h) and females exhibited greater power in a band of longer periods (~4 h). Similarly, ridge period differences in WTs had the same directionality, with WT males having longer periods than females in the τ's band and shorter periods in the τ'l (Fig. 12 vs. Fig. 25). It is remarkable that such similar patterns of sex differences in URs manifested in the populations of mice under study in Chapters 4 and 6. These mice were investigated in our lab years apart, in different animal rooms, very likely have different microbiomes, and were handled by different lab members. They were of different age ranges, and although they are on a similar genetic background (C57BL6) they are from breeding colonies that have never intermixed, and thus there is undoubtedly some genetic drift between

these populations. Nevertheless, these sex differences in UR measures manifested. IN light of all the potential sources of variance and noise that could exist between these studies, such similarities suggest that these UR features are robust and replicable.

In general, effects of *ythdf1* on circadian behavior was more prominent in DD than in LD. *Ythdf* KO and HET mice stably entrained to light dark cycle, showing no difference in phase angle of entrainment or entrained period compared to WT mice. Upon release into DD, without the masking effects of light, differences across sex and genotype emerged in active and inactive phase activity, and onset variability.

Overall, several effects of the *ythdf1* KO were observed. In an idiosyncratic manner, genotype affected three traits: (1) LSP amplitude (Fig. 22), (2) total activity (Fig. 23), (3) and ultradian power structure (Fig. 27D & 30F). LSP amplitude is a measure of the total rhythmic power present at a specific circadian period. It captures the structure of the circadian system because circadian rhythms may have power distributed broadly around a given peak period, or may contain a great deal of circadian power at a narrow range around the peak; the latter would have much higher LSP power (PN value). WT females had greater LSP power than WT males, and in females (but not in males) *ythfd1* KO decreased LSP power; this effect was present in both LD and DD.Total activity was also greater in WT females, as was dark phase activity, and ythdf1 KO also reduced dark phase activity, again in females only. Although it is not clear it this is a specifically circadian effect of *ythdf1* KO, i.e., activity is less diurnal in KO mice, or if activity is simply lower in general. Why only females show this difference is less clear, though because females have more LSP power than males and greater activity ((Iwahana et al., 2008; Kuljis et al., 2013; Stowie & Glass, 2015), and may reflect a floor effect of average total activity. Finally, ultradian power structure in the active phase exhibited the expected pattern of male and

female power in WT mice (In LDF and DD). In both male and female KO mice however, UR power structure was modestly lower that WTs, in a few narrow regions of the UR range, in LD. In DD< there were no differences between WT and KO mice in either sex for this measure. Overall, whereas UR power structure differed markedly between males and females in WT mice, there were essentially no differences in UR power in KO mice. In sum, the effects of *ythdf*1 KO, where present, were more prominent in females than males. Moreover, in most instances where the circadian system exhibited a sex difference (activity, LPS power, UR parameters), this sex difference was no longer present in *ythdf1* KO mice. In a few instances however, the *ythdf1* mutation revealed sex differences: circadian period in DD was longer in females than males in both KOs and HETs, but not WTs. A similar pattern was true of onset variability in DD, with KO unmasking a sex difference not evident in WTs.

Relating the present work to the small literature that currently exists on RNA methylation and circadian rhythms: in line with previously reported results, of the effect of m6A methylation on circadian period, KOs and HETs trended toward having differ periods than WTs; but inconsistent with prior reports, period trended toward being shorter rather than longer (J. M. Fustin et al., 2013; Fustin et al., 2018), though these differences were rather modest. It should be noted that *Ythdf1* is not the only reader of m6A methylation (Jiang et al., 2021; Meyer & Jaffrey, 2017) another of which has already been implicated in circadian function (Zhong et al., 2018), and thus the present data do not reflect an exhaustive examination of the effects of RNA methylation on circadian rhythms,

Taken together, the m6A methylation reader *ythdf1* affects both the circadian and ultradian systems and has implications for sex differences therein. In line with earlier chapters (Riggle et al., 2022) these results show that sex difference in the circadian system are maintained by more

than just the organizational and activational role of sex hormones. The epigenetic regulation of the circadian clock is also sexually differentiated. In addition, these results for the first time implicate a role of epigenetic regulatory mechanisms in ultradian rhythms: m6A KO induces several modest changes in the ultradian system and eliminates UR sex differences. As differences in the ultradian and circadian systems were not consistent, ultradian effects of *ythdf1* KO observed here are unlikely to merely reflect a by-product of some effects of YTHDF1 in the circadian system. Rather, I propose that epigenetic regulation of 'RNA reading' may directly participate in the expression of ultradian rhythms.

Chapter 7: General Discussion:

The work described here documents rigorous investigations of rhythmic processes and sex differences therein. In Chapter 3, I showed that mice homozygous for a functional deletion in the Period-2 gene (*Per2*$^{m/m}$ mice) exhibited short free-running circadian periods and eventually lost behavioral circadian rhythmicity in constant darkness (DD). I investigated *Per2*$^{m/m}$ mice in DD for several months and identified a categorical sex difference in the dependence on *Per2* for maintenance of circadian rhythms. Nearly all female *Per2*$^{m/m}$ mice became circadian arrhythmic in DD, whereas free-running rhythms persisted in 37% of males. Remarkably, with extended testing, *Per2*$^{m/m}$ mice did not remain arrhythmic in DD, but after varying intervals spontaneously recovered robust, free-running circadian rhythms, with periods shorter than those expressed prior to arrhythmia. Spontaneous recovery was strikingly sex-biased, occurring in 95% of females and 33% of males. This sort of spontaneous recovery had not been reported previously in arrhythmic per2 mice (although it has been reported previously in a double KO model Per2^{Brdm1}/Rev-Erbα$^{-/-}$, though not extensively studied (Schmutz et al., 2010)), and although I would speculate that this could be due to disproportionate study of males in neuroscience research (Beery & Zucker, 2011; Woitowich et al., 2020), males in fact were less likely to exhibit arrhythmia in the first place, so sex bias is unlikely to be the reason this has escaped attention. Instead, the extended intervals of analyses used here are rare in chronobiology, and likely played a major role in my ability to identify the diverse phenotypes/chronotypes present in the per2^{Brdm1} mutant mouse. Castration in adulthood resulted in male *Per2*$^{m/m}$ mice exhibiting female-like levels of arrhythmia in DD, but did not affect spontaneous recovery. Taken together, the results of Experiment 1 suggest that the circadian pacemaker of many gonad-intact males, but not females, can persist in DD for long intervals without a functional PER2 protein; these female circadian

clocks may be incapable of sustaining persistent coherent circadian organization, resulting in transient cycles of circadian organization and arrhythmia.

In Chapter 4, I shifted focus to the ultradian system. Circadian rhythms provide daily temporal structure to cellular and organismal biological processes, ranging from gene expression to cognitive attention. Higher-frequency (intra-daily) ultradian rhythms are similarly ubiquitous but have garnered far less empirical study, in part because of the properties that define them—multimodal periods, non-stationarity, circadian harmonics, and diurnal modulation - pose challenges to their accurate and precise quantification. Wavelet analyses are ideally suited to address these challenges, but wavelet-based measurement of ultradian rhythms has remained largely idiographic. So, in Experiment 2, I undertook the development of a novel analytical approach, based on the discrete and continuous wavelet transforms, in order to permit quantification of rhythmic power distribution across a broad ultradian spectrum, as well as precise identification of period within empirically-determined ultradian bands. I also sought to generate wavelet analyses that allowed data reduction: the result of which could be a quantitative value(s) that could be abstracted from the normalized wavelet matrices and aggregated across individuals within treatment groups to allow group-level analyses of experimental treatments, thereby circumventing limitations of idiographic approaches.

The accuracy and precision of these wavelet analyses were validated using extensive *in silico* and *in vivo* models with known ultradian features. Using a spike-recovery paradigm, wherein a simulated circadian waveform was adulterated with a complex, but defined (known) ultradian signal, I found the wavelet analyses to be accurate and precise. This was true for the power distribution analyses and for the period measures. Moreover, I found that splitting the activity data into light-phase and dark-phase activity *prior to* wavelet analyses resulted in more accurate

and precise ultradian measures relative to parsing *after* the wavelet transform, although it should be noted that parsing after was still more accurate than not parsing the data at all. Finally, one critique of the simulations used in Chapter 4 is that they used simulated, rather than real, activity data. To address this potential shortcoming, we used real data from mice with the *per2* mutation in a final simulation. *Per2*$^{m/m}$ mice exhibit a remarkable flexibility in their ability to generate activity that synchronizes with high frequency (4 h period) light dark cycles. These animals allowed us, then, to generate actual (rather than simulated) locomotor activity data that could be driven at known periodicities (essentially, a spike recovery paradigm, at a period of exactly 4 h, except with the spike being generated by the animal's natural ability to synchronize behavior with the light dark cycle, rather than by my artificially generated values). Here again, the results indicated a remarkably accurate recovery of locomotor activity from the wavelet analyses. Taken together, these procedures offer a valid, precise and accurate methodology for quantification of URs

I next examined group-level effects (of sex, gonadectomy, and photoperiod) on mouse URs. The results of these experiments showed that male and female mice yielded robust and repeatable measures of ultradian period and power in home cage locomotor activity, confirming and extending reports of ultradian rhythm modulation by sex, gonadal hormones, and circadian entrainment. Seasonal changes in day length modulated ultradian period and power, and exerted opposite effects in the light and dark phases of the 24-hr day, underscoring the importance of evaluating ultradian rhythms with attention to circadian phase. Sex differences in ultradian rhythms were more prominent at night and depended on gonadal hormones in male mice. In sum, relatively straightforward modifications to the wavelet procedure allowed quantification of ultradian rhythms with appropriate time-frequency resolution, generating accurate and repeatable

measures of period and power which are suitable for group-level analyses. These analytical tools may afford deeper understanding of how ultradian rhythms are generated and respond to interoceptive and exteroceptive cues.

In Chapter 5 (Experiment 3) I returned to further examine the findings from Chapter 3 (Experiment 1). *Per2*$^{m/m}$ mice exhibit circadian arrhythmia constant darkness (DD). But many of these *Per2*$^{m/m}$ mutant mice do not go arrhythmic (ARR) immediately in DD, and instead maintain rhythmicity for many cycles. Indeed, many *Per2*$^{m/m}$ mice never exhibit ARR at all, even in the ones that do so, the onset of ARR in DD ranges from a few days to many weeks across individuals. *Per2*$^{m/m}$ mutant mice likely possess a rapidly-dampening circadian clock, but why only some *Per2*$^{m/m}$ mutant mice exhibit ARR in DD, and why the latency to ARR varies so widely among individuals is not presently known.

Circadian entrainment after-effects enduringly impact behavioral circadian rhythms in DD (Aschoff, 1981). Non-24 h T-cycles alter free-running period in DD, and entrainment to very long photoperiods can profoundly alter the organization of the SCN circadian network. If circadian network organization is relevant to whether *Per2*$^{m/m}$ mice can maintain circadian rhythms in DD, then I predicted that network-altering entrainment aftereffects may affect ARR in DD. Separately, it is also possible that some individual *Per2*$^{m/m}$ mutant mice may simply have a propensity for ARR in DD, for reasons unrelated to the circadian network state. Such a propensity for ARR may be a stable trait in some individuals. If so, then a mouse's chronotype during one interval of exposure to DD may predict its chronotype during a subsequent interval of DD. Alternatively, ARR may reflect an interaction between PER2 and unspecified, stochastic events. To test among these hypotheses, I used a VLD photoperiod to manipulate the circadian network and examined the effects of this manipulation on arrhythmia in DD. Mice were

entrained to very long days and very short days, then put into constant darkness for 110 days; I then allowed them to re-entrain for 30 days, and released them back into constant darkness for a second 110-day interval. The results of these studies again confirm my (Chapter 3) and others' (Zheng et al., 1999) observations of a 'delayed ARR' chronotype in DD among *Per2*$^{m/m}$ mutant mice. Entrainment to very long day lengths, though, did not affect the incidence or emergence of circadian arrhythmia in DD, although in one comparison it appeared that the VLD mice which became ARR did so faster (in DD2). Thus, circadian entrainment aftereffects are unlikely to explain the behavior of *Per2*$^{m/m}$ mice in DD. Finally, a mouse's chronotype in DD1 did not predict its chronotype in DD2, suggesting that a propensity for ARR is not a stable trait, but instead may reflect the state of the circadian network at any point in time, in response to factors that we have yet to specify. Ultimately, at a population level, many *Per2*$^{m/m}$ mutant mice exhibit ARR, but for any given individual *Per2*$^{m/m}$ mouse, ARR in DD is not a stable, repeatable chronotype.

Finally, in Chapter 6, I took a broader view and applied the tools and analyses developed in Chapters 3 and 4, to examine connections between sex differences in the circadian system and epigenetic regulation. Sex differences are pervasive in biological rhythms. Basic temporal features of circadian and ultradian rhythms vary across sex. The neural substrates of the circadian pacemaker are sexually dimorphic, in both electrophysiological and anatomical features. In humans too, men and women experience different clinical outcomes after chronic circadian disruption. And my recent work from Chapter 3 showed that at least one of the core clock genes, *per2* is indispensable for females but not so for males, as it regards the maintenance of biological rhythms in constant darkness. Little is known, however, about how the role of epigenetic regulation of biological rhythms may vary across sex. I examined whether mice with a

knockout of a methylation reader (*ythdf1*) would exhibit altered circadian and ultradian rhythms and if these alterations might vary across sex. Using locomotor activity from *ythdf1* knockout, heterozygote, and wildtype mice, I demonstrated several aspects of circadian and ultradian behavior (activity levels, circadian onset variability, ultradian period, and ultradian power structure) that were altered in the absence of normal *ythdf1*-dependent activity. Collectively, these data implicate m6A in the expression of circadian and ultradian rhythms and suggest a role of epigenetics in shaping the sex differences in multiple levels of biological timing.

Taken together, the studies reported here allowed novel insights into the ways in which the circadian and ultradian systems are sexually differentiated, and affected by internal (hormones, sex, epigenetics) and external (photoperiod) stimuli. I also have created an analysis workflow which holds great promise to advance the study of ultradian rhythms. Collectively the work opens a door for a greater insight into how sex and biological-timekeeping interface, and at the same time challenges long-held dogma and assumptions about the molecular mechanics of the circadian clock (e.g., sex-independence, role of RNA processing).

Limitations

Nevertheless, my work is limited in its ability to uncover the mechanisms of the processes I investigated. Much of the data here is described is quantified observations of behavior and its structure, but the neural and molecular underpinnings of these observations remain elusive. Moreover, limitations to the ways some experiments were conducted constrain insights. For example, an unbalanced number of WTs in Chapter 6, and issues with documentation in the administration of the collaborative effort that yielded these data further reduced sample size, both of which together prevented us from disentangling the effects of sex and genotype from one another. Chapter 5 had a similarly themed issue: because I expected an overall high level of

arrhythmia in DD, I assumed the experiment could be conducted with a sample size of ~10 mice per group. Unexpectedly, the incidence of arrhythmia ~50% lower, and thus it was not possible to robustly statistically characterize many of the quantitative differences I found in this study. Subsequent studies in our lab (conducted in 2021 and 2022) identified much higher rates of ARR in *Per2* females (>80%; J. Love, unpublished data). Ultimately, the reasons why the populations in Chapter 3 and Chapter 5 exhibited such different levels of ARR in DD cannot be specified.

Other shortcomings were related to resource limitation: both gonadectomy studies reported here described would have been greatly improved by having a hormone replacement component (using T, E2, and DHT) to pin down the specific receptors that mediate effects of gonadal hormones on CRs and URs. And in Chapter 4, locomotor activity of animals prior to gonadectomy would have better characterized how the loss of gonadal hormones affected ultradian power structure.

These shortcomings, however, are true of any experiment and reflective of my evolution as a doctoral student. My skills and knowledge evolved and improved throughout this process of investigation. My doctoral contributions may be broader in scope than they are in depth of inquiry, but are nevertheless will represent valuable contributions to the literature.

Beyond the work described in the previous chapters, four broader issues are worthy of further discussion. I treat with each below. briefly.

Sex differences in biological rhythms

Throughout these studies, I regularly replicated prior findings of sex differences in circadian activity and power (Yan & Silver, 2016). But I also described previously-undocumented sex differences in the circadian and ultradian systems of mice. In Chapter 3 I showed that the major clock gene *per2*, which plays a crucial role in the circadian system of diverse taxa from

mammals (Zheng et al., 1999) to (via orthologs) insects (Konopka & Benzer, 1971) is sexually diphenic in its capacity to maintain circadian time. Moreover, I demonstrated that this diphenism is mediated by the activational effects of gonadal hormones, but only those created by the testes. That is: castration of Per2m/m males rendered them female-like in their rates of ARR (increasing the incidence of ARR from <50% to nearly 100%), but ovariectomy of *Per2*$^{m/m}$ females did not render them male-like (i.e., OVx females still exhibited high levels of ARR). Thus, male but not female gonadal hormones are essential for maintaining this sex difference. The SCN exhibits androgen receptors (Iwahana et al., 2008), which would seem a reasonable site to suspect gonadal hormones are acting in males. However, future work will need to address this conjecture. Chapter 5 also found sex differences, here in URs, and also found that gonadectomy caused many of these sex differences to disappear. Finally, Chapter 6 took a more molecular approach, and identified how male and female mice depend on epigenetic regulation of their circadian systems differently; but both seem to rely on epigenetic regulation for maintenance of normal URs.

Chapter 4 replicated observations of sex differences in the ultradian rhythms of rodents (Daan et al., 1975; Painson & Tannenbaum, 1991; Prendergast, Cisse, et al., 2012; Smarr et al., 2017; Wollnik & Turek, 1988) and extended this theme to mice. Furthermore, I invented and extensively validated a methodology for quantifying URs in a light dark cycle. Robust sex differences in the period and power of the ultradian system of mice were quantified. Chapter 6, using an entirely different population of mice, years removed, and derived from a different colony demonstrated remarkably similar ultradian power structure and periods. I also showcased a previously unknown role of RNA processing at the m6A site in the manifestation of these differences. Further work is needed to more fully explore these sex differences in the role of

RNA methylation in CRs. Critical next steps will be to perform immunoprecipitation studies (against YTHDF1) to identify which RNAs are differentially targeted by YTHDF1. I would predict that some clock genes may be identified in such a bioinformatics-based screening, but also many other clock-driven proteins would likely be implicated. Taken together the data presented in this dissertation support the conjecture that male and female circadian and ultradian systems are configured differently at the molecular level, and respond differently to interoceptive cues (hormones, biological sex, epigenetics) and exteroceptive cues (light, normal seasonal photoperiods, exaggerated VLD entrainment aftereffects).

'Spontaneous' circadian recovery in *Per2*$^{m/m}$ mice

Per2$^{m/m}$ Mutants recovered rhythmicity with extended intervals of constant darkness. Even when overall incidence of arrhythmia was reduced in Chapter 5, spontaneous recovery occurred at high rates, especially in females. Spontaneous recovery was also evident after major surgical procedures. Mice routinely exhibited multiple rounds of ARR and recovery in Chapter 3, and in Chapter 5 mice that recovered rhythmicity in DD1 still exhibited ARR and or recovery in DD2, all together suggesting that a single instance of recovery does not permanently alters the circadian network. Given that *per2* is a critical circadian gene, and that many individuals cannot sustain CRs in the absence of *per2* (even if it may take extended intervals of DD for this to happen), it becomes an interesting question to ask: when mice eventually lose CRs in DD which circadian clock genes mediate this spontaneous recovery? Future work may profitably seek to examine which circadian genes are required for recovery in *Per2*$^{m/m}$ mutant mice.

Evaluation of Circadian Arrhythmia in Behavioral Data

The chronotype of Per2$^{m/m}$ mutant presented here was performed by an individual expert scorer who was blind to all experimental manipulations, other than the fact that the records were

from mice, and that the mice were transferred to D on a particular date. Inevitably, operationally defining and measuring ARR in this way introduces a degree of subjectivity into the results. This may have factored into the decreased incidence observed in Chapter 5: PIR data in chapter 5 were much sparser that those obtained in Chapters 3, 4 or 6., and this may have affected the subjective assessment of ARR. Nevertheless, the scoring was ultimately confirmed by both the Fast Fourier Transform and Lomb-Scargle Periodogram. Still, a lingering problem surrounds the level of circadian power that defines ARR. There is not a consensus in the literature (Bunger et al., 2000; Oster et al., 2002; Van Der Horst et al., 1999; Zheng et al., 1999). Using no detectable rhythmicity in the circadian range of the χ^2, FFT or LSP periodogram is one approach, but in preliminary analyses, when such measures were compared to our subjective impressions of actograms, false positives and false negatives were very common. Frequently, mice which appeared clearly rhythmic did not show any peaks in the circadian domain of the periodogram, but had a very prominent peak at 12 hours, which impeded easy quantitative-based scoring of arrhythmia. Similar problems affected evaluations of spontaneous circadian recovery. It would be useful to establish a quantitative algorithm that would permit purely objective assignment of the ARR chronotype, and the re-emergence of the recovered rhythmic phenotype.

Wavelet Analyses

Finally, one of the most meaningful contributions in this dissertation is the invention of a novel workflow for wavelet-based analyses of URs. The techniques developed and described here were robust enough to allow replication (across experiments performed years apart in different animals, reared in different labs): the detection of a strikingly similar sex-specific patterns of UR power structure and UR period (reported in Chapter 4 and in Chapter 6). Moreover, Chapter 6, extended the utility of this analysis to include a modification of

measurement of parsed URs in constant darkness. And again, in Chapter 6 when DD data were parsed into “active” and “inactive” phases, I saw UR power and period that was strikingly similar to the values I saw when activity data were parsed into “dark” and “light” phases (in Chs. 4 and 6), suggesting not only that this method reliably deals with the problem of activity phase-specific parsing in constant darkness, but also, importantly, that ultradian power structure is not simply a consequence of masking effects generated by the presence of a light-dark cycle, but is spontaneously generated by mice even in the absence of periodic environmental input – the hallmark of a truly endogenous rhythm.

References:

Abe, M., Herzog, E. D., Yamazaki, S., Straume, M., Tei, H., Sakaki, Y., Menaker, M., & Block, G. D. (2002). Circadian rhythms in isolated brain regions. *J Neurosci*, *22*(1), 350-356. https://www.ncbi.nlm.nih.gov/pubmed/11756518

Abraham, D., Dallmann, R., Steinlechner, S., Albrecht, U., Eichele, G., & Oster, H. (2006). Restoration of circadian rhythmicity in circadian clock-deficient mice in constant light. *J Biol Rhythms*, *21*(3), 169-176. https://doi.org/10.1177/0748730406288040

Ahima, R. S., & Antwi, D. A. (2008). Brain regulation of appetite and satiety. *Endocrinology and metabolism clinics of North America*, *37*(4), 811-823.

Akhtar, R. A., Reddy, A. B., Maywood, E. S., Clayton, J. D., King, V. M., Smith, A. G., Gant, T. W., Hastings, M. H., & Kyriacou, C. P. (2002). Circadian cycling of the mouse liver transcriptome, as revealed by cDNA microarray, is driven by the suprachiasmatic nucleus. *Curr Biol*, *12*(7), 540-550. https://doi.org/10.1016/s0960-9822(02)00759-5

Albrecht, U., Zheng, B., Larkin, D., Sun, Z. S., & Lee, C. C. (2001). MPer1 and mper2 are essential for normal resetting of the circadian clock. *Journal of biological rhythms*, *16*(2), 100-104.

Appenroth, D., Nord, A., Hazlerigg, D. G., & Wagner, G. C. (2021). Body Temperature and Activity Rhythms Under Different Photoperiods in High Arctic Svalbard ptarmigan (Lagopus muta hyperborea). *Front Physiol*, *12*, 633866. https://doi.org/10.3389/fphys.2021.633866

Aschoff, J. (1981). Freerunning and entrained circadian rhythms. In *Biological rhythms* (pp. 81-93). Springer.

Asher, G., Gatfield, D., Stratmann, M., Reinke, H., Dibner, C., Kreppel, F., Mostoslavsky, R., Alt, F. W., & Schibler, U. (2008). SIRT1 regulates circadian clock gene expression through PER2 deacetylation. *Cell*, *134*(2), 317-328.

Aten, S., Hansen, K. F., Snider, K., Wheaton, K., Kalidindi, A., Garcia, A., Alzate-Correa, D., Hoyt, K. R., & Obrietan, K. (2018). miR-132 couples the circadian clock to daily rhythms of neuronal plasticity and cognition. *Learn Mem*, *25*(5), 214-229. https://doi.org/10.1101/lm.047191.117

Aviram, R., Dandavate, V., Manella, G., Golik, M., & Asher, G. (2021). Ultradian rhythms of AKT phosphorylation and gene expression emerge in the absence of the circadian clock components Per1 and Per2. *PLoS Biol*, *19*(12), e3001492. https://doi.org/10.1371/journal.pbio.3001492

Azzi, A., Dallmann, R., Casserly, A., Rehrauer, H., Patrignani, A., Maier, B., Kramer, A., & Brown, S. A. (2014). Circadian behavior is light-reprogrammed by plastic DNA methylation. *Nat Neurosci*, *17*(3), 377-382. https://doi.org/10.1038/nn.3651

Azzi, A., Evans, J. A., Leise, T., Myung, J., Takumi, T., Davidson, A. J., & Brown, S. A. (2017). Network Dynamics Mediate Circadian Clock Plasticity. *Neuron*, *93*(2), 441-450. https://doi.org/10.1016/j.neuron.2016.12.022

Bae, K., Jin, X., Maywood, E. S., Hastings, M. H., Reppert, S. M., & Weaver, D. R. (2001). Differential functions of mPer1, mPer2, and mPer3 in the SCN circadian clock. *Neuron*, *30*(2), 525-536.

Bailey, M., & Silver, R. (2014). Sex differences in circadian timing systems: implications for disease. *Front Neuroendocrinol*, *35*(1), 111-139. https://doi.org/10.1016/j.yfrne.2013.11.003

Balsalobre, A. (2002). Clock genes in mammalian peripheral tissues. *Cell Tissue Res*, *309*(1), 193-199. https://doi.org/10.1007/s00441-002-0585-0

Beale, A., Guibal, C., Tamai, T. K., Klotz, L., Cowen, S., Peyric, E., Reynoso, V. H., Yamamoto, Y., & Whitmore, D. (2013). Circadian rhythms in Mexican blind cavefish Astyanax mexicanus in the lab and in the field. *Nature Communications*, *4*. https://doi.org/ARTN 2769 10.1038/ncomms3769

Beery, A. K. (2018). Inclusion of females does not increase variability in rodent research studies. *Current opinion in behavioral sciences*, *23*, 143-149.

Beery, A. K., & Zucker, I. (2011). Sex bias in neuroscience and biomedical research. *Neuroscience & Biobehavioral Reviews*, *35*(3), 565-572.

Belchetz, P. E., Plant, T. M., Nakai, Y., Keogh, E. J., & Knobil, E. (1978). Hypophysial responses to continuous and intermittent delivery of hypopthalamic gonadotropin-releasing hormone. *Science*, *202*(4368), 631-633. https://doi.org/10.1126/science.100883

Beymer, M., Henningsen, J., Bahougne, T., & Simonneaux, V. (2016). The role of kisspeptin and RFRP in the circadian control of female reproduction. *Mol Cell Endocrinol*, *438*, 89-99. https://doi.org/10.1016/j.mce.2016.06.026

Bixler, E. O., Papaliaga, M. N., Vgontzas, A. N., LIN, H. M., Pejovic, S., Karataraki, M., VELA-BUENO, A., & Chrousos, G. P. (2009). Women sleep objectively better than men and the sleep of young women is more resilient to external stressors: effects of age and menopause. *Journal of sleep research*, *18*(2), 221-228.

Blattner, M. S., & Mahoney, M. M. (2012). Circadian parameters are altered in two strains of mice with transgenic modifications of estrogen receptor subtype 1. *Genes Brain Behav*, *11*(7), 828-836. https://doi.org/10.1111/j.1601-183X.2012.00831.x

Blessing, W., & Ootsuka, Y. (2016). Timing of activities of daily life is jaggy: how episodic ultradian changes in body and brain temperature are integrated into this process. *Temperature*, *3*(3), 371-383.

Bloch, G., Barnes, B. M., Gerkema, M. P., & Helm, B. (2013). Animal activity around the clock with no overt circadian rhythms: patterns, mechanisms and adaptive value. *Proceedings of the Royal Society B: Biological Sciences*, *280*(1765), 20130019.

Blum, I. D., Zhu, L., Moquin, L., Kokoeva, M. V., Gratton, A., Giros, B., & Storch, K.-F. (2014). A highly tunable dopaminergic oscillator generates ultradian rhythms of behavioral arousal. *Elife*, *3*, e05105.

Bourguignon, C., & Storch, K. F. (2017). Control of Rest:Activity by a Dopaminergic Ultradian Oscillator and the Circadian Clock. *Front Neurol*, *8*, 614. https://doi.org/10.3389/fneur.2017.00614

Brockman, R., Bunick, D., & Mahoney, M. M. (2011). Estradiol deficiency during development modulates the expression of circadian and daily rhythms in male and female aromatase knockout mice. *Hormones and Behavior*, *60*(4), 439-447. https://doi.org/10.1016/j.yhbeh.2011.07.011

Buijs, R. M., Ruiz, M. A. G., Hernández, R. M., & Cortés, B. R. (2019). The suprachiasmatic nucleus; a responsive clock regulating homeostasis by daily changing the setpoints of physiological parameters. *Autonomic Neuroscience*, *218*, 43-50.

Bunger, M. K., Wilsbacher, L. D., Moran, S. M., Clendenin, C., Radcliffe, L. A., Hogenesch, J. B., Simon, M. C., Takahashi, J. S., & Bradfield, C. A. (2000). Mop3 is an essential component of the master circadian pacemaker in mammals. *Cell*, *103*(7), 1009-1017.

Burdakov, D., Liss, B., & Ashcroft, F. M. (2003). Orexin excites GABAergic neurons of the arcuate nucleus by activating the sodium—calcium exchanger. *Journal of Neuroscience*, *23*(12), 4951-4957.

Butler, M. P., Karatsoreos, I., Kriegsfeld, L. J., & Silver, R. (2017). Circadian regulation of endocrine functions. In *Mammalian Hormone-Behavior Systems* (pp. 345-369). Elsevier.

Cai, W., Rambaud, J., Teboul, M., Masse, I., Benoit, G., Gustafsson, J. A., Delaunay, F., Laudet, V., & Pongratz, I. (2008). Expression levels of estrogen receptor beta are modulated by components of the molecular clock. *Mol Cell Biol*, *28*(2), 784-793. https://doi.org/10.1128/MCB.00233-07

Cain, S. W., Dennison, C. F., Zeitzer, J. M., Guzik, A. M., Khalsa, S. B. S., Santhi, N., Schoen, M. W., Czeisler, C. A., & Duffy, J. F. (2010). Sex differences in phase angle of entrainment and melatonin amplitude in humans. *Journal of biological rhythms*, *25*(4), 288-296.

Cannon, W. B. (1929). Organization for physiological homeostasis. *Physiological reviews*, *9*(3), 399-431.

Cardone, L., Hirayama, J., Giordano, F., Tamaru, T., Palvimo, J. J., & Sassone-Corsi, P. (2005). Circadian clock control by SUMOylation of BMAL1. *Science*, *309*(5739), 1390-1394.

Cassone, V. M. (2014). Avian circadian organization: a chorus of clocks. *Frontiers in neuroendocrinology*, *35*(1), 76-88.

Cermakian, N., Monaco, L., Pando, M. P., Dierich, A., & Sassone-Corsi, P. (2001). Altered behavioral rhythms and clock gene expression in mice with a targeted mutation in the Period1 gene. *EMBO J*, *20*(15), 3967-3974. https://doi.org/10.1093/emboj/20.15.3967

Chang, A.-M., Duffy, J. F., Buxton, O. M., Lane, J. M., Aeschbach, D., Anderson, C., Bjonnes, A. C., Cain, S. W., Cohen, D. A., & Frayling, T. M. (2019). Chronotype Genetic variant in PER2 is associated with intrinsic circadian period in humans. *Scientific reports*, *9*(1), 1-10.

Cobb, C. S., Pope, S. K., & Williamson, R. (1995). Circadian rhythms to light-dark cycles in the lesser octopus, Eledone clrrhosa. *Marine & Freshwater Behaviour & Phy*, *26*(1), 47-57.

Collado, P., Beyer, C., Hutchison, J., & Holman, S. (1995). Hypothalamic distribution of astrocytes is gender-related in Mongolian gerbils. *Neuroscience Letters*, *184*(2), 86-89.

Cox, K. H., & Takahashi, J. S. (2019). Circadian clock genes and the transcriptional architecture of the clock mechanism. *Journal of molecular endocrinology*, *63*(4), R93-R102.

Daan, S., Damassa, D., Pittendrigh, C. S., & Smith, E. R. (1975). An effect of castration and testosterone replacement on a circadian pacemaker in mice (Mus musculus). *Proceedings of the National Academy of Sciences*, *72*(9), 3744-3747.

Daan, S., & Pittendrigh, C. (1976). A functional analysis of circadian pacemakers in nocturnal rodents V. Pacemaker structure: A clock for all seasons. *J Comp Physiol*, *106*(3), 333-355.

Daan, S., Spoelstra, K., Albrecht, U., Schmutz, I., Daan, M., Daan, B., Rienks, F., Poletaeva, I., Dell'Omo, G., Vyssotski, A., & Lipp, H. P. (2011). Lab mice in the field: unorthodox daily activity and effects of a dysfunctional circadian clock allele. *J Biol Rhythms*, *26*(2), 118-129. https://doi.org/10.1177/0748730410397645

Davidson, A. J., Castanon-Cervantes, O., Leise, T. L., Molyneux, P. C., & Harrington, M. E. (2009). Visualizing jet lag in the mouse suprachiasmatic nucleus and peripheral circadian timing system. *European Journal of Neuroscience*, *29*(1), 171-180.

Davis, F. C., Darrow, J. M., & Menaker, M. (1983). Sex differences in the circadian control of hamster wheel-running activity. *American Journal of Physiology-Regulatory, Integrative and Comparative Physiology*, *244*(1), R93-R105.

DeBruyne, J. P., Noton, E., Lambert, C. M., Maywood, E. S., Weaver, D. R., & Reppert, S. M. (2006). A clock shock: mouse CLOCK is not required for circadian oscillator function. *Neuron*, *50*(3), 465-477.

DeCoursey, P. J., Walker, J. K., & Smith, S. A. (2000). A circadian pacemaker in free-living chipmunks: essential for survival? *J Comp Physiol A*, *186*(2), 169-180. https://doi.org/10.1007/s003590050017

Doi, M., Hirayama, J., & Sassone-Corsi, P. (2006). Circadian regulator CLOCK is a histone acetyltransferase. *Cell*, *125*(3), 497-508.

Dowse, H., Umemori, J., & Koide, T. (2010). Ultradian components in the locomotor activity rhythms of the genetically normal mouse, Mus musculus. *J Exp Biol*, *213*(Pt 10), 1788-1795. https://doi.org/10.1242/jeb.038877

Duffy, J. F., Cain, S. W., Chang, A.-M., Phillips, A. J., Münch, M. Y., Gronfier, C., Wyatt, J. K., Dijk, D.-J., Wright, K. P., & Czeisler, C. A. (2011). Sex difference in the near-24-hour intrinsic period of the human circadian timing system. *Proceedings of the National Academy of Sciences*, *108*(Supplement 3), 15602-15608.

Duffy, J. F., Viswanathan, N., & Davis, F. C. (1999). Free-running circadian period does not shorten with age in female Syrian hamsters. *Neurosci Lett*, *271*(2), 77-80. https://doi.org/10.1016/s0304-3940(99)00519-4

Dunlap, J. C., & Loros, J. J. (2006). How fungi keep time: circadian system in Neurospora and other fungi. *Current Opinion in Microbiology*, *9*(6), 579-587. https://doi.org/10.1016/j.mib.2006.10.008

Easton, A., Arbuzova, J., & Turek, F. W. (2003). The circadian Clock mutation increases exploratory activity and escape-seeking behavior. *Genes Brain Behav*, *2*(1), 11-19. https://doi.org/10.1034/j.1601-183x.2003.00002.x

Edgar, D. M., Martin, C. E., & Dement, W. C. (1991). Activity feedback to the mammalian circadian pacemaker: influence on observed measures of rhythm period length. *Journal of biological rhythms*, *6*(3), 185-199.

Edgar, R. S., Green, E. W., Zhao, Y., van Ooijen, G., Olmedo, M., Qin, X., Xu, Y., Pan, M., Valekunja, U. K., Feeney, K. A., Maywood, E. S., Hastings, M. H., Baliga, N. S., Merrow, M., Millar, A. J., Johnson, C. H., Kyriacou, C. P., O'Neill, J. S., & Reddy, A. B. (2012). Peroxiredoxins are conserved markers of circadian rhythms. *Nature*, *485*(7399), 459-464. https://doi.org/10.1038/nature11088

Elderbrock, E. K., Hau, M., & Greives, T. J. (2020). Sex steroids modulate circadian behavioral rhythms in captive animals, but does this matter in the wild? *Hormones and Behavior*, *128*, 104900. https://doi.org/10.1016/j.yhbeh.2020.104900

Erkert, H. G., & Schardt, U. (1991). Social Entrainment of Circadian Activity Rhythms in Common Marmosets, Callithrix j. jacchus (Primates) 1. *Ethology*, *87*(3-4), 189-202.

Etchegaray, J. P., Yang, X., DeBruyne, J. P., Peters, A., Weaver, D. R., Jenuwein, T., & Reppert, S. M. (2006). The polycomb group protein EZH2 is required for mammalian circadian clock function. *J Biol Chem*, *281*(30), 21209-21215. https://doi.org/10.1074/jbc.M603722200

Evans, J. A., & Davidson, A. J. (2013). Health consequences of circadian disruption in humans and animal models. *Prog Mol Biol Transl Sci*, *119*, 283-323. https://doi.org/10.1016/B978-0-12-396971-2.00010-5

Evans, J. A., Elliott, J. A., & Gorman, M. R. (2005). Circadian entrainment and phase resetting differ markedly under dimly illuminated versus completely dark nights. *Behavioural brain research*, *162*(1), 116-126.

Evans, J. A., & Gorman, M. R. (2016). In synch but not in step: Circadian clock circuits regulating plasticity in daily rhythms. *Neuroscience*, *320*, 259-280. https://doi.org/10.1016/j.neuroscience.2016.01.072

Evans, J. A., Leise, T. L., Castanon-Cervantes, O., & Davidson, A. J. (2013). Dynamic interactions mediated by nonredundant signaling mechanisms couple circadian clock neurons. *Neuron*, *80*(4), 973-983.

Evans, J. A., Suen, T.-C., Callif, B. L., Mitchell, A. S., Castanon-Cervantes, O., Baker, K. M., Kloehn, I., Baba, K., Teubner, B. J., & Ehlen, J. C. (2015). Shell neurons of the master circadian clock coordinate the phase of tissue clocks throughout the brain and body. *BMC biology*, *13*(1), 1-15.

Feillet, C., Guerin, S., Lonchampt, M., Dacquet, C., Gustafsson, J. A., Delaunay, F., & Teboul, M. (2016). Sexual Dimorphism in Circadian Physiology Is Altered in LXRalpha Deficient Mice. *PLoS One*, *11*(3), e0150665. https://doi.org/10.1371/journal.pone.0150665

Fernandez, F., Lu, D., Ha, P., Costacurta, P., Chavez, R., Heller, H. C., & Ruby, N. F. (2014). Dysrhythmia in the suprachiasmatic nucleus inhibits memory processing. *Science*, *346*(6211), 854-857.

Fischer, D., Lombardi, D. A., Marucci-Wellman, H., & Roenneberg, T. (2017). Chronotypes in the US–influence of age and sex. *PLoS One*, *12*(6), e0178782.

Fitzgerald, K., & Zucker, I. (1976). Circadian organization of the estrous cycle of the golden hamster. *Proceedings of the National Academy of Sciences*, *73*(8), 2923-2927.

Fuller, C. A., Lydic, R., Sulzman, F. M., Albers, H. E., Tepper, B., & Moore-Ede, M. C. (1981). Circadian rhythm of body temperature persists after suprachiasmatic lesions in the squirrel monkey. *American Journal of Physiology-Regulatory, Integrative and Comparative Physiology*, *241*(5), R385-R391.

Fustin, J.-M., Doi, M., Yamaguchi, Y., Hida, H., Nishimura, S., Yoshida, M., Isagawa, T., Morioka, M. S., Kakeya, H., & Manabe, I. (2013). RNA-methylation-dependent RNA processing controls the speed of the circadian clock. *Cell*, *155*(4), 793-806.

Fustin, J. M., Doi, M., Yamaguchi, Y., Hida, H., Nishimura, S., Yoshida, M., Isagawa, T., Morioka, M. S., Kakeya, H., Manabe, I., & Okamura, H. (2013). RNA-methylation-dependent RNA processing controls the speed of the circadian clock. *Cell*, *155*(4), 793-806. https://doi.org/10.1016/j.cell.2013.10.026

Fustin, J. M., Kojima, R., Itoh, K., Chang, H. Y., Ye, S., Zhuang, B., Oji, A., Gibo, S., Narasimamurthy, R., Virshup, D., Kurosawa, G., Doi, M., Manabe, I., Ishihama, Y., Ikawa, M., & Okamura, H. (2018). Two Ck1delta transcripts regulated by m6A methylation code for two

antagonistic kinases in the control of the circadian clock. *Proc Natl Acad Sci U S A*, *115*(23), 5980-5985. https://doi.org/10.1073/pnas.1721371115

Gerkema, M. P., Daan, S., Wilbrink, M., Hop, M. W., & van der Leest, F. (1993). Phase control of ultradian feeding rhythms in the common vole (Microtus arvalis): the roles of light and the circadian system. *J Biol Rhythms*, *8*(2), 151-171. https://doi.org/10.1177/074873049300800205

Gerkema, M. P., Groos, G. A., & Daan, S. (1990). Differential elimination of circadian and ultradian rhythmicity by hypothalamic lesions in the common vole, Microtus arvalis. *J Biol Rhythms*, *5*(2), 81-95. https://doi.org/10.1177/074873049000500201

Gerkema, M. P., & van der Leest, F. (1991). Ongoing ultradian activity rhythms in the common vole, Microtus arvalis, during deprivations of food, water and rest. *J Comp Physiol A*, *168*(5), 591-597. https://doi.org/10.1007/BF00215081

Gerkema, M. P., & Verhulst, S. (1990). Warning against an unseen predator: a functional aspect of synchronous feeding in the common vole, Microtus arvalis. *Animal behaviour*, *40*(6), 1169-1178.

Gerstner, J. R., & Yin, J. C. (2010). Circadian rhythms and memory formation. *Nature Reviews Neuroscience*, *11*(8), 577-588.

Gery, S., Virk, R., Chumakov, K., Yu, A., & Koeffler, H. (2007). The clock gene Per2 links the circadian system to the estrogen receptor. *Oncogene*, *26*(57), 7916-7920.

Gibson, E. M., Wang, C., Tjho, S., Khattar, N., & Kriegsfeld, L. J. (2010). Experimental 'jet lag' inhibits adult neurogenesis and produces long-term cognitive deficits in female hamsters. *PLoS One*, *5*(12), e15267. https://doi.org/10.1371/journal.pone.0015267

Glaser, F. T., & Stanewsky, R. (2005). Temperature synchronization of the Drosophila circadian clock. *Curr Biol*, *15*(15), 1352-1363. https://doi.org/10.1016/j.cub.2005.06.056

Goh, G. H., Maloney, S. K., Mark, P. J., & Blache, D. (2019). Episodic Ultradian Events-Ultradian Rhythms. *Biology (Basel)*, *8*(1). https://doi.org/10.3390/biology8010015

Golombek, D. A., & Rosenstein, R. E. (2010). Physiology of circadian entrainment. *Physiological reviews*, *90*(3), 1063-1102.

Gorman, M. R., Freeman, D. A., & Zucker, I. (1997). Photoperiodism in hamsters: abrupt versus gradual changes in day length differentially entrain morning and evening circadian oscillators. *Journal of biological rhythms*, *12*(2), 122-135.

Gorman, M. R., & Zucker, I. (1997). Environmental induction of photononresponsiveness in the Siberian hamster, Phodopus sungorus. *Am J Physiol*, *272*(3 Pt 2), R887-895. https://doi.org/10.1152/ajpregu.1997.272.3.R887

Granados-Fuentes, D., Prolo, L. M., Abraham, U., & Herzog, E. D. (2004). The suprachiasmatic nucleus entrains, but does not sustain, circadian rhythmicity in the olfactory bulb. *J Neurosci*, *24*(3), 615-619. https://doi.org/10.1523/JNEUROSCI.4002-03.2004

Grant, A. D., Newman, M., & Kriegsfeld, L. J. (2020). Ultradian rhythms in heart rate variability and distal body temperature anticipate onset of the luteinizing hormone surge. *Sci Rep*, *10*(1), 20378. https://doi.org/10.1038/s41598-020-76236-6

Grant, A. D., Wilsterman, K., Smarr, B. L., & Kriegsfeld, L. J. (2018). Evidence for a coupled oscillator model of endocrine ultradian rhythms. *Journal of biological rhythms*, *33*(5), 475-496.

Grone, B. P., Chang, D., Bourgin, P., Cao, V., Fernald, R. D., Heller, H. C., & Ruby, N. F. (2011). Acute light exposure suppresses circadian rhythms in clock gene expression. *J Biol Rhythms*, *26*(1), 78-81. https://doi.org/10.1177/0748730410388404

Guillot, A., & Meyer, J.-A. (1997). A cost-benefit analysis of behavioural sequence organization in laboratory mice. *Ethology Ecology & Evolution*, *9*(2), 119-132.

Güldner, F.-H. (1982). Sexual dimorphisms of axo-spine synapses and postsynaptic density material in the suprachiasmatic nucleus of the rat. *Neuroscience Letters*, *28*(2), 145-150.

Güldner, F.-H. (1983). Numbers of neurons and astroglial cells in the suprachiasmatic nucleus of male and female rats. *Experimental Brain Research*, *50*(2-3), 373-376.

Güldner, F.-H. (1984). Suprachiasmatic nucleus: numbers of synaptic appositions and various types of synapses. *Cell and tissue research*, *235*(2), 449-452.

Guzman, D. A., Flesia, A. G., Aon, M. A., Pellegrini, S., Marin, R. H., & Kembro, J. M. (2017). The fractal organization of ultradian rhythms in avian behavior. *Sci Rep*, *7*(1), 684. https://doi.org/10.1038/s41598-017-00743-2

Hagenauer, M. H., King, A. F., Possidente, B., McGinnis, M. Y., Lumia, A. R., Peckham, E. M., & Lee, T. M. (2011). Changes in circadian rhythms during puberty in Rattus norvegicus: developmental time course and gonadal dependency. *Hormones and Behavior*, *60*(1), 46-57. https://doi.org/10.1016/j.yhbeh.2011.03.001

Hara, R., Wan, K., Wakamatsu, H., Aida, R., Moriya, T., Akiyama, M., & Shibata, S. (2001). Restricted feeding entrains liver clock without participation of the suprachiasmatic nucleus. *Genes Cells*, *6*(3), 269-278. https://doi.org/10.1046/j.1365-2443.2001.00419.x

Harang, R., Bonnet, G., & Petzold, L. R. (2012). WAVOS: a MATLAB toolkit for wavelet analysis and visualization of oscillatory systems. *BMC research notes*, *5*(1), 1-8.

Haspel, J. A., Anafi, R., Brown, M. K., Cermakian, N., Depner, C., Desplats, P., Gelman, A. E., Haack, M., Jelic, S., & Kim, B. S. (2020). Perfect timing: circadian rhythms, sleep, and immunity—an NIH workshop summary. *JCI insight*, *5*(1).

Hastings, M. H., Maywood, E. S., & Brancaccio, M. (2018). Generation of circadian rhythms in the suprachiasmatic nucleus. *Nature Reviews Neuroscience*, *19*(8), 453-469.

Hazlerigg, D. G., & Tyler, N. J. C. (2019). Activity patterns in mammals: Circadian dominance challenged. *PLoS Biol*, *17*(7), e3000360. https://doi.org/10.1371/journal.pbio.3000360

Heldmaier, G., Steinlechner, S., Ruf, T., Wiesinger, H., & Klingenspor, M. (1989). Photoperiod and thermoregulation in vertebrates: body temperature rhythms and thermogenic acclimation. *J Biol Rhythms*, *4*(2), 251-265. https://www.ncbi.nlm.nih.gov/pubmed/2519592

Herzog, E. D., Hermanstyne, T., Smyllie, N. J., & Hastings, M. H. (2017). Regulating the Suprachiasmatic Nucleus (SCN) Circadian Clockwork: Interplay between Cell-Autonomous and Circuit-Level Mechanisms. *Cold Spring Harb Perspect Biol*, *9*(1). https://doi.org/10.1101/cshperspect.a027706

Hill, R. (1992). Mammalian Energetics. Interdisciplinary Views of Metabolism and Reproduction.

Hirayama, J., Sahar, S., Grimaldi, B., Tamaru, T., Takamatsu, K., Nakahata, Y., & Sassone-Corsi, P. (2007). CLOCK-mediated acetylation of BMAL1 controls circadian function. *Nature*, *450*(7172), 1086-1090.

Hofman, M., Zhou, J. N., & Swaab, D. (1996). Suprachiasmatic nucleus of the human brain: an immunocytochemical and morphometric analysis. *The Anatomical Record: An Official Publication of the American Association of Anatomists*, *244*(4), 552-562.

Horvath, T. L., Cela, V., & van der Beek, E. M. (1998). Gender-specific apposition between vasoactive intestinal peptide-containing axons and gonadotrophin-releasing hormone-producing neurons in the rat. *Brain Res*, *795*(1-2), 277-281. https://doi.org/10.1016/s0006-8993(98)00208-x

Hut, R. A., Pilorz, V., Boerema, A. S., Strijkstra, A. M., & Daan, S. (2011). Working for food shifts nocturnal mouse activity into the day. *PLoS One*, *6*(3), e17527. https://doi.org/10.1371/journal.pone.0017527

Inouye, S.-I., & Kawamura, H. (1979). Persistence of circadian rhythmicity in a mammalian hypothalamic" island" containing the suprachiasmatic nucleus. *Proceedings of the National Academy of Sciences*, *76*(11), 5962-5966.

Isomura, A., & Kageyama, R. (2014). Ultradian oscillations and pulses: coordinating cellular responses and cell fate decisions. *Development*, *141*(19), 3627-3636.

Iwahana, E., Karatsoreos, I., Shibata, S., & Silver, R. (2008). Gonadectomy reveals sex differences in circadian rhythms and suprachiasmatic nucleus androgen receptors in mice. *Hormones and Behavior*, *53*(3), 422-430.

Izumo, M., Pejchal, M., Schook, A. C., Lange, R. P., Walisser, J. A., Sato, T. R., Wang, X., Bradfield, C. A., & Takahashi, J. S. (2014). Differential effects of light and feeding on circadian organization of peripheral clocks in a forebrain Bmal1 mutant. *Elife*, *3*, e04617.

Jansen, H. T., Leise, T., Stenhouse, G., Pigeon, K., Kasworm, W., Teisberg, J., Radandt, T., Dallmann, R., Brown, S., & Robbins, C. T. (2016). The bear circadian clock doesn't 'sleep'during winter dormancy. *Frontiers in zoology*, *13*(1), 42.

Jiang, X., Liu, B., Nie, Z., Duan, L., Xiong, Q., Jin, Z., Yang, C., & Chen, Y. (2021). The role of m6A modification in the biological functions and diseases. *Signal Transduct Target Ther*, *6*(1), 74. https://doi.org/10.1038/s41392-020-00450-x

Johnson, C. H. (1999). Forty years of PRCs-what have we learned? *Chronobiology international*, *16*(6), 711-743.

Jones, S. E., Tyrrell, J., Wood, A. R., Beaumont, R. N., Ruth, K. S., Tuke, M. A., Yaghootkar, H., Hu, Y., Teder-Laving, M., & Hayward, C. (2016). Genome-wide association analyses in 128,266 individuals identifies new morningness and sleep duration loci. *PLoS genetics*, *12*(8), e1006125.

Joye, D. A., & Evans, J. A. (2021). Sex differences in daily timekeeping and circadian clock circuits. Seminars in Cell & Developmental Biology,

Kaiya, H., Kangawa, K., & Miyazato, M. (2013). Update on ghrelin biology in birds. *Gen Comp Endocrinol*, *190*, 170-175. https://doi.org/10.1016/j.ygcen.2013.04.014

Kampf-Lassin, A., Wei, J., Galang, J., & Prendergast, B. J. (2011). Experience-independent development of the hamster circadian visual system. *PLoS One*, *6*(4), e16048. https://doi.org/10.1371/journal.pone.0016048

Karatsoreos, I. N., Butler, M. P., LeSauter, J., & Silver, R. (2011). Androgens modulate structure and function of the suprachiasmatic nucleus brain clock. *Endocrinology*, *152*(5), 1970-1978.

Katada, S., & Sassone-Corsi, P. (2010). The histone methyltransferase MLL1 permits the oscillation of circadian gene expression. *Nature structural & molecular biology*, *17*(12), 1414.

Kidd, P. B., Young, M. W., & Siggia, E. D. (2015). Temperature compensation and temperature sensation in the circadian clock. *Proceedings of the National Academy of Sciences*, *112*(46), E6284-E6292.

Kleitman, N. (1982). Basic rest-activity cycle—22 years later. *Sleep*, *5*(4), 311-317.

Klerman, E. B., Rimmer, D. W., Dijk, D. J., Kronauer, R. E., Rizzo, J. F., 3rd, & Czeisler, C. A. (1998). Nonphotic entrainment of the human circadian pacemaker. *Am J Physiol*, *274*(4 Pt 2), R991-996. https://doi.org/10.1152/ajpregu.1998.274.4.r991

Ko, C. H., & Takahashi, J. S. (2006). Molecular components of the mammalian circadian clock. *Human molecular genetics*, *15*(suppl_2), R271-R277.

Koike, N., Yoo, S. H., Huang, H. C., Kumar, V., Lee, C., Kim, T. K., & Takahashi, J. S. (2012). Transcriptional architecture and chromatin landscape of the core circadian clock in mammals. *Science*, *338*(6105), 349-354. https://doi.org/10.1126/science.1226339

Konopka, R. J., & Benzer, S. (1971). Clock mutants of Drosophila melanogaster. *Proceedings of the National Academy of Sciences*, *68*(9), 2112-2116.

Krajnak, K., Kashon, M. L., Rosewell, K. L., & Wise, P. M. (1998). Sex differences in the daily rhythm of vasoactive intestinal polypeptide but not arginine vasopressin messenger ribonucleic acid in the suprachiasmatic nuclei. *Endocrinology*, *139*(10), 4189-4196. https://doi.org/10.1210/endo.139.10.6259

Kriegsfeld, L. J. (2013). Circadian regulation of kisspeptin in female reproductive functioning. *Adv Exp Med Biol*, *784*, 385-410. https://doi.org/10.1007/978-1-4614-6199-9_18

Kriegsfeld, L. J., & Silver, R. (2006). The regulation of neuroendocrine function: timing is everything. *Hormones and Behavior*, *49*(5), 557-574.

Krishnan, V., & Collop, N. A. (2006). Gender differences in sleep disorders. *Current opinion in pulmonary medicine*, *12*(6), 383-389.

Krizo, J. A., & Mintz, E. M. (2015). Sex differences in behavioral circadian rhythms in laboratory rodents. *Frontiers in Endocrinology*, *5*, 234.

Kuljis, D. A., Loh, D. H., Truong, D., Vosko, A. M., Ong, M. L., McClusky, R., Arnold, A. P., & Colwell, C. S. (2013). Gonadal-and sex-chromosome-dependent sex differences in the circadian system. *Endocrinology*, *154*(4), 1501-1512.

Lahiri, K., Vallone, D., Gondi, S. B., Santoriello, C., Dickmeis, T., & Foulkes, N. S. (2005). Temperature regulates transcription in the zebrafish circadian clock. *PLoS Biol*, *3*(11), e351. https://doi.org/10.1371/journal.pbio.0030351

Lee, H., Chen, R., Lee, Y., Yoo, S., & Lee, C. (2009). Essential roles of CKIdelta and CKIepsilon in the mammalian circadian clock. *Proc Natl Acad Sci U S A*, *106*(50), 21359-21364. https://doi.org/10.1073/pnas.0906651106

Lehman, M. N., Silver, R., Gladstone, W. R., Kahn, R. M., Gibson, M., & Bittman, E. L. (1987). Circadian rhythmicity restored by neural transplant. Immunocytochemical characterization of the graft and its integration with the host brain. *J Neurosci*, *7*(6), 1626-1638. https://www.ncbi.nlm.nih.gov/pubmed/3598638

Leise, T. L. (2013). Wavelet analysis of circadian and ultradian behavioral rhythms. *Journal of circadian rhythms*, *11*(1), 5.

Leise, T. L. (2015). Wavelet-based analysis of circadian behavioral rhythms. *Methods Enzymol*, *551*, 95-119. https://doi.org/10.1016/bs.mie.2014.10.011

Leise, T. L. (2017). Analysis of Nonstationary Time Series for Biological Rhythms Research. *J Biol Rhythms*, *32*(3), 187-194. https://doi.org/10.1177/0748730417709105

Leise, T. L., & Harrington, M. E. (2011). Wavelet-based time series analysis of circadian rhythms. *Journal of biological rhythms*, *26*(5), 454-463.

LeSauter, J., Lehman, M. N., & Silver, R. (1996). Restoration of circadian rhythmicity by transplants of SCN "micropunches". *J Biol Rhythms*, *11*(2), 163-171. https://doi.org/10.1177/074873049601100208

Lewis, C. J., Pan, T., & Kalsotra, A. (2017). RNA modifications and structures cooperate to guide RNA-protein interactions. *Nat Rev Mol Cell Biol*, *18*(3), 202-210. https://doi.org/10.1038/nrm.2016.163

Li, Z., Wang, Y., Sun, K. K., Wang, K., Sun, Z. S., Zhao, M., & Wang, J. (2015). Sex-related difference in food-anticipatory activity of mice. *Hormones and Behavior*, *70*, 38-46. https://doi.org/10.1016/j.yhbeh.2015.02.004

Lilly, J. M., & Olhede, S. C. (2010). On the analytic wavelet transform. *IEEE transactions on information theory*, *56*(8), 4135-4156.

Lilly, J. M., & Olhede, S. C. (2012). Generalized Morse wavelets as a superfamily of analytic wavelets. *IEEE Transactions on Signal Processing*, *60*(11), 6036-6041.

Lindman, H. R. (1974). *Analysis of variance in complex experimental designs*. W. H. Freeman.

Liu, A. C., Welsh, D. K., Ko, C. H., Tran, H. G., Zhang, E. E., Priest, A. A., Buhr, E. D., Singer, O., Meeker, K., & Verma, I. M. (2007). Intercellular coupling confers robustness against mutations in the SCN circadian clock network. *Cell*, *129*(3), 605-616.

Liu, L., Shen, H., & Wang, Y. (2017). CRY2 is suppressed by FOXM1 mediated promoter hypermethylation in breast cancer. *Biochemical and biophysical research communications*, *490*(1), 44-50.

Liu, Y., Tsinoremas, N. F., Johnson, C. H., Lebedeva, N. V., Golden, S. S., Ishiura, M., & Kondo, T. (1995). Circadian orchestration of gene expression in cyanobacteria. *Genes & development*, *9*(12), 1469-1478.

Logan, R. W., & McClung, C. A. (2019). Rhythms of life: circadian disruption and brain disorders across the lifespan. *Nature Reviews Neuroscience*, *20*(1), 49-65.

Low-Zeddies, S. S., & Takahashi, J. S. (2001). Chimera analysis of the Clock mutation in mice shows that complex cellular integration determines circadian behavior. *Cell*, *105*(1), 25-42.

Lyall, L. M., Wyse, C. A., Celis-Morales, C. A., Lyall, D. M., Cullen, B., Mackay, D., Ward, J., Graham, N., Strawbridge, R. J., & Gill, J. M. (2018). Seasonality of depressive symptoms in women but not in men: A cross-sectional study in the UK Biobank cohort. *Journal of affective disorders*, *229*, 296-305.

Mackinnon, P., & Bulmer, M. (1974). Sexual differentiation in the phase of the circadian rhythm of [35S] methionine incorporation into cerebral proteins, and of serum gonadotrophin levels. *Journal of Endocrinology*, *62*(2), 257-265.

Mahoney, M. M. (2010). Shift work, jet lag, and female reproduction. *International journal of endocrinology*, *2010*.

Mahoney, M. M., Ramanathan, C., Hagenauer, M. H., Thompson, R. C., Smale, L., & Lee, T. (2009). Daily rhythms and sex differences in vasoactive intestinal polypeptide, VIPR2 receptor and arginine vasopressin mRNA in the suprachiasmatic nucleus of a diurnal rodent, Arvicanthis niloticus. *Eur J Neurosci*, *30*(8), 1537-1543. https://doi.org/10.1111/j.1460-9568.2009.06936.x

Marimuthu, G., Rajan, S., & Chandrashekaran, M. (1981). Social entrainment of the circadian rhythm in the flight activity of the microchiropteran bat Hipposideros speoris. *Behavioral Ecology and Sociobiology*, *8*(2), 147-150.

Mather, J. G. (1981). Wheel-running activity: a new interpretation. *Mammal Review*, *11*(1), 41-51.

McClung, C. R. (2006). Plant circadian rhythms. *Plant Cell*, *18*(4), 792-803. https://doi.org/10.1105/tpc.106.040980

McEwen, B. S., & Wingfield, J. C. (2010). What is in a name? Integrating homeostasis, allostasis and stress. *Hormones and Behavior*, *57*(2), 105-111. https://doi.org/10.1016/j.yhbeh.2009.09.011

McMaster, A., Jangani, M., Sommer, P., Han, N., Brass, A., Beesley, S., Lu, W., Berry, A., Loudon, A., Donn, R., & Ray, D. W. (2011). Ultradian cortisol pulsatility encodes a distinct, biologically important signal. *PLoS One*, *6*(1), e15766. https://doi.org/10.1371/journal.pone.0015766

Meisel, D. V., Byrne, R., Kuba, M., Griebel, U., & Mather, J. (2002). *Circadian rhythmus in Octopus vulgaris*. na.

Meyer-Bernstein, E. L., Jetton, A. E., Matsumoto, S.-i., Markuns, J. F., Lehman, M. N., & Bittman, E. L. (1999). Effects of suprachiasmatic transplants on circadian rhythms of neuroendocrine function in golden hamsters. *Endocrinology*, *140*(1), 207-218.

Meyer, K. D., & Jaffrey, S. R. (2017). Rethinking m(6)A Readers, Writers, and Erasers. *Annu Rev Cell Dev Biol*, *33*, 319-342. https://doi.org/10.1146/annurev-cellbio-100616-060758

Miyata, K., Kuwaki, T., & Ootsuka, Y. (2016). The integrated ultradian organization of behavior and physiology in mice and the contribution of orexin to the ultradian patterning. *Neuroscience*, *334*, 119-133.

Mohawk, J. A., Baer, M. L., & Menaker, M. (2009). The methamphetamine-sensitive circadian oscillator does not employ canonical clock genes. *Proceedings of the National Academy of Sciences*, *106*(9), 3519-3524.

Mohawk, J. A., Green, C. B., & Takahashi, J. S. (2012). Central and Peripheral Circadian Clocks in Mammals. *Annual Review of Neuroscience, Vol 35*, *35*, 445-462. https://doi.org/10.1146/annurev-neuro-060909-153128

Mong, J. A., Baker, F. C., Mahoney, M. M., Paul, K. N., Schwartz, M. D., Semba, K., & Silver, R. (2011). Sleep, rhythms, and the endocrine brain: influence of sex and gonadal hormones. *Journal of Neuroscience*, *31*(45), 16107-16116.

Moore, R. Y., & Eichler, V. B. (1972). Loss of a circadian adrenal corticosterone rhythm following suprachiasmatic lesions in the rat. *Brain research*.

Morin, L. P., Fitzgerald, K. M., & Zucker, I. (1977). Estradiol shortens the period of hamster circadian rhythms. *Science*, *196*(4287), 305-307.

Mosko, S., & Moore, R. Y. (1978). Neonatal suprachiasmatic nucleus ablation: absence of functional and morphological plasticity. *Proceedings of the National Academy of Sciences*, *75*(12), 6243-6246.

Mrosovsky, N. (1996). Locomotor activity and non-photic influences on circadian clocks. *Biological Reviews of the Cambridge Philosophical Society*, *71*(3), 343-372.

Myung, J., Hong, S., DeWoskin, D., De Schutter, E., Forger, D. B., & Takumi, T. (2015). GABA-mediated repulsive coupling between circadian clock neurons in the SCN encodes seasonal time. *Proceedings of the National Academy of Sciences*, *112*(29), E3920-E3929.

Nakamura, T. J., Moriya, T., Inoue, S., Shimazoe, T., Watanabe, S., Ebihara, S., & Shinohara, K. (2005). Estrogen differentially regulates expression of Per1 and Per2 genes between central and peripheral clocks and between reproductive and nonreproductive tissues in female rats. *J Neurosci Res*, *82*(5), 622-630. https://doi.org/10.1002/jnr.20677

Nakamura, T. J., Sellix, M. T., Menaker, M., & Block, G. D. (2008). Estrogen directly modulates circadian rhythms of PER2 expression in the uterus. *Am J Physiol Endocrinol Metab*, *295*(5), E1025-1031. https://doi.org/10.1152/ajpendo.90392.2008

Nakamura, T. J., Shinohara, K., Funabashi, T., & Kimura, F. (2001). Effect of estrogen on the expression of Cry1 and Cry2 mRNAs in the suprachiasmatic nucleus of female rats. *Neuroscience Research*, *41*(3), 251-255.

Nakamura, T. J., Takasu, N. N., & Nakamura, W. (2016). The suprachiasmatic nucleus: age-related decline in biological rhythms. *The Journal of Physiological Sciences*, *66*(5), 367-374.

Niimi, K., & Takahashi, E. (2019). New system to examine the activity and water and food intake of germ-free mice in a sealed positive-pressure cage. *Heliyon*, *5*(8), e02176.

O'Neill, J. S., & Reddy, A. B. (2011). Circadian clocks in human red blood cells. *Nature*, *469*(7331), 498-503.

Ochi, M., Sono, S., Sei, H., Oishi, K., Kobayashi, H., Morita, Y., & Ishida, N. (2003). Sex difference in circadian period of body temperature in Clock mutant mice with Jcl/ICR background. *Neurosci Lett*, *347*(3), 163-166. https://doi.org/10.1016/s0304-3940(03)00688-8

Ohta, H., Yamazaki, S., & McMahon, D. G. (2005). Constant light desynchronizes mammalian clock neurons. *Nature neuroscience*, *8*(3), 267-269.

Oster, H., Yasui, A., van der Horst, G. T., & Albrecht, U. (2002). Disruption of mCry2 restores circadian rhythmicity in mPer2 mutant mice. *Genes & development*, *16*(20), 2633-2638.

Ouyang, Y., Andersson, C. R., Kondo, T., Golden, S. S., & Johnson, C. H. (1998). Resonating circadian clocks enhance fitness in cyanobacteria. *Proceedings of the National Academy of Sciences*, *95*(15), 8660-8664.

Pacha, J., & Sumova, A. (2013). Circadian regulation of epithelial functions in the intestine. *Acta Physiol (Oxf)*, *208*(1), 11-24. https://doi.org/10.1111/apha.12090

Painson, J. C., & Tannenbaum, G. S. (1991). Sexual dimorphism of somatostatin and growth hormone-releasing factor signaling in the control of pulsatile growth hormone secretion in the rat. *Endocrinology*, *128*(6), 2858-2866. https://doi.org/10.1210/endo-128-6-2858

Panda, S., Hogenesch, J. B., & Kay, S. A. (2002). Circadian rhythms from flies to human. *Nature*, *417*(6886), 329-335.

Panda, S., Nayak, S. K., Campo, B., Walker, J. R., Hogenesch, J. B., & Jegla, T. (2005). Illumination of the melanopsin signaling pathway. *Science*, *307*(5709), 600-604.

Patton, A. P., & Hastings, M. H. (2018). The suprachiasmatic nucleus. *Curr Biol*, *28*(15), R816-R822. https://doi.org/10.1016/j.cub.2018.06.052

Paul, M. J., Zucker, I., & Schwartz, W. J. (2008). Tracking the seasons: the internal calendars of vertebrates. *Philosophical Transactions of the Royal Society B: Biological Sciences*, *363*(1490), 341-361.

Pendergast, J. S., & Yamazaki, S. (2018). The mysterious food-entrainable oscillator: insights from mutant and engineered mouse models. *Journal of biological rhythms*, *33*(5), 458-474.

Pernold, K., Rullman, E., & Ulfhake, B. (2021). Major oscillations in spontaneous home-cage activity in C57BL/6 mice housed under constant conditions. *Sci Rep*, *11*(1), 4961. https://doi.org/10.1038/s41598-021-84141-9

Pilorz, V., Helfrich-Forster, C., & Oster, H. (2018). The role of the circadian clock system in physiology. *Pflugers Arch*, *470*(2), 227-239. https://doi.org/10.1007/s00424-017-2103-y

Pilorz, V., Kolms, B., & Oster, H. (2020). Rapid Jetlag Resetting of Behavioral, Physiological, and Molecular Rhythms in Proestrous Female Mice. *J Biol Rhythms*, *35*(6), 612-627. https://doi.org/10.1177/0748730420965291

Pilorz, V., & Steinlechner, S. (2008). Low reproductive success in Per1 and Per2 mutant mouse females due to accelerated ageing? *Reproduction*, *135*(4), 559-568. https://doi.org/10.1530/REP-07-0434

Pilorz, V., Steinlechner, S., & Oster, H. (2009). Age and oestrus cycle-related changes in glucocorticoid excretion and wheel-running activity in female mice carrying mutations in the circadian clock genes Per1 and Per2. *Physiol Behav*, *96*(1), 57-63. https://doi.org/10.1016/j.physbeh.2008.08.010

Pittendrigh, C. S. (1960). Circadian rhythms and the circadian organization of living systems. Cold Spring Harbor symposia on quantitative biology,

Pittendrigh, C. S., & Minis, D. H. (1972). Circadian systems: longevity as a function of circadian resonance in Drosophila melanogaster. *Proceedings of the National Academy of Sciences*, *69*(6), 1537-1539.

Preitner, N., Damiola, F., Zakany, J., Duboule, D., Albrecht, U., & Schibler, U. (2002). The orphan nuclear receptor REV-ERBα controls circadian transcription within the positive limb of the mammalian circadian oscillator. *Cell*, *110*(2), 251-260.

Prendergast, B. J., Beery, A. K., Paul, M. J., & Zucker, I. (2012). Enhancement and suppression of ultradian and circadian rhythms across the female hamster reproductive cycle. *J Biol Rhythms*, *27*(3), 246-256. https://doi.org/10.1177/0748730412441315

Prendergast, B. J., Cable, E. J., Stevenson, T. J., Onishi, K. G., Zucker, I., & Kay, L. M. (2015). Circadian disruption alters the effects of lipopolysaccharide treatment on circadian and ultradian locomotor activity and body temperature rhythms of female Siberian hamsters. *Journal of biological rhythms*, *30*(6), 543-556.

Prendergast, B. J., Cisse, Y. M., Cable, E. J., & Zucker, I. (2012). Dissociation of ultradian and circadian phenotypes in female and male Siberian hamsters. *Journal of biological rhythms*, *27*(4), 287-298.

Prendergast, B. J., Onishi, K. G., & Zucker, I. (2013). Neonatal monosodium glutamate treatment counteracts circadian arrhythmicity induced by phase shifts of the light–dark cycle in female and male Siberian hamsters. *Brain research*, *1521*, 51-58.

Prendergast, B. J., Onishi, K. G., & Zucker, I. (2014). Female mice liberated for inclusion in neuroscience and biomedical research. *Neuroscience & Biobehavioral Reviews*, *40*, 1-5.

Prendergast, B. J., & Zucker, I. (2012). Photoperiodic influences on ultradian rhythms of male Siberian hamsters. *PLoS One*, *7*(7), e41723. https://doi.org/10.1371/journal.pone.0041723

Prendergast, B. J., & Zucker, I. (2012). Photoperiodic influences on ultradian rhythms of male Siberian hamsters.

Prendergast, B. J., & Zucker, I. (2016). Ultradian rhythms in mammalian physiology and behavior. *Current opinion in neurobiology*, *40*, 150-154.

Price, T. S., Baggs, J. E., Curtis, A. M., FitzGerald, G. A., & Hogenesch, J. B. (2008). WAVECLOCK: wavelet analysis of circadian oscillation. *Bioinformatics*, *24*(23), 2794-2795.

Qian, J., Morris, C. J., Caputo, R., Wang, W., Garaulet, M., & Scheer, F. A. (2019). Sex differences in the circadian misalignment effects on energy regulation. *Proceedings of the National Academy of Sciences*, *116*(47), 23806-23812.

Ralph, M. R., Foster, R. G., Davis, F. C., & Menaker, M. (1990). Transplanted suprachiasmatic nucleus determines circadian period. *Science*, *247*(4945), 975-978.

Ramp, C., Delarue, J., Palsboll, P. J., Sears, R., & Hammond, P. S. (2015). Adapting to a warmer ocean--seasonal shift of baleen whale movements over three decades. *PLoS One*, *10*(3), e0121374. https://doi.org/10.1371/journal.pone.0121374

Reddy, A., Field, M., Maywood, E., & Hastings, M. (2002). Differential resynchronisation of circadian clock gene expression within the suprachiasmatic nuclei of mice subjected to experimental jet lag. *Journal of Neuroscience*, *22*(17), 7326-7330.

Reebs, S. G., & Mrosovsky, N. (1989). Effects of induced wheel running on the circadian activity rhythms of Syrian hamsters: entrainment and phase response curve. *Journal of biological rhythms*, *4*(1), 39-48.

Refinetti, R. (2002). Compression and expansion of circadian rhythm in mice under long and short photoperiods. *Integr Physiol Behav Sci*, *37*(2), 114-127. https://doi.org/10.1007/BF02688824

Refinetti, R., Cornélissen, G., & Halberg, F. (2007). Procedures for numerical analysis of circadian rhythms. *Biological Rhythm Research*, *38*(4), 275-325.

Reppert, S., Perlow, M., Ungerleider, L., Mishkin, M., Tamarkin, L., Orloff, D., Hoffman, H., & Klein, D. (1981). Effects of damage to the suprachiasmatic area of the anterior hypothalamus on the daily melatonin and cortisol rhythms in the rhesus monkey. *Journal of Neuroscience*, *1*(12), 1414-1425.

Richter, C. P. (1965). Biological clocks in medicine and psychiatry.

Riede, S. J., van der Vinne, V., & Hut, R. A. (2017). The flexible clock: predictive and reactive homeostasis, energy balance and the circadian regulation of sleep–wake timing. *Journal of Experimental Biology*, *220*(5), 738-749.

Riggle, J. P., Onishi, K. G., Love, J. A., Beach, D. E., Zucker, I., & Prendergast, B. J. (2022). Spontaneous Recovery of Circadian Organization in Mice Lacking a Core Component of the Molecular Clockwork. *J Biol Rhythms*, *37*(1), 94-109. https://doi.org/10.1177/07487304211060896

Ripperger, J. A., Jud, C., & Albrecht, U. (2011). The daily rhythm of mice. *FEBS Lett*, *585*(10), 1384-1392. https://doi.org/10.1016/j.febslet.2011.02.027

Robinson, S. M., Fox, T. O., Dikkes, P., & Pearlstein, R. A. (1986). Sex differences in the shape of the sexually dimorphic nucleus of the preoptic area and suprachiasmatic nucleus of the rat: 3-D computer reconstructions and morphometrics. *Brain research*, *371*(2), 380-384.

Rood, B. D., Stott, R. T., You, S., Smith, C. J., Woodbury, M. E., & De Vries, G. J. (2013). Site of origin of and sex differences in the vasopressin innervation of the mouse (Mus musculus) brain. *J Comp Neurol*, *521*(10), 2321-2358. https://doi.org/10.1002/cne.23288

Roper, T. J. (1976). Sex differences in circadian wheel running rhythms in the Mongolian gerbil. *Physiol Behav*, *17*(3), 549-551. https://doi.org/10.1016/0031-9384(76)90121-9

Ruby, N. F., Hwang, C. E., Wessells, C., Fernandez, F., Zhang, P., Sapolsky, R., & Heller, H. C. (2008). Hippocampal-dependent learning requires a functional circadian system. *Proceedings of the National Academy of Sciences*, *105*(40), 15593-15598.

Ruf, T. (1999). The Lomb-Scargle periodogram in biological rhythm research: analysis of incomplete and unequally spaced time-series. *Biological Rhythm Research*, *30*(2), 178-201.

Sahar, S., & Sassone-Corsi, P. (2013). The epigenetic language of circadian clocks. In *Circadian clocks* (pp. 29-44). Springer.

Sakamoto, K., Nagase, T., Fukui, H., Horikawa, K., Okada, T., Tanaka, H., Sato, K., Miyake, Y., Ohara, O., Kako, K., & Ishida, N. (1998). Multitissue circadian expression of rat period homolog (rPer2) mRNA is governed by the mammalian circadian clock, the suprachiasmatic nucleus in the brain. *J Biol Chem*, *273*(42), 27039-27042. https://doi.org/10.1074/jbc.273.42.27039

Sato, T. K., Panda, S., Miraglia, L. J., Reyes, T. M., Rudic, R. D., McNamara, P., Naik, K. A., FitzGerald, G. A., Kay, S. A., & Hogenesch, J. B. (2004). A functional genomics strategy reveals Rora as a component of the mammalian circadian clock. *Neuron*, *43*(4), 527-537.

Savvidis, C., & Koutsilieris, M. (2012). Circadian rhythm disruption in cancer biology. *Mol Med*, *18*, 1249-1260. https://doi.org/10.2119/molmed.2012.00077

Scannapieco, E., Pasquali, V., & Renzi, P. (2009). Circadian and ultradian motor activity rhythms under 21h and 28h lighting cycles. *Biological Rhythm Research*, *40*(4), 307-316.

Schmutz, I., Ripperger, J. A., Baeriswyl-Aebischer, S., & Albrecht, U. (2010). The mammalian clock component PERIOD2 coordinates circadian output by interaction with nuclear receptors. *Genes & development*, *24*(4), 345-357.

Schroeder, A. M., Truong, D., Loh, D. H., Jordan, M. C., Roos, K. P., & Colwell, C. S. (2012). Voluntary scheduled exercise alters diurnal rhythms of behaviour, physiology and gene expression in wild-type and vasoactive intestinal peptide-deficient mice. *The Journal of Physiology*, *590*(23), 6213-6226.

Schull, J., Walker, J., Fitzgerald, K., Hiilivirta, L., Ruckdeschel, J., Schumacher, D., Stanger, D., & McEachron, D. L. (1989). Effects of sex, thyro-parathyroidectomy, and light regime on levels and circadian rhythms of wheel-running in rats. *Physiol Behav*, *46*(3), 341-346. https://doi.org/10.1016/0031-9384(89)90001-2

Schwartz, W. J., Gross, R. A., & Morton, M. T. (1987). The suprachiasmatic nuclei contain a tetrodotoxin-resistant circadian pacemaker. *Proceedings of the National Academy of Sciences*, *84*(6), 1694-1698.

Schwartz, W. J., Tavakoli-Nezhad, M., Lambert, C. M., Weaver, D. R., & Horacio, O. (2011). Distinct patterns of Period gene expression in the suprachiasmatic nucleus underlie circadian clock photoentrainment by advances or delays. *Proceedings of the National Academy of Sciences*, *108*(41), 17219-17224.

Schwartz, W. J., & Zimmerman, P. (1990). Circadian timekeeping in BALB/c and C57BL/6 inbred mouse strains. *J Neurosci*, *10*(11), 3685-3694. https://www.ncbi.nlm.nih.gov/pubmed/2230953

Sherwin, C. (1998). Voluntary wheel running: a review and novel interpretation. *Animal behaviour*, *56*(1), 11-27.

Shi, H., Zhang, X., Weng, Y.-L., Lu, Z., Liu, Y., Lu, Z., Li, J., Hao, P., Zhang, Y., & Zhang, F. (2018). m6A facilitates hippocampus-dependent learning and memory through YTHDF1. *Nature*, *563*(7730), 249-253.

Shi, S., Hida, A., McGuinness, O. P., Wasserman, D. H., Yamazaki, S., & Johnson, C. H. (2010). Circadian clock gene Bmal1 is not essential; functional replacement with its paralog, Bmal2. *Current biology*, *20*(4), 316-321.

Siebert, U., & Wollnik, F. (1991). Wheel-running activity rhythms in two inbred strains of laboratory rats under different photoperiods. *Physiol Behav*, *50*(6), 1137-1143. https://doi.org/10.1016/0031-9384(91)90574-8

Siepka, S. M., & Takahashi, J. S. (2005). Forward genetic screens to identify circadian rhythm mutants in mice. In *Methods in enzymology* (Vol. 393, pp. 219-229). Elsevier.

Siepka, S. M., Yoo, S.-H., Park, J., Lee, C., & Takahashi, J. S. (2007). Genetics and neurobiology of circadian clocks in mammals. Cold Spring Harbor symposia on quantitative biology,

Silver, R. (2018). Cells have sex chromosomes and circadian clocks: Implications for organismal level functions. *Physiology & behavior*, *187*, 6-12.

Silver, R., Lehman, M. N., Gibson, M., Gladstone, W. R., & Bittman, E. L. (1990). Dispersed cell suspensions of fetal SCN restore circadian rhythmicity in SCN-lesioned adult hamsters. *Brain Res*, *525*(1), 45-58. https://doi.org/10.1016/0006-8993(90)91319-c

Smarr, B., Cutler, T., Loh, D. H., Kudo, T., Kuljis, D., Kriegsfeld, L., Ghiani, C. A., & Colwell, C. S. (2019). Circadian dysfunction in the Q175 model of Huntington's disease: Network analysis. *Journal of neuroscience research*, *97*(12), 1606-1623.

Smarr, B. L., Grant, A. D., Zucker, I., Prendergast, B. J., & Kriegsfeld, L. J. (2017). Sex differences in variability across timescales in BALB/c mice. *Biology of sex differences*, *8*(1), 1-7.

Smarr, B. L., Jennings, K. J., Driscoll, J. R., & Kriegsfeld, L. J. (2014). A time to remember: the role of circadian clocks in learning and memory. *Behavioral neuroscience*, *128*(3), 283.

Smarr, B. L., Zucker, I., & Kriegsfeld, L. J. (2016). Detection of successful and unsuccessful pregnancies in mice within hours of pairing through frequency analysis of high temporal resolution core body temperature data. *PLoS One*, *11*(7), e0160127.

Spoelstra, K., Wikelski, M., Daan, S., Loudon, A. S., & Hau, M. (2016). Natural selection against a circadian clock gene mutation in mice. *Proc Natl Acad Sci U S A*, *113*(3), 686-691. https://doi.org/10.1073/pnas.1516442113

Stavreva, D. A., Wiench, M., John, S., Conway-Campbell, B. L., McKenna, M. A., Pooley, J. R., Johnson, T. A., Voss, T. C., Lightman, S. L., & Hager, G. L. (2009). Ultradian hormone stimulation induces glucocorticoid receptor-mediated pulses of gene transcription. *Nat Cell Biol*, *11*(9), 1093-1102. https://doi.org/10.1038/ncb1922

Steinlechner, S., Jacobmeier, B., Scherbarth, F., Dernbach, H., Kruse, F., & Albrecht, U. (2002). Robust circadian rhythmicity of Per1 and Per2 mutant mice in constant light, and dynamics of Per1 and Per2 gene expression under long and short photoperiods. *J Biol Rhythms*, *17*(3), 202-209. https://doi.org/10.1177/074873040201700303

Stephan, F. K. (1983). Circadian rhythms in the rat: constant darkness, entrainment to T cycles and to skeleton photoperiods. *Physiol Behav*, *30*(3), 451-462. https://doi.org/10.1016/0031-9384(83)90152-x

Stephan, F. K., & Zucker, I. (1972). Circadian rhythms in drinking behavior and locomotor activity of rats are eliminated by hypothalamic lesions. *Proceedings of the National Academy of Sciences*, *69*(6), 1583-1586.

Stevenson, T. J., Prendergast, B. J., & Nelson, R. J. (2017). Mammalian seasonal rhythms: Behavior and neuroendocrine substrates.

Stevenson, T. J., Visser, M. E., Arnold, W., Barrett, P., Biello, S., Dawson, A., Denlinger, D. L., Dominoni, D., Ebling, F. J., Elton, S., Evans, N., Ferguson, H. M., Foster, R. G., Hau, M., Haydon, D. T., Hazlerigg, D. G., Heideman, P., Hopcraft, J. G., Jonsson, N. N., . . . Helm, B. (2015). Disrupted seasonal biology impacts health, food security and ecosystems. *Proc Biol Sci*, *282*(1817), 20151453. https://doi.org/10.1098/rspb.2015.1453

Stojkovic, K., Wing, S. S., & Cermakian, N. (2014). A central role for ubiquitination within a circadian clock protein modification code. *Frontiers in molecular neuroscience*, *7*, 69.

Storch, K.-F., Lipan, O., Leykin, I., Viswanathan, N., Davis, F. C., Wong, W. H., & Weitz, C. J. (2002). Extensive and divergent circadian gene expression in liver and heart. *Nature*, *417*(6884), 78-83.

Stowie, A. C., & Glass, J. D. (2015). Longitudinal Study of Changes in Daily Activity Rhythms over the Lifespan in Individual Male and Female C57BL/6J Mice. *J Biol Rhythms*, *30*(6), 563-568. https://doi.org/10.1177/0748730415598023

Sujino, M., Masumoto, K. H., Yamaguchi, S., van der Horst, G. T., Okamura, H., & Inouye, S. T. (2003). Suprachiasmatic nucleus grafts restore circadian behavioral rhythms of genetically arrhythmic mice. *Curr Biol*, *13*(8), 664-668. https://doi.org/10.1016/s0960-9822(03)00222-7

Sumova, A., Travnickova, Z., Peters, R., Schwartz, W. J., & Illnerova, H. (1995). The rat suprachiasmatic nucleus is a clock for all seasons. *Proceedings of the National Academy of Sciences*, *92*(17), 7754-7758.

Swaab, D. F., Fliers, E., & Partiman, T. S. (1985). The suprachiasmatic nucleus of the human brain in relation to sex, age and senile dementia. *Brain Res*, *342*(1), 37-44. https://doi.org/10.1016/0006-8993(85)91350-2

Tackenberg, M. C., & Hughey, J. J. (2021). The risks of using the chi-square periodogram to estimate the period of biological rhythms. *PLoS Comput Biol*, *17*(1), e1008567. https://doi.org/10.1371/journal.pcbi.1008567

Tahara, Y., Kuroda, H., Saito, K., Nakajima, Y., Kubo, Y., Ohnishi, N., Seo, Y., Otsuka, M., Fuse, Y., & Ohura, Y. (2012). In vivo monitoring of peripheral circadian clocks in the mouse. *Current biology*, *22*(11), 1029-1034.

Takahashi, J. S., & Menaker, M. (1980). Interaction of estradiol and progesterone: effects on circadian locomotor rhythm of female golden hamsters. *American Journal of Physiology-Regulatory, Integrative and Comparative Physiology*, *239*(5), R497-R504.

Tataroglu, Ö., Davidson, A. J., Benvenuto, L. J., & Menaker, M. (2006). The methamphetamine-sensitive circadian oscillator (MASCO) in mice. *Journal of biological rhythms*, *21*(3), 185-194.

Tataroglu, O., & Emery, P. (2015). The molecular ticks of the Drosophila circadian clock. *Curr Opin Insect Sci*, *7*, 51-57. https://doi.org/10.1016/j.cois.2015.01.002

Terazono, H., Mutoh, T., Yamaguchi, S., Kobayashi, M., Akiyama, M., Udo, R., Ohdo, S., Okamura, H., & Shibata, S. (2003). Adrenergic regulation of clock gene expression in mouse liver. *Proc Natl Acad Sci U S A*, *100*(11), 6795-6800. https://doi.org/10.1073/pnas.0936797100

Toh, K. L., Jones, C. R., He, Y., Eide, E. J., Hinz, W. A., Virshup, D. M., Ptáček, L. J., & Fu, Y.-H. (2001). An hPer2 phosphorylation site mutation in familial advanced sleep phase syndrome. *Science*, *291*(5506), 1040-1043.

Truett, G. E., Heeger, P., Mynatt, R. L., Truett, A. A., Walker, J. A., & Warman, M. L. (2000). Preparation of PCR-quality mouse genomic DNA with hot sodium hydroxide and tris (HotSHOT). *Biotechniques*, *29*(1), 52, 54. https://doi.org/10.2144/00291bm09

Turek, F. W. (2016). Circadian clocks: Not your grandfather's clock. *Science*, *354*(6315), 992-993. https://doi.org/10.1126/science.aal2613

Ueda, H. R., Hayashi, S., Chen, W., Sano, M., Machida, M., Shigeyoshi, Y., Iino, M., & Hashimoto, S. (2005). System-level identification of transcriptional circuits underlying mammalian circadian clocks. *Nature genetics*, *37*(2), 187-192.

Van Der Horst, G. T., Muijtjens, M., Kobayashi, K., Takano, R., Kanno, S.-i., Takao, M., de Wit, J., Verkerk, A., Eker, A. P., & van Leenen, D. (1999). Mammalian Cry1 and Cry2 are essential for maintenance of circadian rhythms. *Nature*, *398*(6728), 627-630.

van der Veen, D. R., & Gerkema, M. P. (2017). Unmasking ultradian rhythms in gene expression. *FASEB J*, *31*(2), 743-750. https://doi.org/10.1096/fj.201600872R

van Oort, B. E., Tyler, N. J., Gerkema, M. P., Folkow, L., & Stokkan, K. A. (2007). Where clocks are redundant: weak circadian mechanisms in reindeer living under polar photic conditions. *Naturwissenschaften*, *94*(3), 183-194. https://doi.org/10.1007/s00114-006-0174-2

van Rosmalen, L., & Hut, R. A. (2021). Negative Energy Balance Enhances Ultradian Rhythmicity in Spring-Programmed Voles. *J Biol Rhythms*, *36*(4), 359-368. https://doi.org/10.1177/07487304211005640

Vansteensel, M. J., Michel, S., & Meijer, J. H. (2008). Organization of cell and tissue circadian pacemakers: a comparison among species. *Brain Research Reviews*, *58*(1), 18-47. https://doi.org/10.1016/j.brainresrev.2007.10.009

Veldhuis, J. (2008). Pulsatile hormone secretion: mechanisms, significance and evaluation. In *Ultradian Rhythms from Molecules to Mind* (pp. 229-248). Springer.

Vida, B., Hrabovszky, E., Kalamatianos, T., Coen, C., Liposits, Z., & Kallo, I. (2008). Oestrogen receptor α and β immunoreactive cells in the suprachiasmatic nucleus of mice: distribution, sex differences and regulation by gonadal hormones. *Journal of neuroendocrinology*, *20*(11), 1270-1277.

Vitaterna, M. H., King, D. P., Chang, A. M., Kornhauser, J. M., Lowrey, P. L., McDonald, J. D., Dove, W. F., Pinto, L. H., Turek, F. W., & Takahashi, J. S. (1994). Mutagenesis and mapping of a mouse gene, Clock, essential for circadian behavior. *Science*, *264*(5159), 719-725. https://doi.org/10.1126/science.8171325

Vitaterna, M. H., Selby, C. P., Todo, T., Niwa, H., Thompson, C., Fruechte, E. M., Hitomi, K., Thresher, R. J., Ishikawa, T., Miyazaki, J., Takahashi, J. S., & Sancar, A. (1999). Differential regulation of mammalian Period genes and circadian rhythmicity by cryptochromes 1 and 2. *Proceedings of the National Academy of Sciences*, *96*(21), 12114-12119. https://doi.org/doi:10.1073/pnas.96.21.12114

Walker, W. H., 2nd, Borniger, J. C., Gaudier-Diaz, M. M., Hecmarie Melendez-Fernandez, O., Pascoe, J. L., Courtney DeVries, A., & Nelson, R. J. (2020). Acute exposure to low-level light at night is sufficient to induce neurological changes and depressive-like behavior. *Mol Psychiatry*, *25*(5), 1080-1093. https://doi.org/10.1038/s41380-019-0430-4

Wams, E. J., Riede, S. J., van der Laan, I., ten Bulte, T., & Hut, R. A. (2017). Mechanisms of non-photic entrainment. In *Biological timekeeping: clocks, rhythms and behaviour* (pp. 395-404). Springer.

Wang, G. Z., Hickey, S. L., Shi, L., Huang, H. C., Nakashe, P., Koike, N., Tu, B. P., Takahashi, J. S., & Konopka, G. (2015). Cycling Transcriptional Networks Optimize Energy Utilization on a Genome Scale. *Cell Rep*, *13*(9), 1868-1880. https://doi.org/10.1016/j.celrep.2015.10.043

Wang, L. M., Dragich, J. M., Kudo, T., Odom, I. H., Welsh, D. K., O'Dell, T. J., & Colwell, C. S. (2009). Expression of the circadian clock gene Period2 in the hippocampus: possible implications for synaptic plasticity and learned behaviour. *ASN neuro*, *1*(3), AN20090020.

Wang, X., Zhao, B. S., Roundtree, I. A., Lu, Z., Han, D., Ma, H., Weng, X., Chen, K., Shi, H., & He, C. (2015). N6-methyladenosine modulates messenger RNA translation efficiency. *Cell*, *161*(6), 1388-1399.

Wang, Z. Y., Cable, E. J., Zucker, I., & Prendergast, B. J. (2014). Pregnancy-induced changes in ultradian rhythms persist in circadian arrhythmic Siberian hamsters. *Hormones and Behavior*, *66*(2), 228-237.

Weger, B. D., Gobet, C., Yeung, J., Martin, E., Jimenez, S., Betrisey, B., Foata, F., Berger, B., Balvay, A., & Foussier, A. (2019). The mouse microbiome is required for sex-specific diurnal rhythms of gene expression and metabolism. *Cell metabolism*, *29*(2), 362-382. e368.

Welsh, D. K., Logothetis, D. E., Meister, M., & Reppert, S. M. (1995). Individual neurons dissociated from rat suprachiasmatic nucleus express independently phased circadian firing rhythms. *Neuron*, *14*(4), 697-706.

Whitehead, K., Pan, M., Masumura, K.-i., Bonneau, R., & Baliga, N. S. (2009). Diurnally entrained anticipatory behavior in archaea. *PLoS One*, *4*(5), e5485.

Winfree, A. T. (2001). *The geometry of biological time* (Vol. 12). Springer Science & Business Media.

Woitowich, N. C., Beery, A., & Woodruff, T. (2020). Meta-research: a 10-year follow-up study of sex inclusion in the biological sciences. *Elife*, *9*, e56344.

Wollnik, F., & Dohler, K. D. (1986). Effects of adult or perinatal hormonal environment on ultradian rhythms in locomotor activity of laboratory LEW/Ztm rats. *Physiol Behav*, *38*(2), 229-240. https://doi.org/10.1016/0031-9384(86)90158-7

Wollnik, F., & Turek, F. W. (1988). Estrous correlated modulations of circadian and ultradian wheel-running activity rhythms in LEW/Ztm rats. *Physiology & behavior*, *43*(3), 389-396.

Wu, Y. E., Enoki, R., Oda, Y., Huang, Z. L., Honma, K. I., & Honma, S. (2018). Ultradian calcium rhythms in the paraventricular nucleus and subparaventricular zone in the hypothalamus. *Proc Natl Acad Sci U S A*, *115*(40), E9469-E9478. https://doi.org/10.1073/pnas.1804300115

Xiang, S., Coffelt, S. B., Mao, L., Yuan, L., Cheng, Q., & Hill, S. M. (2008). Period-2: a tumor suppressor gene in breast cancer. *J Circadian Rhythms*, *6*, 4. https://doi.org/10.1186/1740-3391-6-4

Xu, Y., Toh, K., Jones, C., Shin, J.-Y., Fu, Y.-H., & Ptáček, L. (2007). Modeling of a human circadian mutation yields insights into clock regulation by PER2. *Cell*, *128*(1), 59-70.

Yamaguchi, Y., Suzuki, T., Mizoro, Y., Kori, H., Okada, K., Chen, Y., Fustin, J. M., Yamazaki, F., Mizuguchi, N., Zhang, J., Dong, X., Tsujimoto, G., Okuno, Y., Doi, M., & Okamura, H. (2013). Mice genetically deficient in vasopressin V1a and V1b receptors are resistant to jet lag. *Science*, *342*(6154), 85-90. https://doi.org/10.1126/science.1238599

Yamazaki, S., Numano, R., Abe, M., Hida, A., Takahashi, R., Ueda, M., Block, G. D., Sakaki, Y., Menaker, M., & Tei, H. (2000). Resetting central and peripheral circadian oscillators in transgenic rats. *Science*, *288*(5466), 682-685. https://doi.org/10.1126/science.288.5466.682

Yan, L., & Silver, R. (2016). Neuroendocrine underpinnings of sex differences in circadian timing systems. *J Steroid Biochem Mol Biol*, *160*, 118-126. https://doi.org/10.1016/j.jsbmb.2015.10.007

Yang, X., Wood, P. A., Oh, E.-Y., Du-Quiton, J., Ansell, C. M., & Hrushesky, W. J. (2009). Down regulation of circadian clock gene Period 2 accelerates breast cancer growth by altering its daily growth rhythm. *Breast cancer research and treatment*, *117*(2), 423-431.

Yates, F. E., & Yates, L. (2008). Ultradian rhythms as the dynamic signature of life. In *Ultradian Rhythms from Molecules to Mind* (pp. 249-260). Springer.

Yerushalmi, S., & Green, R. M. (2009). Evidence for the adaptive significance of circadian rhythms. *Ecology letters*, *12*(9), 970-981.

Yoo, S.-H., Ko, C. H., Lowrey, P. L., Buhr, E. D., Song, E.-j., Chang, S., Yoo, O. J., Yamazaki, S., Lee, C., & Takahashi, J. S. (2005). A noncanonical E-box enhancer drives mouse Period2 circadian oscillations in vivo. *Proceedings of the National Academy of Sciences*, *102*(7), 2608-2613.

Yoo, S. H., Yamazaki, S., Lowrey, P. L., Shimomura, K., Ko, C. H., Buhr, E. D., Siepka, S. M., Hong, H. K., Oh, W. J., Yoo, O. J., Menaker, M., & Takahashi, J. S. (2004). PERIOD2::LUCIFERASE real-time reporting of circadian dynamics reveals persistent circadian oscillations in mouse peripheral tissues. *Proc Natl Acad Sci U S A*, *101*(15), 5339-5346. https://doi.org/10.1073/pnas.0308709101

Young, M. W., & Kay, S. A. (2001). Time zones: a comparative genetics of circadian clocks. *Nat Rev Genet*, *2*(9), 702-715. https://doi.org/10.1038/35088576

Zhang, H., Wang, L., Shi, K., Shan, D., Zhu, Y., Wang, C., Bai, Y., Yan, T., Zheng, X., & Kong, J. (2019). Apple tree flowering is mediated by low level of melatonin under the regulation of seasonal light signal. *J Pineal Res*, *66*(2), e12551. https://doi.org/10.1111/jpi.12551

Zhang, R., Lahens, N. F., Ballance, H. I., Hughes, M. E., & Hogenesch, J. B. (2014). A circadian gene expression atlas in mammals: implications for biology and medicine. *Proc Natl Acad Sci U S A*, *111*(45), 16219-16224. https://doi.org/10.1073/pnas.1408886111

Zheng, B., Albrecht, U., Kaasik, K., Sage, M., Lu, W., Vaishnav, S., Li, Q., Sun, Z. S., Eichele, G., & Bradley, A. (2001). Nonredundant roles of the mPer1 and mPer2 genes in the mammalian circadian clock. *Cell*, *105*(5), 683-694.

Zheng, B., Larkin, D. W., Albrecht, U., Sun, Z. S., Sage, M., Eichele, G., Lee, C. C., & Bradley, A. (1999). The mPer2 gene encodes a functional component of the mammalian circadian clock. *Nature*, *400*(6740), 169-173.

Zheng, D., Liwinski, T., & Elinav, E. (2020). Interaction between microbiota and immunity in health and disease. *Cell Res*, *30*(6), 492-506. https://doi.org/10.1038/s41422-020-0332-7

Zhong, X., Yu, J., Frazier, K., Weng, X., Li, Y., Cham, C. M., Dolan, K., Zhu, X., Hubert, N., Tao, Y., Lin, F., Martinez-Guryn, K., Huang, Y., Wang, T., Liu, J., He, C., Chang, E. B., & Leone, V. (2018). Circadian Clock Regulation of Hepatic Lipid Metabolism by Modulation of m(6)A mRNA Methylation. *Cell Rep*, *25*(7), 1816-1828 e1814. https://doi.org/10.1016/j.celrep.2018.10.068

Zhu, Y., Stevens, R., Hoffman, A., Tjonneland, A., Vogal, U., Zheng, T., & Hansen, J. (2011). Genome-wide methylation changes in night working women in Denmark: same altered promoter methylation of CLOCK and CRY2 as in breast cancer cases. *Occupational and Environmental Medicine*, *68*(Suppl 1), A18-A18.

Zucker, I., & Beery, A. K. (2010). Males still dominate animal studies. *Nature*, *465*(7299), 690-690.

Zucker, I., Fitzgerald, K. M., & Morin, L. P. (1980). Sex differentiation of te circadian system in the golden hamster. *American Journal of Physiology-Regulatory, Integrative and Comparative Physiology*, *238*(1), R97-R101.

Zucker, I., & Prendergast, B. J. (2020). Sex differences in pharmacokinetics predict adverse drug reactions in women. *Biol Sex Differ*, *11*(1), 32. https://doi.org/10.1186/s13293-020-00308-5

Appendix A: Supplementary Figures

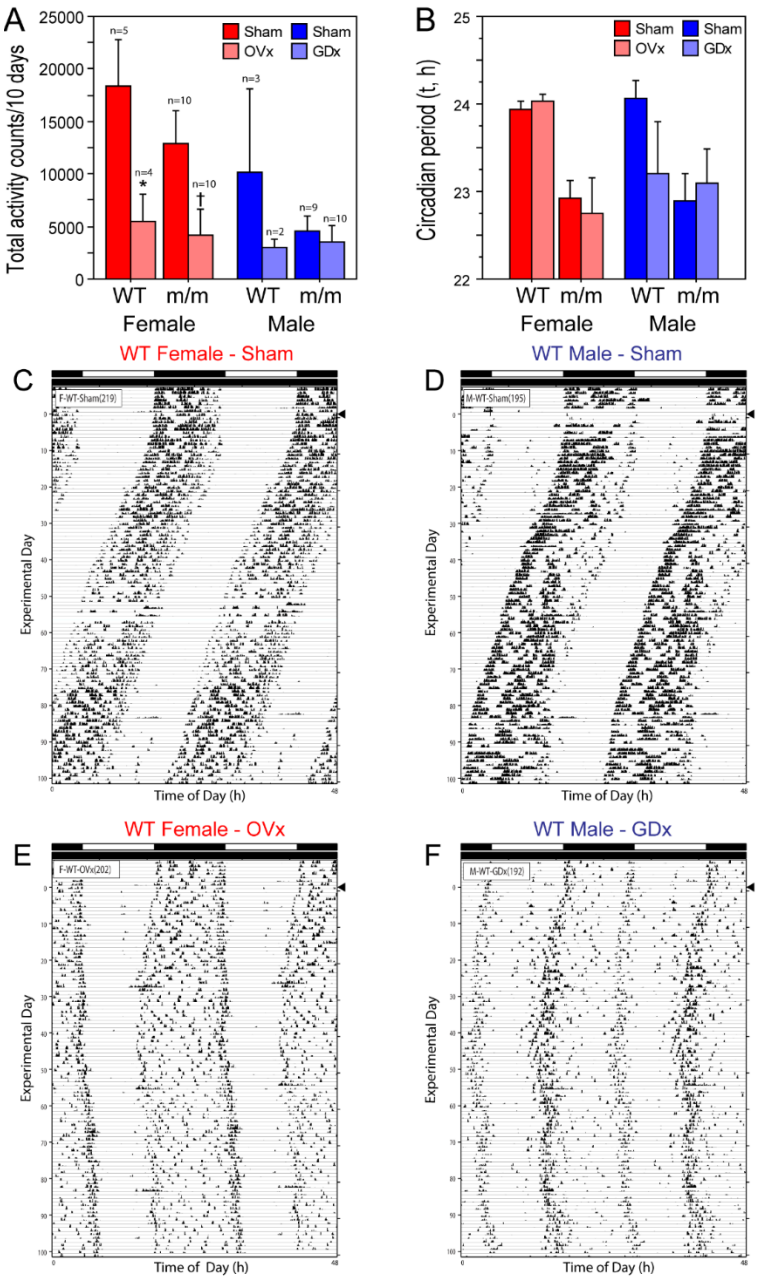

Figure 33: Control procedures

(A) Mean +SEM daily locomotor activity counts (wheel revolutions) of female and male WT and Per2m/m mice that were surgically gonadectomized (females: OVX; males: GDx) or sham

Figure 33, continued: operated, and subsequently housed in a 12L:12D photoperiod. Activity was evaluated over a 10 day interval beginning 2 months after surgery was performed (B) Mean + SEM circadian τ of sham and gonadectomized, male and female, WT and Per2m/m mice in DD. (C-F) Representative double-plotted RW actograms of female and male WT mice that were sham operated (female: panel C; male: panel D or gonadectomized (OVx female: panel E; GDx male: panel F), and maintained in DD for >100 days (transfer from LD to DD indicated by arrowhead; actogram conventions as in Fig. 1).

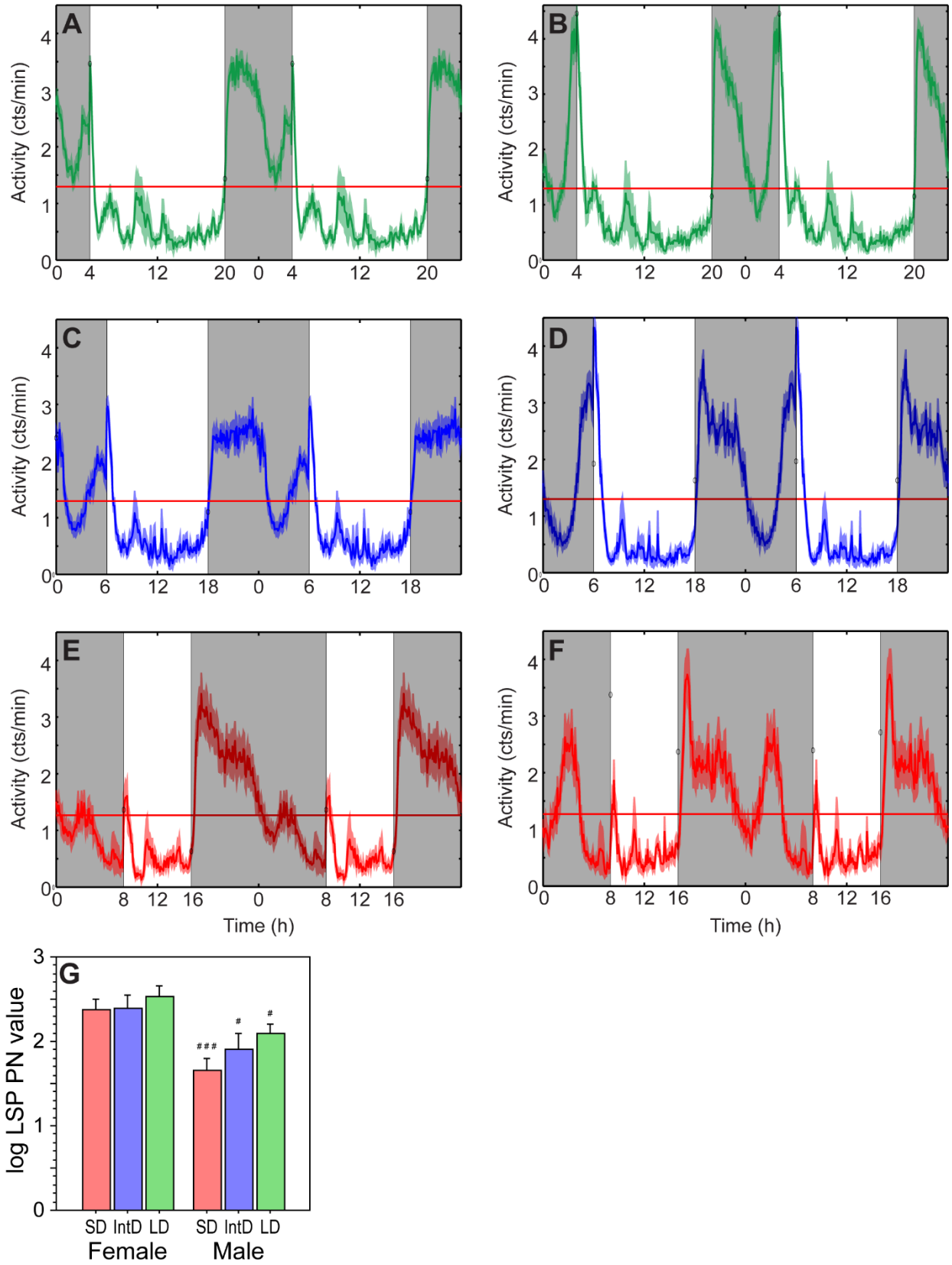

Figure 34. Circadian entrainment to long, intermediate and short photoperiods.

Figure 34, continued: Mean (± SEM) locomotor activity levels (counts/min) of female (left column) and male (right column) mice housed in 16L:8D (A,B green), 12L:12D (C,D blue) or 8L:16D (E,F red). Records are double-plotted to facilitate visualization of nocturnal locomotor activity. Gray shading denotes the dark phase. Horizontal red lines indicate mean locomotor activity levels within each group. (G) Mean (+SEM) power (PN) values obtained from Lomb-Scargle Periodogram analyses of 10 days of locomotor activity of female and male mice housed in 8L:16D (green), 12L:12D (blue) or 16L:8D (red). *# p<0.05, ##p<0.01, ### p<0.001 vs. female within DL.*

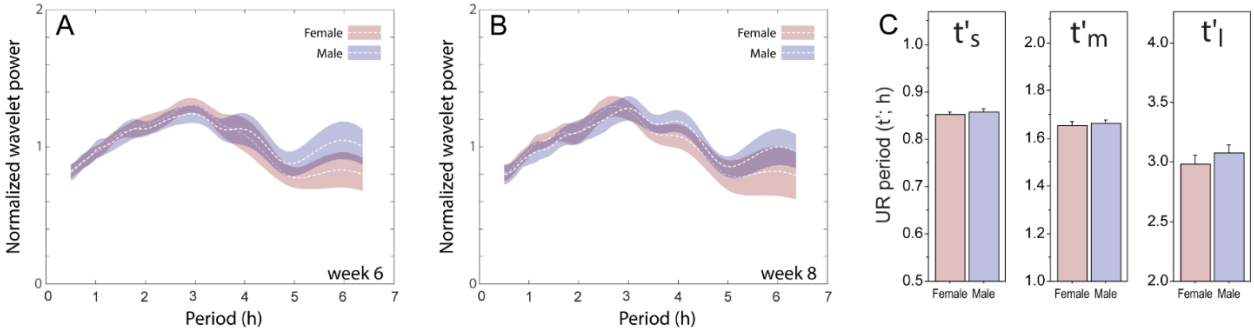

Figure 35. Sex differences in ultradian power and period during the light phase.

Power-period plots (±95% CI) calculated by continuous wavelet transform of 10 days of pre-parsed light phase locomotor activity data from female (red) and male (blue) mice (A) on week 6 and (B) on week 8. Experiment and analysis details, and figure conventions, as in Fig. 4. (C) Mean (± SEM) instantaneous ultradian periods (τ') of pre-parsed light phase locomotor activity data in the τ' in the τ'_s, τ'_m and τ'_l period analysis bands reading.

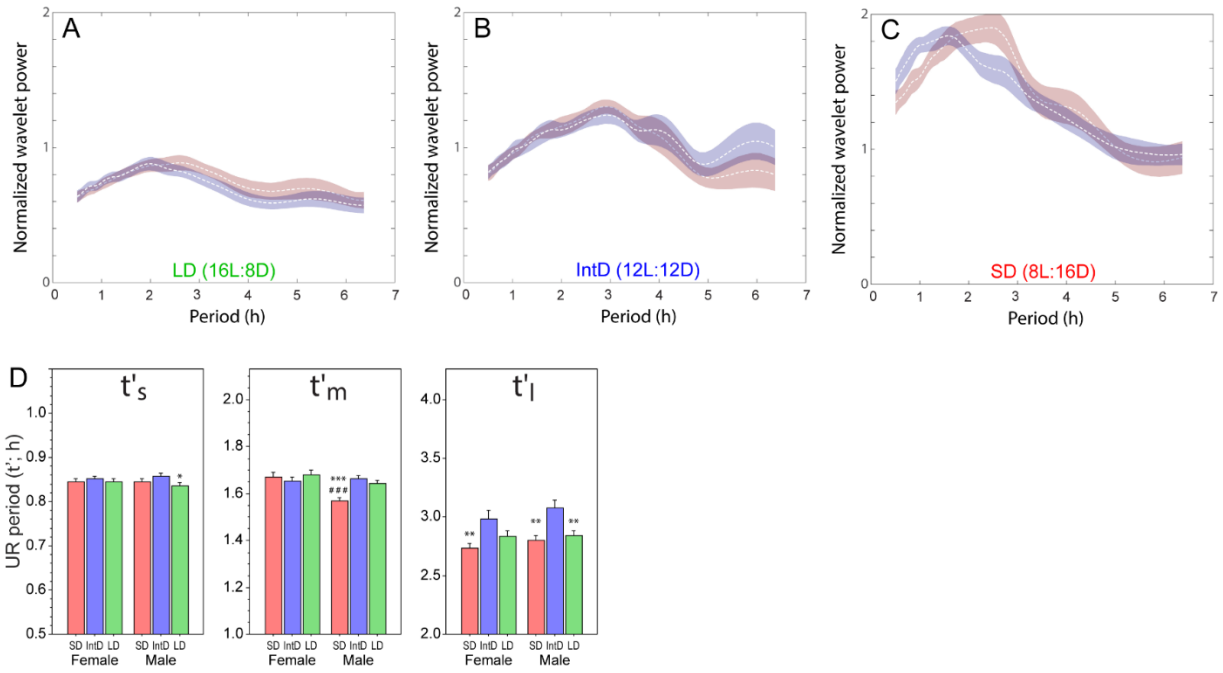

Figure 36. Photoperiodic modulation of ultradian power and period in the light phase.

Power-period plots (±95% CI) calculated by continuous wavelet transform of 10 days of pre-parsed light phase activity data from female and male mice after adaptation to (A) 16L:8D (green), (B) 12L:12D (blue) or (C) 8L:16D (red) photoperiods. See Figure S2 for confirmation of circadian entrainment. (D) Mean (± SEM) instantaneous ultradian periods (τ') of pre-parsed light phase locomotor activity data in the τ' in the τ'_s, τ'_m and τ'_l period analysis bands.* $p<0.05$, ** $p<.01$, ***$p<.001$ vs. IntD value within sex; ### $p<.001$ vs. females, within DL

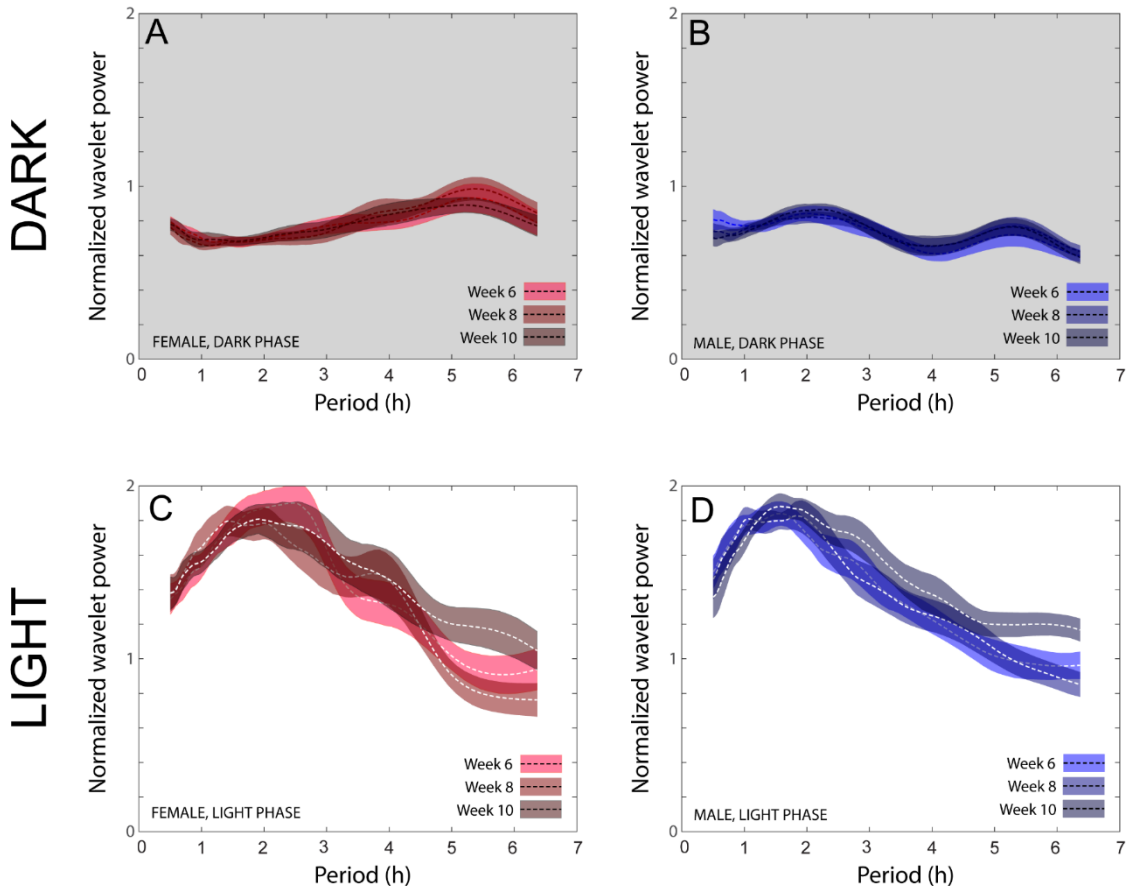

Figure 37. Persistence of short day-induced redistribution of UR power over time.

Power-period plots (±95% CI) calculated by continuous wavelet transform of 10 days of pre-parsed dark phase (A, B) and light phase (C, D) locomotor activity data from female (A, C) and male (B, D) mice after 6, 8 and 10 weeks in short day.

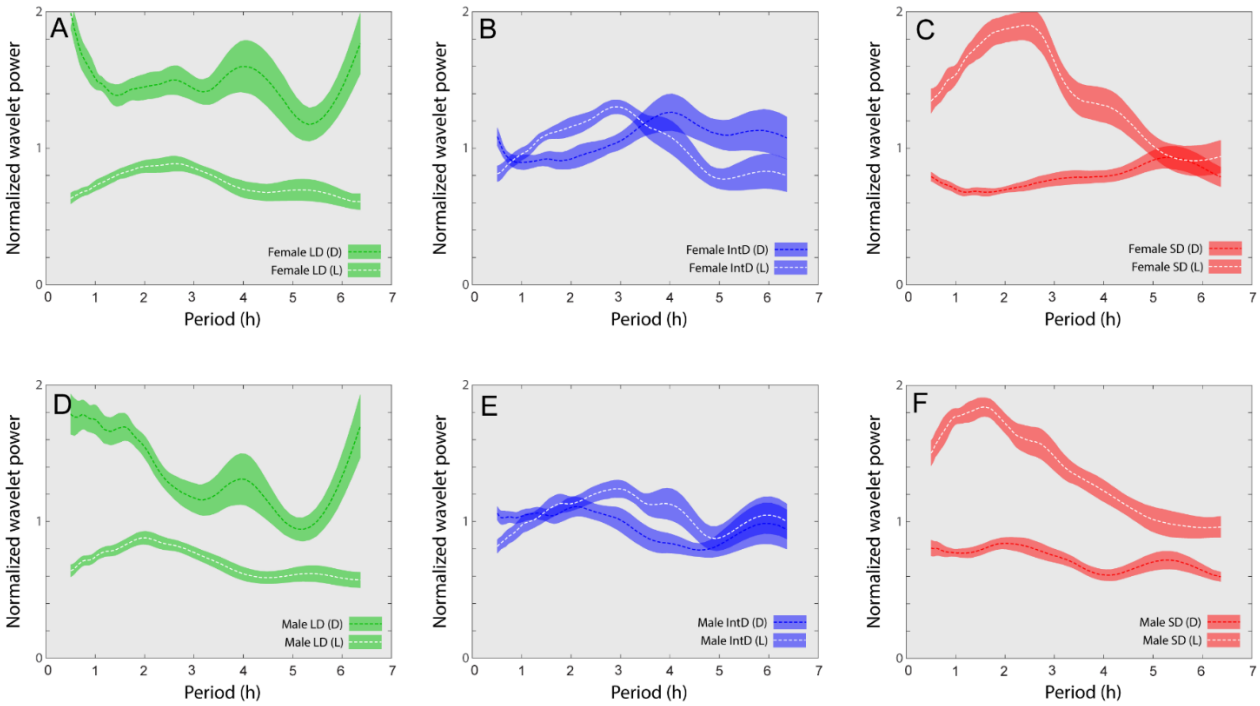

Figure 38. Circadian modulation of UR power in long, intermediate and short photoperiods.

Power-period plots (±95% CI) calculated by continuous wavelet transform of 10 days of pre-parsed dark and light phase locomotor activity data from (A-0C) female and (D-F) male mice after adaptation to 16L:8D (green; panels A and D), 12L:12D (blue; panels B and E) or 8L:16D (red; panels C and F) photoperiods. See Figure S2 for confirmation of circadian entrainment. Within each photoperiod plot, color lines indicate mean wavelet power of dark phase activity, and white lines indicate mean wavelet power of light phase locomotor activity.

Table 0-1: Coeffecient and R^2 values of regressions between interpolated τ values and τ value calculated

A	<u>Interpolated Ultradian Periods Modulated by Circadian Phase</u>			
Analysis window	τ'm			
Method of Calculating Ridge Period	Ridgewalk Function		Ridge Maximum	
Regression Component	R^2	Slope	R^2	Slope
Post-Parsed Dark Phase Data	0.732	0.217	0.815	0.497
Post-Parsed Light Phase Data	0.76	0.279	0.907	0.631

Pre-Parsed Dark Phase Data	0.659	0.228	0.822	0.541
Pre-Parsed Light Phase Data	0.692	0.317	0.901	0.694
Un-Parsed Data	0.34	0.119	0.41	0.283
Analysis window	τ'l			
Method of Calculating Ridge Period	Ridgewalk Function		Ridge Maximum	
Regression Component	R^2	Slope	R^2	Slope
Post-Parsed Dark Phase Data	0.598	0.198	0.803	0.535
Post-Parsed Light Phase Data	0.608	0.238	0.774	0.577
Pre-Parsed Dark Phase Data	0.426	0.233	0.809	0.705
Pre-Parsed Light Phase Data	0.251	0.186	0.76	0.753
Un-Parsed Data	0.365	0.134	0.441	0.33
B	<u>Interpolated Ultradian Periods Not Modulated by Circadian Phase</u>			
Analysis window	τ'm			
Method of Calculating Ridge Period	Ridgewalk Function		Ridge Maximum	
Regression Component	R^2	Slope	R^2	Slope
Post-Parsed Dark Phase Data	0.752	0.266	0.825	0.56
Post-Parsed Light Phase Data	0.773	0.322	0.887	0.719
Pre-Parsed Dark Phase Data	0.659	0.228	0.822	0.541
Pre-Parsed Light Phase Data	0.706	0.301	0.887	0.715
Un-Parsed Data	0.792	0.294	0.879	0.638
Analysis window	τ'l			
Method of Calculating Ridge Period	Ridgewalk Function		Ridge Maximum	

Regression Component	R^2	Slope	R^2	Slope
Post-Parsed Dark Phase Data	0.76	0.347	0.874	0.684
Post-Parsed Light Phase Data	0.781	0.389	0.901	0.783
Pre-Parsed Dark Phase Data	0.426	0.233	0.809	0.705
Pre-Parsed Light Phase Data	0.446	0.281	0.831	0.833
Un-Parsed Data	0.793	0.368	0.903	0.73
C	Ultradian Structure Randomized and Circadian Structure Intact			
Analysis window	τ'm			
Method of Calculating Ridge Period	Ridgewalk Function		Ridge Maximum	
Regression Component	R^2	Slope	R^2	Slope
Post-Parsed Dark Phase Data	0.001	0.003	0.00013	0.002
Post-Parsed Light Phase Data	0.000063	-0.001	0.002	0.009
Pre-Parsed Dark Phase Data	0.004^B	0.007^B	0.000023	0.001
Pre-Parsed Light Phase Data	0.00019	-0.001	0.00013	0.002
Un-Parsed Data	0.0000092	-0.0002	0.00031	0.004
Analysis window	τ'l			
Method of Calculating Ridge Period	Ridgewalk Function		Ridge Maximum	
Regression Component	R^2	Slope	R^2	Slope
Post-Parsed Dark Phase Data	0.001	0.003	0.001	0.009
Post-Parsed Light Phase Data	0.000021	0.001	0.001	-0.008
Pre-Parsed Dark Phase Data	0.00023	0.002	0.00045	0.006
Pre-Parsed Light Phase Data	0.003	-0.008	0.007^A	0.023^A

Un-Parsed Data	0.001	0.003	0.00003	0.001

Note: (A & B). All are significant ($p<0.0001$). (C). Not significant unless denoted. $^{A}P = 0.0073$. $^{B}P = 0.0409$

Appendix B: Supplementary Methods

Generation of artificial activity records for validation of modified wavelet transform workflow. Time series data were evaluated using a modified wavelet transform analyses. Experiments 1.1 - 1.3 evaluated the precision of the CWT workflow and verified that the analysis procedure itself did not generate systematic artifacts in period or power estimates, especially because we concatenated dark and light periods separately for some analyses. To accomplish this we use simulated activity data (artificial activity record) which possessed defined rhythmic features in the UR domain. Artificial activity records mimicked the amplitude and variability inherent in actual activity data generated by mice. Each artificial activity record contained a robust CR in activity, and 2 or 4 unique signals in the UR domain (1 - 6.5 h). Artificial activity records also contained random noise. Procedures for generating artificial activity records were as follows:

1. Each of the simulation experiments (Experiments 1.1 - 1.3) contained 10 treatment groups, and each treatment group ('Group') contained 10 individual simulated 'animals' (i.e., 10 artificial activity records). Each artificial activity record was composed of an 'entrained' CR with a period of 24 h, 2 or 4 URs, each with unique periods.[1]
2. To generate known periodicities in the CR and UR domains, but against a background of naturalistic variance/noise, artificial activity record were generated with constraints that defined the limits of CR and UR period and amplitude but allowed for UR period to vary between simulated Groups and among individuals within each Groups, as well as for random variability to be inserted (inter-individual variability, see Step #4, below).
3. Each Group was assigned a fundamental CR (fCR) period of 24.0 and two different fundamental UR (fUR) periods, which were randomly selected from values bounded by

defined period ranges: faster fURs (fUR1) had periods between 1.07 - 2.13 h, and slower fURs (fUR2) had periods between 2.13 and 4.26 h). This resulted in the generation of 10 different Groups each defined by a fCR of 24.0 h, and two fURs (UR1 [faster] and UR2 [slower]) unique to each treatment Group.

4. Next, artificial activity records for 10 simulated individual 'animals' were generated to populate each Group. To generate individual differences among these subjects (without affecting the mean fUR value of the Group), inter-individual variation was added to the fURs within each artificial activity record. The range of the inter-individual variation was limited by margins that were based on the natural range in variability exhibited in free-running CRs of C57BL6/J mice (mean+sem = 23.8 +0.02, n=10; SD=0.063; 3SD = 0.19, or ±0.8% of the period value; (Schwartz & Zimmerman, 1990)) scaled down into the UR domain. Thus, within a treatment Group, each of the 10 individuals each had a different unique UR (qUR), which was randomly selected, but was bounded in its range to ±0.8% of the defined fUR for that Group. The introduction of inter-individual variation was performed separately for UR1 and UR2 of each simulated animal within each treatment Group.[1]
5. Steps 1-4 were repeated to define fUR periods for each Group and to generate unique qUR periods for each constituent artificial activity record. URs, and the 24 h CR common

[1] Intra-individual (i.e., cycle-to-cycle) variability in the qUR of each member of the treatment Group was added in a later step, but any such experimentally-introduced within-animal period variability from cycle to cycle adhered to the period defined by the qUR.

to all artificial activity records, were generated as square wave functions. artificial activity records were 14,400 min (10 days) in duration.[2]

6. Square wave CRs and URs were generated according to the above schema with a length of 14400 minutes (10 days). All records began with CRs and URs in the ON state. CR and UR phases interacted to generate absolute levels of activity at any point in time. In a given 1 min bin, the CR could be in the ON (active) state, or in the OFF (rest) state; simultaneously, either of the 2 URs could likewise be in an ON or OFF state.

7. To introduce intra-individual variability and random noise, CR and UR state did not obligately code for a fixed amount of activity, rather, the ON or OFF state coded for a probability of activity. Because activity at each point in the artificial activity record resulted from information derived from 3 interacting rhythms (one CR and two URs)[3], a total of 6 permutations of rhythm-states existed at each point in time. The following rules and probabilistic functions were used to determine the absolute activity level (bin value) for each permutation (CR-UR-UR permutation indicated [in brackets]). Probability-driven mean activity levels for a bin with each unique permutation are summarized in Table 1-1.

---

[2] For purposes of clarity, this description considers procedures for artificial activity records adulterated with 2 fURs. In some simulations, (e.g., Expt. 1.1), 4 fURs were interpolated into some artificial activity record records. This was necessary to generate artificial activity records with URs that changed period during the L and D phases ('CR modulated' rhythms; see *Methods*). In these instances, procedures identical to those described here for 2 fURs (and their constituent qURs) were followed, with the only difference being the number of fURs that were randomly generated (4 vs. 2). artificial activity records with 4 fURs were comprised of 2 different fUR1s, and 2 different fUR2s, modulated by circadian phase. For the two fUR1s, one was randomly chosen to be inserted into the active phase of the CR and the other was inserted into the rest phase of the CR; similarly, the two fUR2s were each assigned to a specific circadian phase (see *Methods*). All unique qURs still behaved the same with respect to range of variability around their respective fUR periods. See #7 below for details of quantitative generation of intra-individual variability in records that contained 2 vs. 4 fURs.

[3] Although artificial activity records in the CR modulated group in Experiment 1.1 possessed 4 fURs, note that at any point in time only 2 of the fURs were being expressed, thus even in these records, a maximum of 3 rhythms would be interacting.

a. [OFF-OFF-OFF] If the CR was in the OFF state, and both URs were also in OFF states, then: 99% of the time the bin value = 0, and 1% of the time it was set to a random integer ranging from 0 - 30. This chance was also added to all of the below conditions.

$$\sum_{n=0}^{30}.01 * \ 1/31 * n = .15$$

b. [OFF-ON-OFF] If the CR was in the OFF state, and one of the two URs was in the ON state but the other UR was in the OFF state, then: 79% of the time the bin value = 0, and 20% of the time it was set to a random integer ranging from 0 – 10. 1% of the time it was set to a random integer ranging from 0 - 30.

$$\sum_{n=0}^{20} .2 * \ 1/21 * n + \sum_{n=0}^{30}.01 * \ 1/31 * n = 2.15$$

c. [OFF-ON-ON] If the CR was in the OFF state, but both URs were in the ON states, then: 59% of the time the bin value = 0, 20% of the time it was set to a random integer ranging from 0-30 (additive), and 13.34% of the time it was set to a random integer ranging from 0-20 (interference)[4] 1% of the time it was set to a random integer ranging from 0 - 30.

[4] These two settings were selected in an effort to remain agnostic about the nature of UR-UR interactions when both are in the ON state, The probabilistic range of 0-25 accounts for URs interacting in an additive manner, whereas the range from 0-15 accounts for URs interfering with one another.

$$\sum_{n=0}^{20} .2 * 1/21 * n + \sum_{n=0}^{30} .1334 * \frac{1}{31} * n + \sum_{n=0}^{30}. 01 * 1/31 * n = 4.15$$

d. [ON-OFF-OFF] If the CR was in the ON state, but both URs were in OFF states, then: 49% of the time the bin value = 0, and 50% of the time it was set to a random integer ranging from 0 – 20. 1% of the time it was set to a random integer ranging from 0 - 30.

$$\sum_{n=0}^{20} .5 * 1/21 * n + \sum_{n=0}^{30}. 01 * 1/31 * n = 5.15$$

e. [ON-ON-OFF] If the CR was in the ON state, and one of the two URs was in the ON state but the other UR was in the OFF state, then: 29% of the time the bin value = 0, and 70% of the time it was set to a random ranging from 0 – 20. 1% of the time it was set to a random integer ranging from 0 - 30.

$$\sum_{n=0}^{20} .7 * \frac{1}{21} * n + \sum_{n=0}^{30}. 01 * 1/31 * n = 7.15$$

f. ON-ON-ON] If the CR was in the ON state, and both URs were in the ON states, then: 9% of the time the bin value = 0[5], and 18% of the time it was set to a random integer ranging from 0 - 10 [low activity], 54% of the time it was set to a

[5] Bouts of LMA inactivity (rest, grooming, sleep) occur abundantly during the active phase, thus, the CR ON cannot obligately code for a non-zero integer activity value.

random integer ranging from 0 - 20 [moderate activity], and 18% of the time it was set to a random integer ranging from 0 – 30 [high activity][6]. 1% of the time it was set to a random integer ranging from 0 - 30.

$$\sum_{n=0}^{10} .18 * 1/11 * n + \sum_{n=0}^{20} .54 * 1/21 * n + \sum_{n=0}^{30} .18 * \frac{1}{31} * n +$$

$$\sum_{n=0}^{30} .01 * \frac{1}{31} * n = 9.15$$

CR	UR	UR	UP E.V.	Range	Probability (P0) of 0 value
-	-	-	0.15	0 – 30	P = 0.99
-	+	-	2.15	0 – 30	P = 0.79
-	+	+	4.15	0 – 30	P = 0.59
+	-	-	5.15	0 – 30	P = 0.49
+	+	-	7.15	0 – 30	P = 0.29
+	+	+	9.15	0 – 30	P = 0.09

Table 1-1. Mean activity value for each of the 6 unique permutation bins (UP mean E.V.) activity value being inserted

Note: Table indicates mean value for each unique bin, but probabilistic function ensures bin-to-bin variability, even if they possess the same permutation.

8. For each artificial activity record, a low-amplitude time series of random noise equal in length to each artificial activity record was generated and the random values were

[6] To generate 3 different levels of higher-probability activity during the ON-ON-ON permutation.

subtracted from the artificial activity record generated in Step #7. Noise was generated by creating a square wave with a random period between 0 and 1 minute. When the noise was in the OFF state the bin value = 0, and when noise was in the ON state a random number ranging from 0 – 1 was selected. The resultant random-period high-frequency time series values were then subtracted from the artificial animal time series.

9. Finally, to account for variability in activity level, we assumed the default time series state to be high activity and multiplied each artificial activity record by a decimal between 1.0 & .2 such that it somewhere between 100% to 20% of the default level of activity. As this grouping of 10 artificial activity record is meant to approximate group conditions that might lead to similar activity and temporal structure we wanted groupings to have both similar activity levels while maintaining some variance. To accomplish this for each set of 10 artificial activity record, a random of number was chosen such that 50 % of the time they were set to having high activity, a range of [1 - .6], and 50% of the time they were set to having low activity, a range of [.6-.2]. For each individual artificial activity record within the high and low grouping then a random number was chosen within the corresponding range and the artificial activity record was multiplied by it. Negative value bins resulting from noise subtraction were set to = 0.
10. To evaluate face validity of artificial activity record, they were visually compared to real locomotor activity time series data. See comparisons of artificial activity record and actual activity data in Fig 2.